UNIVERSIDADE FEDERAL FLUMINENSE
INSTITUTO DE GEOCIÊNCIAS
DEPARTAMENTO DE GEOLOGIA E GEOFÍSICA
PROGRAMA DE PÓS-GRADUAÇÃO EM DINÂMICA DOS OCEANOS E DA TERRA

MARIANA BITTENCOURT SEABRA LEBRE

ANALYSIS OF FLOW FACIES IN THE PRE-SALT INTERVAL OF THE SANTOS BASIN

NITERÓI, RJ

2021

MARIANA BITTENCOURT SEABRA LEBRE

ANALYSIS OF FLOW FACIES IN THE PRE-SALT INTERVAL OF THE SANTOS BASIN

Dissertation submitted to Universidade Federal Fluminense as a partial requirement of the graduate program in Ocean and Earth Dynamics to obtain the title of Master in Geology and Geophysics.

Advisor: PhD. Wagner Moreira Lupinacci

NITERÓI - RJ

2021

Ficha catalográfica automática - SDC/BIG
Gerada com informações fornecidas pelo autor

L451a Lebre, Mariana Bittencourt Seabra
Analysis of flow facies in the presalt interval of the Santos Basin / Mariana Bittencourt Seabra Lebre ; Wagner Moreira Lupinacci, orientador ; Antônio Fernando Menezes Freire, coorientador. Niterói, 2021.
224 f. : il.

Dissertação (mestrado)-Universidade Federal Fluminense, Niterói, 2021.

DOI: http://dx.doi.org/10.22409/PPGDOT .2021.m.15659041760

1. Geofísica. 2. Caracterização de Reservatório. 3. Carbonatos do pré-sal. 4. Fácies de Fluxo. 5. Produção intelectual. I. Lupinacci, Wagner Moreira, orientador. II. Menezes Freire, Antônio Fernando, coorientador. III. Universidade Federal Fluminense. Instituto de Geociências. IV. Título.

CDD -

Bibliotecário responsável: Debora do Nascimento - CRB7/6368

ANALYSIS OF FLOW FACIES IN THE PRE-SALT INTERVAL OF THE SANTOS BASIN

MARIANA BITTENCOURT SEABRA LEBRE

Dissertation submitted to Universidade Federal Fluminense as a partial requirement of the graduate program in Ocean and Earth dynamics to obtain the title of Master in Geology and Geophysics.

Approved on October 29th, 2021.

_____

PhD. Elita Selmara de Abreu (Petrobras)

_____

PhD. Guilherme Furlan Chinelatto (Unicamp)

_____

PhD. Antonio Fernando Menezes Freire (GIECAR/GGO/UFF)

_____

PhD. Francisco Romerio Abrantes Junior (GIECAR/GGO/UFF)

_____

PhD. Wagner Moreira Lupinacci (Advisor - GIECAR/GGO/UFF)

Acknowledgments

I gratefully acknowledge all those who in any way contributed to the completion of my master's dissertation. The accomplishment of this project would not have been possible without financial support from Equinor, and the provision of data used in this work by CGG and Agência National do Petróleo, Gás Natural e Biocombustíveis (ANP). Also, I thank the willingness and encouragement from my friends of GIECAR, especially, Fernando Vizeu, Fabio Jr., Mário Martins and Ana Luiza Muniz.

I would like to address special thanks to my colleagues from the research project in the Santos Basin Tone, Raquel, Malu, Dea, and Julia. Also, I want to give an affectionate thanks to Maíra, Igor and Tuany for their assistance and discussions.

I am pleased to thank professor Fernando Freire for all the support, discussions, and feedbacks, his contributions, without a doubt, were very important to my professional journey.

I feel very honored to thank my advisor Wagner Lupinacci for all his support, care, patience and understanding over almost four years of working together. Without a doubt, I could not get where I am today without his support and guidance. Thank you for being an excellent human being, professional, professor, and advisor. You are part of my history as a geophysicist, and I am so grateful for all your support.

I would also wish to mention my friends from the heart who were super important throughout my masters' studies. Natalia, Leila, Aline, Preta, Pedro and Bruna, all my affection and thanks for always listening to me, encouraging, and praying for me.

To my beloved and dear family, the pandemic brought us closer again and I couldn't choose to finish my master's anywhere but at home, and with them. Mom and Dad, thank you so much for always believing in me, supporting me in everything, and thinking I'm the smartest and most capable person in the world. I'm sure your prayers are what helped me to stand firm. Also, I would like to thank my boyfriend, Matheus, for all his support, love, affection, understanding, patience, and care, without you the path would have been much harder and darker.

Last and most important, I would like to thank God, my best friend, my safe haven, and my fortress. If I am who I am today, it is because of Him. Thanks for always helping me, calming me down during the hectic moments of this journey and for bringing light to my darkest days.

Abstract

Rock typing into flow units (FU) is a well-known technique for characterizing flow heterogeneities in reservoirs. Several methods that correlate pore-throat size with permoporosity in the core and well-log domains are available in the literature, being the flow zone indicator (FZI) method the most used in carbonate reservoirs. The pre-salt carbonates from the Santos Basin still present many challenges regarding the characterization of its reservoirs due to the complexity and heterogeneities of such accumulations. Thus, from the analysis of rock data, well log, and seismic volumes, this study aims to estimate the flow facies (FF) of the pre-salt carbonate reservoirs, in the Santos Basin, using porosity and permeability of the nuclear magnetic resonance (NMR) logs as input and compare them with the elemental capture spectroscopy logs (ECS) such as calcium, magnesium, and silica in order to understand their influence in the flow facies behavior. The main reservoirs are found in the coquinas bank commonly known as rudstones and grainstones of the Itapema Formation, and in shrubs and spherulites in situ, as well as reworking facies (e.g., grainstones, rudstones, floastones) from Barra Velha Formation. It was observed that the base of the coquinas presents a more tight carbonates behavior, which can be related to low energy and deeper environments, with lower permoporosities, associated with the presence of fines and/or muddy sediments (e.g., mudstones and laminites), as well as to diagenetic processes such as cementation, mainly of calcite and dolomite. Towards the top of the formation, it observed a greater presence of coquinas with good permoporosity and the best FF, which may indicate high energy and shallower environments, with little or no presence of fine grains. The Barra Velha Formation has the best flow facies at the base of the formation, worsening, normally, from the middle towards the top. Silicification is a major factor in the Barra Velha Formation that ends up influencing permoporosity, decreasing it. Also, the presence of igneous rocks is another factor that decreases permoporosity. Diagenetic factors such as dissolution, silicification, and dolomitization are more intense in the Barra Velha Fm. Integrating rock, well-logs, and seismic data is the key to understanding how the flow facies can be related to depositional environments and how the spatial location of the wells can influence their petrophysical characteristics. From this correlation, it was possible to identify the main behaviors, cycles, and heterogeneities observed in the Barra Velha and Itapema formations. Furthermore, a Bayesian classification was performed to provide a quantitative analysis of the probability of occurrence for each flow facies in a seismic section from the inversion of the volume of acoustic impedance (PI).

Keywords: carbonate reservoirs, permoporosity, pre-salt, Santos Basin, flow facies, RQI, rock-well-seismic, Bayesian classification.

Summary

List of Illustrations

Tables

1. Introduction

Carbonate reservoirs represent around 60% of the petroleum reserves of the world (Chopra et al., 2005) and have a crucial role in the world energetic scenario. From the second half of the year 2000, the carbonate reservoirs in Brazil began to arouse great interest through the discovery of pre-salt plays. The finding and production of this play are causally related to the Santos Basin history, which has a leading part in this process.

The first exploratory well in the pre-salt section of the Santos Basin, the Parati Prospect, was drilled in 2006 to test. Although it was discovered only gas and condensate, which was commercially unattractive, it proved the existence of an active oil system in that portion of the basin, indicating the existence of a new exploratory play in the Santos Basin: the pre-salt play (Petersohn, 2013). In 2006, the discovery of the Tupi Prospect was also announced in the deep-water section. Discovered with oil accumulation in neo-Aptian carbonate reservoirs, the Tupi Prospect would become the first commercial discovery of the Santos Basin pre-salt. Its area allowed this field to be considered the largest ever discovered in Brazil so far. At the end of 2010, the commercial viability of the Tupi Prospect was declared.

Since its discovery was announced by Petrobras in 2007, the pre-salt represents the world's major oil discovery of the past 50 years. Its reserves are composed of large accumulations of oil considered light and with high commercial value. Another important feature is high productivity. In a 2018 survey, the Agência Nacional do Petróleo, Gás Natural e Biocombustíveis (ANP) showed that the average production of the pre-salt wells was approximately 17,000 barrels of oil per day. This represents ten times more than the average production of wells in other offshore areas in Brazil and a thousand times more in onshore areas. In 2020, the pre-salt reached 2.7 million barrels of oil equivalent per day, which represents almost 70% of national production and in February 2021, the production of 71.3% of the total oil produced in Brazil, being responsible for generating 2,044 MMbbl/d of oil and 87.7 MMm^3/d of natural gas.

The economic importance of the carbonate reservoirs of pre-salt brings with them the challenges related to the exploration of these rock types. Carbonates are rocks overly complex and have great difficulties related to the characterization, production, and management of reservoirs. They have a very heterogeneous nature due to the complex combination of depositional and diagenetic processes to which are submitted (Dunham,

1962). The variability of carbonate facies, which have complex textured and depositional characteristics, results in extremely heterogeneous reservoir properties, both vertically and laterally (Mohriak et al., 2015).

In the search for more accurate characterization of reservoirs, new data integration methodologies of different scales have been developed, establishing correlations between the textural, permo-porous, and structural characteristics of the formations. Seismic data provide information on the decametric scale. Meanwhile, well logs provide information on a centimetric scale and rock data provides centimetric and millimetric scales, enabling a more accurate interpretation of the reservoirs. Rock data includes sidewall core samples and thin sections collected in the wells, which are described and analyzed in the laboratory, providing a direct measure of the rocks that compound the reservoirs. The integration of these tools is important to increase knowledge as well as help in the understanding and characterization of these reservoirs.

In several pre-salt fields, diagenetic processes have directly altered and/or reorganized the porosity architecture of the carbonate fabric, consequently affecting the porosity and permeability characteristics of the reservoir rocks (Lima and De Ros, 2019). The Itapema Formation, in the Santos Basin, reservoirs correspond to the bioclastic deposits of bivalves, known as “coquinas”. The Barra Velha Formation contains intervals of fascicular calcite (shrubs) and spherulitic aggregates interspersed with intraclastic deposits that have been reworked from these precipitates (e.g., grainstones, rudstones, packstones) and laminated strata made of syngenetic magnesian clay minerals and siliciclastic mud (e.g., Tosca and Wright, 2014; Wright and Barnett, 2015; Wright and Tosca, 2016; Herlinger Jr. et al., 2017; Lima and De Ros, 2019). Although these carbonate rocks generally have high permoporous properties, they are frequently affected by diagenesis. Among these processes, the occurrence of dissolution features and cementation/substitution of the carbonate fabric by silica minerals greatly modify the reservoir quality and may potentially affect the fluid flow behavior within the reservoir. For these reasons, understanding the processes that originated such diagenetic features, their timing, and distribution in the reservoir is crucial for the pre-salt reservoirs characterization and modeling (Sartorato et al., 2020).

These heterogeneous and non-uniform reservoirs can be divided into multiple homogeneous groups, called flow units (FUs). Each unit presents similarities in terms of grain size, texture, cementation, pore distribution, porosity, and other physical

characteristics controlled by the sediment depositional environment and diagenesis (Altunbay et al., 1994). FUs for reservoir characterization are an effective way to simulate fluid movement and oil-production behavior.

The understanding of variability and spatial distribution of petrophysical properties along a reservoir in distinct lithofacies is crucial to improve reservoir description and exploration. Each porosity within a rock type can generate a permeability variation of several orders of magnitude, indicating the existence of multiple flow units. According to Ebanks (1987), a flow unit (FU) is a representative elementary volume of the total reservoir rock, within which geological and petrophysical properties that affect fluid flow rate are internally consistent and predictably different from properties of other rock volumes.

The premise for the grouping of flow facies is the similarity in flow characteristics which can be affected by grain size, texture, mineralogy, cementation, bedding contacts, permeability barriers, clay content, and petrophysical properties such as porosity and permeability. Therefore, the depositional environment and diagenesis control the hydraulic properties of rocks and, consequently, the reservoir quality control (Altunbay et al., 1994 and Amaefule et al., 1993).

Due to the carbonate reservoir heterogeneities, the Flow Zone Indicator (FZI) Method may produce many flow units, which makes 2D and 3D modeling difficult, especially when using seismic data to restrict spatial variation (Penna and Lupinacci, 2021). Since Amaefule and Altunbay (1993) introduced the concept of FZI based on the Kozeny-Carman model, different flow units estimation methods have been proposed (Mahjour et al., 2017; Kadkhodaie and Kadkhodaie, 2018). Penna and Lupinacci (2020) proposed a modification of the classical FZI permeability versus porosity core measurements. They built and analyzed a cumulative S-curve using the Stratified Modified Lorenz Plot (SMLP) (Gunter et al., 1997) to limit the number of flow units that could be correlated with seismic elastic attributes and observed at large scales without losing resolution and maintaining the geological features of the area.

After having carried out a bibliographical review of the concepts and ways of estimating a flow unit, the present work chose to adopt the flow facies nomenclature. The concepts, calculations, and utilities are the same, but the use of "facies" instead of "unit" was adopted as a way to be able to characterize the wells according to the different facies

may present. It is important to highlight that incorporating flow facies into geological models is a difficult task because each FF shows a wide variety of sedimentological facies, with little or no relationship between FF and carbonate facies. That is, the same FF can be associated with different geological facies and different FFs might have the same geological facies. The flow facies were calculated using the porosity and permeability from the NMR log or, when necessary, from the merge of the porosity and permeability of the sonic (DT) and NMR logs. These estimations were made in four wells (A, B, C, and D).

This dissertation has as main objective to estimate, evaluate and compare the flow facies obtained in the Barra Velha and Itapema formations to diagenetic processes, types of depositional environments as well as depositional cycles found in the literature. From the rock-well-seismic correlation, it is identified the impact of diagenesis on permoporosity and, consequently, on the flow facies in each formation. The elemental capture spectroscopy logs (ECS) of calcium, magnesium, and silica also play an important role in understanding the performance of pre-salt carbonate reservoirs. In addition, a feasibility study was carried out for the classification of flow facies in the seismic volume, using data from upscale well logs, which were presented in the form of probability density function (PDFs). This facies classification was performed using the Bayesian classification, which, in short, seeks to estimate the probability of a pattern of variables, in the case of this work, the acoustic impedance (PI), being related to a certain class, that is, the flow facies. For this, it was necessary to define the classes as each flow facies and their respective probabilities related to the PI values, in addition to estimating the likelihoods.

The steps taken to develop this work were organized into six chapters. The second chapter contains a bibliographical review of the main aspects of the Santos Basin as well as the formations that shelter the main reservoirs in this basin. The third chapter describes the step-by-step methods used to estimate and evaluate the flow facies of the Barra Velha and Itapema formations. The fourth chapter shows the methodology used in this dissertation, a brief literature review regarding what a flow unit is and the main methods of estimating them, and a summary of the Bayesian classification. The fifth chapter shows the results of flow facies analysis related to the main reservoir properties obtained through geophysical well logs, rock physics crossplots, and rock, well-log, and seismic correlation. The sixth chapter presents the discussions regarding the results obtained in

the previous chapter, as well as a more in-depth analysis of the diagenetic effects on the flow facies, the possible relationships of the FFs with the different environments, and depositional cycles in the Itapema and Barra Velha formations. Finally, the seventh chapter highlights the conclusions and contributions of the dissertation and presents suggestions for future work.

2. Santos Basin

The Santos Basin is the largest basin offshore and the main producer of hydrocarbonates in the country with a production that has already surpassed the average of 2.7 MMboe/day, appearing as one of the most important Brazilian sedimentary basins in exploratory terms. It extends from the southern coast of the Rio de Janeiro State to the north of the Santa Catarina State, between the latitudes of 23° e 28°S in the southeast portion of the Brazilian passive continental margin (Carlotto et al., 2017). The Cabo Frio high is the northern limit of the basin, and the Florianopolis high is the southern limit, defining its borders with Campos and Pelotas basins, respectively. The Santos Basin is one of the most extensive offshore Brazilian basins covering an area of approximately 350.000 Km^2 up to a bathymetric height of 3.000m (Figure 1) (Moreira et al., 2007). This area is equivalent to almost three times the size of the Campos Basin and accounts for more than 54% of total Brazilian hydrocarbon production according to Agência Nacional do Petróleo, Gás Natural e Biocombustíveis (ANP).

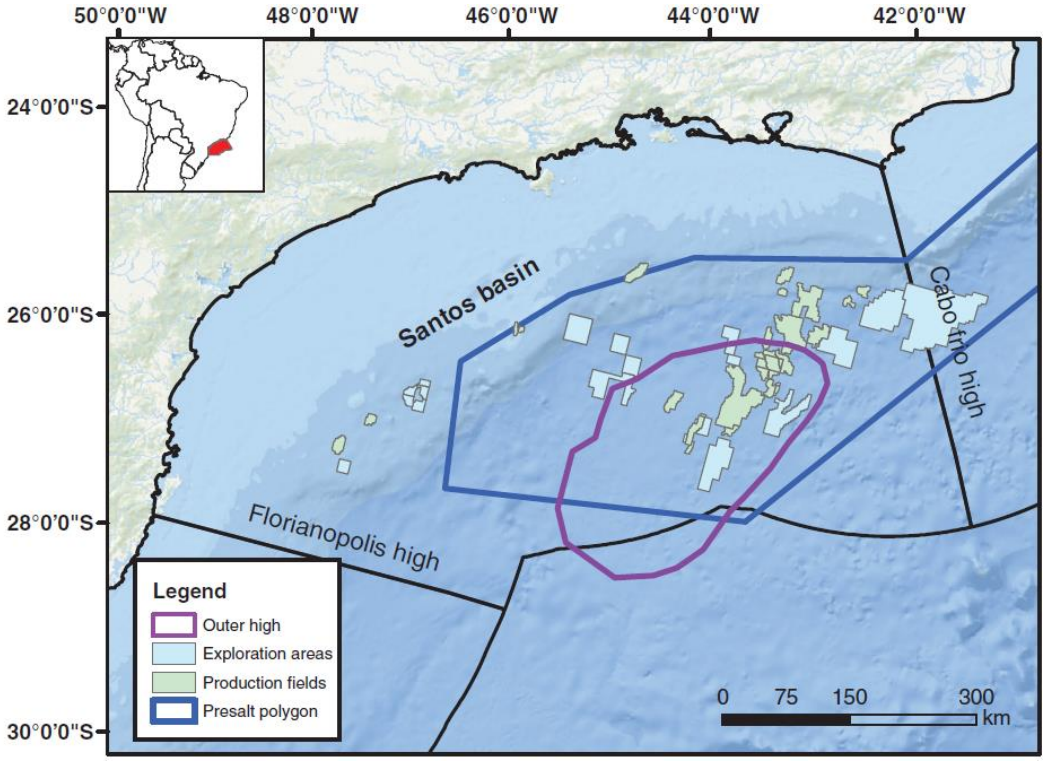

Figure 1: Location map of the Santos Basin. Source: Neves et al., (2019).

The origin of Santos Basin is connected to the Gondwana break-up and the opening of the South Atlantic in the Late Jurassic-Early Cretaceous. These extensional tectonics resulted in the separation between South America and Africa, controlling the

tectono-stratigraphic evolution of the basins in the Brazilian eastern margin. (Chang et al. 1992; Cainelli and Mohriak, 1999; Mohriak et al., 2008). According to Petersohn (2013), the tectonostratigraphic evolution of this basin is characteristic of passive margin, due to the geological records of processes such as lithospheric distension, crustal stretching, continental crust disruption, implantation of oceanic crust, and thermal subsidence.

In the southern basins, growing lithospheric stretching and faults promoted intense volcanism and the formation of half-graben structures (Cainelli and Mohriak, 1999; Mohriak et al., 2008). The stratigraphy of the Santos Basin has been studied by several authors since the 1970s. Pereira and Feijó (1994), with few wells available in the basin, established a chrono-stratigraphic framework in terms of depositional sequences. Moreira et al. (2007), based on a large volume of rock and well data, updated the chronolithostratigraphic framework with an emphasis on the individualization of depositional sequences and divided the basin-fill history of the Santos Basin into three super-sequences: rift, post-rift/sag, and drift (Figure 2). Initially, the weakened and thin continental crust was strongly affected by tensional fractures that later became conduits for magma (Herz, 1977), the intense volcanism characterized by the Camboriú Formation basalts mark the beginning of the rift phase and development of the economic basement of the Santos Basin (Chang et al., 1992; Mohriak et al., 2008). With the gradual evolution of the rift system, the Camboriú Formation was overlain by the fluvio-lacustrine deposits of the Piçarras and Itapema formations, which are dominated by sandstones, siltstones and shales of talc-stevensitic composition and coquinas interlayered with shales, respectively (Moreira et al., 2007).

Thermal contraction of the crust resulted in the subsidence and collapse of crustal domes, generating sag-type basins (Beasley et al., 2010). The post-rift/sag interval is composed of the lacustrine carbonates deposits of the Barra Velha Formation. The formation is bordered at its base by the Pre-Alagoas unconformity, separating the lacustrine carbonates from the older bivalve coquina-dominated lakes (Basso et al., 2020). At the top, the formation is overlain by transitional evaporitic deposits of anhydride and halite, locally with more soluble salts such as carnallite, sylvite, and tachyhydrite of the Ariri Formation (Moreira et al. 2007; Mohriak et al. 2008; Quirk et al. 2013). The post-salt deposits occurred during the drift phase, which is characterized by the development of a passive margin and represents the definitive establishment of marine settings, comprising the Camburi, Frade and Itamambuca Groups (Moreira et al. 2007).

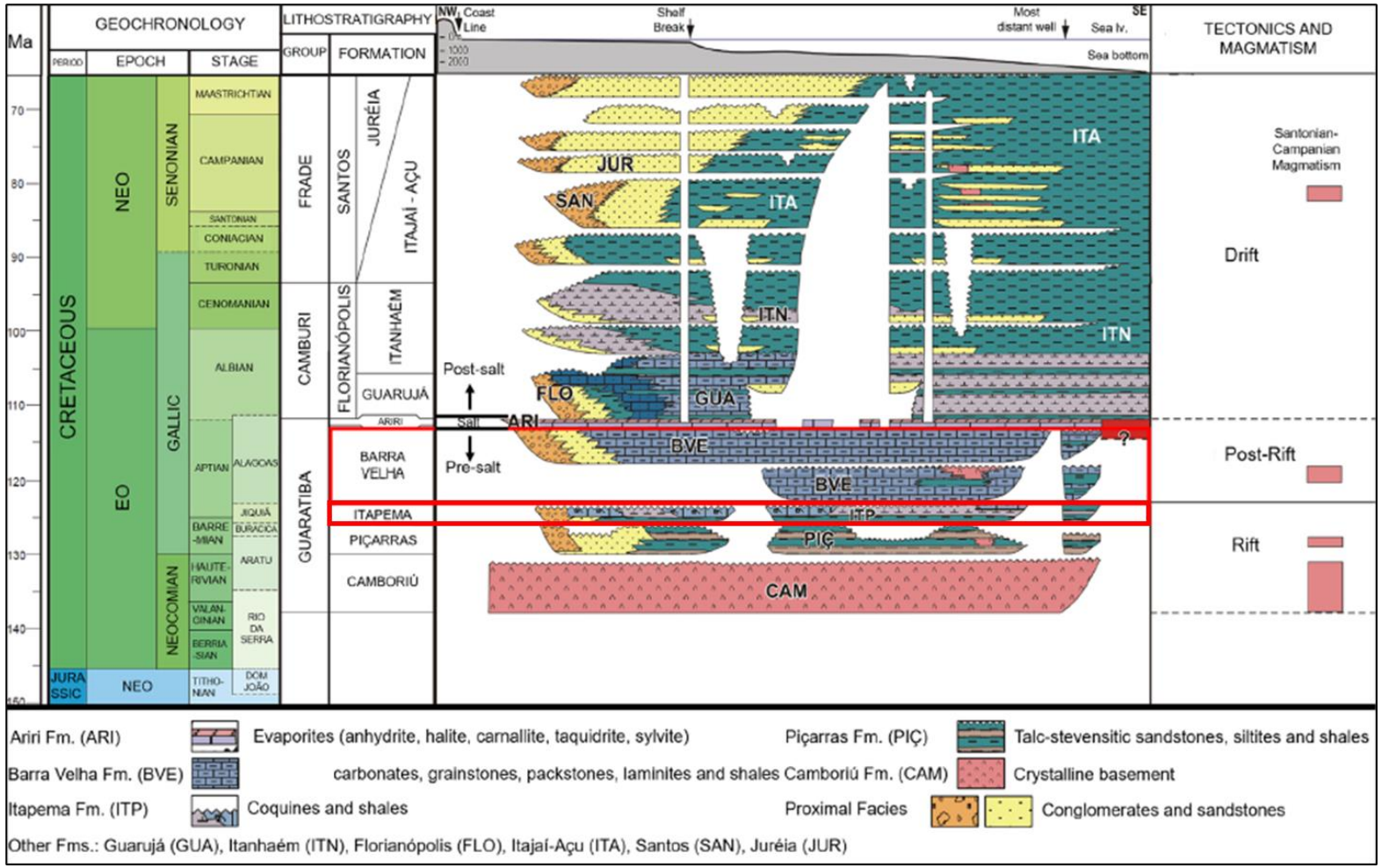

Figure 2: Cretaceous stratigraphic chart for the Santos Basin highlighting the Barra Velha and Itapema formations (Basso et al., 2020, modified from Moreira et al., 2007).

Even though Moreira et al. (2007) have introduced the formations in a passive margin context with the typical tectonic processes distributed in the rift, post-rift, and drift phases, they do not address in detail the issue of tectonic evolution. Thus, in terms of phases of the tectonic framework, other works must be considered.

In this study, the litho-stratigraphic sequences that occur in the basin will be analyzed according to their correlation to the tectonostratigraphic events prevailing at the time. Thus, the sequences were established according to the most recent studies developed by Wright and Barnett (2015) and Buckley et al. (2015), being divided into the lower (or early) rift, upper rift, Sag, and passive margin (or drift) (Figure 3). Each of these sequences was delineated according to the regional unconformities mapped in the seismic sections.

The complexity of lacustrine carbonate deposits is due in part to the variety of control mechanisms associated with their formation. The sedimentary input rate, tectonics and climate in the control of eustatic variations are, in stratigraphy, common conditions to different sedimentary environments. In this case, factors such as temperature and chemical composition of water join the list of protagonists for understanding the lateral distribution and vertical stacking of the facies found.

It is important to highlight the three major unconformities to understand the Barra Velha Formation: the Pre-Alagoas Unconformity (PAU) at the top of the coquina deposits, an internal unconformity called the Intra-Alagoas Unconformity (IAU), and the Salt Base Unconformity (SBU) that caps the formation (Figure 3). Finally, the basin evolved into a passive-margin basin with an early drift supersequence represented by shallow-marine platform carbonates of the Guarujá Formation, followed by platform drowning and deeper-water sediments of the Itanhaém Formation (Gomes et al., 2020).

Buckley et al. (2015) affirm that it is possible to identify in seismic sections the evolution of the rift phase to a tectonic quiescence phase, highlighting the presence of a sag phase. They add that most extensional faults end at the base of the sag phase and can be correlated to Intra-Alagoas unconformity, thus corroborating the statement made by Wright and Barnett (2015) and Silva (2021).

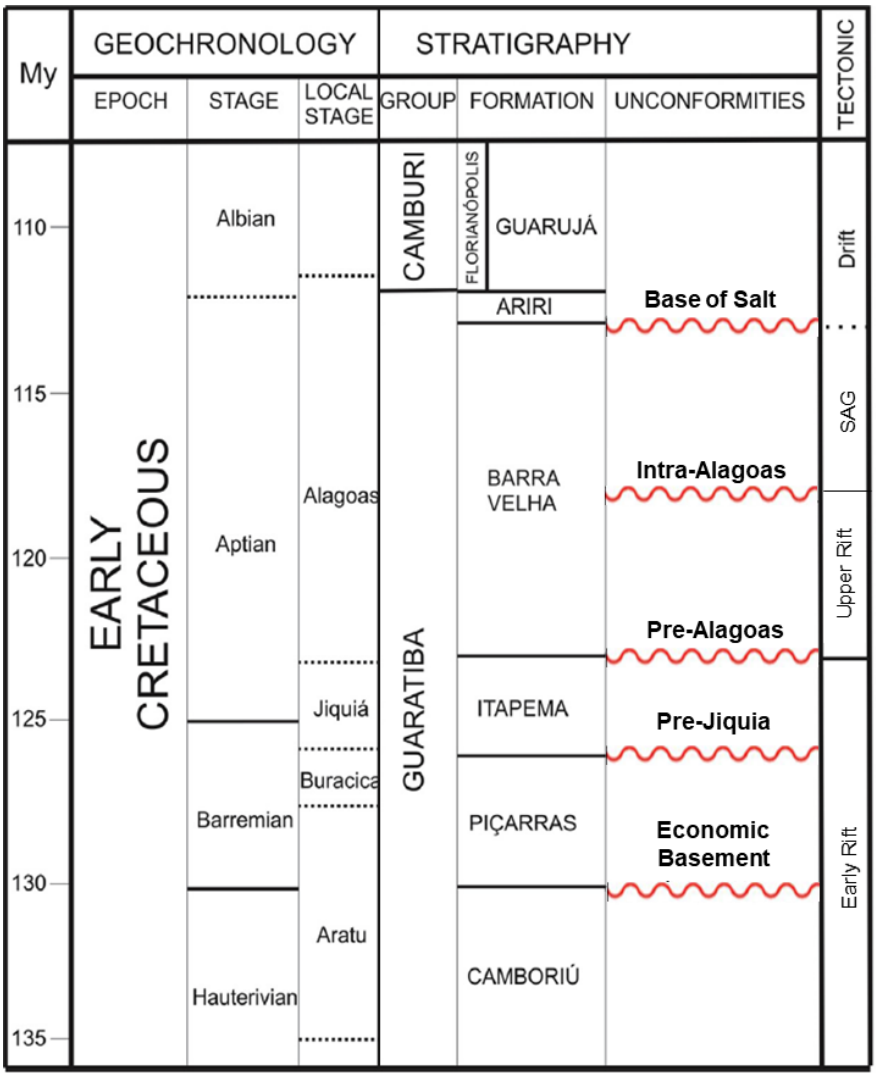

Figure 3: Lower Cretaceous stratigraphic chart for the Santos Basin (Adapted from Buckley et al., 2015; Wright and Barnett, 2015; Neves et al., 2019).

Figure 4 shows a simplified stratigraphic column with the main reflectors interpreted in a seismic section in the Santos Basin: base of the salt surface, Intra-Alagoas and Pre-Alagoas unconformity, and economic basement. The thermal subsidence during the sag phase promoted the development of an extensive and restricted hypersaline gulf, which suffered episodically marine incursions, allowing the formation of thick lacustrine carbonates successions on isolated platforms located in structural highs that were concluded by Liechoscki de Paula Faria et al. (2017) that this actual structure was also a paleohigh throughout Barra Velha deposition. This location remains away from the reach of siliciclastic sedimentation (Gomes et al., 2002; 2008).

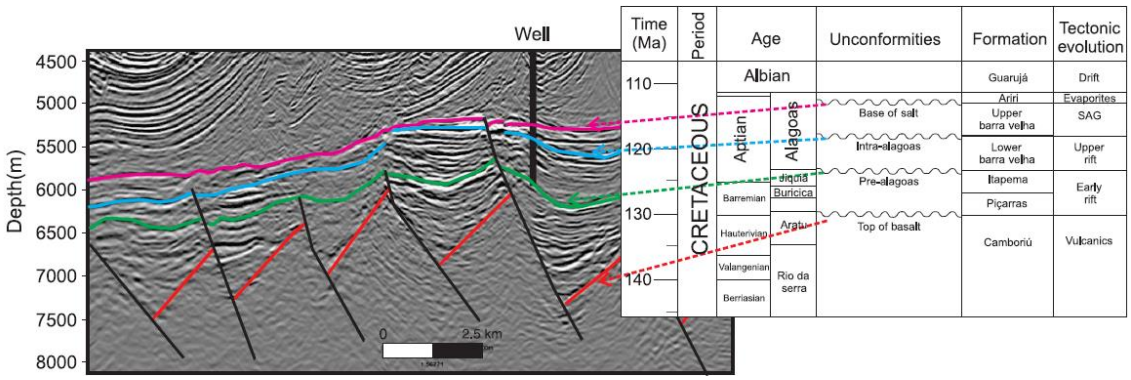

Figure 4: Simplified stratigraphic column showing the main reflectors interpreted in the area (economic basement, pre-Alagoas unconformity, intra-Alagoas unconformity, and base salt surface). Source: Neves et al. (2019).

In general, the seismic facies observed by Buckley et al. (2015) and Ferreira et. al (2019) were classified as carbonate platforms with a large areal extent marked by parallel to subparallel reflectors of moderate amplitude and with gradational or progradational character, isolated buildups, and buildups aligned to main fault zones, which present chaotic reflectors with moderate to low amplitudes, platforms with the presence of nearby evaporites, with chaotic to progradational reflectors with low to moderate amplitudes suggesting sedimentary facies related to reworking by currents or subaerial exposure.

2.1. Itapema Formation

The Itapema Formation was deposited from Neobarremian to Eoaptian and has its base limited by the Jiquiá / Buracica unconformity and its top by the Pre-Alagoas unconformity (Moreira et al., 2007). This last-mentioned unconformity determines its limit with the Barra Velha Fm., and it is relatively easy to be mapped in seismic sections, presenting a regional expression that is known in both the Santos and Campos basins. The age corresponding to the top of Itapema Fm. is not well constrained but is estimated to be around 120 and 123.1 Ma (Moreira et al., 2007).

Briefly speaking, this formation consists of conglomerates and alluvial fans sandstones in the proximal portion and intercalations of carbonate rocks and dark colored shales, because of the high amount of organic matter, in the distal part. According to Moreira et al. (2007), these carbonates are composed of bivalve shells (coquinas) with occurrences of ostracods and gastropods, described as rudstones, grainstones, packstones and wackestones, and exhibit very similar taphonomic, sedimentary, and stratigraphic characteristics (Chinelatto et al., 2020). The Itapema Formation is regionally equivalent to the Coqueiros Formation of the Lagoa Feia Group in the Campos Basin (Moreira et al.,

2007) which was developed between the Barremian-Aptian, during the rift stage of the Gondwana break-up. The coquinas of the Coqueiros Formation have been interpreted as lacustrine deposits located at structural highs deposited under shallow, high-energy conditions, with facies varying between beaches, bars, bioaccumulated banks and storm deposits (Carvalho et al., 2000; Muniz and Bosence, 2015; Mizuno et al., 2018; Oliveira et al., 2019).

According to Kattah (2015), coquinas have become important exploratory targets after discoveries of large accumulations in Buzios and Mero fields in the Santos Basin. High porosities and permeabilities resulting from complex diagenetic processes have preserved part of the primary porosity and developed secondary porosity in thick packages, around 300-400 meters of coquinas (Thompson et al., 2015).

According to Terra et al. (2010), the coquinas are bivalve-rich rocks composed mainly of shells and their fragments, including three types of carbonate rocks: bioaccumulated (when the two valves are preserved, commonly with matrix); packstones/rudstones with matrix and grainstones/rudstones without matrix (when the valves are reworked and have no matrix). The authors emphasize that only the latter type is constituted in reservoir rocks. Thus, the coquinas of the pre-salt reservoirs are classified mainly as grainstones and rudstones without matrix, essentially composed of shells of reworked bivalves. It is noteworthy that despite the emphasis given to coquinas, the shales of this formation are also of paramount importance as they are source rocks. They were deposited during the Jiquiá floor in anoxic lake environments rich in organic matter (Castro, 2019).

Herlinger et al. (2017) performed a petrographic study at Coqueiros Fm. from the Campos Basin. According to the authors, 9% of the samples used were grainstones and 91% were rudstones poorly to well sorted, with a chaotic or subparallel fabric. Bivalves are predominant in the samples and the degree of reworking is quite variable, they are usually fragmented or dissolved and have dimensions ranging from 0.07 to 25 mm, with an average of 2.3 mm. Gastropods are present in some samples and are generally whole and not abraded, with preserved intraparticle porosity. Ostracods occur in smaller amounts and are typically whole, sometimes articulated, and occasionally recrystallized. Furthermore, it is common to have intraclasts of mudstones, volcanic rocks, and siliciclastic grains in small quantities, occurring rarely in the bioclastic rudstones and grainstones.

Pietzsch et al. (2018) presented and discussed a set of geochemical and biostratigraphic data in order to reconstruct the hydrological evolution of the lakes of the rift and post-rift successions associated with the deposition of carbonates from the Barra Velha and Itapema formations. The authors stated that a significant contribution of diagenesis in the samples of analyzed coquinas was discarded and that there is an expectation that carbonates from Itapema Fm. are more calcitic than those of Barra Velha Fm. In addition, they highlighted that the analysis performed, and the generated models point to a more humid environment, due to the presence of fauna of ostracodes, with a greater influence of a drainage system, owing to the lower concentration of strontium observed in the analyzed data at the time that Itapema Fm. has been deposited. The simplified conceptual model illustrating the general geology and hydrology of the lake system at the time of the sediments deposition in Itapema Fm. can be seen in Figure 5.

There are still many questions about Itapema Fm. that remain open due to the lack of studies in this formation. Despite this, a significant amount of work in the Coqueiros Formation, Campos Basin has been carried out. In addition, some recent studies in the Itapema Formation, such as the ones accomplished by Pietzsch et al. (2018), Oliveira et al. (2019) and Chinelatto et al. (2020) have been gaining prominence. Thereby, some relevant discussions and approaches will be presented in the following paragraphs, both on Coqueiros Fm. and the Itapema Fm., thus contributing to a better understanding of aspects such as the depositional environment and the main facies of the Itapema Formation.

According to Guardado et al. (1989), the coquina banks were developed in confined lacustrine environments along the flanks and low angle ridges in high deposits. Carvalho et al. (2000) add that the paleolake of the coquinas sequence presents characteristics of a closed and perennial to an open saline lacustrine environment. This environment would have suffered considerable fluctuations in the water level, due to both tectonic variations and the influence of waves and currents. In addition, an expansive distribution of shallow-water sediments would indicate that the paleolake was strongly influenced by the action of waves. Therefore, the coquinas would have been accumulated due to the action of waves and currents generated by storms and the reworking, transport and redeposition of shells as layers with or without matrix.

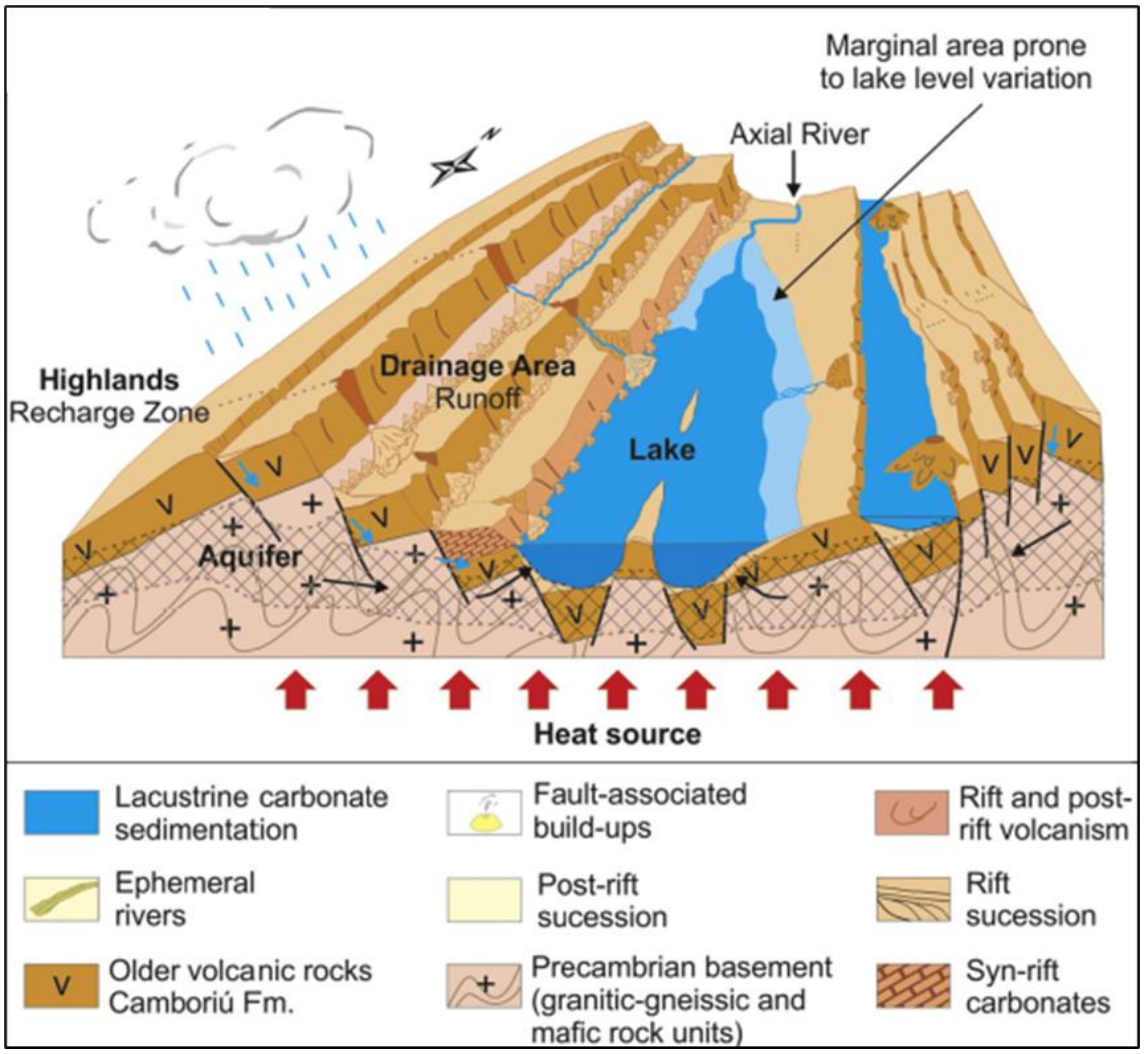

Figure 5: Idealization of the rift phase environment, corresponding to the time of deposition of the Jiquiá sequence, where a deeper lake formed, which could eventually be subjected to water-column stratification. It is a simplified conceptual model illustrating the general geology and hydrology of the pre-salt rift system. Small blue arrows show infiltration to and recharge of the aquifers; long black arrows indicate infiltration of groundwater to the lake basin. Thick red arrows underneath represent geothermal heat, which is assumed to decrease from rift to post-rift phase. Hachured areas propose the presence of aquifers relative to the lake basin, flowing mainly through the fractured crystalline basement. (Source: Modified from Pietzsch et al., 2018).

According to Thompson et al. (2015), the parameters that control the development and distribution of coquinas facies in rift-lake are quite complex and include factors such as climate, water chemistry, basin architecture/platform morphology, catchment geology and siliciclastic sediment influx. All these factors affect molluscan productivity and are associated with one another. For example, lake chemistry is strongly influenced by lake hydrology, which is in turn regulated by fluctuations in climate and evolving tectonic regimes. Carbonate platforms develop on topographic highs created during the rifting and

mollusks are concentrated on carbonate beaches, shoals and bars due to the shallow water, high energy conditions.

Thompson et al. (2015) highlight that the deposition of coquinas in the Coqueiros Fm. occurred in an environment with a strong influence of faults, on low-angle ramps cut by normal faults. The authors also state that the depositional environment of this formation can be interpreted as fluvio-lacustrine, based on the following evidence: 1) the absence of marine fauna; 2) rapid salinity fluctuations when compared to marine sequences; 3) the absence of sedimentary characteristics indicative of marine depositional processes, such as tidal currents and strong wave action; 4) complex vertical and lateral lithofacies assembl (typical of lacustrine environments due to the high frequency of climatic oscillations); 5) presence of minerals with chemical characteristics typical of non-marine environments.

Regarding the distribution of facies, some authors have proposed depositional and sedimentological models related to the coquinas of Coqueiros Fm. Carvalho et al. (2000) defined, within the coquinas sequence, based on the identified facies associations, seven main depositional environments: 1) Bioclastic Sandy Beaches: bioclastic calcarenite units associated with layers of silt, shale and calcilutite. These were deposited on the banks of lakes with siliciclastic sediments mixed with the shells and transported by storm-induced currents; 2) Calcarenitic Bioclastic Beaches: the present calcarenites consist of shell fragments from bivalves, or rarely, from gastropods, which commonly exhibit a high degree of abrasion and micrite content; 3) Marginal: strong presence of fine sediments and interpreted as low gradient deposits to shallow water and low energy lacustrine environments; 4) Bioclastic bars: there is no presence of intercalation of siliciclastics and they are interpreted as the result of amalgamation of calcirudite layers. They suggest high-energy environments and shallow waters, being associated with paleo-highs; 5) Bar fringes/Bioclastic Sheets: represent debris from bivalve shells and, rarely, gastropods, which were spread over the flanks of the bars or in areas with a gentle slope. They are inferred as storm deposits; 6) Bioaccumulation Banks: in situ shells associated with muddy or sandy deposits deposited in a low-energy paleoenvironment and shallow to deep waters; 7) Deep Lacustrine: intercalations of fine siliciclastic sediments and ostracode mudstones that were locally buried and deposited under low hydraulic energy conditions. Thompson et al. (2015) illustrated some of these facies associations, highlighting five main environments as can be seen in Figure 6.

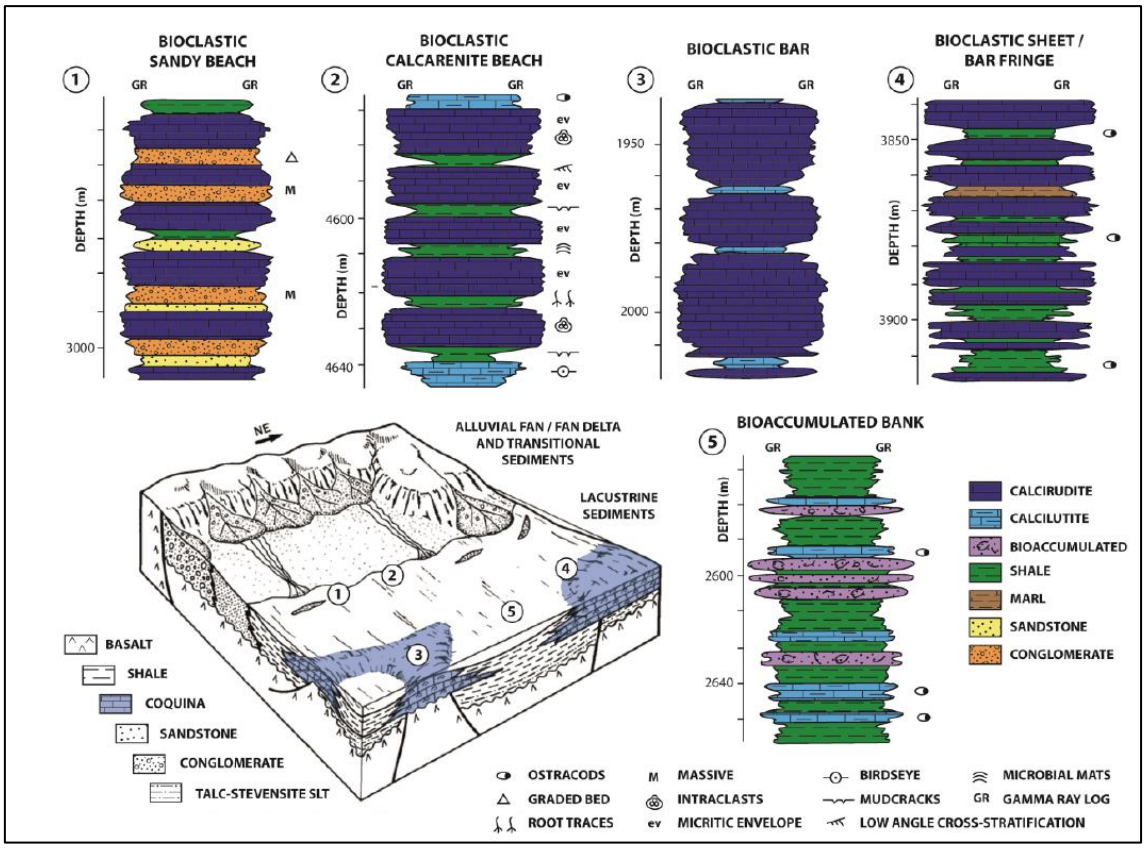

Figure 6: Schematic depositional model of the Coqueiros Formation with facies associations and their relevant locations in the reconstruction. Alluvial fans border the fringe of the basin, in association with topographic highs, and locally form fan deltas at the lake margin. Marl and shale are common lacustrine sediments in basin depocentres, while coquina forms on the flanks of horst blocks and tilted fault blocks, pinching out basinward into fine-grained sediments (Source: Guardado et al., 1989; Carvalho et al., 2000; Thompson et al., 2015).

Based on the integration of petrography, sedimentology, and seismic stratigraphy of the Coqueiros Fm., Goldberg et al. (2017) interpreted that throughout the rift section of the basin, the bioclastic rudstones correspond mostly to gravitational deposits, resedimented from structural highs to deeper lacustrine settings. In petrographic terms, Herlinger et al. (2017) carried out a work where they analyzed, among other lithologies, bioclastic grainstones and rudstones (coquinas). They observed that many of the samples were described as rudstones. In addition, the primary constituents corresponded to bioclasts of bivalves, gastropods and ostracodes, with bivalves being the main component. The authors also pointed out that, in terms of porosity, bioclastic grainstones had, predominantly, moldic and intercrystalline porosity. Dolomitized grainstones and rudstones, on the other hand, were rich in intercrystalline porosity, showing a cyclical variation in porosity ranging from moldic to interparticle.

Herlinger et al. (2017) observed that the bioclastic rocks followed three main evolution pathways, controlled by distinct eogenetic conditions (Figure 7). Pathway 1 was probably related to circulation of interstitial fluids undersaturated with respect to aragonite, most likely lacustrine freshwaters during more humid periods, promoting intense dissolution of the aragonitic bivalves, and the precipitation of calcite prismatic rims in interparticle and intraparticle pores. Pathway 2 was promoted probably where less dilute fluids initially allowed the preservation of the bioclasts, precipitation of calcite prismatic rims and drusiform cement, followed by extensive dissolution of bioclasts and generation of moldic porosity. Pathway 3 developed where limited circulation of fluids slightly supersaturated with respect to aragonite favored the precipitation of thin calcite rims, neomorphism of the bioclasts, and the preservation of interparticle porosity. They add that the common alternation of intervals with predominance of neomorphism and dissolution may indicate frequent oscillation between the environmental conditions mentioned above. Also, the diagenetic variations may be related to climatic control of the composition and level of lacustrine waters, or to tectonically driven hydraulic gradients probably related to faulting along the rift margins.

In the Coqueiros Fm., the coquinas constitute reservoirs with medium porosities in the range of 15 to 20% and medium permeability ranging from < 1 mD to > 500 mD (Horschutz and Scuta, 1992). Despite the high productivity rates, the coquinas present great heterogeneity, with deep lateral and vertical variations, which ends up affecting the evaluation of the reservoirs. These variations are due to diagenetic, biological, topographical, climatic and water level changes (Bruhn et al., 2003).

In general, coquinas have a textural heterogeneity that is related to the depositional environment and the diagenetic processes affecting the sediments, resulting in petrophysical conditions with complex pore systems and a high range of porosity and permeability (Tavares et al., 2015; Corbett et al., 2016; Herlinger et al., 2017; Chinelatto et al., 2018a, b; Belila et al., 2018; Zielinski et al., 2018). In this context, it is necessary to understand how and where the different coquina facies were deposited, their relationship with diagenetic processes and, consequently, their petrophysical characteristics.

Oliveira et al. (2019) performed a facies study and created a conceptual depositional model of the Coqueiros Fm. in the Campos Basin. The main types of facies found by the authors are carbonate, siliciclastic rich in magnesian clay minerals and

hybrids. Carbonate facies are defined as rudstones, grainstones, floatstones, packstones and mudstones composed of bivalves, ostracods and rarely gastropods. The siliciclastic facies are essentially composed of siliciclastic sandstones and mudstones, which occur locally. Stevensitic-rich facies are composed of stevensitic clays and sandstones. Finally, the mixture of bioclasts, siliciclastic grains, stevensite ooids and peloids constitute the hybrid facies.

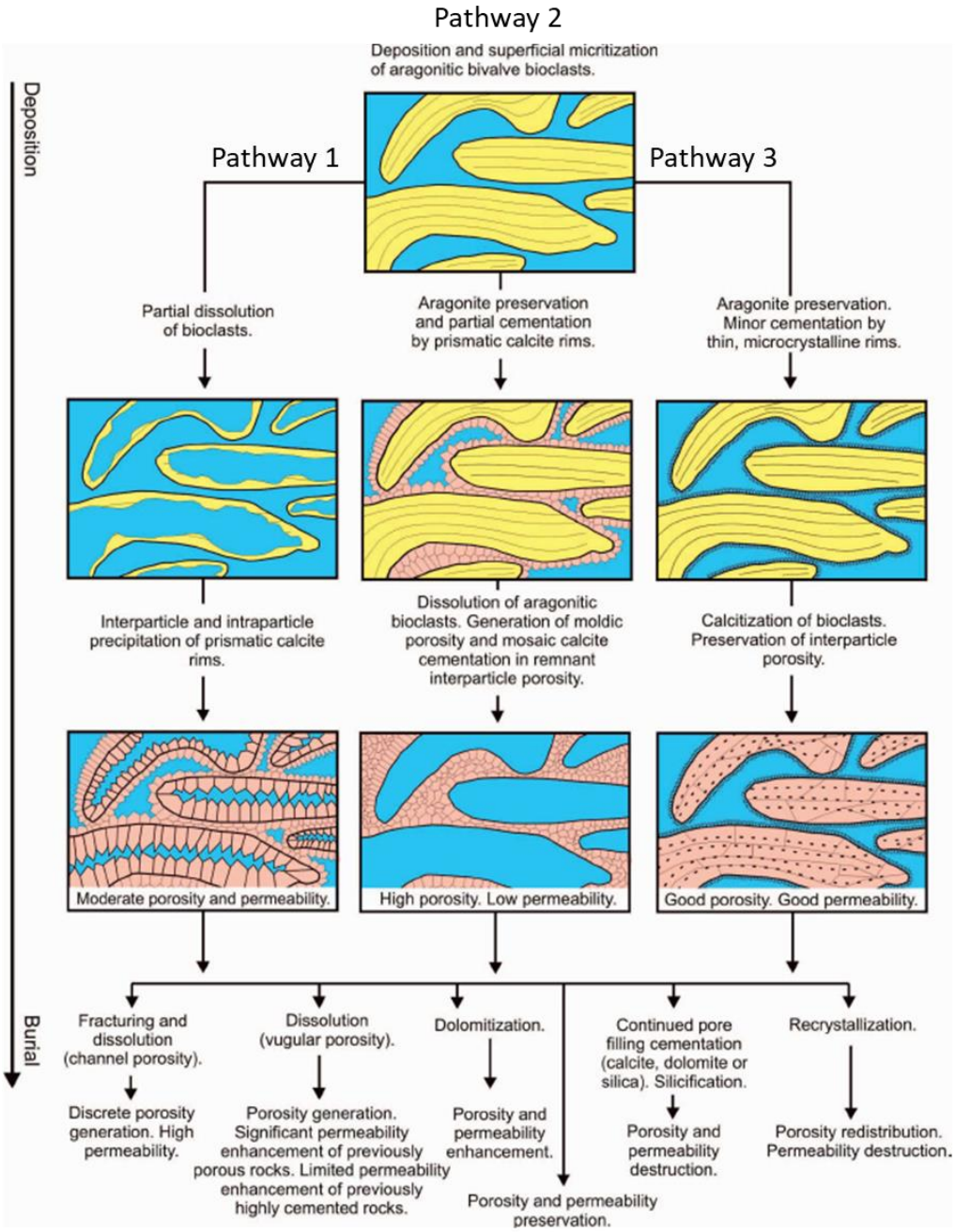

Figure 7: Schematic diagenetic pathways of bioclastic rudstones and grainstones, showing the impact of diagenetic process and products on porosity preservation, enhancement, and destruction and their resulting impact on permeability (Source: Herlinger et al. 2017).

Oliveira et al. (2019) analyzed the primary composition of rocks of two wells (WELL-1 and WELL-2) in the Coqueiros Fm. which are plotted on a ternary diagram quantified by visual estimation of the rock constituents (Figure 8). The vertices of this diagram represent the compositional end members non-carbonate sediments of extrabasinal origin, carbonate sediments of intrabasinal origin and non-carbonate sediments of intrabasinal origin. The non-carbonate extrabasinal sediments are represented by quartz and feldspar grains and fragments of volcanic rocks, while carbonate intrabasinal sediments are composed by bivalves and ostracod bioclasts, coquina intraclasts, gastropods and phosphatic fragments. Non-carbonate intrabasinal sediments include clay peloids and ooids as well as volcanic rock fragments. Rocks with more than 90% of a single component are defined as siliciclastic sandstones and mudstones, stevensite/volcanic enriched sandstones, and carbonate rocks. Rocks mixed with more than one component were designated as hybrid, which were named according to the main composition followed by reference to the secondary principal component (e.g., stevensitic/volcaniclastic hybrid with carbonates).

Rocks described in WELL-1 were predominantly hybrid due to the presence of non-carbonate extrabasinal particles (usually quartz and feldspar grains) and non-carbonate intrabasinal particles (clay ooids and peloids), besides the occurrence of carbonate rocks composed of bioclasts and siliciclastic rocks like siliciclastic sandstones and mudstones, suggesting a strong terrigenous influence and variation of the lake water chemistry. In WELL-2 carbonate rocks are predominate with more than 90% of bioclastic intraclasts, mostly bivalve shells. Igneous rock fragments occur in minor proportions. The rare siliciclastic rocks of this well are mudstones (Figure 8).

Oliveira et al. (2019) state that the depositional environment of the Coqueiros Fm. is characterized by the presence of waves and currents in fair- and storm-weather conditions, as well as by active tectonics. A conceptual depositional model was proposed based on the characteristics of the two geological settings represented by the sedimentary sequence described and interpreted from WELL-1 and WELL-2 (Figure 9).

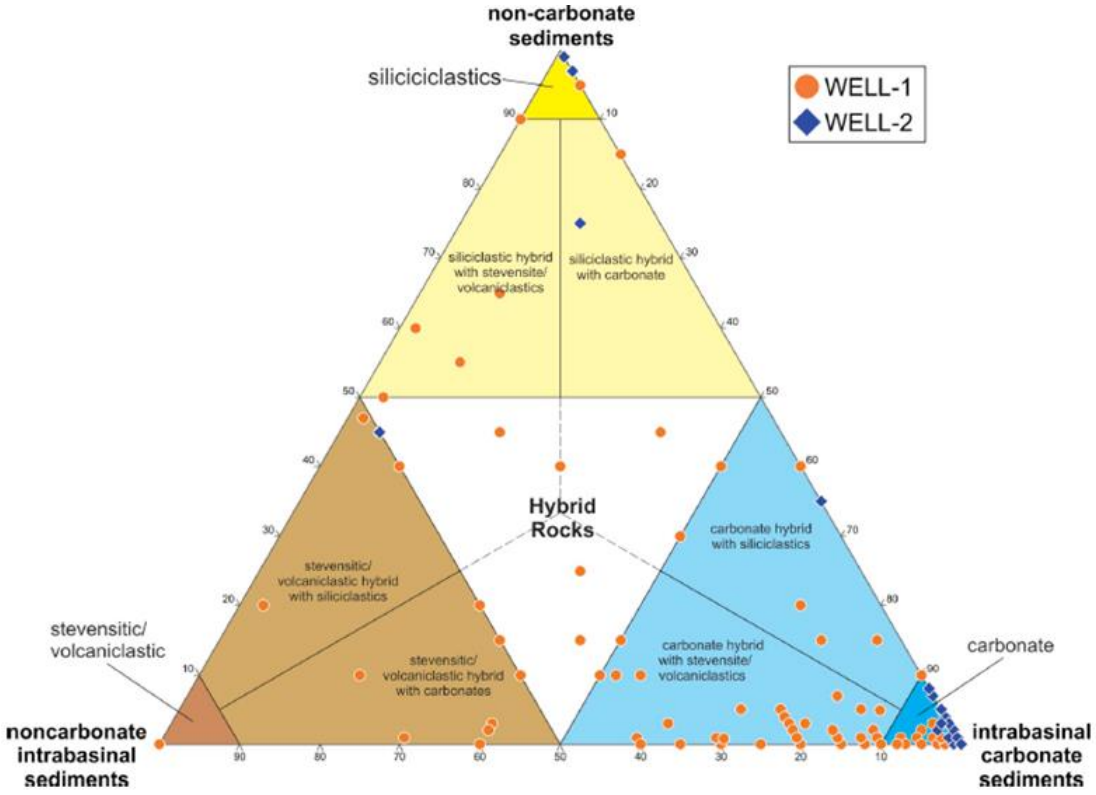

Figure 8: Ternary diagram proposed to classify the studied rocks, based on constituent's composition. wells one and two are represented by 179 points inserted on the diagram. The diagram represents non-carbonate extrabacinal, non-carbonate intrabacinal and carbonate intrabacinal (Source: Oliveira et al., 2019).

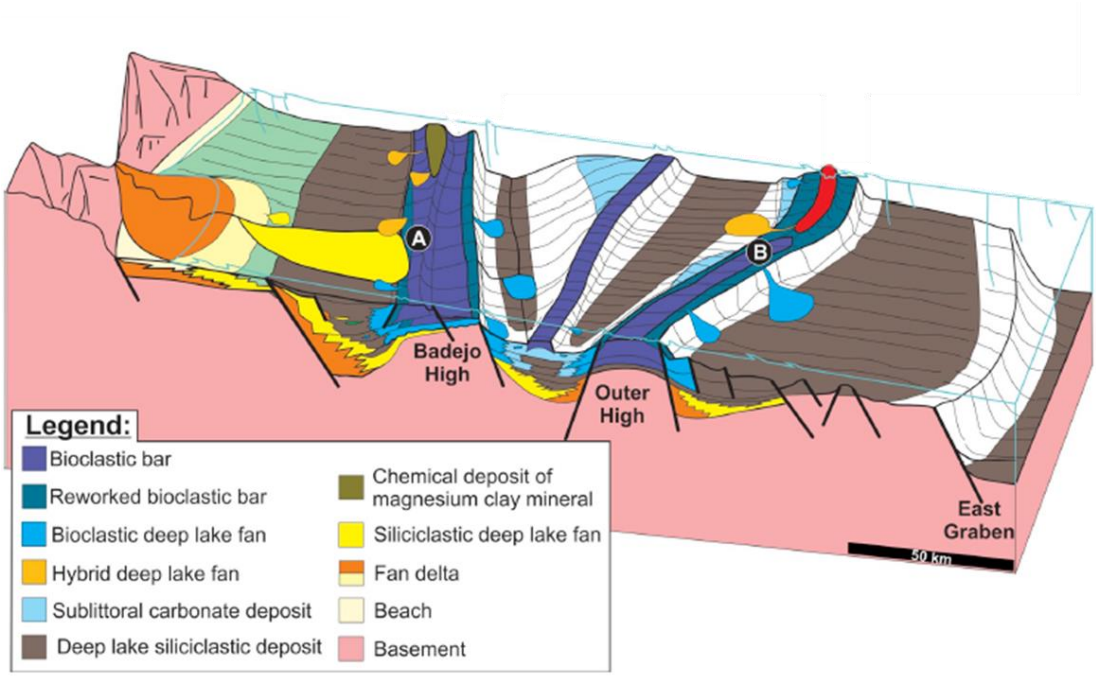

Figure 9: Proposed depositional model of lower Aptian, rift section of the Campos Basin, based on sedimentological analysis of wells 1 and 2 and the structural framework inherited from basement of Campos Basin. The (A) correspond to WELL-1 located in a hybrid ramp, and (B), at the External High, WELL-2 projection, drilled over a bioclastic isolated high (Source: Oliveira et al., 2019).

According to this depositional model, the carbonate sedimentation during the lower Aptian, occurred in a rift lake, with high bivalve productivity associated with basement highs providing ideal conditions for the development of bioclastic bars, which were accumulated by storms and were reworked by fair-weather waves and longshore currents. The structural highs were eventually exposed and eroded during lake levels oscillations. Sandstones were deposited by turbidite currents, close to the lake border, over the Badejo High, on a carbonate ramp affected by intense tectonic activity and submitted to storms action. Regionally, the changes in lake chemistry may favored the precipitation of magnesium rich clay minerals. Occasionally, siliciclastic, carbonate and stevensitic grains were mixed by re-sedimentation in deeper environment by storms and tectonically driven gravitational flows, forming hybrid deposits. Far from the rift border, bioclastic sedimentation predominated on isolated highs on the External High. Siliciclastic mudstones were deposited in structural lows during flooding events. In the structural lows, low energy environment, mud supported carbonates dominated. Finally, in basin grabens, carbonate mudstones interlayer with reworked sediments from structural highs (Oliveira et al., 2019).

Recently, Chinelatto et al. (2020) developed a work based on the coquinas of the Itapema Formation. According to the authors, these rocks have distinct textural characteristics that are related to depositional and diagenetic processes and may end up influencing the porous system and consequently the permeability. In addition, they claim that understanding how the different facies are distributed and their relationship with petrophysics is an essential study in predicting the quality of a reservoir. Thus, the authors classify the shell beds of Itapema Formation through taphonomic characteristics, applying the concept of taphofacies, where the patterns such as orientation of shells, degree of packing, fragmentation, abrasion, and sorting (type of grains) were used to differentiate shell concentrations (Figure 10). Based on their signature of skeletal elements and the biofabric it is possible to recognize deposits influenced by storms, tsunamis, or mass movements, or even whether these deposits formed in situ (Chinelatto et al., 2020).

Chinelatto et al. (2020) performed a geological description and facies definition through one well core available and a total of 11.5m described from which 40 thin sections were analyzed. Then, the taphofacies definition were made through the analysis of well core and thin sections and classify according to the Dunham (1962) and Embry and Klovan (1971) for carbonate rocks. From that point, six taphofacies (Tf-1 – Tf-6)

were described and divided according to their orientation (parallel, oblique, and chaotic) and sorting (well-sorted and unsorted) (Figure 10). Taphofacies Tf-1 and Tf-2 are, respectively, well-sorted and unsorted grainstones/rudstones with parallel-oriented and densely packed shells with a braded valve (Figure 23-A, B). Taphofacies Tf-3 and Tf-4 are, consecutively, well-sorted and unsorted grainstones/rudstones with oblique oriented shells, generally well-preserved but often with high shell dissolution (Figure 10-C, D). Finally, taphofacies Tf-5 and Tf-6 are well-sorted and unsorted grainstones/rudstones with randomly oriented shells and densely packed deposits (Figure 10-E, F). In general, all the well-sorted taphofacies are composed mainly of shells and their fragments, do not show mud matrix or even shell fragments smaller than 0.2 mm, the size of valves varies from 0.5 to 5 mm and shell fragments are the smallest components. The unsorted taphofacies contain grains smaller than 0.2 mm, most of them peloids, and exceedingly small shell fragments.

Chinelatto et al. (2020) related the classifications of coquinas as unsorted and well-sorted to the environmental conditions in which they were probably deposited. According to them, the well-sorted coquinas were interpreted as deposits influenced by storm-induced currents and waves where the energy was sufficient to winnow the finer grains and preserve the primary pores. The taphonomic characteristics indicate storm to shoreface deposits, whereas in unsorted facies the energy was not enough to remove fines grains, being generally associated with distal storm and offshore deposits.

In taphofacies Tf-1 and Tf-3, shells are oriented parallel and oblique to bedding, an effect of high energy environments which are influenced by waves and currents. The reworked deposits are located above the fair-weather wave-base (FWWB) as shoreface and foreshore deposits. Taphofacies Tf-2 and Tf-4, despite displaying taphonomic characteristics similar to Tf-1, show a high diversity of fine grains such as peloids, very small micrite intraclasts, shell debris, and ostracods. The high occurrence of these fine grains indicates low-energy deposits, such as restricted deposits or storm deposits located below the FWWB. Taphofacies Tf-5 and Tf-6 are interpreted as storm-induced concentrations, supported by the chaotic arrangement of shells, occurrence of ostracods and an erosional base of the beds.

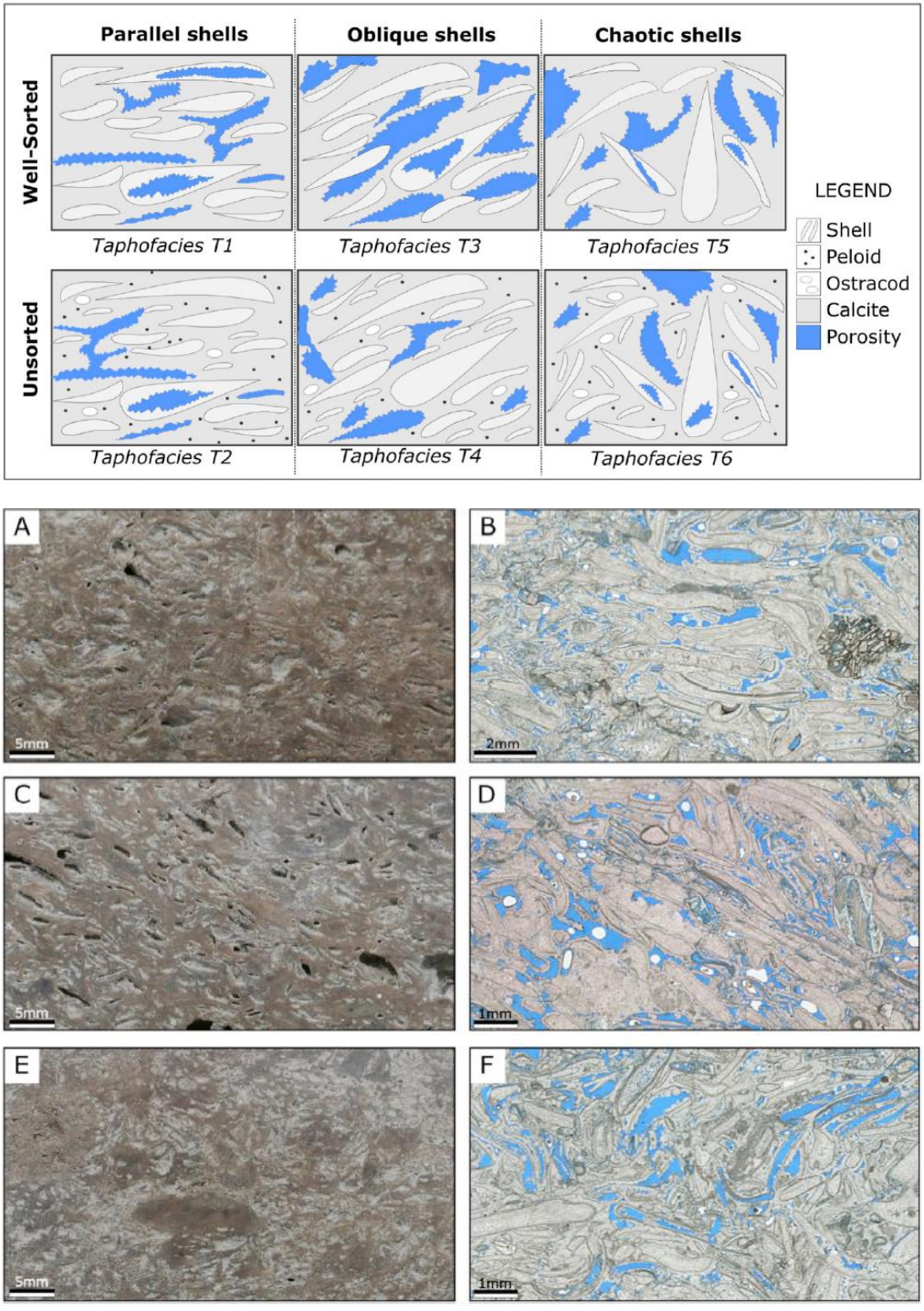

Figure 10: Taphofacies based on shell orientation and sorting and some examples from core photographs and photomicrographs of thin sections. A-B) Shells oriented parallel to the bedding: taphofacies Tf-1-Tf-2, B) Tf-1 composed of whole and fragmented shells and coquinas intraclasts. C-D) Shells with oblique orientation: taphofacies Tf-3-Tf-4; D) Tf-3, the white bubbles reflect the poor Epoxy impregnation. E-F) Shells with chaotic orientation: taphofacies Tf-5-Tf-6, F) Tf-6 with peloids, small shell fragments and intraclasts (Source: Chinelatto et al., 2020).

Fick et al. (2018) simulated the formation of shell concentrations in flume experiments under fair-weather and storm-weather conditions. They conclude that waves, storm-induced currents, the breaker, and the shoaling zone control the distribution of shell accumulation. Figure 11 provides the taphofacies interpretation of the analyzed deposits, indicating the limits of the breaker and shoaling zones during fair-weather (Figure 11-A, C) and storm conditions (Figure 11-B, D). During fair-weather conditions, taphofacies Tf-1 and Tf-3 are formed at the shoreface and foreshore, while Tf-2 occurred below the winnowing zone where peloids could find a good environment to settle. At the same time, in restricted areas, peloids, stevensitic ooids and shells with stevensite layers are formed, besides that, at the lake margin, microbialites and mudstones may occur.

During storm surges, the zone of reworking is wider and storm waves and currents are capable of eroding previously deposited taphofacies (red lines in Figure 11-D). Foreshore and shoreface coquinas may be eroded, transported, and deposited as washover deposits with a mixture of old and fresh shells, whereas at the lake margin, the waves can remove and transporting clay and microbialites clasts. In the deepest areas of the lake, mudstones may have been deposited. According to the analyzed interval, the coquinas occur between the foreshore and offshore transitional, mainly as bioclastic bars and washover fans due to the absence of marginal or deep lake facies that may be represented by a few carbonate intraclasts (Chinelatto et. al., 2020).

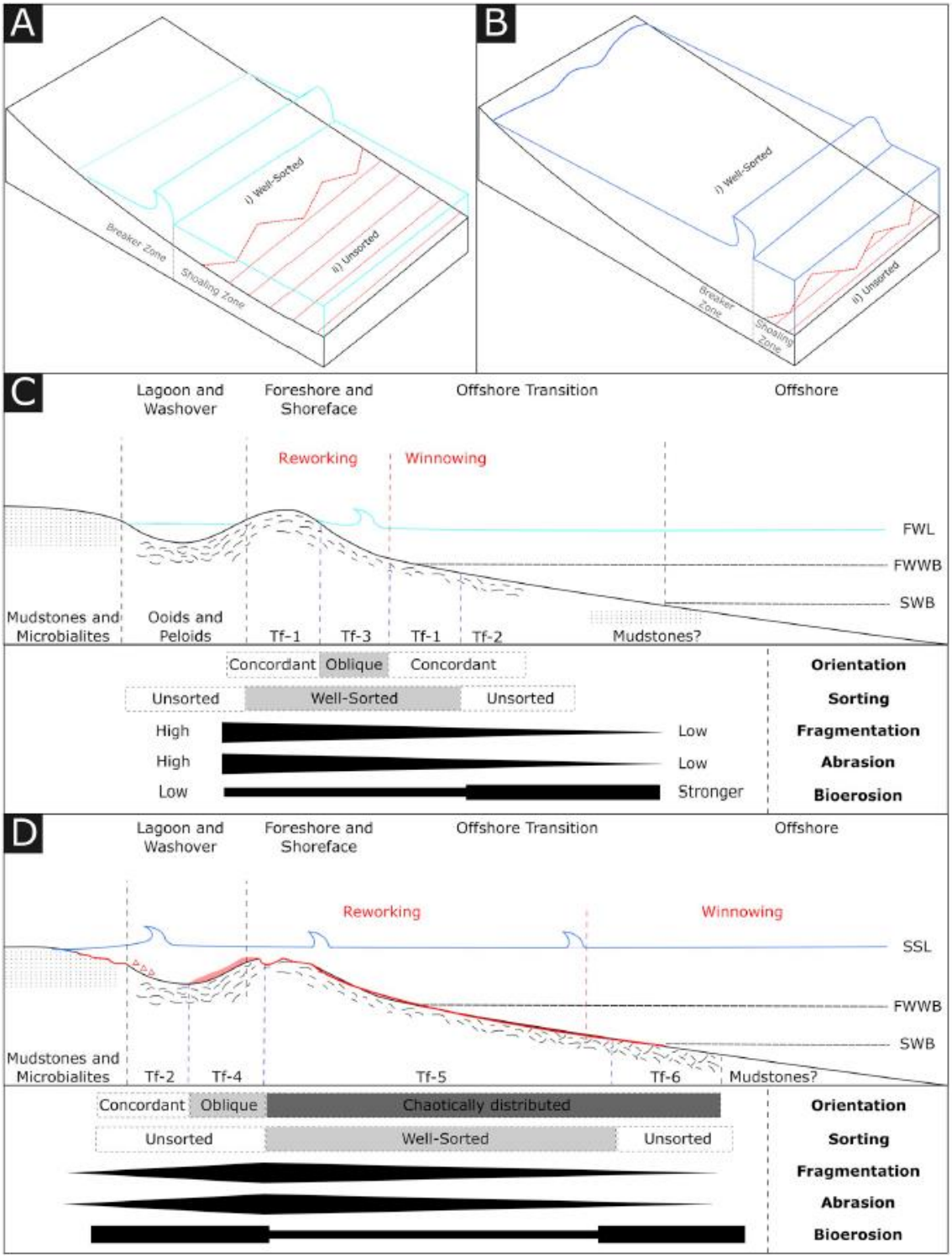

Figure 11: Depositional interpretation of taphofacies under first wave breakpoint (Fick et al., 2018): A, C) Fair-weather conditions; B, D) Storm conditions (Source: Chinelatto et al., 2020).

Besides that, through the analysis of thin sections, x-ray tomography (CT), high resolution tomography (H-CT) and Nuclear Magnetic Resonance (NMR), Chinelatto et al. (2020) quantified the porosity of the taphofacies and classified them according to Choquette and Pray (1970) and Ahr (2008) (Figure 12). Generally, in well-sorted taphofacies primary pores are preserved, consisting mainly of interparticle, intraparticle, moldic and vug porosities. The porosity control varies from depositional to hybrid 1[1] and pores are generally connected. On the other hand, in unsorted taphofacies, preserved primary porosity is uncommon and most pores are moldic and vugs. The porosity control varies from hybrid 1 to diagenetic and the connectivity varies (Ahr 2008). Chinelatto et al. (2020) also state that despite the textural differences between well-sorted and unsorted taphofacies, in general, porosity is good and varies between 10 and 25%, while the permeability has a different and expressive behavior being way lower in unsorted taphofacies than in the well-sorted ones.

It is important to mention the influence of calcite cementation and dissolution between the depositional, hybrid, and diagenetic controls of porosity, and the main pore type found in each group (Figure 12), as observed in the scientific paper developed by Chinelatto et al. (2020). In depositional control, taphofacies Tf-1, Tf-3 and Tf-5 (well-sorted), showed great values of porosity and permeability comparable with the taphofacies Tf-2, Tf-4 and Tf-6 (unsorted) that exhibited finer grains between the shells reducing the interparticle porosity. In hybrid control, the cementation and dissolution may run the improvement or diminution of porosity in all taphofacies. The authors observed that all taphofacies showed high cementation, however, the samples that showed great indices of dissolution were the taphofacies Tf-1, Tf-3 and Tf-5. Finally, in diagenetic control, the Tf-2, Tf-4 and Tf-6 was dominant, the high cementation obstructed the primary pores, and only secondary porosity was observed. Then, Chinelatto et al. (2020) state that for these taphofacies the diagenesis reduces the primary pore, however, the dissolution of shells and matrix will promote the moldic pores and vugs.

[1] based on Ahr (2008): type of porosity that is produced by depositional and diagenetic processes and porosity mainly varies between primary and secondary.

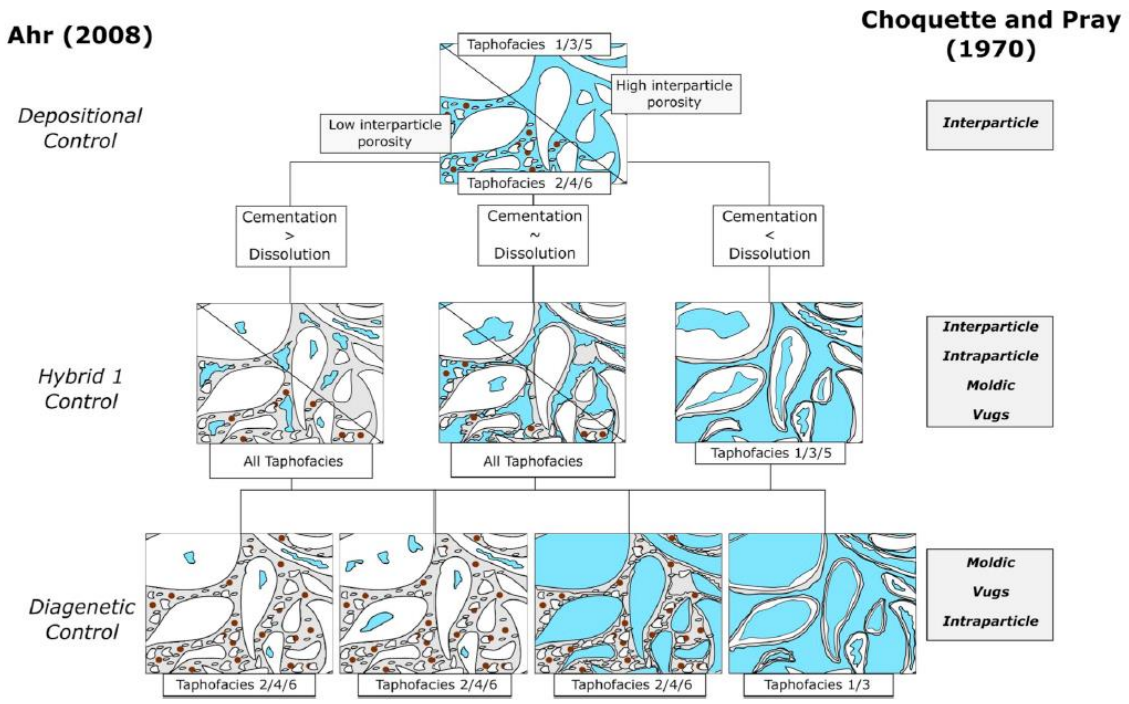

Figure 12: Control of porosity according to Ahr (2008), the influence of calcite cementation (C) and dissolution (D), and main taphofacies found in each type. When the cementation prevails over dissolution (C > D) interparticle pores are reduced, whereas C < D, vugs and molds are created (Source: Chinelatto et al., 2020).

Besides Chinelatto et al. (2020), Herlinger et al. (2017) stated that calcite is the main type of cement found in Itapema Fm. According to them, the diagenesis acting on bioclasts was controlled by the balance between dissolution and neomorphism, mainly calcification of aragonitic bioclasts, favoring the generation of poorly connected mold porosity or the preservation of well-connected interparticle porosity. Distinguishing between neomorphism and calcite cementation is difficult most of the time. Bioclasts are usually covered by calcite edges. Dolomitization and/or the presence of dolomitic cement is not so common. The presence of silica occurs in 44% of the samples, but rarely exceeds more than 2% of the total rock volume. Therefore, chalcedony and quartz occur in small amounts, replacing calcite or, more rarely, filling moldic, interparticle, intraparticle, and vugular pores.

2.2. Barra Velha Formation

The Barra Velha Formation belongs to the Alagoas local stage, of Aptian age. It is limited at the base by the Pre-Alagoas unconformity and at the top by a thick salt layer (Ariri Fm.). As previously seen, the Barra Velha Fm. can be divided through the Intra-Alagoas unconformity, into a lower part, which represents the carbonates of the upper rift, and an upper part, which constitutes the carbonates of the sag phase (Wright and Barnett, 2015; Buckley et al., 2015). According to Wright and Barnett (2015) the thickness of the Barra Velha Fm. varies significantly across the Santos Basin, from more than 500 m to less than 55 m at the top of fault blocks, where it may be locally absent.

This formation contains excellent quality reservoirs (Satzmari and Milani, 2016) and, therefore, it has been the target of several discussions still uncertain about its evolution, such as its depositional environment and the biotic or abiotic origin of these carbonates.

The depositional environment of the Barra Velha Fm. has been the subject of numerous discussions since the early 2000s, being mainly about the type of environment under which the Barra Velha Formation was deposited. First, Dias (2005) attributed a marine depositional environment as a context for the deposition of carbonates from the Macabu Fm. in the Campos Basin (Winter et al., 2007), which is an analog for the Barra Velha Fm. (Moreira et al., 2007). Then, some authors such as Moreira et al. (2007), Carminatti et al. (2008), Gomes et al. (2008), Formigli et al. (2009) and Farias et al. (2019) suggested a transitional depositional environment, under the marine influence. Later, this marine influence would be contested by Wright and Barnett (2015), Muniz and Bosence (2015), Pietzsch et al. (2018), Herlinger et al. (2017), Lima and De Ros (2019) and Gomes et al. (2020) who end up discarding the marine origin of the depositional environment of the Barra Velha Formation.

There is a strong contrast between marine and lake carbonates. In marine environments, the main controls on genetic conditions and on aspects such as stratal architecture, seismic geometry, facies and diagenetic potential are age (Moore, 2001; Herlinger et al., 2017), climate, type of carbonate fabric and changes in sea level (Williams et al., 2011; Wright and Rodriguez, 2018). The deposition of lacustrine carbonates is quite complex, being controlled by local geological configurations through numerous factors such as sedimentary input, temperature variations, climate, tectonics,

fauna, specific geochemical conditions, hydrological (input and output of surface waters, precipitation, and groundwater flow) and water chemistry (Herlinger et al., 2017; Wright and Rodriguez, 2018). This last factor plays an important role in lake environments due to the control it imposes on several processes, including the development of microbial communities, abiotic precipitation of carbonates (Riding 2008; Wright and Barnett 2015), and clay minerals (Calvo et al. 1999; Pozo and Casas 1999; Furquim et al. 2008), and the development of algae, ostracodes, and mollusks (bivalves or gastropods).

Wright and Barnett (2015) state that the absence of marine fossils such as miliolid foraminifera and sulphate minerals such as gypsum and anhydrite show a non-marine, but lacustrine origin. Pietzsch et al. (2018) state that the biostratigraphic components of the pre-salt are based essentially on non-marine ostracods because of the lack of marine fauna in these sequences and, in addition, the carbonates present higher radiogenic signals values when compared to the Aptian marine values, also certifying a lacustrine origin for the pre-salt carbonates (strontium isotopes can be exceptionally sensitive indicators of lacustrine evolution). Muniz and Bosence (2015) interpreted the absence of marine and freshwater biota and the presence of non-marine ostracodes as evidence of a brackish - water - lacustrine environment.

Another widely discussed topic about Barra Velha Fm. is the microbial or chemical origin of its carbonates. Moreira et al. (2007), Carminatti et al. (2008) and Carminatti et al. (2009) mention microbialites as constituent facies of the Barra Velha Fm. and Terra et al. (2010) classify such microbial textures. Muniz and Bosence (2015) state that the carbonates in this formation are partially microbial. Wright and Barnett (2015) state that macro and microscopic evidence of microbial involvement in the production of these carbonates is considerably rare, defending the abiotic origin for the succession of carbonate precipitation. According to Herlinger et al. (2017), recent interpretations suggest that most of the Macabu Fm., analog for Barra Velha Fm., are chemical precipitates, controlled by the geochemistry of alkaline lacustrine waters. Tosca and Wright (2015) also state that evidence of microbial influence on Barra Velha Fm. is absent. Lima and De Ros (2019) cite a hybrid origin (biotic/abiotic), but with an abiotic predominance for pre-salt carbonates. Silva (2018) adds that it is possible that carbonates from Fm. Barra Velha are the result of joint action between biotic and abiotic processes, with an eventual predominance of one process over the other. Thus, the origin of the

carbonates of the Barra Velha Fm. is a controversial issue, which remains under constant discussion and is far from a consensus.

Wright and Barnett (2015) claim that despite the uncertainty about the exact chemical conditions that produce sediments of the Barra Velha Fm., it can be inferred that the lakes in the formation were hyper-alkaline and willing to evaporation. This statement can be supported by the strong presence of magnesium-rich clays (Mg-clay) such as stevensite that is formed under restricted conditions with high pH (>10). In addition, Wright and Barnett (2017) identified possible trends in carbon and oxygen isotopic data from Barra Velha Fm. that can be compared with those of Quaternary lakes in the East African rift, corroborating the statement of shallow and evaporitic lakes for the Barra Velha Formation.

Wright and Barnett (2015) carried out a complete and detailed study, based on the analysis of 1400 m of core samples and more than 3400 thin sections, on the textures and facies of the Barra Velha Fm, in Santos Basin. The authors realized that the carbonates comprise three main components and detrital material derived from them. Such components are represented by shrubs (crystal shrubs), millimetre-scale fibrous laminae, and spherulites. Shrubs are defined as millimetre- to centimetre- sized growths of dense radiating fibrous to bladed calcite. They occur in layers, with predominantly vertical growth positions, being commonly fragmented and mixed with spherulites to form grainstones to wackestones (reworked facies). Also, they are interbedded and interlaminated with spherulitic limestones and laminites and within cyclic packages.

The authors mentioned in the previous paragraph identified, in the collected samples, cyclothems with thicknesses ranging from 0.75 to 5 m. Thus, the carbonates were, in part, cyclically settled into symmetric and asymmetric cyclothems that exhibit three main facies (Figure 13). Facies 1 consists predominantly of shrubs in situ. Facies 2 is dominated by spherulites in situ immersed in a matrix formed by magnesian clays (mainly stevensite) that cover a large part of Barra Velha Fm. Facies 3, on the other hand, consists of laminated detrital limestones composed of fragments of fine sand to silt shrubs, wackestone, and calcimudstone with thicker fragments mainly composed of spherulitites. It is also common the occurrence of reworking formed by fragments of shrubs, mainly in the form of grainstones. Each cyclothem begins with a sharp-based incursion of Facies 3 capping Facies 1 (in situ shrubs), separated in some wells by a thin grainstone composed mainly of reworked shrubs.

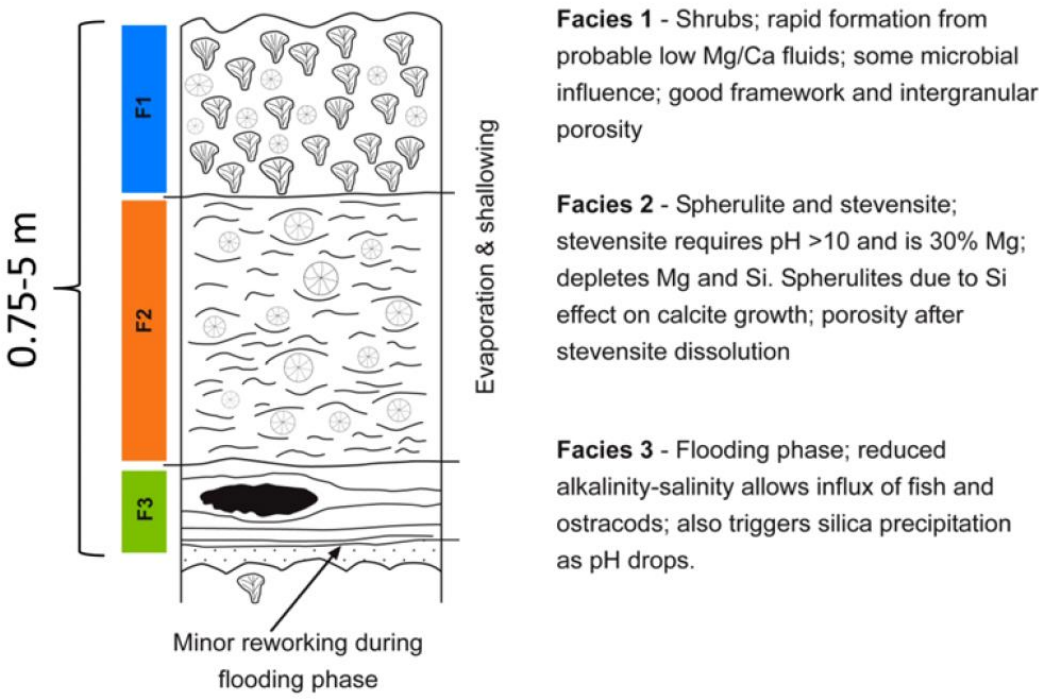

Figure 13: Schematic cyclothem proposed by Wright and Barnett (2015) for the Barra Velha Fm.

Wright and Barnett (2015) establish a relationship between these three facies and the evolution of the depositional environment, seeking to determine the context in which each lithology was preferably deposited. Facies 3 probably accumulated in some protected environment condition or possibly below wave-base in a flooding phase, in which some short rainfall events would occur. This facies may contain desiccation cracks that can suggest a relatively shallow water origin, yet deeper than those of the other facies. In addition, the authors state that the change to Facies 2 may have caused an increase in the rate of evaporation producing highly saturated and alkaline waters that generates a significant change in pH, corroborate by the rare occurrence of non-marine ostracodes and fish. This might suggest that the lake may have become less hostile and with enough fresh water to allow the species to colonize. As a result, when producing super-saturated and alkaline waters, evaporation acted as a trigger for the precipitation of magnesium silicates (stevensite), initially as gels, and calcite spherulites formation within these gels. Wright and Barnett (2015) further explain that, as the rate of precipitation of the gel decreased or ceased, the calcite crystals shrubs (Facies 1) developed and grew in the water column, although they maintained some evidence of the ancient presence of some Mg silicates. The reduction of the precipitation of the gel allowed the rapid growth of structures of shrubs of calcite crystals from the asymmetric growth of spherulites in the lake waters. The relationship between these facies can be seen in Figure 14.

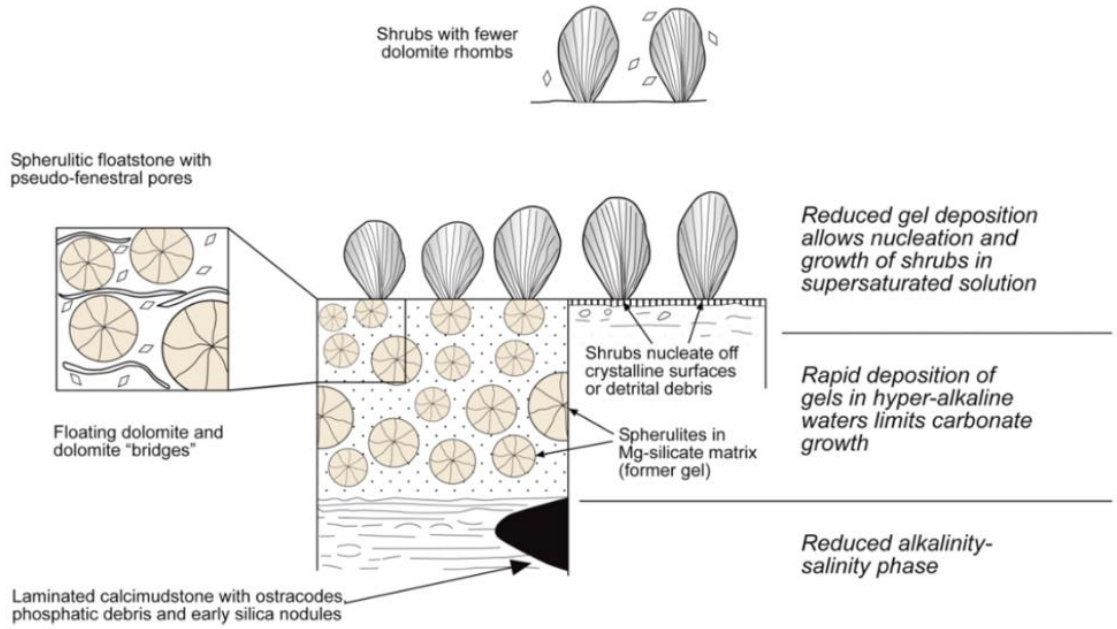

Figure 14: Model to explain relationships between the three main facies types and components in the Barra Velha Formation. (Source: Wright and Barnett, 2015).

According to Wright and Rodriguez (2018), the shrubs and spherulites can be reworked into a range of different textures. While the finest products of rework are associated with laminated carbonate muds, the coarsed ones consist of well-sorted grainstones. These authors highlight that the best reservoir facies correspond to shrubs in situ (Facies 1) and add that well-sorted grainstones can also have excellent reservoir quality. Furthermore, Tosca and Wright (2015) highlight that the formation and subsequent dissolution of stevensitic clays represents a crucial factor in the production of reservoirs with good quality. Jones and Renaut (2010) state that the alternation of calcite or stevensite precipitation in these deposits was related to variations in the pH, Mg and Ca ratio, saturation levels, temperature, and pCO2 in the geochemistry of lacustrine waters.

Muniz and Bosence (2015) carried out a study to analyze facies related to carbonate deposits of Macabu Fm. in the Campos Basin, which is correlated to Barra Velha Fm., in the Santos Basin (Moreira et al., 2007). The authors determined, from the interpretation of the borehole image logs, facies that were divided into four groups. The first corresponds to genetically modified facies such as breccias (BHI-1). The second refers to terrigenous facies and includes shales (BHI-2), marls (BHI-3) and conglomerates (BHI-4). The third is related to allochthonous facies and is represented by mudstones (BHI-5) and by packstones, grainstones and rudstones (BHI-6). The last group

encompasses the autochthonous facies and comprises laminites (BHI-7), stromatolites (BHI-8) and thrombolites (BHI-9).

Subsequently, the interpretation of the depositional environments corresponding to these facies was performed, as shown in Figure 15. Such facies were interpreted as having been formed in four lacustrine depositional environments: deep underwater, intermediate underwater, shallow underwater and subaerial/emergent. In the deep, low-energy, underwater environment, shales (BHI-2) and laminites (BHI-7) are present, which were formed below the storm wave-base (SWB). Also in this environment, but in a little shallower water, are marls (BHI-3). Thrombolites (BHI-9) are rare and were also inserted in the deep lacustrine environment due to their occurrence in association with other low energy facies (BHI-2, BHI-3 and rarely with BHI-8).

The intermediate underwater environment is above the fair-weather wave-base (FWWB) and dominated by stromatolitic (BHI-8) and reworked (BHI-6) facies. Such deposits exhibit structures that can indicate lacustrine margin environments with high to moderate energy. The shallow underwater environment is interpreted as a shallow, low-energy zone with limited accommodation space, where laminites are also present (BHI-7). Finally, the sub-aerial or emergent environment is located in areas of higher topographical relief, which is only occasionally flooded. In this environment there are breccias (BHI-1) that are commonly covered by shales (BHI-2), marls (BHI-3), or laminites (BHI-7), indicating transgressive events and an increase in the level of the lake.

Some authors (Carminatti et al., 2009; De Paula Faria et al., 2017) consider that the Barra Velha Fm. was originated in an environment of high relief carbonate platforms. Wright and Barnett (2017) state that evidence such as the fact that correlations using well logs indicate post-depositional relief, the facies model and provisional isotopic data suggest that the Barra Velha Fm. did not develop as a carbonate platform, but as shallow, evaporitic, and alkaline lakes. Also, according to these authors, the conical mounts interpreted in seismic can be mounds formed by chemical precipitation and/or volcanoes.

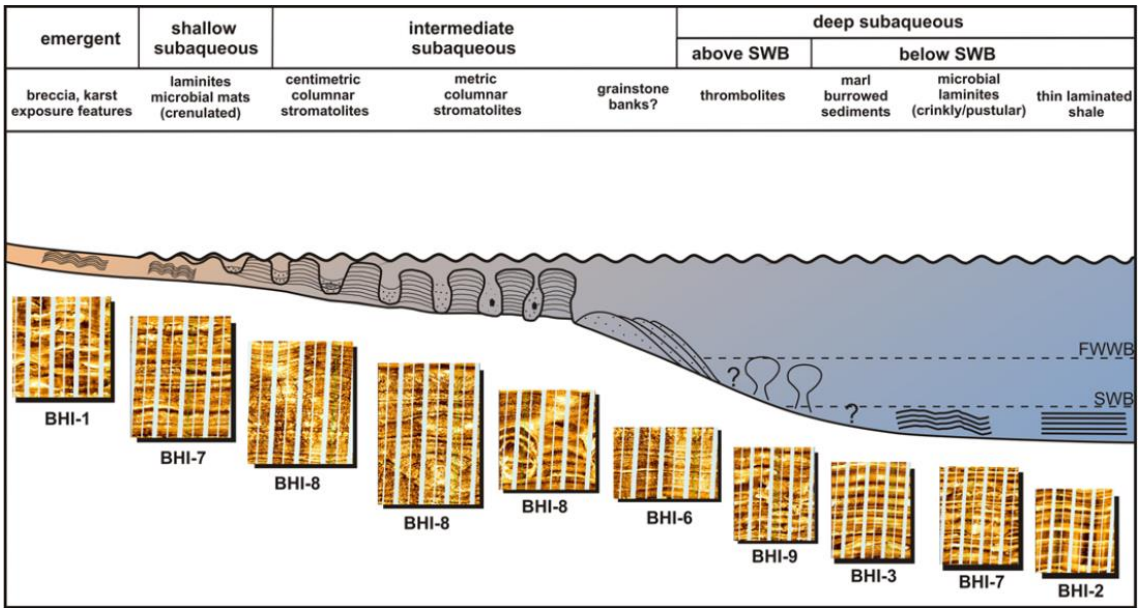

Figure 15: Schematic facies model for borehole image (BHI) facies based on the microbialites of the Macabu Fm, Aptian of the Campos Basin. This scheme takes into account the lake level, the level of wave action and the facies succession. It is also based on the observation of similar facies' occurrence in ancient outcrops and modern deposits, as discussed in the text. FWWB, fairweather wave-base; SWB, storm wave-base (Source: Muniz and Bosence, 2015).

Pietzsch et al. (2018) proposed a simplified model that illustrates the general lacustrine geology and hydrology during the deposition of the Barra Velha Fm. based on a well in the Santos Basin shown in Figure 16. The authors proposed a model formed by shallow, broad lakes that over time became progressively more evaporitic and alkaline, being involved with groundwater infiltration in the Basin and the geothermal heat that tends to decrease from the rift phase to the post-rift. Groundwater recharge to the lake probably occurred through conduits spread across the lake bottom and as infiltration not necessarily connected to them. These fluids mixed with the main body of water, significantly contributing to the chemical and isotopic composition of carbonate rocks.

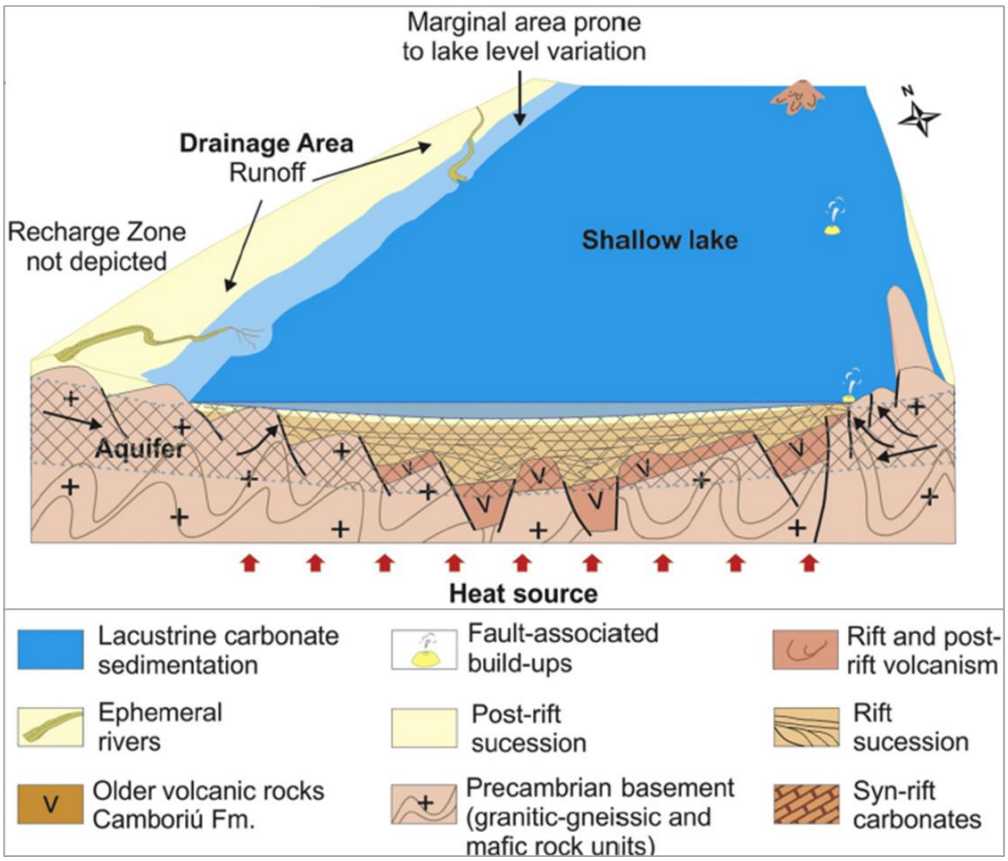

Figure 16: Simplified conceptual model illustrating the Pietzsch's model. Black arrows indicate the groundwater's infiltration in the lacustrine basin and red arrows represent geothermal heat. Shaded areas propose the presence of aquifers flowing mainly through the fractured crystalline basement (Modified from Pietzsch et al., 2018).

Wright and Barnett (2015; 2017) and Wright and Rodriguez (2018) present a depositional model (Figure 17) based on a large volume and variety of data from the Santos Basin, comprising petrographic samples, isotopic and well log data, thin and seismic sections. Furthermore, the authors present strong evidence that supports the depositional model proposed by them and by Pietzsch et al. (2018) from an environment of extensive, hyper-alkaline and shallow evaporitic lakes.

An important work that analyzes the impact of diagenesis on the evolution of the porosity and permeability of carbonates is that developed by Herlinger et al. (2017), in the pre-salt carbonates of Macabu Fm. The authors pointed out that the presence of stevensitic clays was associated with calcite spherulites, more specifically, they stated that the deposits of magnesian clays were frequently replaced by calcite spherulites due to their chemical instability. Such occurrence is similar to that observed by Wright and Barnett (2015) in Facies 2 of the cyclothem for the Barra Velha Fm.

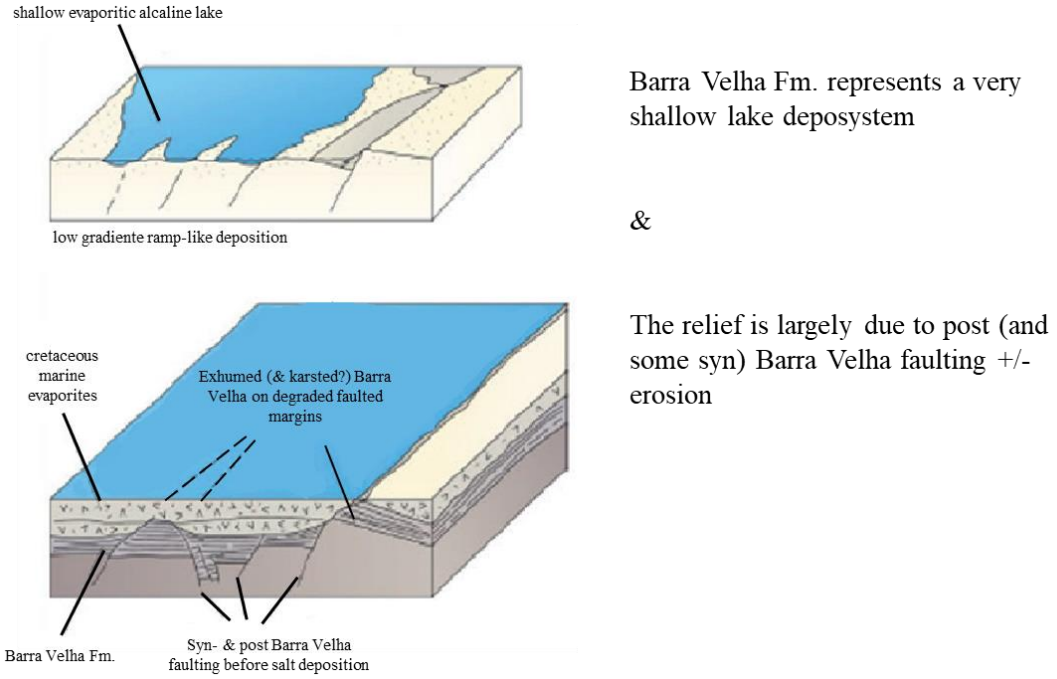

Figure 17: Connected shallow evaporitic lake model consistent with facies, isotopic and thermodynamic evidence. Seismic relief would be owing to syn- and post-depositional faulting (Source: Wright and Rodriguez, 2018).

As mentioned earlier, Herlinger et al. (2017) address the presence of stevensitic clays facies associated with calcitic spherulites in Macabu Fm. from the Campos Basin. When analyzing the diagenetic aspects of this facies, the authors indicate that the deposits of magnesian clays in the sag section were frequently replaced by calcitic spherulites (Figure 18A, B, E and F), dolomite and silica. Dolomite appears to replace stevensite constantly and often completely replaces stevensite and calcitic spherulites. Buchheim and Awramik (2013) emphasize that in cases where stevensite is found preserved it becomes problematic, as it compromises the permo-porosity of the reservoir.

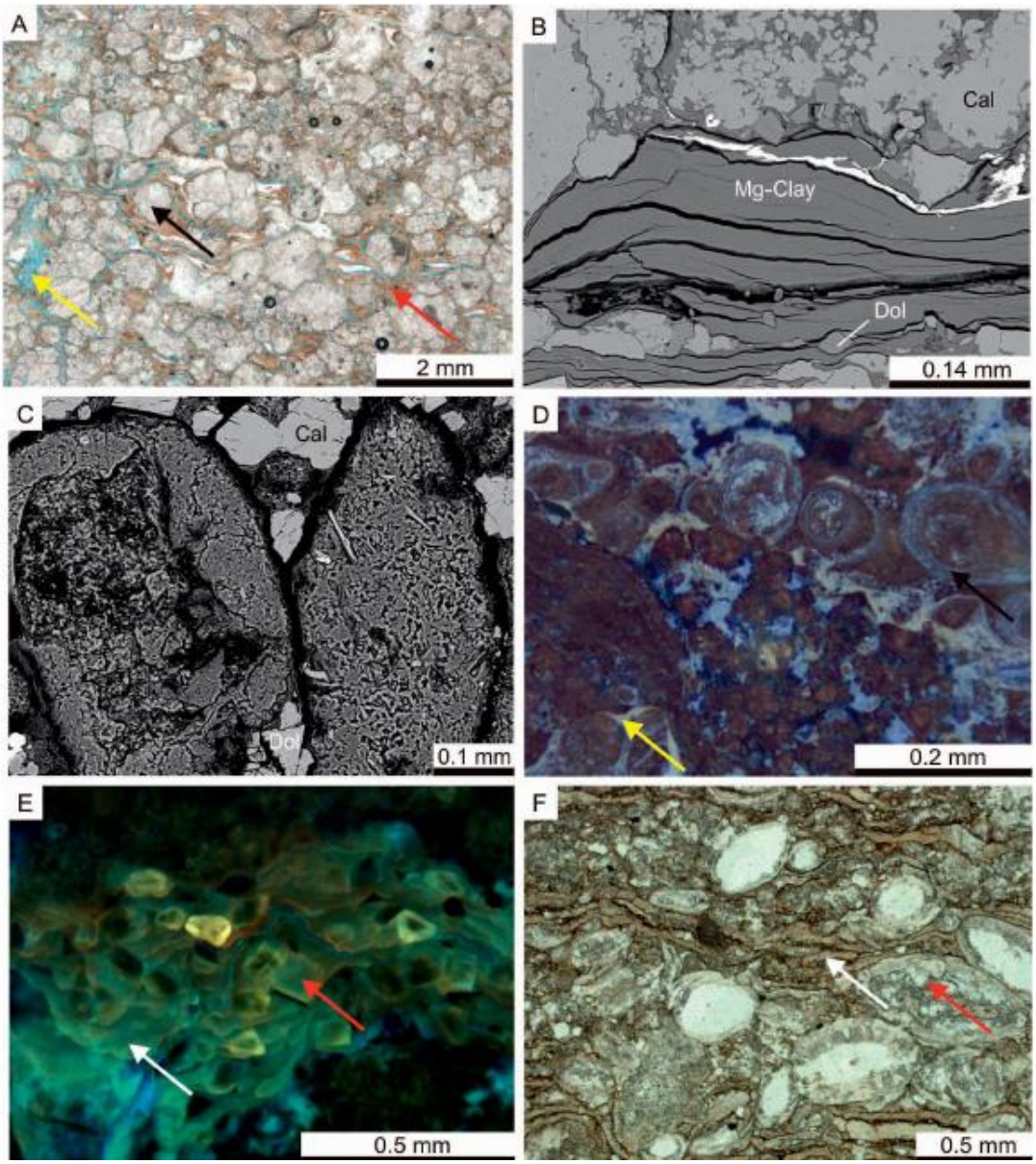

Figure 18: Important characteristics of stevensitic claystones: A) shrunken and partially dissolved (yellow arrow) stevensite laminations (red arrow) replaced by recrystallized calcite spherulites (black arrow). B) Slightly shrunken stevensite (Mg-clay) laminated aggregates, partially replaced by dolomite (Dol) and calcite (Cal). C) Stevensite ooid–peloid. Ooid on the left has a partially dissolved nucleus and an outer massive texture, whereas peloid on the right has a dominantly massive texture. D) Stevensite as ooids (black arrow) and as coatings (yellow arrow) on intraclasts. E) Laminated stevensite aggregates (white arrow) partially replaced by dolomite (red arrow). F) Articulated ostracod bioclast shells (red arrow) filled and replaced by quartz in deformed stevensite laminations replaced by mimetic dolomite (white arrow) (Source: Herlinger et al., 2017).

Lima and De Ros (2019) carried out a detailed petrographic study in seven wells at Macabu Fm., which, as mentioned above, is correlated to Barra Velha Fm. The main facies found by the authors were fascicular calcite crusts, stevensitic clays with calcitic spherulites, rudstones and intraclastic grainstones, laminites, dolostones and cherts (totally silicified rocks). Fascicular calcite crust is the facies equivalent to shrubs (Wright and Barnett, 2015) and stromatolites (Terra et al., 2010).

Lima and De Ros (2019) propose a succession of facies in which laminated magnesian clay deposits with little contribution of clay peloids and siliciclastic grains constitute the substrate into which spherulites are chemically precipitated, replacing and/or displacing this mainly stevensitic matrix. The closer to the water-sediment interface, the more these spherulites grew and became asymmetric, thus originating fascicular calcite aggregates. The distinction between spherulites and fascicular calcite aggregates was probably defined by the greater ionic availability, precipitation rate and accommodation space for the latter. Finally, the fascicular calcite aggregates coalesced, giving rise to fascicular calcite crusts (or shrubs), as shown in Figure 19.

It is important to highlight that according to Armelenti et al. (2016), Herlinger et al. (2017) and Lima and De Ros (2019), the laminated stevensitic deposits were probably deposited in low-energy environments, while the ooids are likely to have been formed under some agitation caused by waves or currents, with peloids probably deposited in intermediate energy conditions. Fine-grained deposits of stevensite and other Mg-silicates occur throughout the whole Aptian Pre-Salt succession, and their recurrent and widespread distribution indicates that they constituted the background of sedimentation in the wide, hyper-alkaline sag lakes.

Lima and De Ros (2019) claim that the salinity of the fluid is an important factor in Mg-clay precipitation. The Mg-clay deposits were commonly dissolved, and/or replaced by silica, calcite, dolomite or magnesite. The widespread dissolution of Mg-clays in the pre-salt deposits probably occurred under eodiagenetic conditions related to the low stability and fast dissolution kinetics of stevensite in a scenario of high pCO_2, with a pH below 8 (Tosca and Wright, 2015). They also analyzed that dissolution of stevensite and other Mg silicates may have occurred either by the influx of CO_2 related to magmatic and/or hydrothermal activity or by the dilution of lacustrine waters owing to relatively more humid climatic conditions. Also, the presence of stevensite indicates that the pre-salt lacustrine environments in the Campos and Santos Basins had high alkalinity

(pH greater than or equal to 10), high concentrations of silica and magnesium and low amounts of CO2. The laminated stevensite was probably deposited in a low energy environment, while the peloids were deposited at times with increased energy from the environment. Figure 20 is a photomicrograph that illustrates the main features in syngenetic and diagenetic constituents of the sag section.

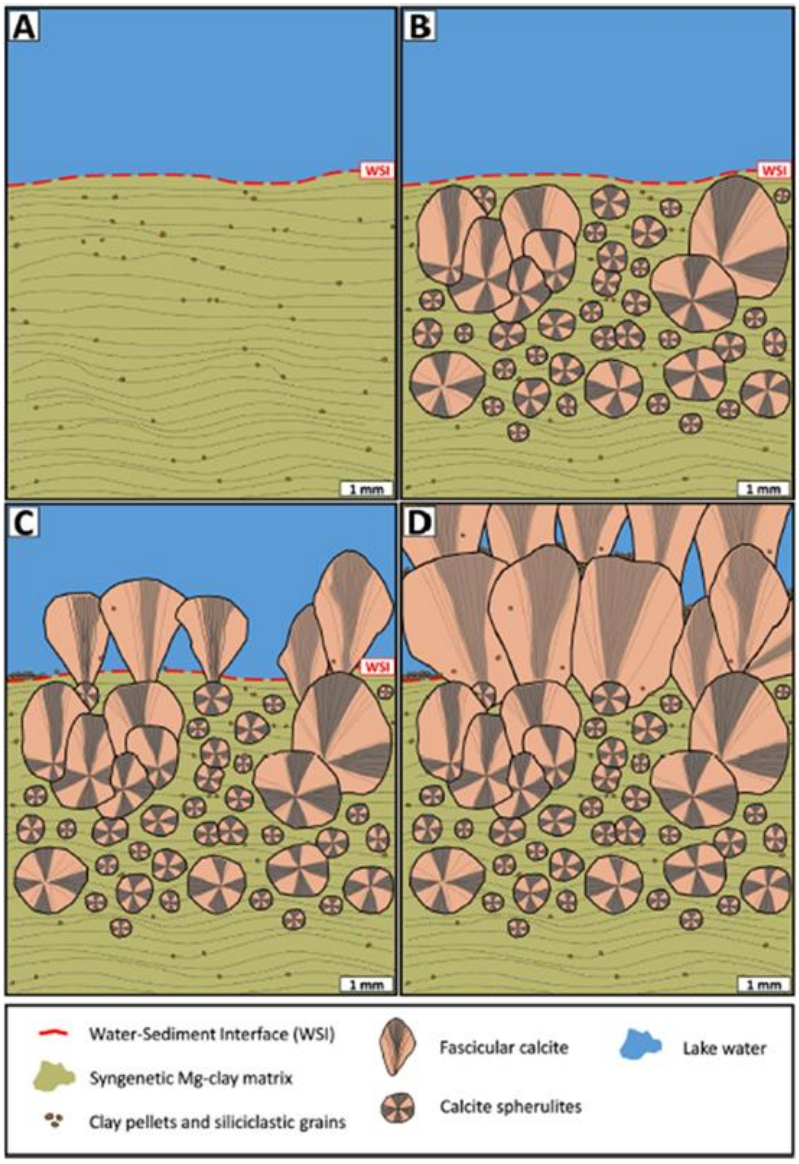

Figure 19: Schematic representation of the genesis of typical Aptian Pre-salt deposits. A) Laminated deposits of syngenetic magnesian clays,with dispersed clay peloids and siliciclastic grains; B) Partial replacement and de formation of the Mg-clay matrix by calcite spherulites. Asymmetrical spherulites formed closer to the water-sediment interface (WSI); C) Non-coalesced fascicular aggregates of calcite precipitated onWSI with inter-aggregate growth-framework porosity. Clay peloids and siliciclastic grains included in some fascicular aggregates; D) Characteristic “cycle” showing the syngenetic crust of coalesced fascicular calcite aggregates at the top, and syngeneticMg-clay matrix partially replaced and displaced by calcite spherulites in themiddle and preserved at the base. Source: Lima and De Ros (2019).

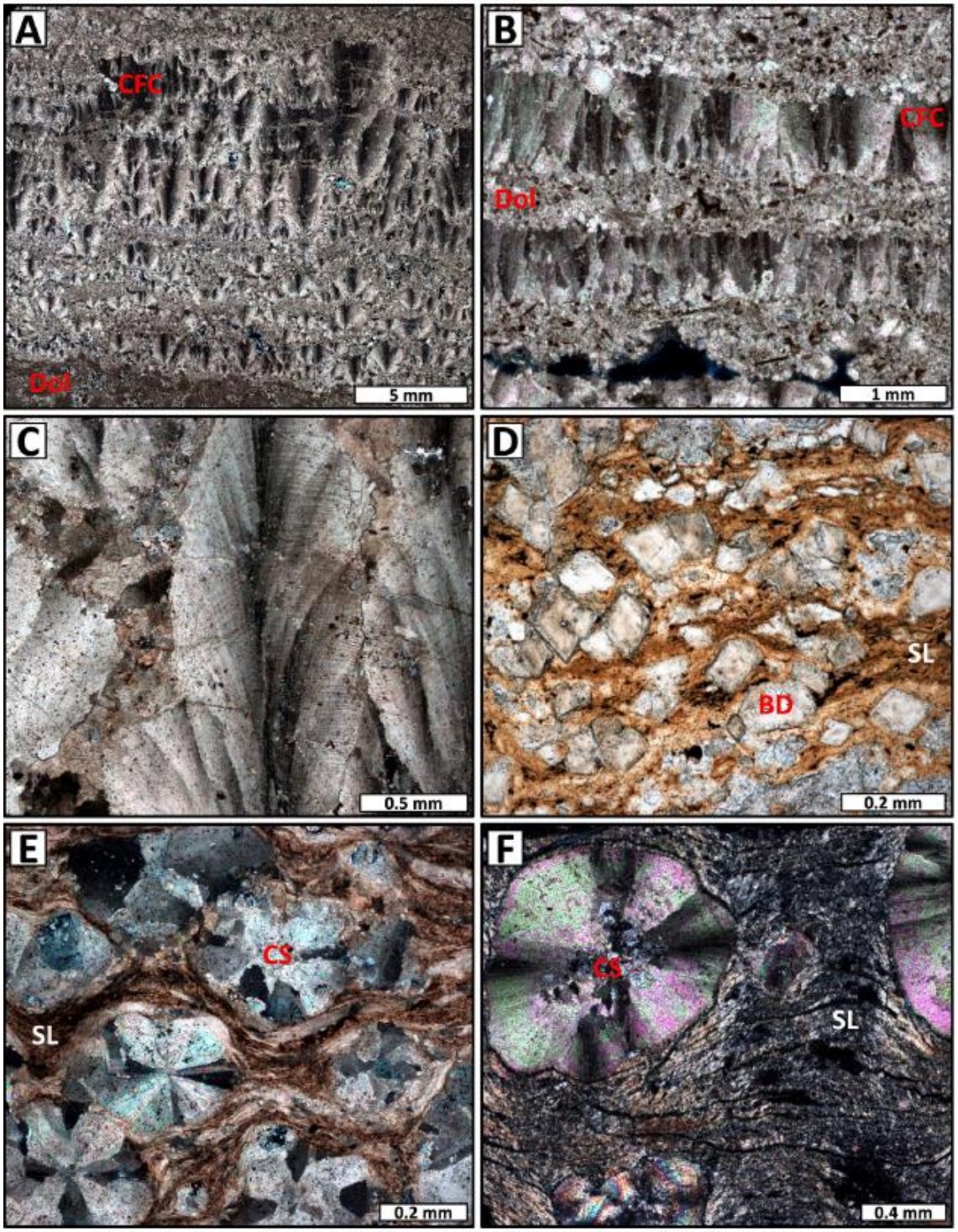

Figure 20: A) and B) Fascicular-optic calcite crusts intercalated (CFC) with granular deposits replaced by dolomite (Dol); (C) Divergent calcite crystal aggregates with fascicular-optic texture; D) Stevensite laminations (SL) replaced and displaced by blocky dolomite (BD); E) Calcite spherulites in the laminated Mg-clay matrix replaced by dolomite; F) Partially silicified calcite spherulites (CS), displacing and replacing Mg-clay laminations. Source: Lima and De Ros (2019).

The most recent work developed by Gomes et al. (2020) analyzed data from eight wells distributed along the horst structure of the Santos Outer High. According to the authors, the main facies present in Fm. Barra Velha in the Santos Basin are mudstones (magnesian clays, calcite, dolomite and silica), spherulitites, shrubs and reworked facies such as grainstones, packstones and wackestones. From this, a new facies classification scheme is proposed, based on the relative abundance of three components: mudstones, spherulitites and shrubs. The ternary diagram (Figure 21) shows the proposed classification based on the combination of the three components where there is no evidence of significant rework. The most abundant component provides a rock name and the minor component provides a qualifying adjective.

The combination of more than 50% shrubs and less than 10% mud separates spherulitic shrubstone from shrubby spherulitestone, and rocks with more than 10% mud are divided according to the proportion of the two components. Spherulitic shrubstone with mud and shrubby spherulitestone with mud are divided by the 50% shrub content. A rock with less than 10% shrubs is divided according to mud and spherulite proportions into muddy spherulitestone, if the proportion of spherulites is higher than 70% and spherulitic mudstone otherwise. The term mudstone is applied to all samples that comprise more than 90% fine-grained components which include Mg-clays, microcrystalline calcite, dolomite, and silica, and the nature of the fine-grained component can be specified by adding an adjective (Mg-clay, calcitic, dolomitic or siliceous mudstone) (Figure 21). Besides, an adjective for the main diagenetic event can be added, for example, dolomitic spherulitestone, silicified spherulitestone or dissolved spherulitestone.

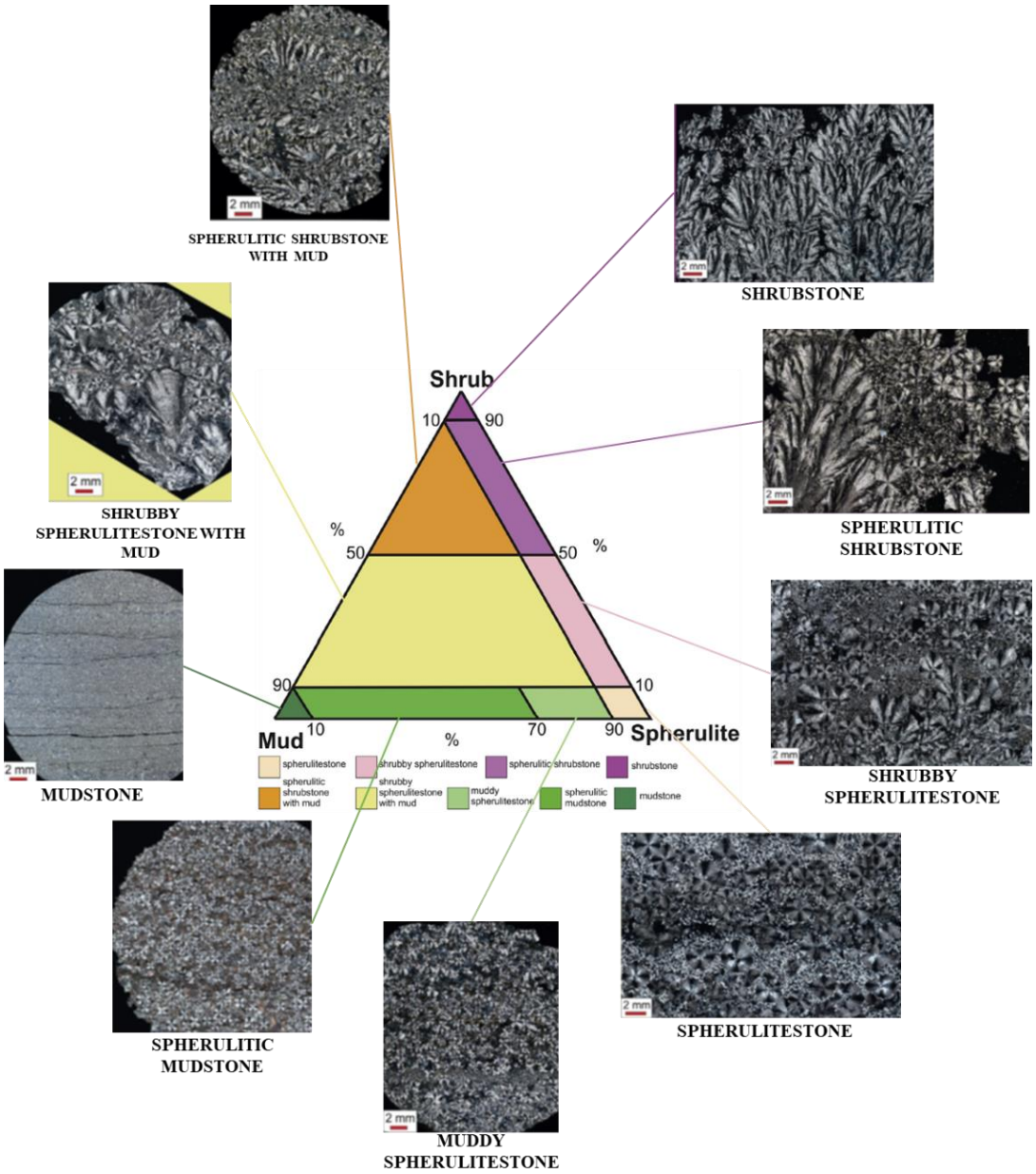

Figure 21: Ternary diagram showing the facies classification for sediment generated in situ for the Barra Velha Formation. Source: Gomes et al. (2020). Facies classification. Shrubstone: comprising fascicular-optic calcite crust with framework porosity; spherulitic shrubstone: comprising fascicular optic shrubs, calcite spherulites and microcrystalline dolomite with inter-particle porosity; shrubby spherulitestone: comprising fascicular optic shrubs, calcite spherulites and microcrystalline dolomite with inter-particle porosity; spherulitestone: comprising calcite spherulites and rhombohedral dolomite with inter-particle porosity; spherulitic shrubstone with mud: comprising calcite shrubs, calcite spherulites and Mg-clays locally replaced by dolomite; shrubby spherulitestone with mud: comprising fascicular calcite shrubs, calcite spherulites and Mg-clays; muddy spherulitestone: comprising calcite spherulites and Mg-clays; spherulitic mudstone: comprising calcite spherulites and Mg-clays; and Mg-clay mudstone. All images are XP and were impregnated with blue epoxy resin to highlight the porosity. Modified from Gomes et al. (2020).

Gomes et al. (2020) also identified that there are reworked facies composed by intraclasts (fragments of shrubs and spherulites), with grain-size varying from fine to very coarse, moderate to poor sorting, and massive to cross-stratified units. Therefore, the authors proposed a set of three ternary diagrams to cover all the facies recognized from the Barra Velha Fm. (Figure 22), separated into in-situ and reworked facies. Mudstone may be in situ or reworked, and this is further classified according to mineralogical composition.

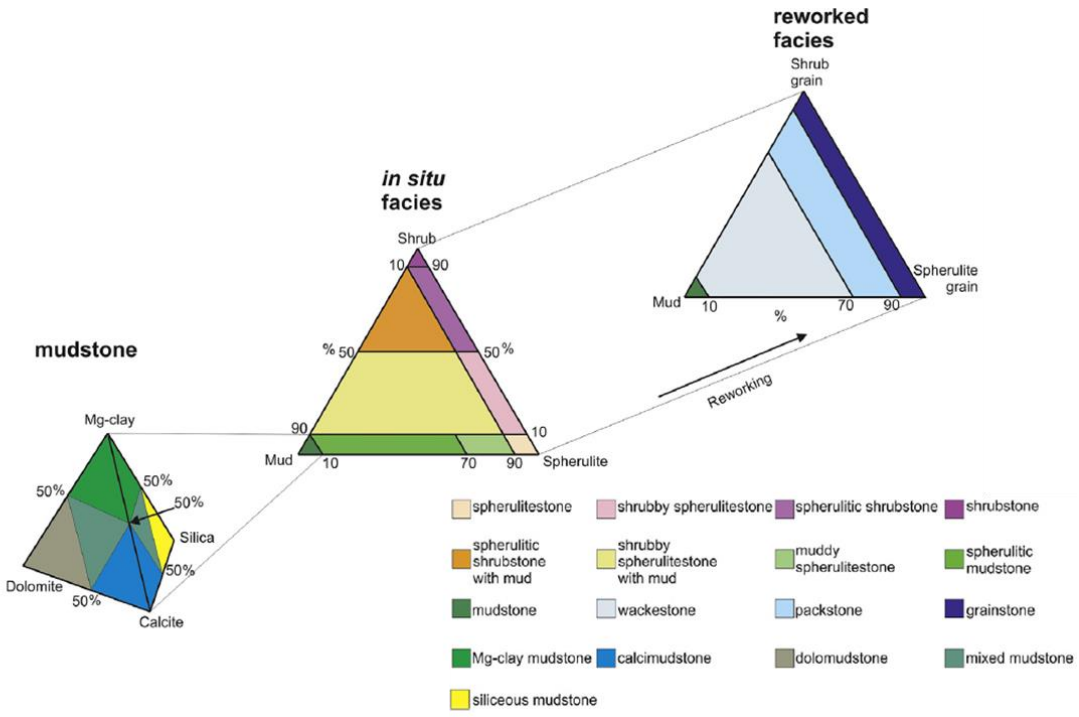

Figure 22: New classification scheme, comprising three triangular diagrams, proposed to describe all facies within the Barra Velha Formation. Source: Gomes et al. (2020).

They also proposed two alternative facies stacking patterns that can be identified in the Barra Velha reservoirs (Figure 23). The first can be characterized by a non-reservoir interval with an upward-increasing shrub pattern transition from mudstone to spherulitic mudstone, muddy spherulitestone, shrubby spherulitestone with mud and lastly to spherulitic shrubstone with mud (Figure 23-a), as well as by a reservoir interval with an upward-increasing shrub pattern from spherulitestone to shrubby spherulitestone, spherulitic shrubstone and finally to shrubstone (Figure 23-b). The second proposal is described as the upward-increasing spherulite pattern that would be shrub dominated at the base, with a gradual transition upward to spherulitestone in reservoir intervals (Figure 23-d) and, in non-reservoir intervals, a gradual upwards transition from spherulitic shrubstone with mud to mudstone (Figure 23-c). Researchers like Wright and Barnett

(2015), Muniz and Bosence (2015), Wright and Barnett (2017), Liechoscki de Paula Faria et al. (2017), Arienti et al. (2018), Artagão (2018), Sartorato (2018), Tanaka et al. (2018), Lima and De Ros (2019) and Farias et al. (2019) suggest a dominance of spherulites within the lower part of the basic cycle and shrubs within the upper part, as it has been shown in the facies stacking pattern of upward increasing shrub.

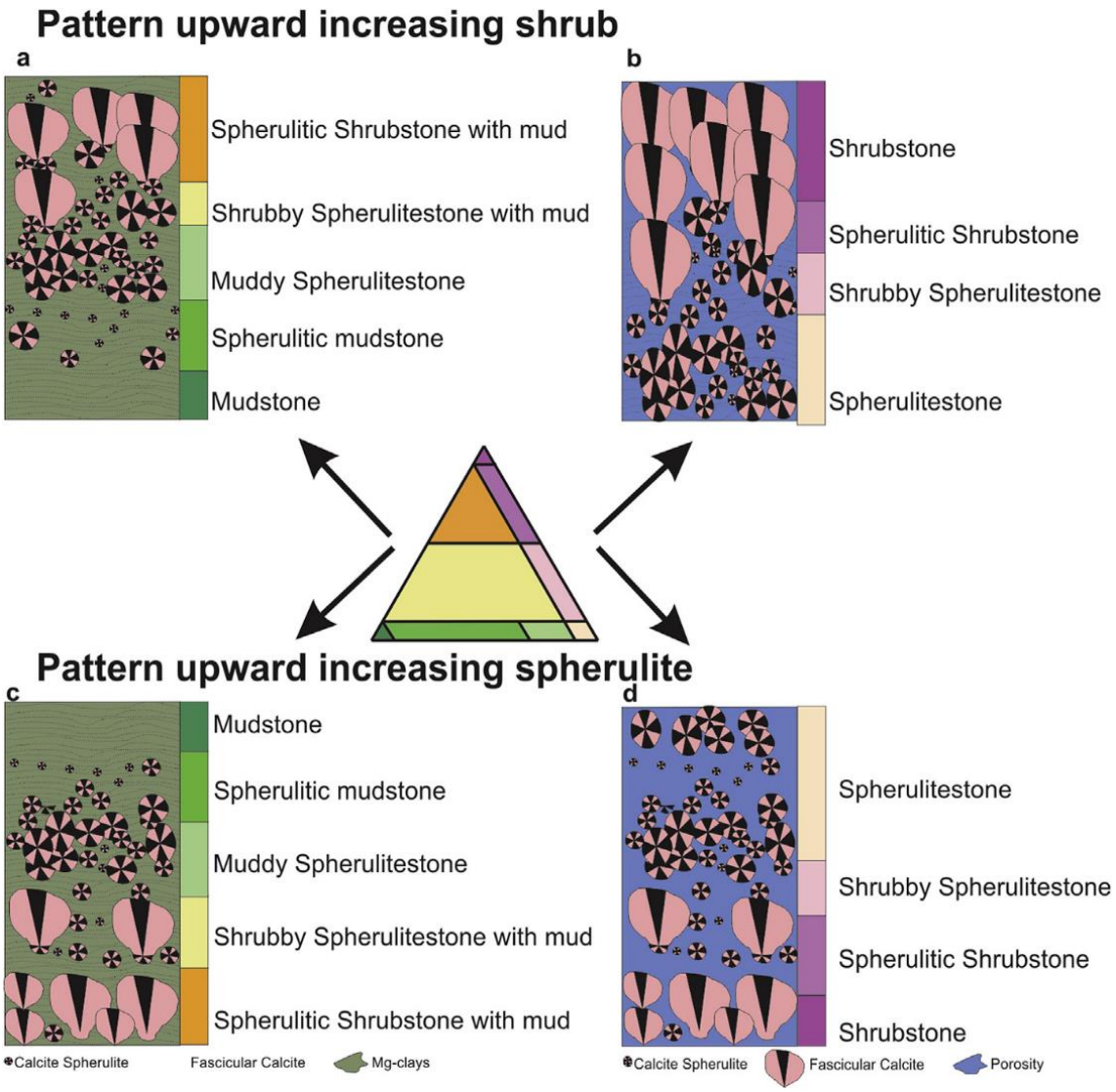

Figure 23: Two models (upward-increasing shrub and upward-increasing spherulite) of facies stacking for elementary cycles in the Barra Velha Formation based on core descriptions and two types of cycle. a) and c) non-reservoir and b) and d) reservoir. Source: Gomes et al. (2020).

These two alternative facies stacking patterns (Figure 23) suggested for a basic cycle within both reservoir and non-reservoir intervals can be interpreted using concepts derived from a traditional sequence stratigraphic approach for marine carbonate sediments based on the changes in water depth. In lacustrine systems changes in facies may be linked to water depth via physical controls such as the depth of wave-base,

biological controls such as the photic zone depth and/or chemical controls such as evaporative concentration (Gomes et al., 2020).

According to the concepts mentioned above, Gomes et al. (2020) proposed three possible types of environments where those facies succession were deposited. The first is the humid to arid climate model with lake-level fluctuation (Figure 24-a). In humid climate, it is assumed that the precipitation rate is greater than that of evaporation (P > E), so there would be an increase in the fluvial detrital input, and an increase in the lake level, resulting in lower concentration, dilution, and a drop in pH, then, with that there would be mudstone precipitation. In times of arid climate, it is assumed that the precipitation rate is lower than the evaporation rate (P < E), so there would be a reduction in the entry of fluvial detrital sediments and a drop in lake level, resulting in a lake with evaporative concentration and a rise in pH. These conditions would lead to precipitation of magnesian clays with spherulites and shrubs. This interpretation is a modification of the Wright and Barnett (2015, 2017) model incorporating the detrital grain distribution.

The second is the semi-arid to arid shallow lake climate model. In times of semi-arid climate, the precipitation rate is very close to the evaporation rate (P≈E), there is less aeolian detrital input (dust) and mudstone precipitation. In times of arid climate, the precipitation rate is lower than the evaporation rate (P < E), there is an increase of aeolian detrital input (dust), a reduction in the lake level, a rising in the pH of the lake, allowing the precipitation of shrubs and spherulite, and magnesian clays with spherulites growing therein, as seen in Figure 24-b. This interpretation is a modification of the model by Farias et al. (2019). According to Farias et al. (2019) the lakes were formed by hybrid brines that received influx from two sources: drainage brines containing HCO3 formed by the weathering caused immediately after the deposition of basalts and hydrothermal brines rich in CaCl2 formed by the reaction in depth between sea water and the basalt of the barrier by where the brine has infiltrated. So, these brines would have saturated the lake in CaCo3 (calcium carbonate).

The third is constant lake level controlled by spill point model. In this case, climate-induced changes alter the inflow of fluvial and aeolian detrital inputs, pH, and stratification of the lake. As it was possible to see in previous models, at times of lower pH the mudstones were more likely to precipitate, while when the pH was higher, that is,

the alkalinity increased, the environment was more prone to precipitation of magnesian clays with spherulites and shrubs (Figure 24-c).

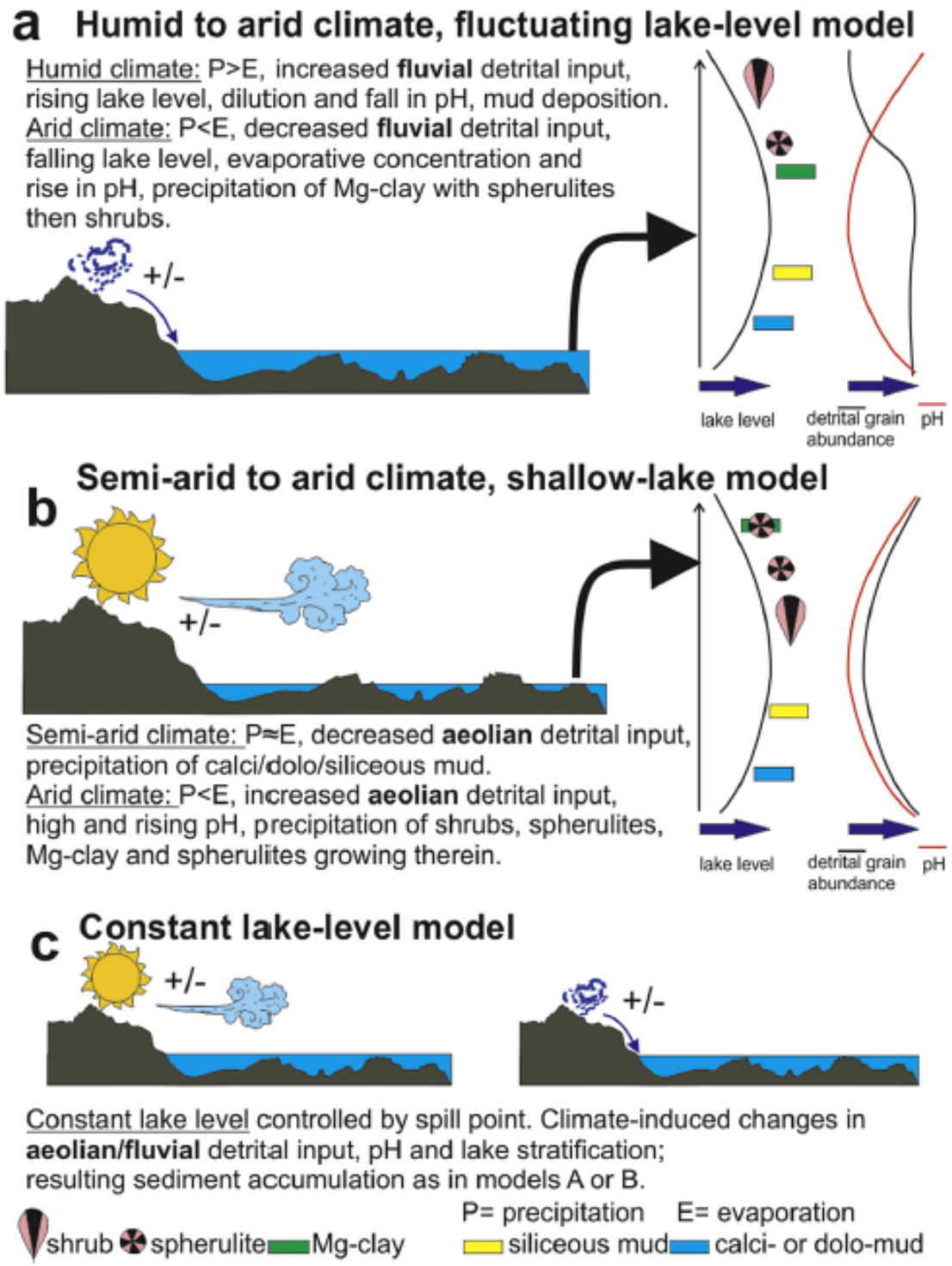

Figure 24: Alternative conceptual models to explain temporal variations of detrital material within the Barra Velha Formation: a) Humid to arid climate, fluctuating lake-level model. b) Semi-arid to arid climate, shallow lake model. c) Constant lake level controlled by spill point. Black arrows point at the stage of the model for the lake x-section. Source: Gomes et al. (2020).

Wright (2020) created a five-stage model (Figure 25) for the development of cyclothems (Figure 13) proposed by Wright and Barnett (2015) for Barra Velha Fm. In stage 1, the lake has waters with reduced alkalinity and salinity, introducing favorable conditions for the colonization of fish and ostracods. Also, the precipitation of silica in the form of gels is propitious, which would later form silica nodules. The accumulation of fine-grained carbonates implies deposition in a lower-energy setting, probably below wave-base (Figure 25-1). Stage 2 represents the point when evaporation triggered the formation and deposition of magnesium silicate gels, which would be the precursors of magnesian clays. These gels are assumed to have been deposited below the wave-base (Figure 25-2). In stage 3 there was the precipitation of calcite as spherulites within the magnesium silicate gels below the wave-base, and locally growing up-dip as shrubs where gels were not accumulating or had been removed by falling wave-base (Figure 25-3). Finally, in stage 4, the deposition of magnesium silicate gels ceased, allowing the growth of spherulites, reaching the sediment-water interface, which originated the shrubs and may also have occurred in shallower regions. Above the wave-base, it is common to find reworking of previously deposited facies (Figure 25-4).

As mentioned before, Herlinger et al. (2017) discuss the role of diagenesis in Macabu Fm. of the Campos Basin. The authors claim that the stevensitic deposits were mainly replaced by spherulites, dolomite and silica. Lima and De Ros (2019) agree and add that magnesian clays are easily dissolved and/or replaced. The primary porosity of the shrubs and the dissolution of stevensite constitute the main reservoirs of Macabu Fm. Wright and Barnett (2017) and Herlinger et al. (2017) mention that the Mg-matrix is later dissolved, preserving only syngenetic and eodiagenetic constituents, shrubs and spherulites, and generating secondary porosity. Therefore, the preservation, dissolution, and replacement of stevensite exert an important control on the quality of reservoirs. The dissolution of the stevensite provided magnesium and silica, favoring dolomitization and silicification, commonly observed in Barra Velha and Macabu formations (Herlinger et al., 2017). Wright and Barnett (2021), who carried out a study at Barra Velha Fm. in the Santos Basin confirm the fact that the dissolution of magnesian clays is a very important factor for the generation of porosity. Also, they state that the presence of silica and dolomite, in addition to magnesian clays, spherulitites, shrubs and reworked facies are common in the Barra Velha Fm. of the Santos Basin.

Thus, despite the great attention that Barra Velha Fm. has recently received in the academy, it is noticed that many aspects related to its origin and deposits still remain uncertain. Therefore, due to the complexity of the Barra Velha Fm., further analysis of various aspects of its constitution would still be needed.

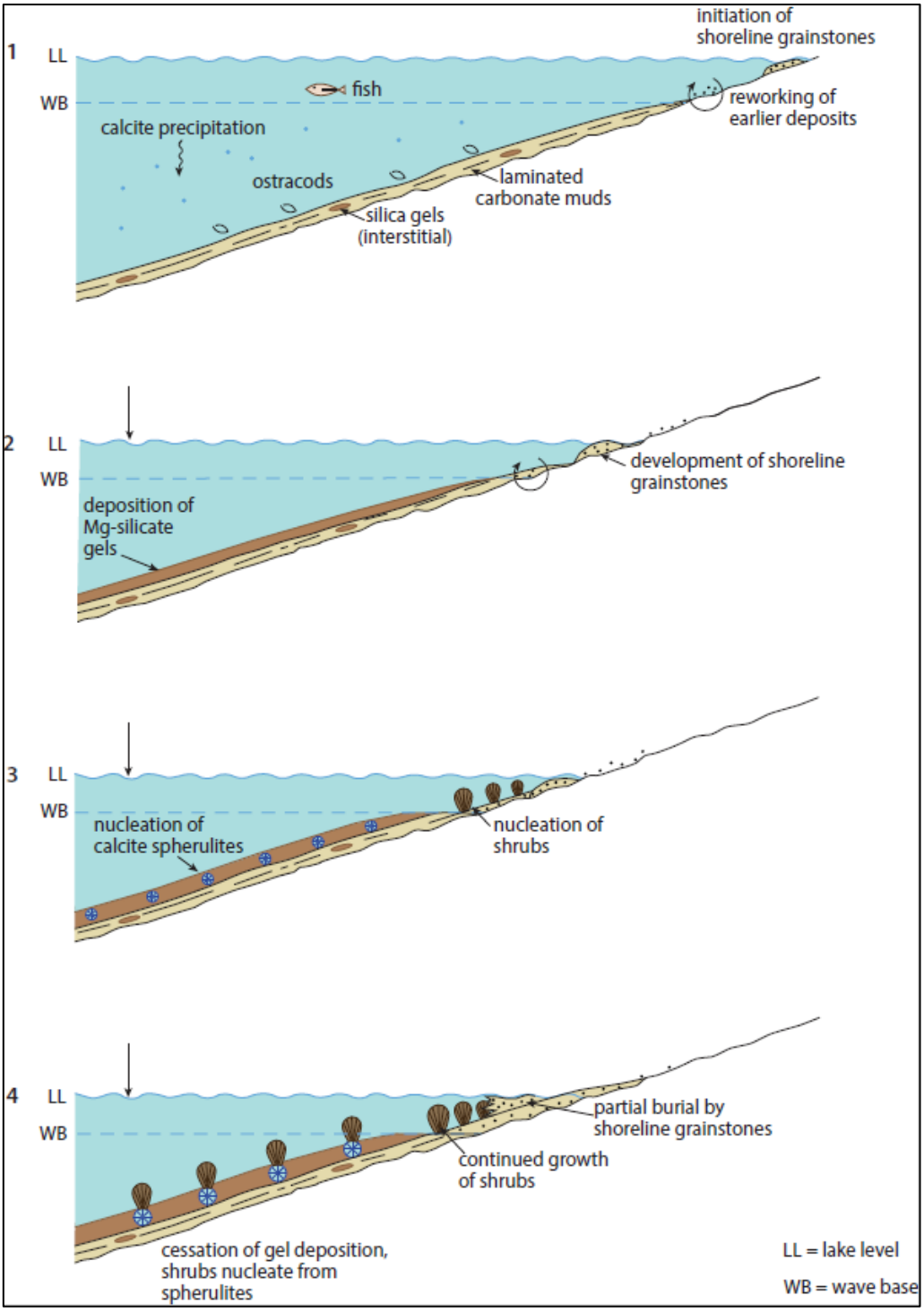

Figure 25: Model proposed by Wright (2020) for the cyclothems from Wright and Barnett (2015) of Barra Velha Fm., Santos Basin. WB: Wave base, LL: lake level. Vertical black arrow: Shallow depth of lake compared to stage 1. Source: Wright (2020).

3. Flow units classification

A flow unit (FU) is a stratigraphically continuous interval of similar reservoir process speed that maintains the geologic framework and characteristics of rock types. Rock type are representative reservoir units with a distinct porosity-permeability relationship. These units are deposited under similar conditions, and they have experienced similar diagenetic processes (Gunter et al., 1997).

Reservoir rock typing is an important step in any reservoir characterization and modeling study. By definition, a rock type is defined as a set of properties that several rocks have in common. The rock type attributes can be sedimentary (such as lithology, fossil content, sedimentary textures, diagenesis, or general microfacies), petrophysical (electrical logs), or reservoir parameters (porosity, permeability, and capillary pressure). Generally, it can be stated that any meaningful classification of reservoir rocks, which differentiates and describes them based on special characteristics of the reservoir, can be attributed to rock typing. Such characteristics could be related to sedimentary attitudes (sedimentary rock typing), petrophysical well logs (electrofacies), pore system properties (flow unit), as well as can be extended to seismic data (seismic facies). In fact, the rock typing technique can effectively be used for unraveling the reservoir heterogeneity, for describing the reservoir zones, and for the interpretation of fluid flow within the reservoir (Kadkhodaie and Kadkhodaie., 2018).

Rock typing into flow units (FU) plays a decisive role in the construction of static and dynamic models of an oil field. A better understanding to predict how liquids will infiltrate the subsurface during the reservoir's life cycle is needed in order to make the best decisions. Reservoir characterization through flow units is an effective way to simulate fluid movement and oil-production performance within the geological nature. For this reason, it is important to understand the variability and spatial distribution of petrophysical properties along a reservoir. Understanding these variations of pore geometry in distinct lithofacies is crucial to improve reservoir description and exploration. Each porosity within a rock type, can generate a permeability variation of several orders of magnitude, indicating the existence of multiple flow units. In carbonate settings, dealing with rock typing is complex and can generate a large quantity of units because of diagenetic processes such as dissolution, cementation, and silicification. (Penna and Lupinacci, 2020).

The concept of flow units was first proposed by Hearn et al (1984) where he defined the flow units (FUs) as a reservoir zone that is laterally and vertically continuous, having similar permeability, porosity, and bedding. Ebanks (1987) stated that the FUs represents mappable portions of an elementary volume of the total reservoir rock in which the geological and petrophysical properties that affect fluid flow rate, are internally consistent, and predictably different from properties of other rock volumes. Qiu et al. (1996) consider that flow unit is a naturally occurring fluid flow channel due to the heterogeneity of the reservoir, the baffle, and the by-pass conditions. Mu et al. (1996) state that flow unit is a reservoir unit that is consistent with percolation characteristic due to boundary constraints, discontinuous thin barrier layers, various sedimentary micro-interfaces, small faults, and permeability differences within an oil body. Gunter et al (1997) claimed that is a continuous stratigraphic range with similar reservoir process velocities that honor the geological structure while maintaining facies characteristics. Dezfoolian (2013) said that variations in pore geometrical attributes can define the existence of distinct zones with similar fluid flow characteristics. Finally, Tiab and Donaldson (2000) said that a flow unit consists of a continuous body, along a specific reservoir volume, where the petrophysical and fluid properties are practically constant, uniquely characterizing its static and dynamic communication with the well. Tiab and Donaldson (2004) add that a FU may be composed of one or more lithologies, it is correlatable at the interval scale, recognizable from wire-line data, and may be hydraulically connect to other flow units.

Among the available methods for identifying flow units and Rock/Pore Types in many reservoir settings, it can highlight: (1) the Lorenz curve, (2) the K/Phie ratio isoline graph, (3) Winland R35 (Rock/Pore Types) and (4) RQI and FZI (reservoir quality index and flow zone indicators) (Nascimento, 2015). However, on this present study, we use the method proposed by Penna and Lupinacci (2020) that consists of a modification of the classical flow zone indicator (FZI) permeability vs. porosity rock typing, analyzing a cumulative S-curve like the Lorenz method.

This section will briefly present a bibliographic review of the main methods used to estimate Flow Units such as Flow Zone Indication (FZI) (Amaefule and Altunbay, 1993) and Lorenz by discretization of the cumulative permeability S-curve. The focus will be on the FZI method that was the one used in this work.

Heterogeneous and non-uniform systems are formed by multiple homogeneous groups of FU. The premise for this grouping is the similarity in flow characteristics which are affected by grain size, sorting, texture (packing, angularity, grain shape, homogeneity), mineralogy, cementation, bedding contacts, permeability barriers, clay content, pore size, pore distribution, tortuosity, and by petrophysical properties such as porosity, permeability, and capillary pressure. Therefore, the depositional environment and diagenesis control the hydraulic properties of rocks, and consequently, the reservoir quality control (Altunbay et al., 1994 and Amaefule et al., 1993).

All rock typing methods mentioned above have pros and cons, especially considering the complexity degree of the geological setting and the quantity of data available. Nevertheless, all share a similar limitation: the lack of integration with different resolutions and data scales. In several examples, rock typing can quantify small-scale flow characteristics in the core and well-log domain but fails when extrapolate these properties to the whole reservoir (Penna and Lupinacci, 2021).

3.1. Lorenz Method

Lorenz (1905) developed an equation with the aim of describing the inequality of wealth distribution of a population using a graphical representation of income distribution. This concept is appropriate to use in different areas of competence to describe how heterogeneous is the sample space. From that, many authors have used this method in petrophysics.

The traditional Lorenz coefficient used in reservoir property modeling focuses on a plot of cumulative flow capacity (Fm) against cumulative thickness (Hm), which are represented for Equation (1 below (Schmalz and Rhame, 1950; Craig, 1972; Lake and Jensen, 1991; Zahaf and Tiab, 2002):

$$Fm = \frac{\sum_{i=1}^{i=m} k_i h_i}{\sum_{i=1}^{i=n} k_i h_i}, \qquad Hm = \frac{\sum_{i=1}^{i=m} h_i}{\sum_{i=1}^{i=n} h_i}, \tag{1}$$

where k is the cumulative flow capacity and h is the depth.

According to Fitch (2013), two alternative versions of Lorenz method were developed: the first one using porosity and permeability directly and the second one using a single property against depth increment. The basic technique is the same for each method, i.e., to calculate the Lorenz coefficient. The cumulative of a certain property (e.g., cumulative flow capacity, permeability, or porosity) sorted from low to high values,

is plotted on the y-axis, and a second cumulative of another property (e.g., storage capacity, porosity, or depth increment) is plotted on the x-axis (Figure 26). In a purely homogeneous formation, the two cumulative properties will increase by a constant value, giving a straight diagonal line of perfect equality (grey line in Figure 26). An increase in the heterogeneity of the property will move the Lorenz curve further away from the line of perfect equality. The Lorenz coefficient (Lc) is calculated as twice the area between the Lorenz curve and the line of perfect equality, a purely homogeneous system returns a Lc value equal to zero, and a heterogeneous system return a Lc value greater than zero, close to one.

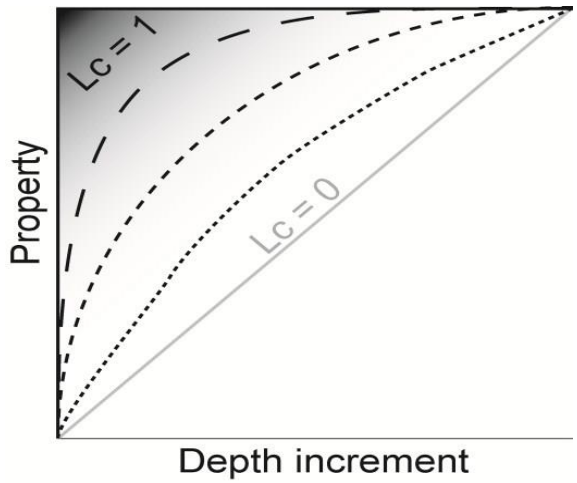

Figure 26: Schematic illustration of a Lorenz plot. A cumulative of a property (flow capacity, permeability, or porosity), sorted from in descending order (y-axis) and a second cumulative property storage capacity, porosity, or depth increment) is plotted on the x-axis. The diagonal straight line (grey one) corresponds to the line of perfectly equality, Lc=0, and the other lines represent Lorenz curves for increasing Lc values until get to Lc=1 (black lines) (Source: Fitch et al., 2013).

Lorenz coefficients provide a simple, graphic-based, approach to visualizing and quantifying heterogeneity in a dataset. As heterogeneity can only alternate between zero and one, different datasets can be easily compared regardless the scale of original measurements. The traditional method, normalizing data according to sample thickness, is generally used for investigations of porosity and permeability heterogeneity in core measurements (Schmalz and Rhame, 1950; Craig, 1971; Lake and Jensen, 1991; Zahaf and Tiab, 2002). Sample heterogeneity will be influenced by its size (Lake and Jensen, 1991; Dutilleul, 1993), that is why this normalization is extremely important in core studies.

Quantifying heterogeneity in the continuous data allows a complete reservoir succession to be analyzed, capturing the impact of bed thickness in controlling the proportion and range of porosity and permeability values. Estimating heterogeneity from core plugs alone would inevitably not provide an understanding of the formation.

Therefore, the Lorenz coefficient can be used as a measure of heterogeneity in a dataset to obtain a single value of numerical variation where zero is homogeneous and one is maximum heterogeneity. Also, can be used to compare data from different tools (measuring either the same property or different properties), data at different scales of measurement, and data for different reservoir types.

In petrophysical studies, the Lorenz plot is modified to variables as flow capacity (or permeability) versus storage capacity (or porosity).

3.1.1 Stratigraphic modified Lorenz plots (SMLP)

According to Gunter et al. (1997), the Stratigraphic Modified Lorenz Plot can evaluate the number of FUs according to cumulative storage capacity vs. cumulative flow-capacity S-curve, ordered in the stratigraphic sequence. If the data is continuous (smoothed), it should be constructed using every sample available. It offers a guide as to how many flow units are necessary to honor the geologic framework. The equation to calculate a unique value of cumulative flow capacity (k_H) is:

$$k_H = k_1 (H_1 - H_2) + k_2 (H_2 - H_3) + \cdots k_i (H_i - H_{i+1}), \quad (2)$$

where the term $(H_i - H_{i+1})$ is the depth difference between following samples i and $i + 1$. An analogous equation calculates the cumulative storage (φ_H) capacity:

$$\varphi_H = \varphi_1 (H_1 - H_2) + \varphi_2 (H_2 - H_3) + \cdots \varphi_i (H_i - H_{i+1}), \quad (3)$$

The slope variation analysis in the segments of the k_H vs φ_H plot is interpreted as the main flow units in the dataset. Steeper parts of the curve are called “speed zones” and relates with better quality facies in terms of flow capacity. On the other hand, flat segments shall be interpreted as seals or baffles zones.

According to Gunter et al. (1997), the shape of SMLP curve is indicative of the flow performance of the reservoir, and the final flow units should retain this character (Figure 27). Segments with steep slopes have a greater percentage of reservoir flow capacity (or permeability) relative to storage capacity (or porosity), and, by definition, have a high reservoir process speed. They are called speed zones. Segments with neither

flow nor storage capacity are seals or baffle zones. Preliminary flow units (speed zones, baffles, and seals) are interpreted by selecting changes in slope or inflection points (Figure 28).

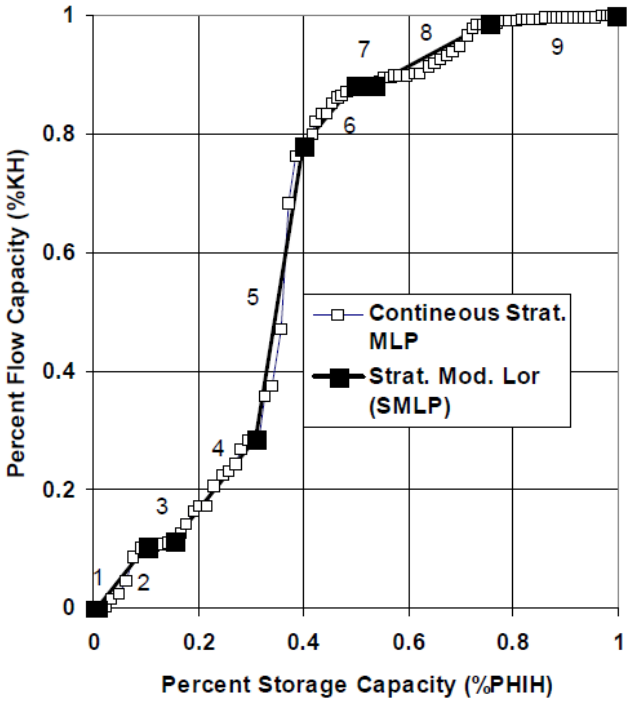

Figure 27: Interpreted continuous Stratigraphic Modified Lorenz Plot (SMLP) (Source: Gunter et al., 1997).

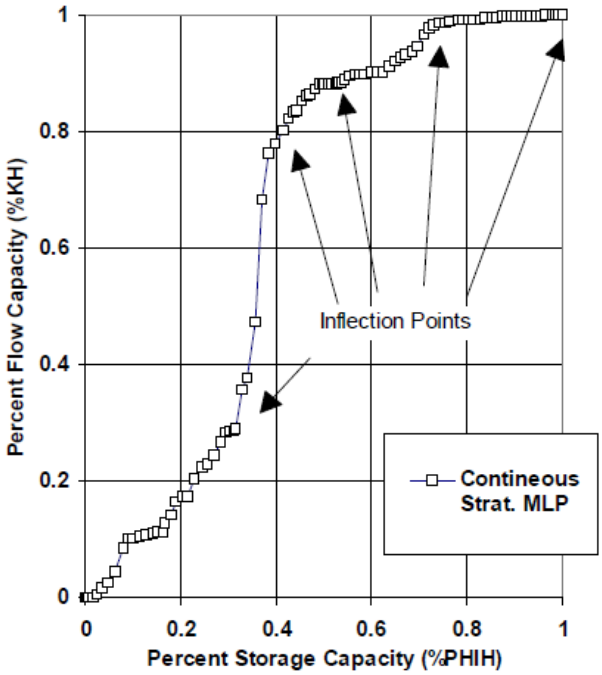

Figure 28: Uninterpreted SMLP (Source: Gunter et al., 1997).

Storage capacity and flow capacity were calculated for the Barra Velha and Itapema formations using the Eqs. 2 and 3 rearranging the data in crescent-depth values.

Then, the SMLP was built plotting the normalized values of both variables, as shown in Figure 29 (Penna and Lupinacci, 2021).

Analyzing the slope variation of the curve in Figure 29, Penna and Lupinacci (2021) deduced a minimum number of four main FUs (black lines, lower orders) for the reservoir of the Mero Field, although it was possible to observe more FUs as a higher-order variation (green lines). To ensure a good correlation of obtaining flow units with the available spatial data, in this case, the seismic data that has a lower vertical resolution, the number of four flow units was considered ideal. Furthermore, the amount of flow units found in the literature is restricted to four or five when the intention is to make an upscale to the seismic domain.

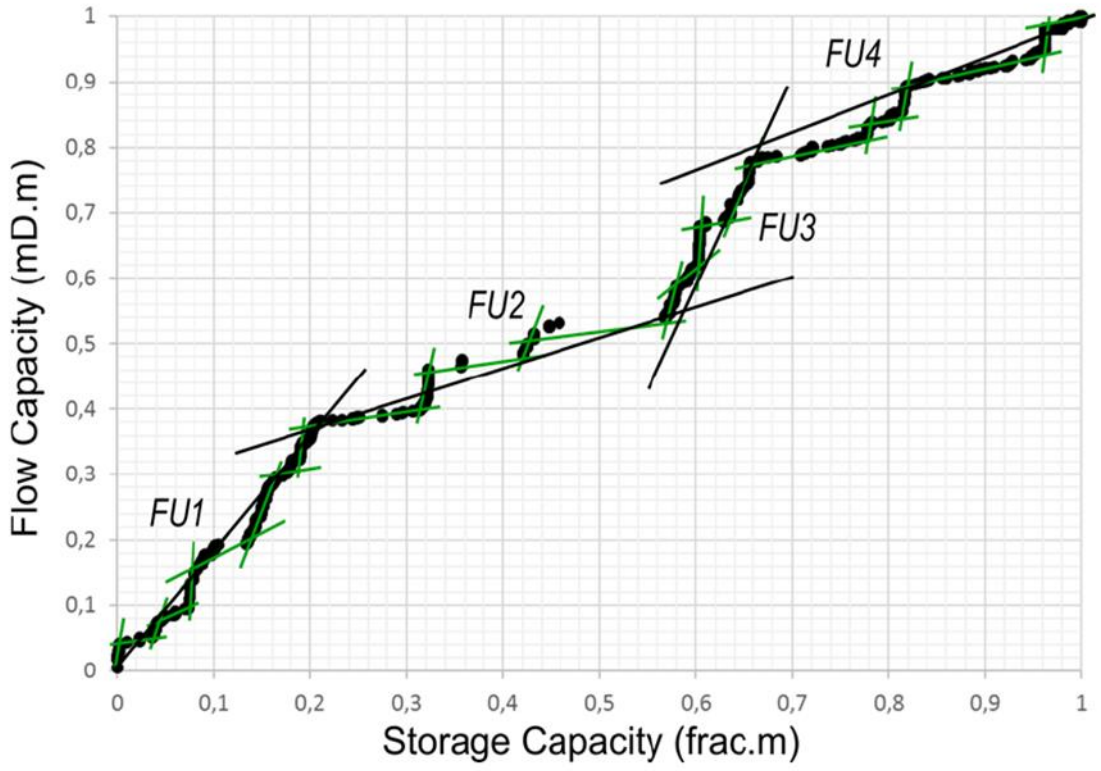

Figure 29: Stratigraphic Modified Lorenz (SMLP) plot from the core permeability and porosity laboratory samples. The high orders of flow units are represented by green lines and the lower order by black lines (Source: Penna and Lupinacci, 2021).

Penna and Lupinacci (2020) proposed an approach from the Lorenz method to analyze a cumulative S-curve of permeability vs. porosity, which removes vertical core and plug sampling bias present in Eqs. (2 and(3. The graphic shown in Figure 30 was constructed by porosity values sorted in increasing order and the sum of its corresponding permeability. Then, the porosity cut-offs values to discretize the LPFU (Lorenz Plot flow units) analyzing the changes of the S-curve slope, was determined.

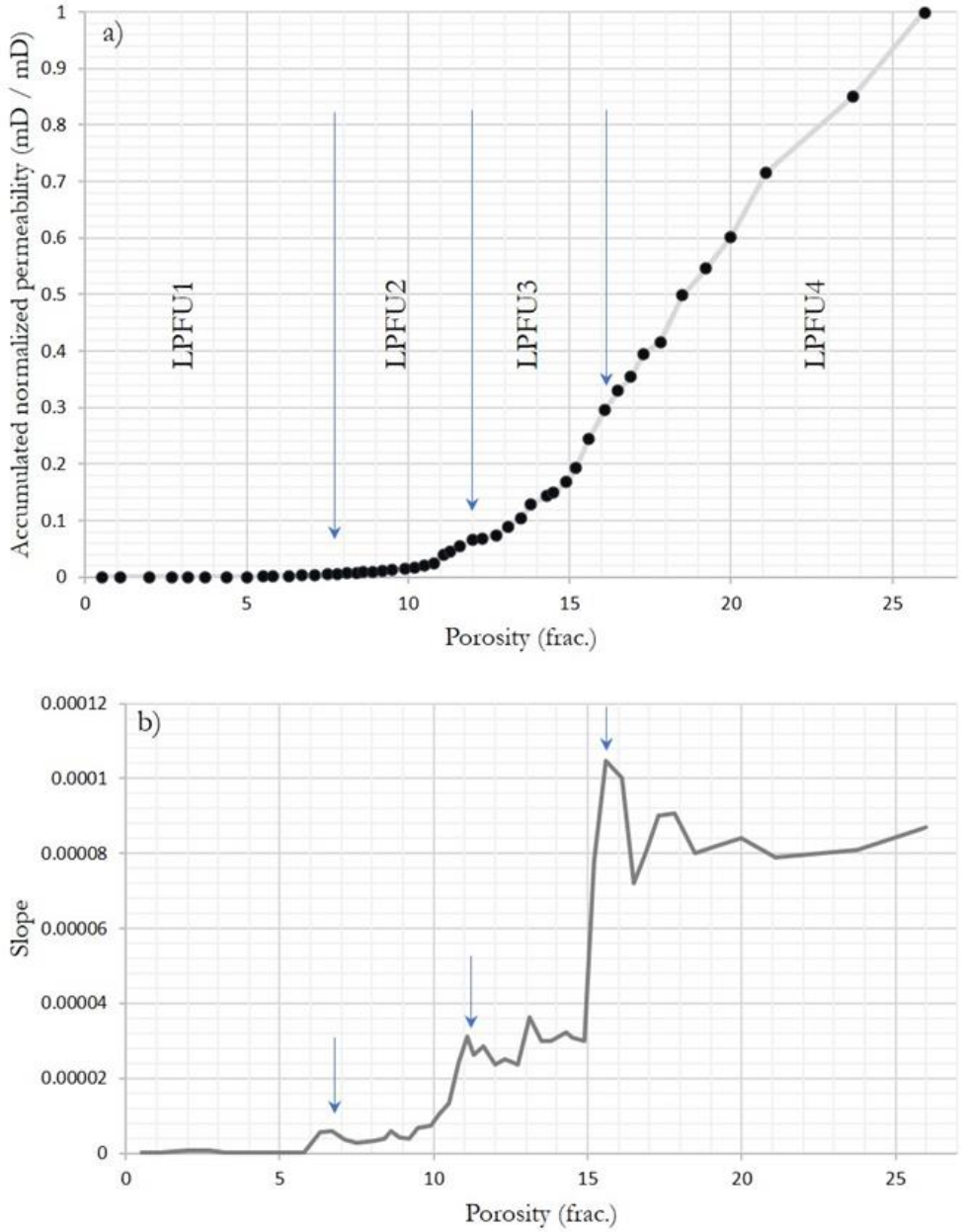

Figure 30: a) Cumulative permeability S-curve plot for the modified LPFU classification; b) the porosity cutoffs to discretize the LPFUs were interpreted as the major changes in the slope (Source: Penna and Lupinacci, 2020).

It is possible to note that as seen in the SMLP (Figure 29), the cumulative S-curve (Figure 30) also suggests a larger number of FUs to the reservoir. However, Penna and Lupinacci (2020) chose to interpret only major changes in flow performance (i.e., greatest slope variations in the Lorenz plots).

Thus, to construct the Lorenz's S-Curve, the following steps were used: (a) calculate percentiles of the porosity and permeability core and plug dataset; (b) sort porosity values in increasing order; (c) accumulate and normalize the percentiles of permeability values; and finally (d) calculate the slope of the curve for each sample.

The interpretation of each LPFU calculated by Penna and Lupinacci (2020) showed in Figure 30 is like the one described above by Gunter et al. (1997). Given this, LPFU1, where the curve does not show any detachment from the horizontal axis and none or little cumulative permeability, can be considered a flow barriers or no-flow zones in reservoir dynamic modeling. LPFU2 is interpreted as the beginning of the curve detachment from the X-axis until the first ramp up of the line. This unit also has little storage capacity but shows a better flow capacity than the first. LPFU3 and LPFU4 are interpreted as the following meaningful changes in the slope, having better porosity and permeability properties. LPFU3 indicates medium to good reservoir facies in terms of fluid performance, with porosities varying from 11 to 15%, decent flow capacity. Finally, LPFU4, presenting a steeper ramp (speed zone), is the best FU, and significantly contributes to the reservoir-flow performance. Table 1 describes the cut-off ranges used considering the classification in both the Barra Velha and Itapema formations.

Table 1 : FU and porosities cut-offs used in the S-curve of Figure 30.

	Porosity cut-offs
LPFU1	below 6 %
LPFU2	6 to 11 %
LPFU3	11 to 15 %
LPFU4	above 15 %

3.2. Fluid Zone Indicator (FZI) Method

Knowledge of porosity and permeability distribution is crucial to effectively define a reservoir. Many authors have noted the relevance of these parameters, both for planning and operating completion strategies and for building representative simulation models for successful reservoir management (Shirer et al., 1978; Stiles et al., 1988; Chopra et al., 1987).

Since Amaefule and Altunbay (1993) have introduced the flow zone indicator (FZI) concept based on the Carman-Kozeny model, FZI is widely used to classify rocks with similar flow behavior in reservoirs settings. Studies have shown that the FZI is mostly related to petrophysical properties, such as porosity, permeability, surface area, pore size distribution, mean pore-throat size and nuclear magnetic resonance relaxation (NMR) data (Ohen and Ajufo, 1995; Basbug and Karpyn 2007; D'Windt et al., 2018, Dezfoolian, 2013). FZI is considered a robust method of permeability estimation and reservoir prediction in terms of flow heterogeneities due to petrophysical correlations between permeability and flow units.

On the classical plot, the relationship between permeability and porosity is not causal. Whereas porosity is generally independent of grain size, permeability is strongly dependent on grain size. For example, in a reservoir, porosity and permeability may be directly proportional. However, in the same reservoir, there may be both high and low permeability zones with equal porosity values. Therefore, the traditional plot cannot be used reliably to estimate accurate permeability from porosity data. Several researchers have noticed the inadequacy of this classical approach and have proposed alternative models for relating porosity to permeability (Stiles et al., 1988; Dorfman et al., 1990; Dubrule and Haldorsen, 1986; Timur, 1968; Wendt et al., 1986). It can be concluded that combinations of different for any given rock type, the different porosity/permeability relationships are evidence of the existence of different hydraulic flow units (HFUs). Therefore, FZI depends on depositional texture and mineralogical content (Dezfoolian, 2013).

The hydraulic quality of a rock is a function of mineralogy (i.e., type, abundance, morphology, and location relative to pore throats) and texture (i.e., grain size, grain shape, sorting, and packing). Alterations of these geological attributes usually indicate the existence of distinct rock units with similar pore throat attributes (Dezfoolian, 2013).

Their characterization is vital to accurate zoning of reservoirs into units with similar hydraulic properties. The mean hydraulic unit radius (r_{mn}) concept showed in equation below is the key to unraveling the hydraulic units and relating porosity, permeability, and capillary pressure (Bird et al., 1960):

$$r_{mn} = \frac{\text{Cross Sectional Area}}{\text{Wetted Perimeter}} = \frac{\text{Volume Open to Flow}}{\text{Wetted Surface Area}}, \quad (4)$$

Koseny (1927) and Carman (1937) considered the reservoir rock to be composed of a bundle of capillary tubes due the concept of the mean hydraulic radius. The mean hydraulic radius can be related to the surface area per unit grain volume (S_{gv}), effective porosity (φ_e), tortuosity (τ) and permeability (k) as follows:

$$k = \frac{\varphi_e^3}{(1-\varphi_e)^2}\left[\frac{1}{2\tau^2 S_{gv}^2}\right], \quad (5)$$

Then, the generalized form of Koseny-Carman relationship is:

$$k = \frac{\varphi_e^3}{(1-\varphi_e)^2}\left[\frac{1}{F_s\tau^2 S_{gv}^2}\right], \quad (6)$$

where F_s is the shape factor (2 is for a circular cylinder). The term $F_s\tau^2$ has been classically referred to as the Koseny constant. This constant is variable and varies between hydraulic units but is constant within a given unit.

The problem of the variability of the Kozeny constant is addressed dividing both sides of Eq. (6 by effective porosity (φ_e) and taking the square root of both sides:

$$\sqrt{\frac{k}{\varphi_e}} = \left[\frac{\varphi_e}{1-\varphi_e}\right]\left[\frac{1}{\sqrt{F_s}\tau S_{gv}}\right], \quad (7)$$

where k is in μm^2.

However, if permeability is presented in millidarcies, then the following parameter can be defined:

$$\text{RQI}\ (\mu m) = 0.0314\sqrt{\frac{k}{\varphi_e}}, \quad (8)$$

with:

$$\varphi_z = \frac{\varphi_e}{1 - \varphi_e}, \quad (9)$$

where RQI (μm) is the Reservoir Quality Index and φ_z is defined as the pore volume-to-grain volume ratio.

The FZI rock typing is a more complex estimate than Lorenz approach because considers the tortuosity, mean hydraulic radius, surface area per unit grain volume, porosity, and permeability (Amaefule and Altunbay, 1993). Finally, the Flow Zone Indicator (FZI), that is a useful approach to describe the porosity and permeability of a pore system (Amaefule et al., 1993), is defined by:

$$\mathrm{FZI} = \frac{1}{\sqrt{F_s}\tau S_{gv}} = \frac{\mathrm{RQI}}{\varphi_z}, \quad (10)$$

where FZI is in μm.

Besides that, the FZI equation indicates that for any hydraulic unit, on a log-log plot of RQI vs. φ_z, all samples will lie on a straight line with the same unit slope. Samples with different FZI values will lie on other parallel lines. The value of the FZI constant can be determined from the intercept of the unit-slope straight line at $\varphi_z = 1$. Samples that lie on the same straight line have similar pore throat attributes and, thereby, constitute a hydraulic unit (Shenawi et al., 2009).

In short, the FZI is intrinsic to a reservoir and is such that rocks or associations of rocks with identical values are expected to have identical hydraulic behaviors. According to Amaefule et al. (1993), it is a unique parameter that incorporates different lithological attributes in the discrimination of distinct pore geometries and facies. Rocks with a narrow range of FZI values belong to a single hydraulic flow unit, i.e., they have similar flow properties (Prasad, 2003; Kadkhodaie-Ilkhchi and Amini, 2009). Besides, in this method, the greater the magnitude of the FZI (which is directly proportional to the permeability), the better the flow unit (better permoporosity).

3.2.1. Modified fluid zone indication (FZI) classification

Graph analysis is enough to discretize the sample space into “n” flow units. Shenawi et al. (2009) introduced a way to automate and minimize display errors, from a notation named Hydraulic Units (HU):

$$\mathrm{HU} = \mathrm{Round}\,[\,2\,.\ln(\mathrm{FZI}) + 10.6], \qquad (11)$$

Once the hydraulic units are calculated, each rock sample, represented by the pair φ_e and k, will have a value of HU. Samples with the same HU value are grouped (each group has a different coloration) so that the different flow units (FU) are individualized (Figure 31). The best flow units are those that have the highest magnitudes of "HU", which is directly proportional to permeability (Nascimento, 2015).

As it was already seen, the FZI classification is a common method of reservoir rock typing into flow units. The reservoir quality index (RQI), detailed in Eq. 8, is the net result of the porosity contribution to the permeability, which, sometimes, are ruled by the pore size, shape, and distribution. RQI and FZI are the key parameters for measuring the potential of the petrophysical properties of a rock sequence, assessing the ability of the reservoir for storing and accumulating hydrocarbons (Li et al., 2017). Nevertheless, diagenetic factors can obliterate the primary porosity or generate connected or isolated karsts and vuggy structures. As previously seen, studies in pre-salt of the Campos and Santos Basin show how the balance between dissolution and neomorphism, redeposition of sediments into deep lacustrine settings, replacement of minerals, dolomitization, silicification, and dissolution affect many levels of porosity in Brazilian carbonate rocks (Herlinger et al., 2017; Wright and Barnett, 2018; Lima and De Ros., 2019; Chinelatto et al., 2020; Gomes, 2020, among others).

Considering the high level of heterogeneity in the pre-salt carbonate reservoirs, Penna and Lupinacci (2020) built a semi-log graph from the data obtained from the typical FZI /RQI rock typing workflow (Eqs. 8 and 10) in the Barra Velha and Itapema formations. It is possible to see the large amount of flow units generated shown in Figure 31.

Working with this amount of FU during the construction of the geologic and dynamic modeling is categorically problematic since the FUs often do not correlate with the stratigraphic depositional facies and 3D modeling trends are usually made in most reservoirs characterization. Penna and Lupinaci (2020) preferred to discretize FZI rock typing in a permeability cumulative S-curve, using percentiles of the k and φ_e dataset (Figure 32-a) and analyzing the slope variation (Figure 32-b), like the workflow described in the Lorenz method section. Both workflows are equivalent, apart from the fact that the FZI value itself is an estimate of the pore throat size. To create the FZI S-curve, it is

necessary to do the following steps: a) calculate porosity and permeability percentiles of the core and plug dataset; b) calculate the RQI and FZI using Eqs. 5 to 10 and the percentiles values; c) order the data with increasing values of log(FZI); d) accumulate and normalize the percentiles of permeability values; e) calculate the slope of the curve for each sample.

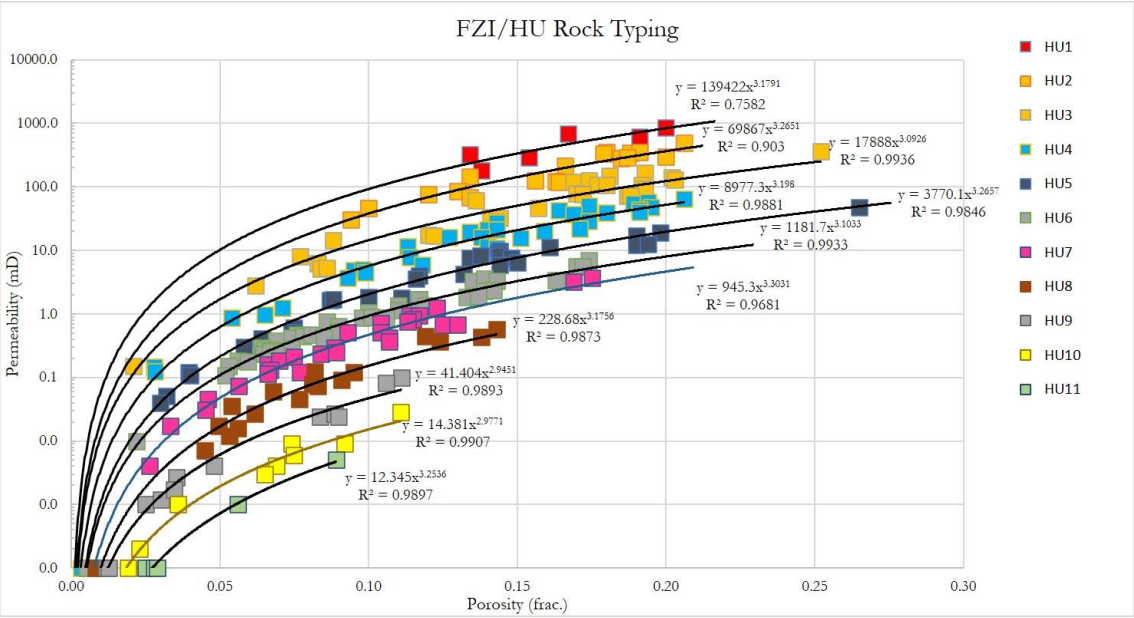

Figure 31: Usual FZI/HU workflow applied in the pre-salt carbonate reservoirs, calculating 11 hydraulic units in the Barra Velha and Itapema formations, (source: Penna and Lupinacci 2020).

Figure 32 shows the S-curve percentiles plot of permeability versus log(FZI). The FUs were discretized by analyzing the values of log(FZI) corresponding to major changes in the slope, like what have done to the Lorenz plot. Four major flow units were identified and named FZI1, FZI2, FZI3, and FZI4 (Penna and Lupinacci, 2020).

FZI1 corresponds to the initial flat segment of the curve, with poor flow performance and, probably, a barrier or baffle zone. FZI2 relates to the initial detachment of the curve, with reduces but considerable flow capacity in the seismic scale. FZI3 relates to the first ramp up after the FZI2 cut-off value, and an increasingly steep curve. This is the higher point of permeability of the reservoir rock. FZI4 corresponds to the better flow characteristics and relates with the final step of the S-curve. Table 2 summarizes the log(FZI) cut-offs rock typing according to the S-curve values, taken from Figure 32, using the FZI method (Nascimento, 2015; Penna and Lupinacci, 2021).

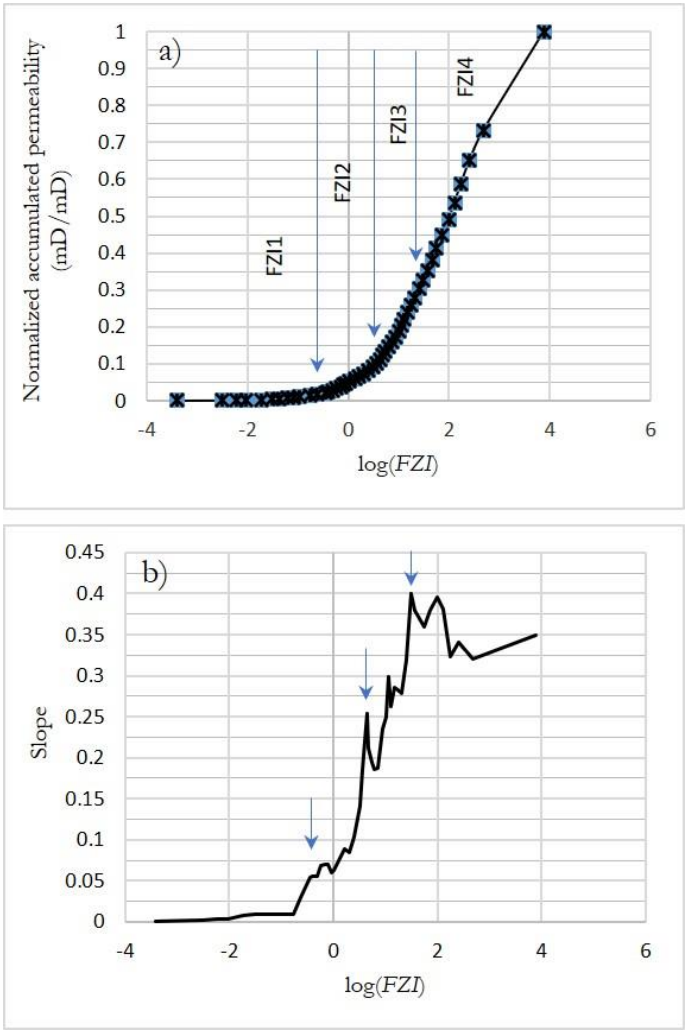

Figure 32: (a) Cumulative permeability S-Curve plot; (b) The log(FZI) cut-offs to discretize the FUs were interpreted as the major changes in the slope.

Table 2: FU and log(FZI) cut-offs used in the S-curve of Figure 32.

	Log(**FZI**) values
FZI1	below -0.5
FZI2	-0.5 to 0.67
FZI3	0.67 to 1.49
FZI4	above 1.49

Analyzing each variation of the slope in Figure 32, it would be easy to find 11 FUs or more. However, it is important to interpret only the main changes in the percentiles of the cumulative S-curve, because when thinking about using the flow units on a larger scale, without losing resolution, it is necessary to limit the number of FUs to be used, making them more likely to be subsequently detected in seismic volumes.

4. Methodology

This chapter details the entire workflow performed in the dissertation, including the methodology and procedures executed to estimate the flow facies in the carbonate reservoirs of the Barra Velha and Itapema formations. For this, data from four wells and a post-stacking seismic volume migrated at depth (PSDM) from a field located in the Santos Basin were used. The rock and well data are composed of geophysical well-logs, sidewall and core sample descriptions, thin sections description, and some pictures from core and sidewall samples provided by ANP. From the integration of these data, it was possible to obtain reliable parameters and relevant results to the evaluation and estimation of flow facies.

The methodology used in this work is presented in chronological order, aiming to identify and refine possible problems that may influence the final product, which is the flow facies estimation. All steps of the workflow were carried out for four wells (wells A, B, C, and D). These wells were chosen based on the greater availability of the rock description and, chiefly, the elemental capture spectroscopy logs (ECS) of calcium, magnesium, and silica, to identify their impact on the flow facies, as well as to integrate them with the other geophysical well-logs more effectively.

4.1. Rock typing into flow units

Rock typing into flow units (FUs) plays a pivotal role in constructing static and dynamic models of petroleum reservoirs. FU is an important technique to define flow heterogeneities and produce reliable estimates of petrophysical properties such as porosity and permeability. The FUs are grouping into facies with the same petrophysical characteristics, regardless of their geological deposition configuration or lithological definition.

This section will discuss and show which methodology was chosen to estimate the Flow Units, the singularities of this method, and the effort to find the one that could best fit given the geological configurations and particularities of the field studied. Besides that will display how the qualitative and quantitative results obtained through the flow units in the wells are generated and their correlation to the elemental capture spectroscopy logs (ECS) of calcium, magnesium, and silica, as well as gamma-ray, clay volume, and acoustic impedance logs. Then, the evaluation of how the flow facies behave in a correlation between petrophysical and elastic parameters will be presented, and, finally,

the extrapolation of the flow facies to the seismic scale and the Bayesian classification of these facies will be made. Figure 33 summarizes all the steps performed during the process of estimating the flow facies of the Barra Velha and Itapema formations in the four wells analyzed in this work.

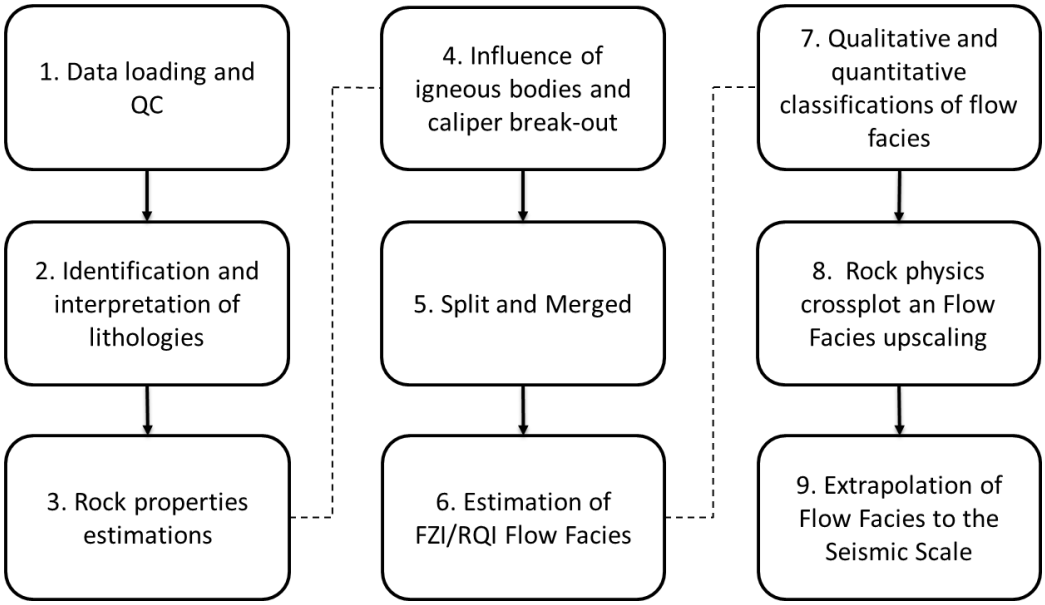

Figure 33: Workflow adopted for the preparation of this work.

4.1.1. Data loading and quality control

The first stage of the rock typing into flow units consisted of loading the curves and analyzing the quality of data for each well in the study area.

Subsequently, the curve depths were verified. Well-logs from different datasets are often not correctly aligned at all depths due to the difficulty of depth control during acquisition. Thus, some curves showed the need to carry out the depth adjustment performed through comparison with a reference curve based on the depth information for each formation found in the well reports provided by ANP. In Well D, it was necessary to adjust the depth of 11cm downwards in the ECS logs (Mg, Ca, and Si) and nuclear magnetic resonance (total and effective porosity, permeability, and free fluid) logs. In Well A, it was also necessary to adjust the ECS curves (Mg, Ca, and Si) and the permeability curve by NMR. The depth adjustment in this well was done by merging the curves performed in different runs, thus reaching the depth present in the well reports.

An important aspect verified in this step was the sampling rate of each curve. To execute the calculation of several parameters, such as clay volume, porosity, permeability and to perform crossplots and charts, the input curves need to be in the same dataset.

However, the program does not allow curves with different sampling rates to be allocated in the same dataset, requiring their resampling. Thus, to join the curves with different sampling rates a resampling was made, putting the curves with a lower sampling rate (best sampled) in datasets with a higher sampling rate (worst sampled). Otherwise, data could have been created and this is not appropriate.

Table 3 shows an assessment of the main geophysical logs used in this work that were available in the wells. After this survey, it was found that the four wells had the ECS logs of silica (Si), magnesium (Mg), and calcium (Ca), and three of them have thin-section data and sidewll samples description (Table 4).

Table 3: Table with information on the main well logs found and used in the wells presented in this work.

wells	well-logs								
	CAL	GR	RES	DEN	DT	NMR	Ca	Mg	Si
A	X	X	X	X	X	X	X	X	X
B	X	X	X	X	X	X	X	X	X
C	X	X	X	X	X	X	X	X	X
D	X	X	X	X	X	X	X	X	X

Table 4: Table with information from the main reports and images present in each well used in this dissertation.

wells	Composite log	well Final Report	Thin section description and images	Sidewall samples description	Core images	Sidewall samples images	Lab. Porosity and permeability
A	X	X	X	X			X
B	X	X			X	X	X
C	X	X	X	X	X		X
D	X	X	X	X	X	X	X

It is worth mentioning that the central point of this work is not to analyze in detail the descriptions of each of the thin sections, as well as the sidewall core and plug images. Instead, the focus is on estimating and evaluating flow facies at larger scales such as well-log and seismic scales. However, it is extremely important to understand and bear in mind the main characteristics that can be found in the descriptions of rock samples in order to discover their diagenetic history that ends up influencing the estimates of the flow facies.

Figure 34 shows the layouts with the ECS logs that were used as a constrain in order to choose what wells would be performed in this work. Therefore, we used four (A, B, C, and D) over ten wells available in the pre-salt section of the Santos Basin. It is worth mentioning that this figure has the distance between the wells, but it does not have the horizontal scale or the spatial position of each well.

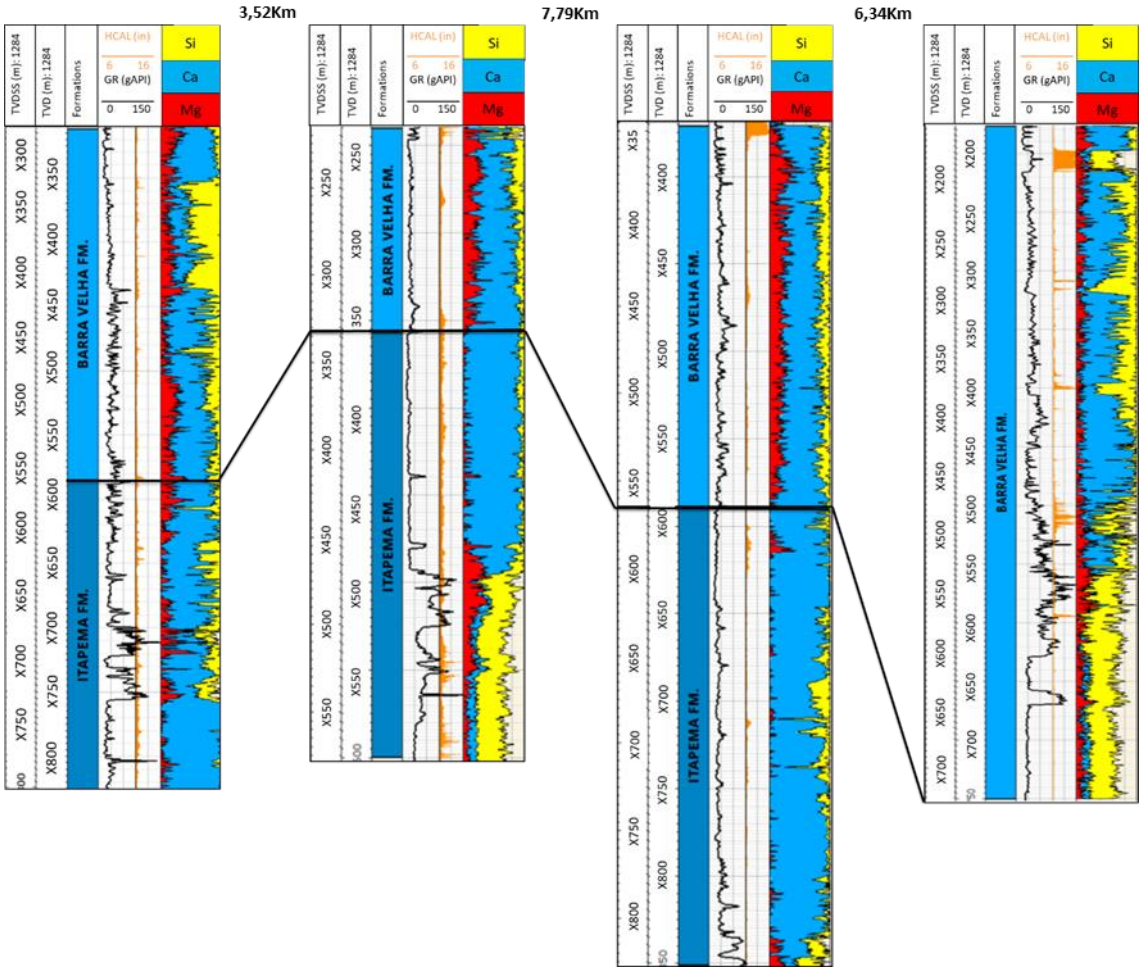

Figure 34: Layout of the four wells used in this work placed in order from left to right: Well A, B, C, and D. Track 1 and 2: depths in true vertical depth subsea (TVDSS) and true vertical depth (TVD), respectively; Track 2: formations (Barra Velha and Itapema); Track 3: Caliper log (HCAL) in orange and gamma-ray log (GR) in black; Track 4: ECS logs of silica (yellow), calcium (blue) and magnesium (red). The figure does not have the horizontal scale or the spatial position of each well.

Another extremely important step in the quality control of the well logs is the preliminary analysis of the caliper log (HCAL). Through this analysis, it is possible to identify whether the information extracted from the interpretation of well logs is reliable or not. This geophysical well log plays an important role in the quality control of the curves by providing information about the diameter of the well. Such information allows the identification of possible areas of invasions and washover that can affect the responses of the geophysical logs. Besides, this step turns out to be important due to the significant presence of igneous rocks in the study area that can be related to alterations in caliper values, indicating washover zones that can compromise the reading of tools that are sensitive to any changes in the wellbore wall. As the estimations of the flow units directly depend on the petrophysical logs (porosity and permeability), a careful analysis of these logs must be carried out in an attempt to identify anomalous values that can compromise the final result of the FUs. Thus, the analysis and identification of variations in the caliper were performed for each of the wells, aiming at recognizing possible alterations that could compromise the responses of the logs.

4.1.2 Identification and interpretation of lithologies

In the reservoir characterization process, the use of well logs is important to identify and interpret the lithologies. In this work, the classification was made by consulting the thin section's description, composite log's description, the Final Report's description, and through the interpretation of geophysical logs, such as gamma-ray (GR) and photoelectric (PEFZ) combined with other logs.

Then, based on the responses of the GR and PEFZ, as well as the responses of the other logs, when necessary, and the descriptions of sidewall sample and/or core data, an attempt was made to establish a relationship between the behavior observed in the well logs and the main lithologies described from the rocks. Thus, the main types of lithologies present were identified and determined. From this information obtained by the integrated analysis of rock and well-log data, as well as by the available reports, the limits of the Itapema and Barra Velha formations were defined.

4.1.3. Rock properties estimation

At this stage, estimations of rock properties were performed using the main geophysical logs required. The permeabilities used in this dissertation were estimated by the Timur-Coates method (Kenyon, 1997; Kenyon et al., 1988; Coates et al., 1999) for

both the NMR and the sonic logs. In addition, porosity was also calculated by the sonic log, the clay volume (Vclay) by the Larionov (1969) for the old rocks method using the gamma-ray (GR) curve as input parameter, and, finally, the acoustic impedance (PI) was estimated using the sonic (DT) and density (RHOZ) logs and will be detailed in the "rock physics crossplot" section.

Estimating the physical properties of the rock is an extremely important step for the evaluation of the wells. The porosity and permeability curves from the Nuclear Magnetic Resonance (NMR) method were mostly used due to the good correlation they presented with the laboratory data provided by the ANP. However, due to the possible influence of igneous bodies, and their natural fractures, on the responses and reliability of the tools, in some wells, porosity and permeability were also estimated by the sonic (DT) log.

The development and application of nuclear magnetic resonance (NMR) techniques in the evaluation of formations provide relevant information about the pore space and the distribution and behavior of fluids in the pores (Schön, 2015). The porosity coming from the NMR tool is essentially independent of the matrix, that is, the tool is only sensitive to the fluids in the pores. Boyd et al. (2015) state that this property makes the porosity determined from the NMR log the most frequently used, when available, especially in a geological context as heterogeneous as those found in the pre-salt carbonates.

NMR logs are effective in predicting permeability (Coates et al., 1999; Dunn et al., 2002) and porosity (Schön, 2015). The permeability models derived from the NMR log are based on a combination of empirical and theoretical relationships. They are typically calibrated in a zone of interest and verified, where possible, with rock data. The most used models are known as SDR (Schlumberger-Doll-Research) and Timur-Coates (Kenyon, 1997; Kenyon et al., 1988; Coates et al., 1999). It is important to highlight that in this work only the permeability based on the Timur-Coates equation (1968) is used and it is described as:

$$\mathrm{KTIM} = \left(\frac{\emptyset}{C_2}\right)^{m_2} \times \left(\frac{\mathrm{BVM}}{\mathrm{BVI}}\right)^{n_2}, \qquad (12)$$

where BVI is the bound fluid index, BVM is the free fluid, $\emptyset$ is the total porosity, and C, m, and n are parameters of the statistical model, whose values can be derived from experimental NMR data obtained from lateral samples and/or cores.

The free fluid (BVM), total porosity (PHIT), effective porosity (PHIE), and permeability (KTIM) from NMR were calculated by the companies responsible for the acquisition based on cutoff values determined from laboratory measurements. To verify the reliability of the curves provided by the companies, the effective porosity and permeability curves were compared with the porosity and permeability values measured in the laboratory for the four wells. This comparison can be seen in Figure 35.

The sonic log (DT), also known as slowness, transit time interval, and/or acoustic log, measures the time that a compressional sound pulse takes to cross a given distance in a given element (Kearey et al., 2009). Generally, the unit of this measurement is expressed in μs/ft (microseconds per foot) on a scale of 140 to 40. When considering the propagation of compressional waves through two similar rocks, the one that contains more fluids inside the pores, that is, greater porosity will result in a longer transit time (Δt) than the other with less fluids, and therefore, less porosity (Girão, 2004).

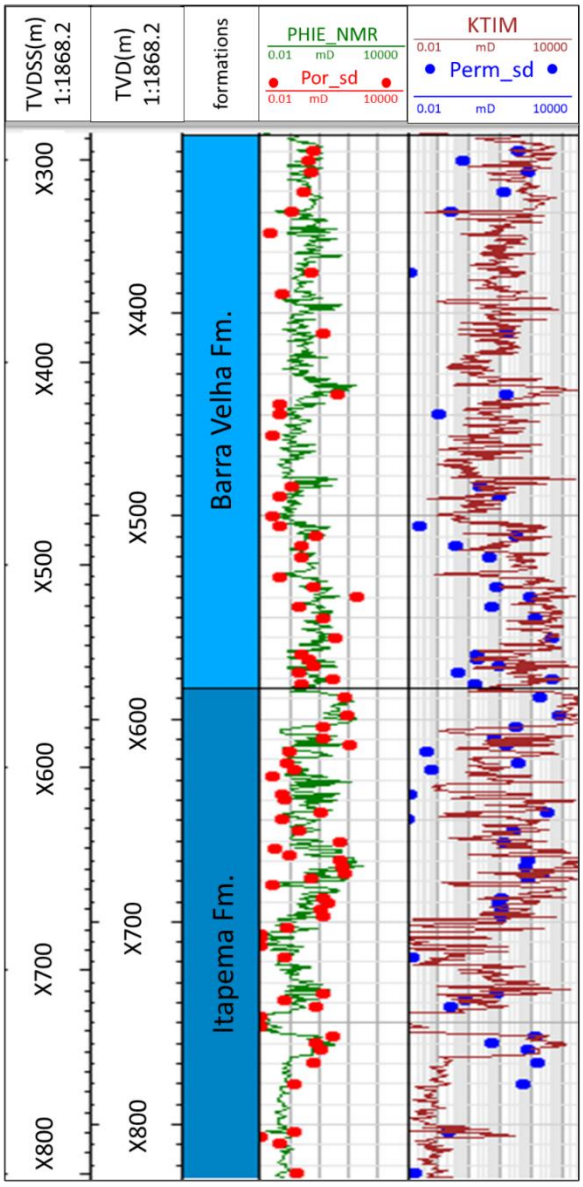

Figure 35: Effective porosity of the NMR (PHIE_NMR) log and petrophysical porosity from laboratory measurements (track 4) and permeability of the NMR log (KTIM) and petrophysical permeability from laboratory measurements (track 5) of Well A.

Often, the sonic log shows a direct relationship between the wave propagation time and the porosity of rocks. However, the estimation of porosity by DT log may have a factor that reduces the reliability of this tool, which is the presence of clay. The possible presence of clay in the permoporous layers increases the amount of interstitial water (water pressured by capillary action), attenuates the speed of sound, and increases the recorded Δt, and as the increase in transit time is associated with increases in porosity, the tool can end up recording unreliable results in muddier areas.

The total porosity estimated from the sonic log, in consolidated sandstones and carbonates with intergranular and intercrystalline porosity, can be calculated by the following equation (Wyllie et al., 1956):

$$\varphi_{t,DT} = \frac{\Delta t_{log} - \Delta t_{ma}}{\Delta t_f - \Delta t_{ma}}, \quad (13)$$

where Δt_{ma} is the transit time interval in the rock matrix, Δt_f the fluid transit time, and Δt_{log} the formation transit time. The calculation of effective porosity through the sonic log ($\varphi_{e,DT}$) is given by:

$$\varphi_{e,DT} = \varphi_{t,DT} - (V_{clay} \times \varphi_{t,DT,clay}), \quad (14)$$

From these estimates, it was possible to calculate the permeability ($KTIM_{\_DT}$) using the Coates Equation (1999) for clean zones:

$$KTIM_{\_DT} = k_c \times PHIE_{\_DT}^{4} \times \left(\frac{1 - Swirr}{Swirr}\right)^2, \quad (15)$$

else:

$$KTIM_{\_DT} = k_c \times PHIE_{\_DT}^{4} \times \left(\frac{PHIT_{DT} - PHIE_{DT} \times Swirr}{PHIE_{DT} \times Swirr}\right)^2, \quad (16)$$

where $PHIT_{\_DT}$ and $PHIE_{\_DT}$ was named as the total and effective porosities from sonic log (DT), respectively, Swirr is irreducible water saturation and k_c is a constant.

The existence of fines grains/clay in reservoir rocks is a factor that can hinder the evaluation of the formation, as their presence can obstruct the porous connections, considerably reducing the porosity and permeability values and negatively impacting the productibility of hydrocarbons (Lebre, 2019). Thus, depending on the fines/clay content in a given region of a formation, this may represent a reservoir of low permo-porous quality.

One of the most used methods to determine the clay volume is based on the use of the gamma-ray log (GR). Thus, for comparison purposes and to aid in the quantitative analyses, the clay volume was calculated for the four wells using the GR log as input.

Initially, the gamma-ray curve was analyzed in order to provide the necessary parameters for the calculation of the Gamma Ray Index (IGR), used in conventional clay estimation calculations (Vclay):

$$IGR = \frac{GR - GR_{min}}{GR_{max} - GR_{min}}. \quad (17)$$

Based on the age of the rock, the Larionov equation (1969) for old rocks was used to determine the clay content:

$$V_{clay} = 0{,}33\ [2^{2{,}0 \times IGR} - 1]. \quad (18)$$

The analysis of the clay volume curves, obtained from equations Eqs. 18 and 19, together with the gamma-ray, nuclear magnetic resonance, as well as ECS logs helped to understand and identify the zones where it was possible to find the worst and best flow facies.

4.1.4. Influence of igneous bodies

The pre-salt carbonates in the Santos Basin are known for their uniqueness and the complex environment that was formed, so it is already expected that challenges will be encountered when working in the fields from this basin. In some oil fields, in the deep-water portion in the Santos Basin, there are several occurrences of igneous rock observed during the process of well-drilling (Penna and Lupinacci, 2021).

The presence of igneous bodies along the reservoir layering is a matter of concern for production and reservoir management (Zhao et al., 2019). Identification and characterization of igneous rocks have been a strategic task for the development of oil-producing areas in Brazil. The impact of magmatic emplacement on the depositional history of a sedimentary basin directly influences processes of both generation and migration of hydrocarbons (Rodrigues, 1995; Thomaz-Filho et al., 2008), the establishment of structural patterns for trapping hydrocarbons, and the generation of favorable reservoir conditions induced by the diagenetic evolution of pore water-related to hydrothermal vents processes (Planke et al., 2005; Holford et al., 2013).

Extrusive and intrusive igneous rocks can act like flow barriers and even as permeability corridors if fracturing is high enough (Penna et al., 2019). The studies carried out in the field so far have identified five wells out of ten evaluated with the presence of igneous bodies, and in this present work two of four wells (Figure 36 and Figure 37) showed the presence of these rocks. Therefore it is important to analyze how they may affect the well log responses.

The presence of igneous rocks can affect the feasibility of some specific tools such as the NMR and HCAL logs due to the high incidence of natural fractures that may be related to these rocks. In most cases when igneous bodies are detectable, the caliper breakout may be evident due to the high level of faults and fractures caused by magmatic events (Zhao et al., 2019). The NMR tool is extremely sensible to washover zones since is placed and runs close to the wellbore wall (Coates et al., 1999), and for that reason, any change or event that occurs near the wellbore wall can affect its good functioning. Moreover, the NMR log is a measure of the magnetic field through the relaxation time of spins, and due to the presence of ferrous materials, these spins may respond unexpectedly.

On the other hand, the sonic tool works centered and the pads do not touch the wellbore wall, being more reliable to measure and evaluate the porosity and permeability in intervals with the presence of igneous rocks and caliper breakout. It is important to highlight that in the presence of washover zones, the reliability of both tools is compromised, but in the next section will be possible to identify that the DT log presented more coherent responses in these intervals.

It is noteworthy that the main goal of this work is to estimate the flow facies and their responses in the pre-salt carbonate reservoirs. As the presence of igneous rocks is a reality in the analyzed wells, there is a need to identify them and perform quality control of the geophysical logs responses, evaluating whether the results obtained by these tools are optimistic or pessimistic and if they hinder or not the estimation of the flow facies.

4.1.5. Split and merge tools

For the purpose of generating more reliable flow facies estimates, the split and merge of the porosity and permeability curves from DT and NMR logs in intervals with the presence of igneous rocks were performed. In summary, this means that at igneous intervals it was utilized the sonic log and for the rest the NMR log was used.

Figure 36 andFigure 37 show examples of the split and merge tools that were used in the porosity and permeability logs at intervals with the presence of igneous bodies and caliper breakout for the two wells (B and D, respectively) used in this dissertation. Analyzing the PHIE_NMR (effective porosity by Nuclear Magnetic Resonance) and PHIE_DT (effective porosity by sonic) logs it is possible to notice, in the same interval, different responses for each tool. As mentioned earlier, the NMR tool is overly sensitive

to washover zones that, in this case, may be related to the presence of igneous rocks. Therefore, NMR logs may have unreliable values for these specific intervals.

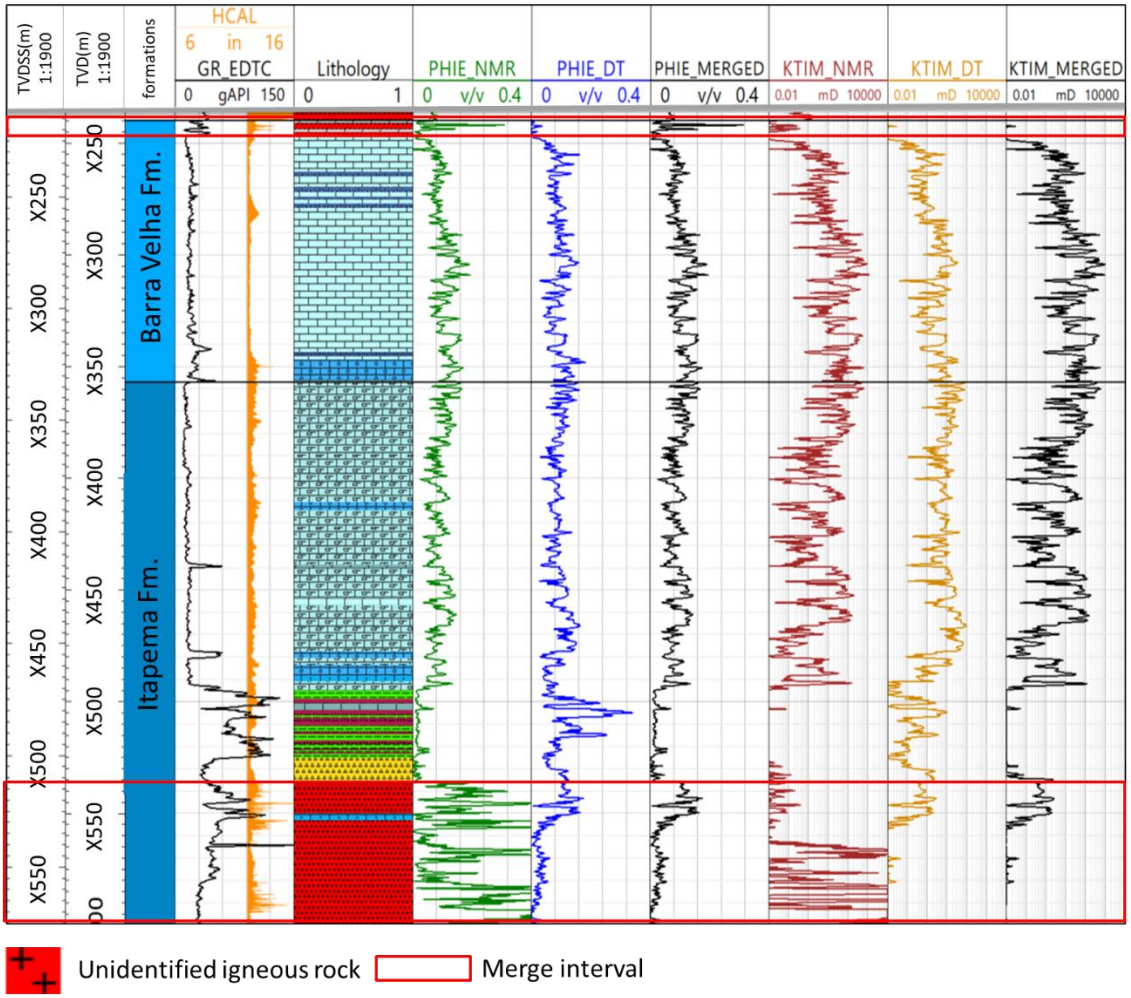

Figure 36: Layout with well-logs used to merge the porosity and permeability curves in Well B. Tracks: 1 and 2) depth by TVDSS and TVD, respectively; 3) formations (Barra Velha and Itapema); 4) Composite log lithology; 5) gamma-ray (GR_EDTC) and caliper (HCAL); 6) porosity by NMR (PHIE_NMR); 7) porosity by Sonic (PHIE_DT); 8) merged porosity (PHIE_merged); 9) Sonic permeability (KTIM_DT); 10) permeability by NMR (KTIM_NMR); 11) merged permeability (KTIM_merged).

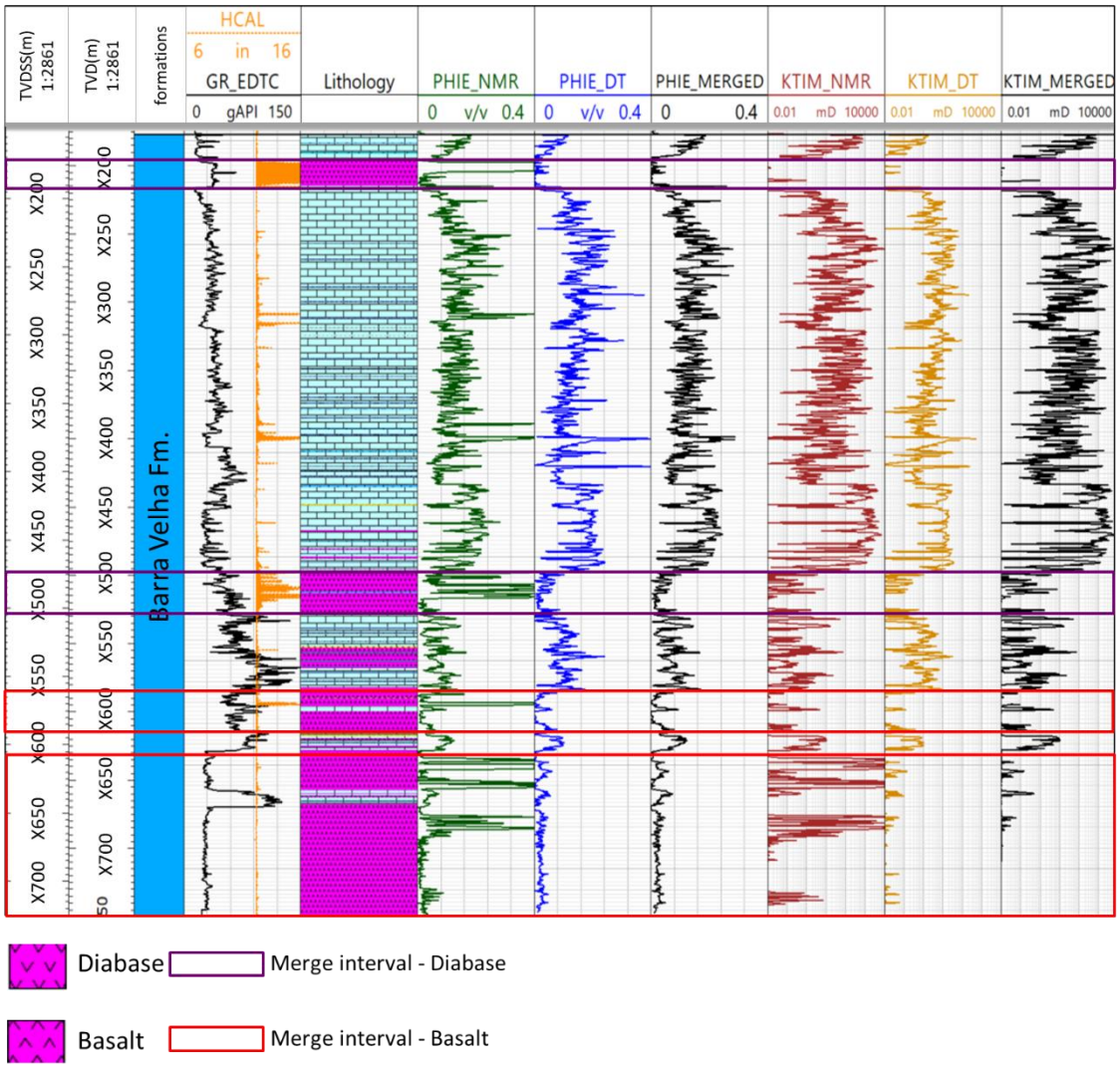

Figure 37: Layout with well-logs used to merge the porosity and permeability curves in Well D. Tracks: 1 and 2) depth by TVDSS and TVD, respectively; 3) formations (Barra Velha); 4) Composite log lithology; 5) gamma-ray (GR_EDTC) and caliper (HCAL); 6) porosity by NMR (PHIE_NMR); 7) porosity by Sonic (PHIE_DT); 8) merged porosity (PHIE_merged); 9) Sonic permeability (KTIM_DT); 10) permeability by NMR (KTIM_NMR); 11) merged permeability (KTIM_merged).

The red and the purple squares highlighted in both Figure 36 and Figure 37 show that the NMR porosity and permeability logs reach anomalous values presenting several spurious points (spikes). On the other hand, the DT porosity and permeability logs have more optimistic values in these intervals, being considered a more reliable tool to be used in these specific zones. Thereby, it is necessary to evaluate and carry out quality control at intervals with the presence of igneous rocks, especially in the porosity and permeability curves which are the input parameters to estimate the flow facies. If the anomalous values of porosity and permeability recorded by the NMR log in these intervals were considered,

the generated flow facies would be overestimated and would end up not representing reliably the flow characteristics of the area.

After performing the individual analysis of the logs and their respective responses at each interval, a sort of “cut” (split) was performed in the porosity and permeability logs in the areas where the presence of igneous rocks was identified. After completing this cut, the PHIE_DT and KTIM_DT curves in the igneous areas and the PHIE_NMR and KTIM_NMR for the rest of the formation were placed on the same track in order to merge the curves. The PHIE_merged and KTIM_merged logs represent the porosity and permeability curves with the merged done, which consists of the union of the PHIE_DT and PHIE_NMR logs as well as the KTIM_DT with KTIM_NMR.

Then, in short, in the wells with igneous rocks and washover zones the methodology used was: PHIE_DT and KTIM_DT for the igneous intervals and PHIE_NMR and KTIM_NMR for the rest. The PHIE_merged and KTIM_merged are the junction of these two curves, forming the final curve used in the estimates of flow facies in Wells B and D.

4.1.6. Flow facies estimation

As already pointed out in section 3, several methods for reservoir rock typing into Flow Units are available in the literature and each one has its limitations and advantages depending on the complexity of the geological settings. Every method is a pursuit to find a connection of the pore-throat size, that is, between permeability (k) and porosity (ϕ). In this work, it was decided to use one of the most popular correlations that express k as a function of ϕ found in Kozeny's equations which were developed by Kozeny (1927) and Carman (1937) also known as the Carman-Kozeny model.

Amaefule and Altunbay (1993) introduced the Flow Zone Indicator (FZI) concept derived from the Carman-Kozeny equations, being widely used to classify rocks with similar characteristics and behavior. The FZI method is considered a robust method of permeability estimation and reservoir prediction in terms of flow heterogeneities, due to the petrophysical correlations between permeability and Flow Units (Aggoun et al., 2006; Pritchard et al., 2010; Emami Niri and Lumley, 2016; Iravani et al., 2018).

Thus, in the present work, the focus will be directed to the FZI method. In the FZI analysis, the first step is to calculate the Reservoir Quality Index (RQI), defined in section 3.2 by Eq. (8, where φ_e and k is represented by the effective porosity and permeability

of the nuclear magnetic resonance (NMR) logs, respectively. After that, the FZI is calculated by Eq. (10). Taking the logarithm on both sides and rearranging the equation, the result is:

$$\log \mathrm{RQI} = \log \mathrm{FZI} + \log \phi_z. \quad (19)$$

Considering Eq. (19), it can be assumed that a constant value of FZI produces an inclined straight line in the log-log plot of RQI versus φ_z. All samples with similar FZl values will lie on a straight line with a unit slope. Samples with different FZI values will lie on other parallel lines. The constant value of the FZI can be determined from the intercept of the unit slope straight line at ϕ_z=1. Samples that lie on the same straight line have similar pore throat attributes and, thereby, constitute a flow unit (Amaefule and Altunbay., 1993).

It is worth highlighting that there was not enough data to estimate the cut-off values for the field studied in this dissertation, so it was decided to adopt the values found in the article developed by Penna and Lupinacci (2020). The authors used percentiles and a cumulative S-curve from approximately 500m of core samples taken in different stratigraphic intervals. This dataset was composed of 1700 laboratory core and plug samples of porosity and permeability from 17 wells containing both Barra Velha and Itapema formations in the pre-salt of the Santos Basin. They proposed a methodology for better calculating the seismic derived petrophysical volumes, characterizing large-scale flow characteristics of the reservoir considering flow units as constraints.

Penna and Lupinacci (2020) calculated a significant number of flow units that correlates with seismic elastic attributes and respond to the large-scale flow characteristics in the reservoir, maintaining part of the local flow complexity. Within each FU, they established petrophysical relations that calculate more accurate the seismic 3D volumes derived from porosity and permeability and compared to volumes calculated using sedimentological k-Φ relations. Samples with similar flow characteristics and, consequently, similar FZI values, cluster around a corresponding unit slope, determining a FU. Samples with different FZI values are plotted on different parallel lines and grouped in distinct flow units.

The cutoff values of each FU were defined by the calculations developed by Penna and Lupinacci (2020) taken from Gunter et al. (1997), which are based on the SMPL (Stratigraphy Modified Lorenz Plot) method that uses the Storage Capacity and Flow

Capacity. The SMLP was constructed by plotting the normalized values of both variables, as shown in Figure 29.

The analysis of each FU is accomplished by observing the slope of the curve: flat segments correspond to seals or baffle zones, as they may present some level of porosity, but have no contribution of permeability. Steep segments correspond to “speed zones” of the reservoir, they can have low or high porosity, but provide major contributions to the reservoir flow performance in terms of fluid movement (Figure 32).

It is possible to measure different scales in the SMLP plot. There are higher and lower orders of slope variations, Penna and Lupinacci (2021) considered the number of four main FUs in a lower-frequency (black lines) as a minimum number of units, even though it is possible to observe more FUs as a higher-frequency (green lines) order (Figure 29). Besides, they set down this number of four FUs to guarantee a better correlation with the seismic data which has a lower vertical resolution. It is worth mentioning that in the literature when the main goal is to do an upscale and identify the flow units in seismic volumes, the maximum number of FUs found are between 4 and 6.

Due to the high heterogeneity of the field that ends up producing a large number of FU, Penna and Lupinacci (2020) preferred to discretize the FZI rock typing in the permeability cumulative S-curve, using percentiles of the permeability and porosity datasets and analyzing the slope variation, like the workflow described in section 2. The steps to build an FZI S-curve are:

i. Calculate porosity and permeability percentiles of the core dataset.

ii. Calculate RQI and FZI values using Eqs. 8 and 10, and the percentiles values.

iii. Order the data with increasing values of Ln(FZI).

iv. Accumulate and normalize the percentiles of permeability values.

v. Calculate the slope of the curve for each sample.

Figure 32 shows the RQI/FZI S-curve percentiles plot of permeability versus Ln(FZI) (Figure 32-a) with the corresponding slope variation (Figure 32-b). Two ranges are observable in the derivative data: one on a small scale (higher-order) related to metric variations, and the other on a large scale (lower-order) related to decametre variations.

The four decameters flow units (FU) were discretized by analyzing the values of Ln(FZI) corresponding to major changes in the slope.

It is important to mention that this dissertation is going to use the flow facies (FF) nomenclature to characterize the wells according to the different facies associated with the flow performance they may present. The flow facies concept that will be used in this work is based on the flow units model described above. Therefore, the four flow units identified in the work developed by Penna and Lupinacci (2020; 2021) will be called flow facies and will be divided into FF1, FF2, FF3, and FF4.

FF1 is considered a barrier zone with near-zero permeability. FF2 relates to the initial detachment of the curve, with very reduced flow capacity in the decametre scale. FF3 corresponds to the first ramp up after the FF2 cut-off value and an increasingly steep curve being able to represent a reservoir rock with good permeability and flow performance. Lastly, FF4 corresponds to the better flow characteristics and relates to the final step of the S-curve (Figure 38) (Penna and Lupinacci, 2020). The cut-offs values of Ln(FZI) and its corresponding colors used for the segmentation of each rock typing are shown in Table 5.

Thus, the cut-offs for the flow units pre-established by Penna and Lupinacci (2020) were applied to well-log data to estimate the flow facies (FF). It is important to highlight that incorporating flow facies into geological models is a difficult task because each FF shows a wide variety of lithological facies, with little or no relationship between FF and these facies. That is, the same flow facies can be associated with different geological facies and different flow facies might group the same geological facies.

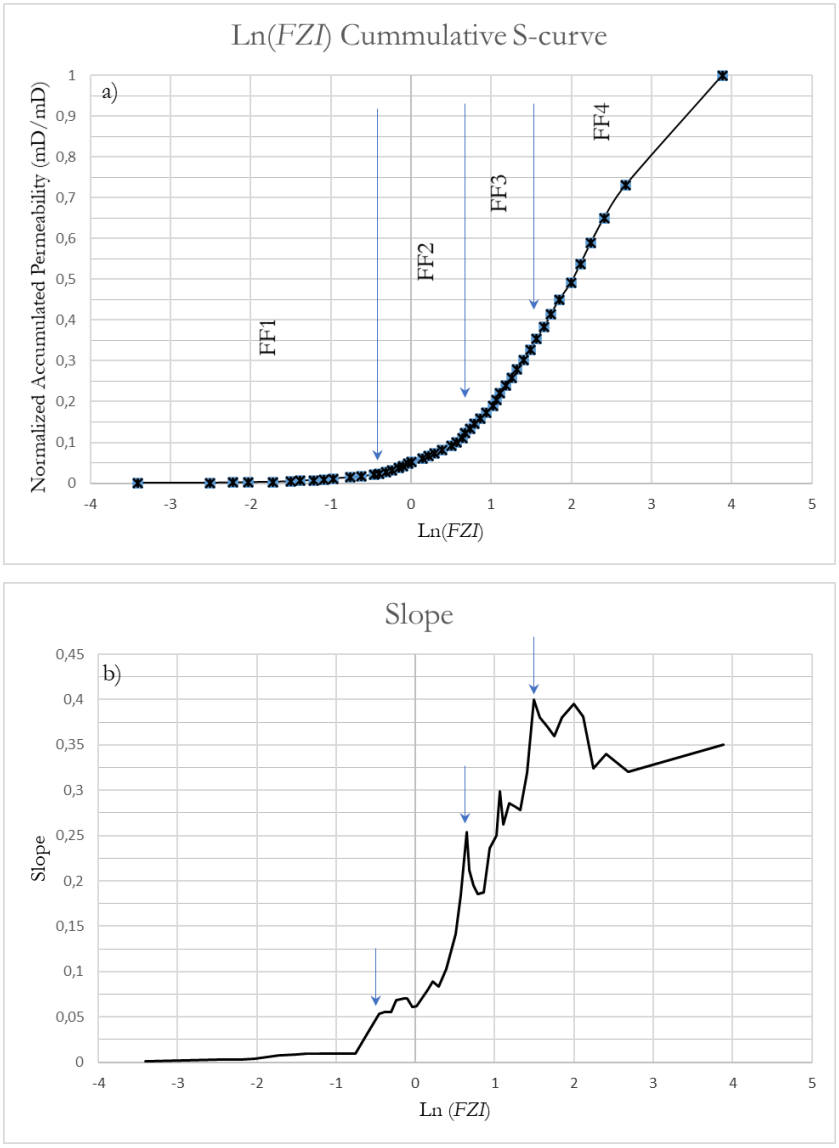

Figure 38: (a) Cumulative permeability S-Curve plot; (b) The Ln(FZI) cut-offs to discretize the FF were interpreted as the major changes in the slope (Modified from Penna and Lupinacci, 2020).

Table 5: FUs and Ln(FZI) cut-offs used in the S-curve of Figure 38.

Flow facies	Ln (FZI) cutoffs values
FF1	below -0.5
FF2	-0.5 to 0.67
FF3	0.67 to 1.49
FF4	above 1.49

4.1.7. Qualitative and quantitative classifications of flow facies

Carrying out the qualitative and quantitative classification of the flow facies in carbonates, which are rocks with little chemical composition, texturally complex, heterogeneous, and strongly affected by diagenesis, it was necessary to consider the geophysical well logs that may help to identify the presence of some diagenetic activity. Therefore, rock data such as thin-sections and sidewall core samples, in addition to ECS logs (Mg, Si, and Ca), clay volume (Vclay), gamma-ray (GR), porosity, permeability, and acoustic impedance (PI) were the main well logs used in the qualitative and quantitative analyzes. The quantitative response of the well-logs, together with the analysis of the rock data, helped to understand the flow responses found in each interval and each formation of the analyzed wells. Although flow facies have no direct correlation with lithologic facies, understanding the environments and diagenetic processes present in each lithotype is important because it can help identify the predominant flowe facies cycles in both Barra Velha and Itapema formations of each well.

The well logs used to estimate the flow facies were the effective porosity and permeability by resonance (CMRP_3MS/PHIE_NMR, and KTIM/KTIM_NMR, respectively) in wells without the presence of igneous rocks and in wells with the presence of igneous rocks, the porosity and permeability logs merged (PHIE_MERGED and KTIM_MERGED) were used. In addition, the ECS logs of calcium (Ca), Silica (Si), and Magnesium (Mg) as well as the GR, Vclay and PI logs were used to evaluate and relate the flow facies found and their responses to these curves.

It noticed that, for the Barra Velha Formation, in the four analyzed wells, where there is a significant increase in the silica content and a decrease in the calcium content, porosity and permeability tend to decrease. The increase of the GR curve, and consequently of Vclay, due to the presence of clay and/or organic matter (shales) and the presence of fine grains (laminites/mudstones), also reduce the permoporosity. Therefore, it is important to analyze how the Vclay, Si, Mg and Ca logs behave because their responses may indicate regions with greater silicification and/or silica, quartz, calcite, or dolomite cement, as well as areas with the presence of cleaner or dirtier carbonates. In the Itapema Formation, the presence of silica still acts as an important factor influencing permoporosity however the silica content is significantly lower than the found in the Barra Velha Fm. Also, calcitic cement seems to have an important role in decreasing the porosity and permeability values. The igneous intervals have a great impact on both

formations regarding the porosity and permeability values, representing the worst flow facies, together with the regions where there is a predominance of muddy facies and/or fine grains.

The quantitative analysis of the curves was made by the arithmetic mean and median values of the main parameters (acoustic and reservoir) and the main lithology and type of cement present in each flow facies in the Barra Velha and Itapema formations in the four wells studied.

The arithmetic mean was calculated by summing all the values of a given dataset and dividing them by the number of elements of this set (Figure 39-b). The median is a statistical measure that represents the value between the greater half and the lower half of a sample, a population, or a probability distribution. In simple terms, the median can be a single middle value of an odd dataset or can also be the mean of the two numbers located in the middle when the dataset is even (Figure 39-a). These numbers must be listed from the smallest to largest values.

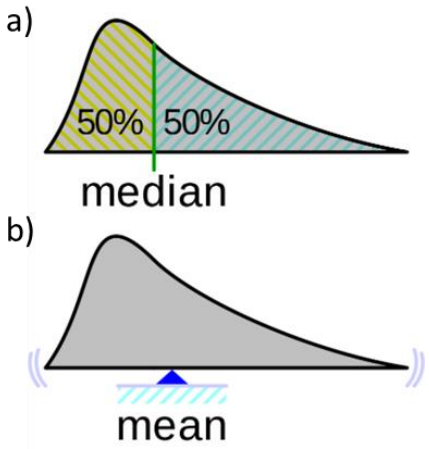

Figure 39: Geometric visualization of the a) median and b) mean of an arbitrary probability density function (Source: Modified from Cmglee, CC BY-SA 3.0 via Wikimedia Commons).

As the reservoir properties present great variability along the analyzed wells, a quantitatively comparison of these properties between the Itapema and Barra Velha formations in the studied field was made. For this purpose, arithmetic means and medians of the following properties were calculated: PHIE, silica (Si), calcium (Ca), magnesium (Mg), KTIM, Acoustic Impedance (PI), GR, V_{clay} for each flow facies. The calculation of the arithmetic mean (μ) was performed using the following equation:

$$\mu = \frac{\sum_{i=1}^{n} x_i}{n}, \quad (20)$$

in which i is the number of each sample; x is the measured property of a given dataset; n is the total number of samples.

In the median calculation for the odd dataset, the middle number will represent the median of the dataset, and is represented by the equation below:

$$\text{Median } (x) = x_{(n+1)}/2, \quad (21)$$

For a set x of n elements.

For even observation numbers, there is no distinct middle value, so the median is generally defined by the arithmetic mean of the two middle values, represented by:

$$\text{Median } (x) = \frac{x_{\left(\frac{n}{2}\right)} + x_{\left(\frac{n}{2}\right)+1}}{2}, \quad (22)$$

It is important to point out that the choice for the use of the median was made because the curves with asymmetric values (e.g. permeability logs) usually present large amounts of spurious points and may end up pulling the mean, generating overestimated values. In lithologically and depositionally complex contexts such as those found in some pre-salt carbonate reservoirs, it is necessary to use the median to find more reliable values, since this statistical measure does not take into account either very high values or very low values that can pull the average up or down. The quantitative analyzes were presented in table shapes, pie charts, as well as in bar graphs, and were made for each flow facies for both Itapema and Barra Velha formations.

4.1.8. Rock physics crossplot and flow facies upscaling

Rock physics allows us to correlate petrophysical parameters with elastic parameters, representing an important step in the characterization of reservoirs. According to Avseth et al. (2005), the correlation between such parameters can avoid ambiguities in seismic interpretation, in addition to playing an important role in seismic inversion. In this work, the calculation of acoustic impedance (PI), acoustic inversion, as well as the generation of probability and density functions (PDFs), and the seismic model of the probability of occurrence of flow facies through the Bayesian classification were

made using only one acoustic parameter. Thus, at this stage, when using density curves (RHOZ) and compressional sonic transit times (DTCO) the following acoustic parameters were calculated:

(I) P wave velocity (V_p)

The primary or P waves are so-called because they are the first to be recorded by seismographs. Also known as compressional or longitudinal waves, they propagate by uniaxial deformation (compression and expansion) in the direction of wave propagation. The movement of particles associated with the passage of this wave involves oscillation, around a fixed point, in the propagation direction (Kearey et al., 2009). P wave velocity can be determined from the compressional sonic log (DTCO) since it corresponds to the inverse of the sonic transit time, that is:

$$V_p = \frac{1}{DTCO}, \quad (23)$$

Also, to calculate the compressional velocity (V_p) it is necessary to pay attention to the unit. In general, transit time curves are in μs/ft. Therefore, unit conversion was necessary to obtain speeds in m/s. For this, the calculated values of V_p (Eq. (23) were multiplied by the constant 304.800.

(II) Acoustic Impedance (PI)

In an interface between different layers of rocks, lithologies, and elastic parameters, there is usually a change in the speed of wave propagation. This variation is a result of the different physical properties of lithologies. In such an interface, the energy contained in an incident seismic pulse is separated into transmitted and reflected pulses. The relative proportions of transmitted and reflected energies are determined by the contrasts of compression and shear velocities, densities, and angle of incidence (Aki and Richards, 1980). Acoustic impedance (PI) depends on the compressional propagation speed (V_p) and rock density (RHOZ), being defined as:

$$PI = RHOZ \times V_p, \quad (24)$$

The analyzes of the crossplots of PHIE_NMR vs. PI and Ln(FZI) vs. PI performed in this work aims to obtain information about the flow facies of each well and their relationships with acoustic and petrophysical properties. In addition, it is sought to understand how these aspects are related to the observed heterogeneities, assisting in the identification of patterns that can be recognized and reflected in the seismic volume.

In order to minimize the errors between the well and seismic scales and to visualize the flow facies in the seismic volume without losing vertical resolution, the main geophysical well-logs used for the evaluation and quantitative analysis such as porosity (PHIE), permeability (KTIM), acoustic impedance (PI), clay volume (Vclay) and Ln(FZI) were upscaled to seismic scale. Thus, from the upscale of the Ln(FZI), and using the cutoff values present in Table 5 as a constrain, it was possible to obtain the flow facies in seismic scale. These curves will be identified from the suffix _UPS, which indicates that the upscale was made.

The upscale was performed through the Backus average (Backus, 1962; Tiwary et al., 2011), with a frequency of 100Hz and a sampling rate of 5 meters. Figure 40 shows the curves in the well-domain and after applying the upscale (blue curves) for just one well as an example, since the upscale was made for all the four wells. In all wells, the upscale curves showed good responses when compared to the original ones, maintaining the main characteristics of the original curves. However, we observed that several thinner layers of FF ceased to exist after the upscale.

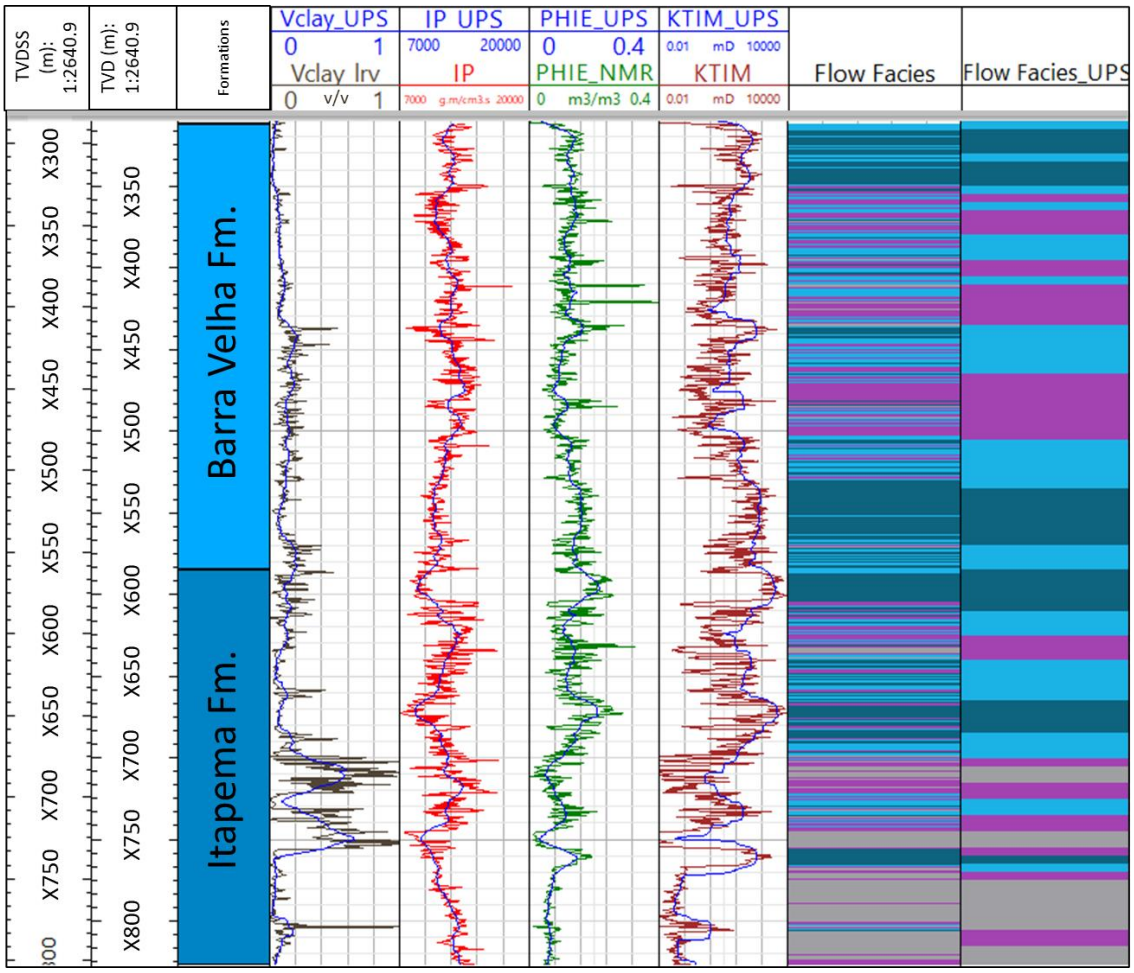

Figure 40: Layout with the geophysical logs in well domain and after the upscale (blue curves; suffix_UPS) in Well A. Tracks: 1 and 2) depth by TVDSS and TVD, respectively; 3) formations (Itapema and Barra Velha); 4) Vclay in well domain (black curve) and with upscaling (blue curve); 5) acoustic impedance (in well domain (red curve) and with upscaling (blue curve); 6) effective porosity by NMR (PHIE_NMR) in well domain (green curve) and with upscaling (blue curve); 7) permeability by NMR (KTIM) in well domain (marsala curve) and with upscaling (blue curve); 8) Flow facies in well domain; 9) Flow facies with upscaling (Flow facies_UPS).

4.1.9. Rock-well-seismic extrapolation

Data integration is decisive for an adequate characterization of reservoirs. In carbonate reservoirs, which present great lateral and vertical variation, this procedure is essential for a more robust representation of its properties.

Core or sidewall sample data provides direct and accurate information about the composition and properties of the rock. Thus, rock data are essential for reducing uncertainties and for calibrating with analyzes from well logs.

The integration between well and seismic data is also of great relevance. Well data has a high vertical resolution when compared to seismic data. These, in turn, have great spatial continuity and lateral resolution. This property of the seismic data allows the identification of structural aspects, the geometry of the deposits, and their lateral variations. Thus, the integration between well and seismic allows features observed in the wells to be correlated with certain reflectors in the seismic sections. In addition, this correlation allows the identification of the possible lateral continuity of certain patterns observed in the geophysical well logs.

Strasser (2006) and Catuneanu (2019) clarify that the geological stratigraphic cyclicity can be observed at different scales. At each scale of observation (i.e., core and plug data, well log, and seismic data), the construction of a stratigraphic framework for a reservoir is represented by sequences, and their component systems tracts and depositional systems.

According to Catuneanu (2019), the core plug-scales, system tracts and component depositional systems consist of sedimentological cycles (such as beds and bed sets), typically observed at scales of 1 to 10 m. At large scales, the systems tracts and depositional systems consist of lower-rank stratigraphic cycles, also known as sequences (hundreds of meters thick). For instance, on shorter time scales, stratigraphic cyclicity is usually controlled by tidal cycles, storm/fair-weather cycles, and climate changes. Tectonic events, compaction, and long glacial cycles define long-term changes, which define the sequences. This cyclicity reasoning can also be applied to the FUs definition as one of the major factors controlling porosity obliteration and dissolution are possibly related to stratigraphic events, in shorter or longer time scales of observations.

Rock typing for flow units in centimetric data and metric data produces different results, although all may represent the same geological construction process. Thus,

determining the large-scale and core-plug-scale flow performance are equally important and comprise different stages of the geological building process from a reservoir (Penna and Lupinacci, 2020).

From the correlation between the rock, well and the seismic data, this present work intends to verify if the heterogeneities observed in the well domain can be identified in the seismic domain and whether these characteristics have lateral continuity or not. Furthermore, one of the objectives of this correlation is to evaluate the behavior of the flow facies observed in the wells and in the seismic volume in both Barra Velha and Itapema formations.

Since the seismic data used was in depth, there was no need to generate a velocity model, time-to-depth conversion, or do the seismic-well tie. Thus, the seismic interpretation was carried out in depth and consisted of identifying the main faults, recognizing the main reflectors – which in general are those with greater amplitude and great lateral continuity – and interpreting the stratigraphic units delimited by well data.

An interpretation of arbitrary lines that cross the regions where the wells are located was made. These lines were generated in the SW-NE direction to better visualize the regional faults and fractures that cut through the study area since these same faults and fractures have an SW-NE preferential trend, being almost South-North. The main unconformities and faults were mapped and the types of seismic features in the vicinity of the wells in the arbitrary lines were identified, aiming to analyze them.

In addition to the upscale of the geophysical well logs, the Bayesian classification was made with the aim of providing a quantitative analysis of the probability of occurrence of each flow facies, given the upscaled well logs as input. Bayes' theorem describes the conditional probability of some event occurring given that a previous event has already occurred, that is, it describes the posterior probability considering an a priori probability. The posterior probability of the model m given the observed data z, P (m | z), described by the Bayes theorem would be assumed by:

$$P\,(m|z) = \frac{P(m) \times P(z|m)}{P(z)}, \tag{25}$$

where P(m) and P(z) are the probabilities of observing m and z independently, respectively, and P(z|m) is the conditional probability of z given m.

Given the discretization of FF using seismic-derived acoustic property volume, it is possible to rewrite Eq.(25 as:

$$\mathrm{PP(FF|PI)} = \frac{\mathrm{P(FF)} \times \mathrm{P\ (PI|FF)}}{\mathrm{P(PI)}}, \tag{26}$$

where P(FF) is an a priori estimate of the probability of occurrence for each flow facies. For this, a relative flow facies count is made for each well. The term P(PI | FF) is the likelihood and corresponds to the adjusted a priori probability density function (PDF) for each FF based on the P-impedance (PI) values.

As stated before, the Bayesian classification uses the Bayes Theorem to estimate the probability that a pattern of variables is related to a certain class. For that, first, it is necessary to define these classes. Their respective probabilities and likelihoods must be known or, practically, estimated (Mello, 2020).

When doing a simple experiment with four different classes, represented by the four flow facies (C1, C2, C3, and C4, for example), and only one continuous variable, the acoustic impedance (x, hypothetically), the distribution of sampled measures in each of the classes could be transformed into a probability density function (PDF). The integral (Eq. (27) of this function would describe for each class, the probability of the impedance variable being sampled within a given interval, and the total area under the complete function must be equal to 1 (Figure 41):

$$\mathrm{P\ (a < x < b)} = \int_{\mathrm{a}}^{\mathrm{b}} \mathrm{f(x|\ C_i)dx}, \tag{27}$$

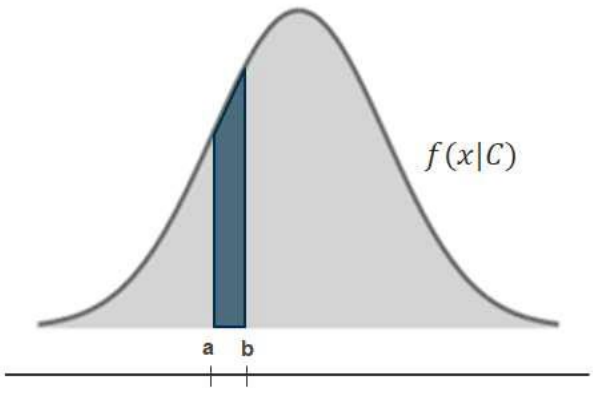

Figure 41: Probability density function of a class C analyzed in an interval between a and b (Source: Mello, 2020).

Therefore, in this work, the acoustic parameter (PI), which is a continuous variable, was used to calculate the probabilities associated with the different classes represented by the petrophysical characteristics of the rock group in different flow facies.

After carrying out the Bayesian classification and the PDFs, a flow facies probability occurrence model from the results of the acoustic impedance volume inversion will be generated for the four wells analyzed in this dissertation. This will be done with the aim of analyzing the lateral distribution of these flow facies along the wells in the seismic volume.

Finally, this section will be covered and discussed in more detail in chapter 5. It is important to mention that a detailed bibliographical review was not carried out regarding the bayesian classification or the probability density function (PDF) since it is not the main objective of this work, being just an increment aiming at a more robust discussion.

5. Results

In this chapter, the results referring to the phases described in section 4 will be presented. These analyzes were done for each formation as well as for the entire well. These results are the outcome of qualitative and quantitative rock and well-log data analysis of four wells in the pre-salt region of a field in the Santos Basin.

The estimation of the flow facies in the wells was performed from the NMR effective porosity and permeability, named PHIE_NMR and KTIM_NMR, respectively, in cases where there was no occurrence of igneous rocks along the formations (wells A and C). In cases where the presence of igneous rocks was noted (wells B and D), the suffix “merged” was used (PHIE_merged and KTIM_merged, i.e., merge of the Sonic and the NMR curves in igneous intervals). It is noteworthy that at this stage, all curves have already gone through all steps of quality control. For each studied well, qualitative, and quantitative analyzes were made at the well scale, and for the seismic scale (upscaled curves) only the quantitative ones. Then, a statistical analysis of each well and for all wells together was performed, and at last, a Bayesian classification of the flow facies in the seismic volume was made.

Two layouts were generated for each well and will be shown in similar ways, the first contains conventional logs, the nuclear magnetic resonance logs, the ECS logs (Ca, Mg, and Si), porosity and permeability data measured in the laboratory (Por_sd and Perm_sd, respectively), as well as some estimated logs, such as porosity and permeability by the sonic (DT), acoustic impedance (PI), and clay volume (Vclay). The second layout presents the flow facies and the main curves used to estimate them. In addition, it has the main curves considered to perform quantitative analyzes such as gamma-ray (GR), clay volume (Vclay), acoustic impedance (PI), types of cement, main lithologies, as well as the ECS logs of calcium (Ca), magnesium (Mg) and Silica (Si). Putting all this information together, it was possible to identify patterns and trends, as well as cycles associated with changes in the behavior of these curves, which end up directly reflecting in the flow facies behavior. Finally, it is noteworthy that the second layout also displayed the curves with the upscale made from the Backus average, with the final aim of extrapolating the results to the seismic volume. The upscale curves are on the same track as the original curves but differentiated by the blue color.

As already seen, flow facies have no direct correlation with lithological facies. However, the diagenetic effects that occur in rocks over time, such as silicification, dolomitization, dissolution, and cementation are indirectly estimated using them. Hence, an important step in understanding the flow facies bahvaior is to comprehend the diagenetic action in both Itapema and Barra Velha formations for the four wells.

5.1. Formation evaluation

Before the interpretation and generation of results from the geophysical well-logs, the analysis of the reports available for the four wells was carried out. Such analysis was fundamental for the initial recognition of the main lithologies present in the Itapema and Barra Velha formations, as well as their corresponding depths. The reports used correspond to composite logs, sidewall core samples, core plug samples, petrographic analysis reports, final exploratory well reports, and petrophysics reports.

Only three of the four wells have the Itapema Formation (wells A, B, and C), and they have coquinas as the most predominant lithology. These coquinas can be found in the form of rudstones, grainstones, floatstones, and packstones. Rudstones, grainstones, and floatstones are predominant in the formation in the three analyzed wells. The second most recurrent lithology is mudstones and laminites, which also make up a significant part of the formation. There is also the occurrence of intervals with the presence of shales rich in organic matter and limestone that appear in more than one well, but with a lower frequency. Such limestones are different from those found in the Barra Velha Formation. Thus, it is observed that the presence of coquinas, mainly in the form of rudstones, grainstones, and floatstones, is always the majority at Itapema Fm in the wells analyzed in this work. Other lithologies described in Itapema Fm. correspond to dolomites that occur punctually, and unidentified igneous that appears only in a well at the base of the Itapema Formation.

All the wells have Barra Velha Formation and limestones are the predominant lithology, composing an average of 75% of the formation in the analyzed wells. The vast majority of these limestones are described as in situ shrubs and spherulites, as well as reworked of these shrubs and spherulites in the form of grainstones. Furthermore, it is common to find cherts, and laminites in smaller proportions. Dolomite was found in three of the four wells, but it occurs with low frequency. Basalt and diabase were identified

only in one well. Other lithologies such as carbonate breccia, wackestones, and packstones occur punctually and with little significance.

From the analysis of the reports, it was possible to relate the response of the geophysical well logs with the descriptions of the sidewall core sample. In some wells, significant increases in the GR log were identified in the middle of the Itapema Fm. and near the top of Barra Velha Fm. According to the information in the sidewall core sample descriptions, in some wells such peaks are associated with shales, mudstones, and/or laminites from Itapema Fm. and in other wells, they correspond to mudstones or laminated rich carbonates from Barra Velha Fm. The characteristic GR peaks near the top of the latter formation may be associated with the [2]Lula Mark that occurs typically in several wells in the Santos Basin.

In addition to the behavior of the GR log, it was possible to observe that in all wells the increase in the ECS log of silica in the Itapema Formation represented a decrease in permoporosity and calcium content. Furthermore, the base of this formation appears to be more cemented and/or more closed, due to the low porosity and permeability values. In some wells, this decrease in permoporosity may be associated with the presence of calcite cement and/or fine grains. The magnesium content does not show any significant trend in this formation, and it is not possible to find a plausible relationship between its increase or decrease influencing permoporosity. In the Barra Velha Formation, it was observed that the ECS logs of silica and magnesium are considerably higher than in the Itapema Fm. and both generate a negative impact on permoporosity, reducing it. The calcium content is lower in the Barra Velha than in Itapema Formation and in the intervals where it increases, there is a consequent increase in porosity and permeability. The silica and magnesium content tends to increase from the middle to the top of the Barra Velha Fm. in some wells. It is noteworthy that these analyzes are more effective for intervals without the presence of igneous rocks, however, in general, where there are igneous rocks and in their surroundings (contact metamorphism), the porosities and permeabilities are usually low and the silica and magnesium contents higher.

[2] According to Wright and Barnett (2017), Neves et al. (2019) and Wright (2020) the Lula Mark is a package of about 20.8 to 28.5m, characterized by a series of shallowing and drowning cycles towards the top that presents nine GR peaks and occurs in several Wells in the Santos Basin.

5.2. Qualitative evaluation of flow facies

After analyzing the reports, interpretation and calculations were performed using the geophysical well-logs. In a first visual analysis of the curves, it was possible to identify some main patterns and behaviors in the Itapema and Barra Velha formations. In general, the Itapema Fm. varied more significantly across the analyzed wells. In two out of three wells (A and B), the Itapema Fm. is more heterogeneous, presenting specific intervals with high values of gamma rays – which seem to reflect a formation with a high clay content – and presenting low permoporous properties. One of these two wells, in addition to exhibiting an interval with the presence of fines and/or clay, has at its base an unidentified igneous rock that ends up influencing in the heterogeneity found in this well. Only the Well C has low gamma-ray values throughout the formation and a more homogeneous behavior, typical of the Itapema Fm., and, therefore, better permoporous properties. In addition, the ECS logs of magnesium and silica are higher in the first two wells, where there is a more heterogeneous Itapema Fm. than in the last well mentioned. Thus, in general, the worst flow facies have their highest concentrations from the base to the middle of the formation.

Previous analysis of the curves in the Barra Velha Fm. showed a more heterogeneous character for this formation, mainly concerning the behavior of the GR and ECS logs. Thus, it was possible to identify some distinct behaviors. Three of the four wells (A, C and D) that have the Barra Velha Formation, presented permoporous properties well distributed throughout the entire formation interval, despite exhibiting considerable variations in gamma-ray values and a higher fines content, especially in the middle and near the top of the formation. These wells showed a drop in the quality of permoporous properties, with a considerable decrease in the region closest to the top of Barra Velha Fm. Also, in two of these three wells (A and D), there is a very peculiar behavior of the silica log in the middle to the top part of this formation, which considerably affects almost all geophysical logs. Among these two wells, one of them shows the presence of igneous rocks described as diabase and basalt throughout almost the entire formation, in addition to an outstanding interval with the presence of fines, which ends up affecting, even more, the response of the logs. Finally, the Well C has a more homogeneous character, low gamma-ray values, and a good distribution of permo-porous properties throughout the formation.

The four wells mentioned above and in the previous sections were selected according to the amount of information and well logs available that would assist in the development of this work. Therefore, the criterion used to choose these four wells was to give greater emphasis to wells that have behavior that can impact the flow facies estimates.

The Itapema Formation, except for Well B - which has the presence of unidentified igneous at its base - has similar characteristics showing intervals with the presence of fines and/or clay rich in organic matter, sometimes in the base, sometimes in the middle of the formation, and consequently worst permoporosities. With the exceptions of these intervals, the formation has good permoporous properties and lower GR values.

In the Barra Velha Formation, the Well A has very peculiar characteristics regarding the behavior of the silica log as well as GR, Well B has a more homogeneous characteristic in this formation, with few variations of GR and good flow facies over the entire range. Well C presents significant variations in GR, as well as a higher content of magnesium than silica, a characteristic that is uncommon to be found in the Barra Velha Formation along the wells. And finally, Well D presents intercalations of diabase and basalt, mainly at the base to the middle of the formation, in addition to intervals with high gamma-ray values that configure the presence of fines, also presenting high values of silica throughout the entire interval.

WELL A

The data and results of the formation evaluation for Well A are presented in Figure 42. The caliper log (HCAL) has a good response over the interval, showing no considerable changes. In the Itapema Formation, only small punctual washovers zones are observed, visualized through spikes in the curves, but nothing that compromises the final result. The effective porosity curves from the resonance log (PHIE_NMR) and the sonic log (PHIE_DT) are well-calibrated with laboratory data, with PHIE_NMR being slightly more calibrated than PHIE_DT. In addition to porosity, the permeability through the resonance log (KTIM_NMR) is also visually better calibrated than the permeability through the sonic (KTIM_DT).

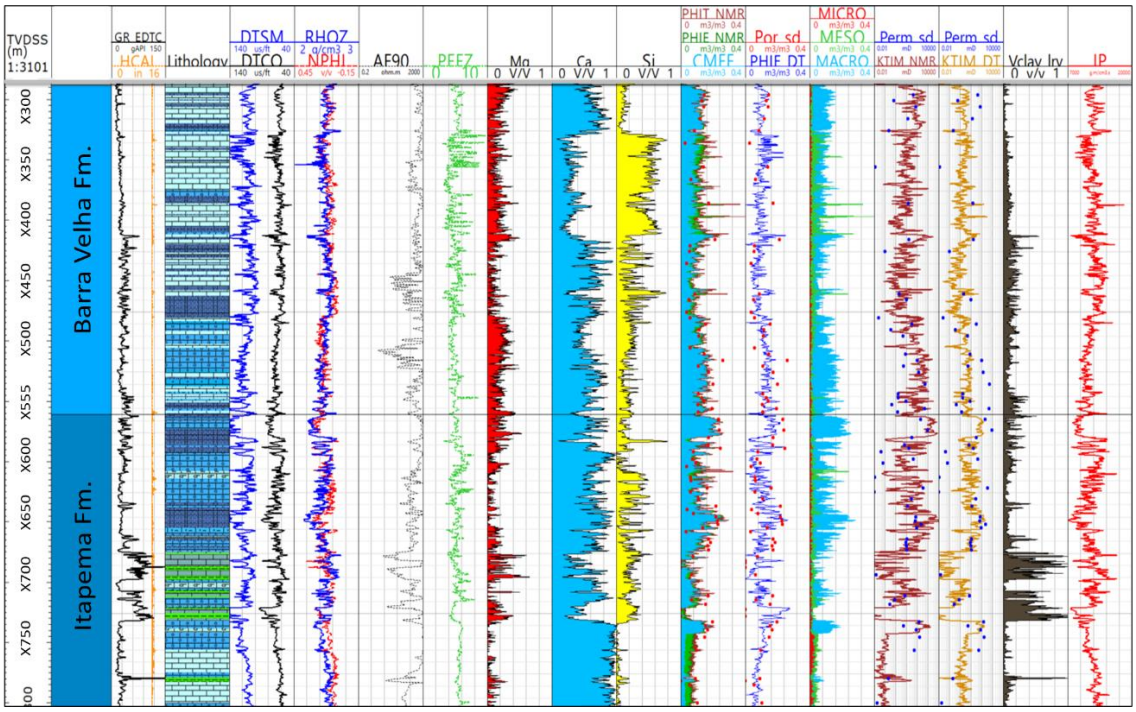

Figure 42: Layout with conventional, NMR, and estimated well-logs and porosity and permeability side core samples (red and blue dots, respectively). Tracks: 1) depth by TVDSS; 2) formations; 3) Gamma rays (GR_EDTC) and caliper (HCAL); 4) Lithology by composite log; 5) Sonic transit time (DTCO and DTSM); 6) Density and neutron (RHOZ and NPHI); 7) Deep resistivity (AT90); 8) Photoelectric (PEFZ); 9) Mg ECS log; 10) Si ECS log; 11) Ca ECS log; 12) Total porosity (PHIT_NMR), effective porosity (PHIE_NMR) and Free Fluid (CMFF) by NMR; 13) Effective porosity by Sonic (PHIE_DT); 14) Micro, Meso and Macro porosity; 15) permeability by NMR (KTIM_NMR); 16) Permeability by Sonic (KTIM_DT); 17) clay volume (Vclay); and 18) Acoustic Impedance (7000-20000 g.m/cm3.s).

The Itapema Fm. reveals some heterogeneous behavior, having intervals with greater GR values and low porosity and permeability, as well as low GR values related to low permoporosity. The base of the formation is where it can be observed the gamma-ray log with considerably low values as well as the porosity and permeability. In the middle of the formation, it is possible to see that the GR value increases significantly, as well as the permoporosity decreases. In these intervals, samples of mudstones and laminites were collected. It is also possible to notice that the permoporosity increases towards the top of the formation.

Figure 43 shows the main flow facies associated with this formation and the curves after performing the upscale (blue curves). It is possible to notice that the geophysical well logs with the upscale showed good responses when compared to the original curves. The worst flow facies are in an area comprising the base and the middle of the formation. The base of the Itapema (X800 to X745m) has a predominance of FF1,

associated with low values of porosity, permeability, and Vclay, as well as high values of calcium content (Ca), presence of calcitic cement, and thin sections and sidewall samples described mostly as grainstones. In addition, it was identified through the pressure gradient graph that the oil/water contact is close to the base of this formation, making it possible, then, to raise the hypothesis of a possible contribution of water in the cementation of the coquinas at the base of this zone.

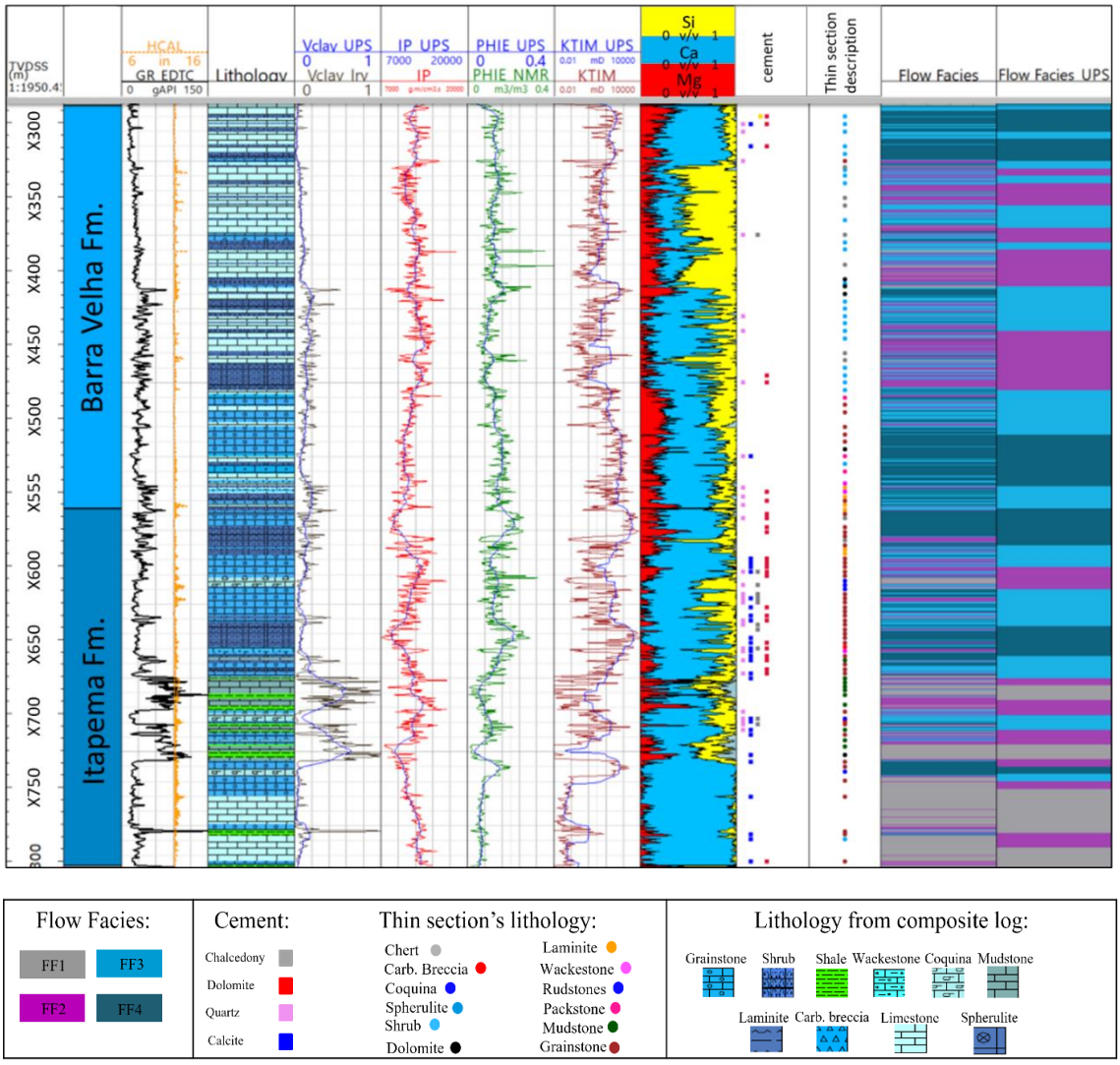

Figure 43: Layout with the main curves used to estimate the flow facies in Well A and their respective upscaled curves (blue). Tracks: 1) depth by TVDSS; 2) formations; 3) GR and HCAL; 4) Lithology; 5) Vclay (v/v); 6) PI (7000-20000 g.m/cm3.s); 7) Porosity NMR (PHIE_NMR); 8) Permeability NMR (KTIM); 9) ECS logs (Si, Ca and Mg); 10) Types of cement according to the petrographic report;11) Lithology according to the thin section description; 12) flow facies in well-domain; 13) Upscaled flow facies.

Although some intervals have layers of FF3 and FF4 associated with a sudden improvement in permoporous properties, the region where mudstone samples were collected (X731 – X675m) has a predominance of FF1 and FF2, combined with high values of GR, Vclay, low values of PHIE and KTIM, as well as sometimes low and sometimes medium values of PI. In these intervals, calcite, quartz, and chalcedony cement were collected, the latter two possibly being associated with the presence of high silica (Si) content.

Toward the top of this formation, there is an improvement in permoporous properties as well as a decrease in GR and Vclay, and lower values of PI, with a predominance of FF4. Near the interface of the top of the Itapema Formation and the base of the Barra Velha Formation (X580 – X560m), there is an FF4 interval of approximately ~20m, a decrease in the silica content, and an increase in the calcium content. In this interval samples of grainstones, floatstones, and few occurrences of laminite were collected, in addition, the predominant cement is dolomite.

The Barra Velha Fm. has, in general, a more peculiar behavior when compared to the Itapema Formation, especially for the ECS and GR logs. It is observed that the best permoporosities are present at the base of this formation, where samples of grainstones, shrubs, and few samples of laminite were collected. On the other hand, the middle part of the formation shows lower and more variable values of porosity and, mainly of permeability, where samples of cherts and shrubs with the presence of quartz and chalcedony cement were collected.

Throughout the formation, it is possible to notice the predominance of quartz cement, which may denote the strong influence of silica across the interval. The values of Si and Ca show opposite directions, influencing the changes in the behavior of the porosity and permeability logs, and, therefore, the estimated flow facies. The Mg content along the formation is greater than in Itapema Fm. Finally, the GR and Vclay tend to decrease towards the top of the formation, having the highest values in the middle of the formation.

In this formation, it is possible to notice a more significant effect of the ECS logs, mainly of calcium and silica, in the calculated flow facies. There are three different types of behavior associated with these logs. There is a cycle that relates the low silica and the high calcium content values with high permoporosity, another that presents an increase

in silica, decrease in calcium and lower porosity and permeability values, and a third one that denotes a mixed behavior, where there are intervals in which the silica content is considered the highest of the formation, the calcium content the lowest and the porosity and permeability have reasonable values, presenting a slight decrease when compared to the previous interval. Furthermore, it was observed that throughout the formation, permeability values are more susceptible to more sudden variations than porosity values.

At the base (X561 – X506m) there is a predominance of FF4, lower silica content, higher Ca values, low Vclay and PI values. The sidewall core and thin section samples in this interval mention the predominant presence of grainstones, shrubs, and laminites, only one occurrence of dolomite, and the predominance of dolomite cement followed by quartz cement.

Then, from X506 to X418m there are intercalations between FF2 and FF3, medium Si values (with the presence of some high peaks), lower Ca content values, lower porosity, and permeability values. The behavior of these curves indicates that the presence of silica possibly causes an effect on the permoporosity of this interval. The values of GR and Vclay show a slight increase, not significantly impacting the values of the other logs. The samples collected at these depths point to shrubs and chert, as well as to the presence of quartz cement and dolomite.

Between X412.4 and X329.3m a peculiar behavior of the logs is observed. In this interval, it is possible to notice a slight decrease in porosity and permeability values when compared to the previous interval, as well as the predominance of FF2 interspersed with FF3 and FF1. In addition, there is a decrease in GR, and Vclay values. The silica content is the highest of the entire formation, reaching an average of around 50%, while the calcium content has the lowest formation value (~30%). The sidewall core and thin section samples mention the presence of cherts, shrubs with quartz and chalcedony cementation, and dolomite.

Finally, very close to the top of the formation, in the range of X325 and X289m, there is a greater presence of FF4 interspersed with FF3, with GR values gradually decreasing and Vclay with values close to zero, the PHIE, KTIM, and Ca increasing as well as the significant decrease of Si from the base towards the top of this interval. The presence of shrubs is predominant in this interval, in addition to the presence of calcite

cement, quartz, and dolomite that possibly did not fill the pore space completely and/or were partially dissolved.

WELL B

Figure 44 shows the data and results of the formation evaluation for Well B. The caliper log has some washover zones intervals in the Itapema Formation, mainly in the area where an igneous rock was identified, while in the Barra Velha Formation the HCAL appears be more "calm". This well has laboratory data, making the rock and well log calibration possible. Then, it could be observed that both the NMR and sonic logs had, in general, a good fit with the rock data. It is noteworthy that, visually, the NMR porosity and permeability logs showed a slightly more refined fit than the sonic, except for the base of Itapema, where a sample of unidentified igneous rock was collected.

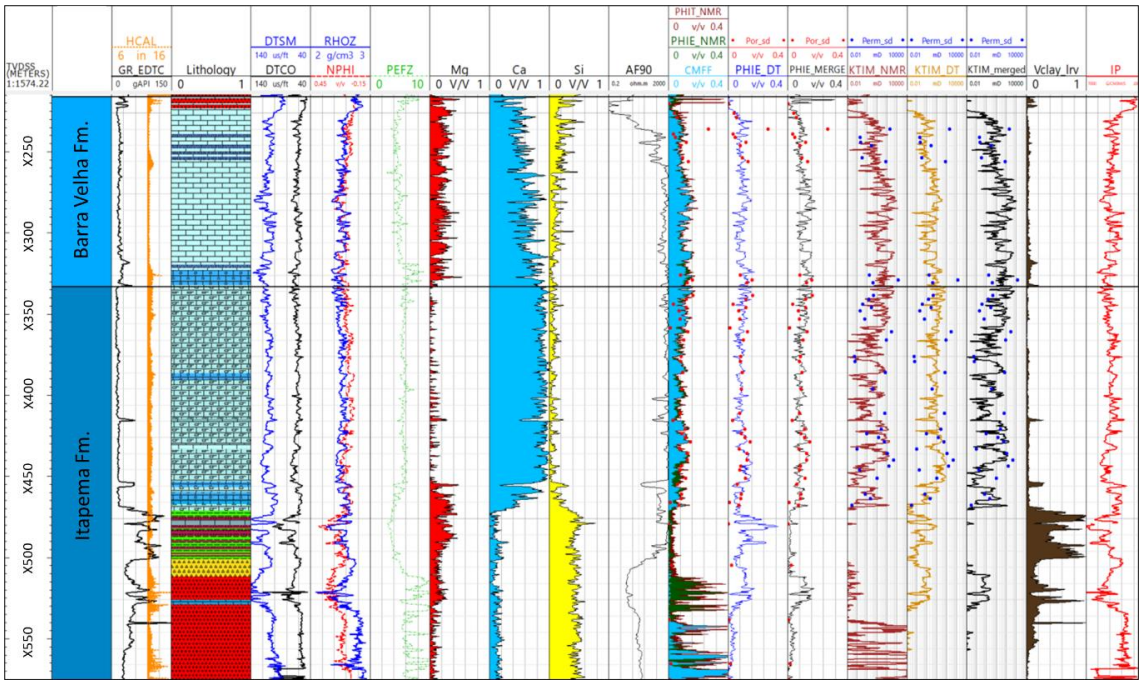

Figure 44: Layout with conventional, NMR, and estimated well logs and porosity and permeability side core samples (red and blue dots, respectively). Tracks: 1) depth by TVDSS; 2) formations; 3) Gamma rays (GR_EDTC) and caliper (HCAL); 4) Lithology by composite log; 5) Sonic transit time (DTCO and DTSM); 6) Density and neutron (RHOZ and NPHI); 7) Deep resistivity (AT90); 8) Photoelectric (PEFZ); 9) Mg ECS log; 10) Si ECS log; 11) Ca ECS log; 12) Total porosity (PHIT_NMR), effective porosity (PHIE_NMR) and Free Fluid (CMFF) by NMR; 13) Effective porosity by Sonic (PHIE_DT); 14) merged porosity (PHIE_NMR and PHIE_DT); 15) permeability by NMR (KTIM_NMR); 16) Permeability by Sonic (KTIM_DT); 17) merged permeability (KTIM_NMR and KTIM_DT); 18) clay volume (Vclay); and 19) Acoustic Impedance (7000-20000 g.m/cm3.s).

In this well, the Itapema Fm. presents high values of GR at its base, decreasing towards the top. The base of the formation is marked by the presence of igneous rocks and a breakout in the caliper log, which ends up influencing the reading of some geophysical logs such as NMR. In the igneous interval, the merge between the curves of the sonic and NMR logs was made, being the sonic log to be used in this specific region. Note that porosity and permeability values are extremely low, being close to zero. In the region covering depths between X575.83 and X500.56m, sidewall core samples of unidentified igneous, volcanic breccia, and packstones were collected. This region has low permoporosity, in addition to low calcium content, very high PI, and high silica content. It is important to highlight that the contact metamorphism caused by the igneous rocks may be responsible for the decrease in permoporosity in this interval.

Right after this interval, there is a zone where the GR values are very high, inferring the presence of fines grains and muddy facies, corroborated by the high values of Vclay. This region (X500.56 to X471.62m) is also characterized by low permoporosity, low Ca, high Si, and higher Mg content. The analyzes of the descriptions of lateral samples point to intercalations of mudstones, shales, and siltstones.

The clean character of the region near the top of the formation, between the depths of X471.62 to X5332.53m, is confirmed by the clay volume (Vclay), which presents very low values. In addition, this interval has excellent permo-porous characteristics, as well as a significant increase in calcium content and a sharp decrease in silica content. In general, porosity and permeability as well as calcium content increase towards the top of the formation while Si content and PI decrease. In this interval, samples of coquinas were collected, and some more specific ones were identified as grainstones.

The Barra Velha Formation presents a more homogeneous behavior when compared to the Itapema Formation, with low GR and Vclay values, good permoporosity, low silica content, high calcium content, and higher magnesium content, in addition to lower PI values. Permoporosity decreases at the top and PI increases due to the presence of igneous rock. The main samples collected point to the presence of spherulites, shrubs, and grainstones.

Figure 45 shows the main flow facies associated with Itapema and Barra Velha formations and the curves after performing the upscale (blue curves). It is possible to notice that for both formations, the well logs with the upscale showed good responses

when compared to the original curves. It can be observed that in the same way that the intervals with the presence of muddy facies and/or fine grains represented the worst flow facies (FF1, and FF2) in Well A, this also occurs in Well B.

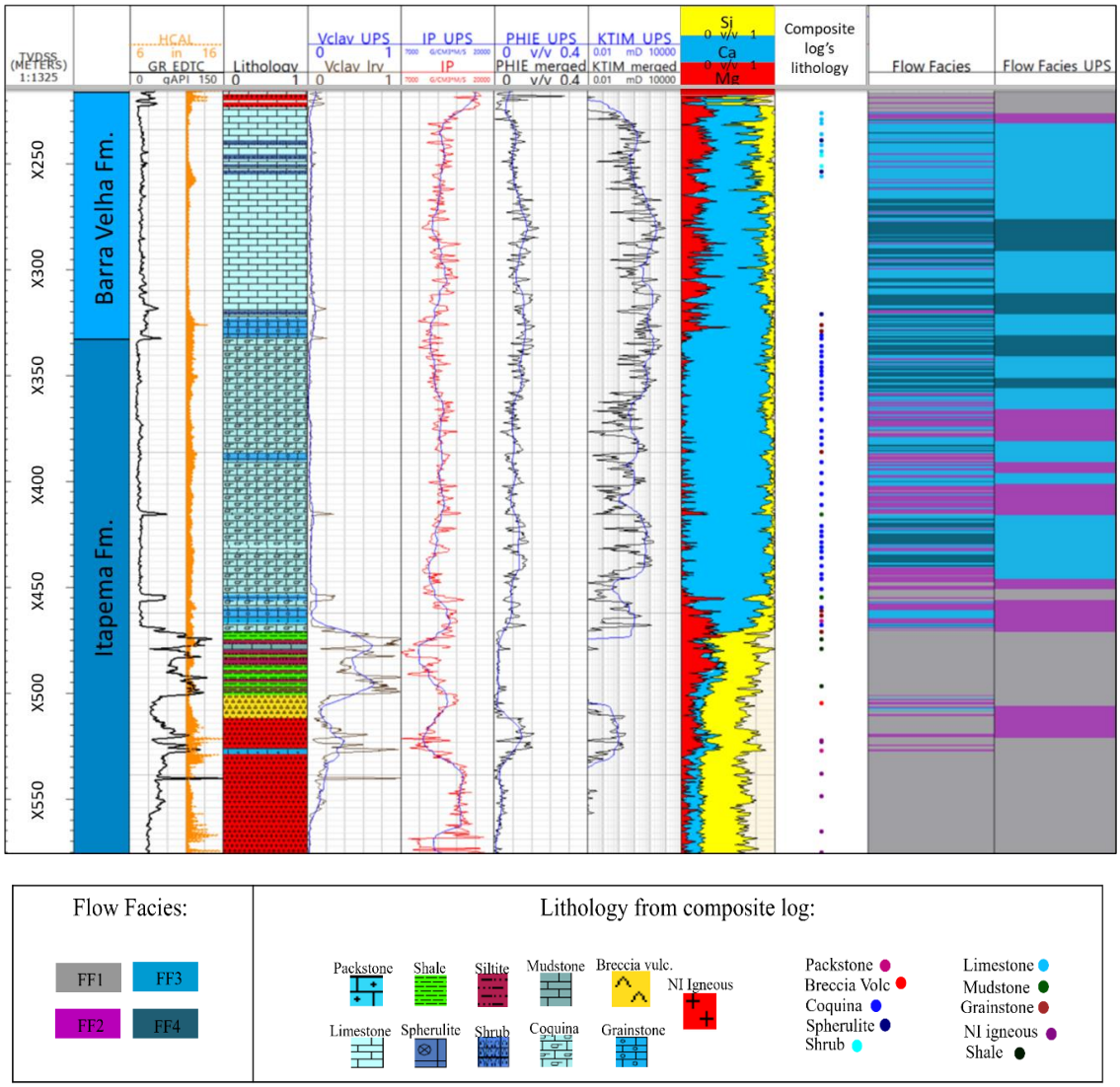

Figure 45: Layout with the main curves used to estimate the flow facies in Well B, and their respective upscaled curves (blue). Tracks: 1) depth by TVDSS; 2) formations; 3) GR and HCAL; 4) Lithology from composite log; 5) Vclay (v/v); 6) PI (7000-20000 g.m/cm3.s); 7) Porosity merged; 8) Permeability merged; 9) ECS logs (Si, Ca and Mg); 10) Lithology according to the composite log's description; 12) flow facies in well-domain; 13) Upscaled flow facies.

The base of the Itapema Formation has the presence of igneous rocks, in addition to shales, mudstones, siltite and volcanic breccias. The GR and Vclay values are considerably high, as well as the silica content, which mostly represents FF1. It is possible to notice that in the region between X439.9 – X415.22m, where the permoporosity starts to increase, the silica content decreases, and the calcium content increases, FF4 layers

start to appear. Soon after this interval, from X415.22 to X327.69m, it is possible to see FF2 layers, associated with a decrease in permoporosity. Finally, near the top of the formation, the porosities and permeabilities increase again, and, thus, layers of FF4 interspersed with FF3 reappear. Therefore, it can be observed that there is a trend from the bottom to the top of the improvement in permoporous properties, decrease in Si, increase in Ca, and improvement in flow facies.

As the Barra Velha Formation presents a more homogeneous behavior of the curves, it was to be expected that there would not be great variations in the flow facies. The porosities and permeabilities are considered good throughout the formation, the silica content increases towards the top, the calcium content decreases and there is a predominance of intercalations of FF3 and FF4, with thin and few layers of FF2.

It is noteworthy that this well has neither a detailed description of a sidewall core sample nor a description of petrographic thin section, which makes it difficult to interpret and understand the possible diagenetic processes that may have occurred along the formations. On the other hand, it is possible to notice that the presence of igneous rock has a great influence on the logs and that, in general, it presents itself as FF1. In addition to this, facies described as mudstones, siltstones and shales also represent FF1. Furthermore, it is noted that where there is high Si content and low Ca, there is a predominance of the worst flow facies (FF1 and FF2). The high values of silica and magnesium at the base of Itapema Fm. may be linked to hydrothermal fluids due to the strong presence of igneous which may have served as a source of these minerals. Furthermore, in the Itapema Fm., a higher magnesium content is associated with the worst flow facies, but in Barra Velha Fm. although the Mg content is higher than in the Itapema Fm., it does not have a significant influence on the porosity and permeability logs.

WELL C

The data and results of the evaluation of formations and the main well logs for Well C are shown in Figure 46. The HCAL has small changes throughout the formations, not significantly compromising the responses of the geophysical well logs in these intervals. The available laboratory porosity data show a good correlation with the effective porosity curve calculated by the NMR (PHIE_NMR). In turn, in the Itapema Formation, the permeability measured in the laboratory has a reasonable correlation with the permeability curve of the NMR (KTIM_NMR).

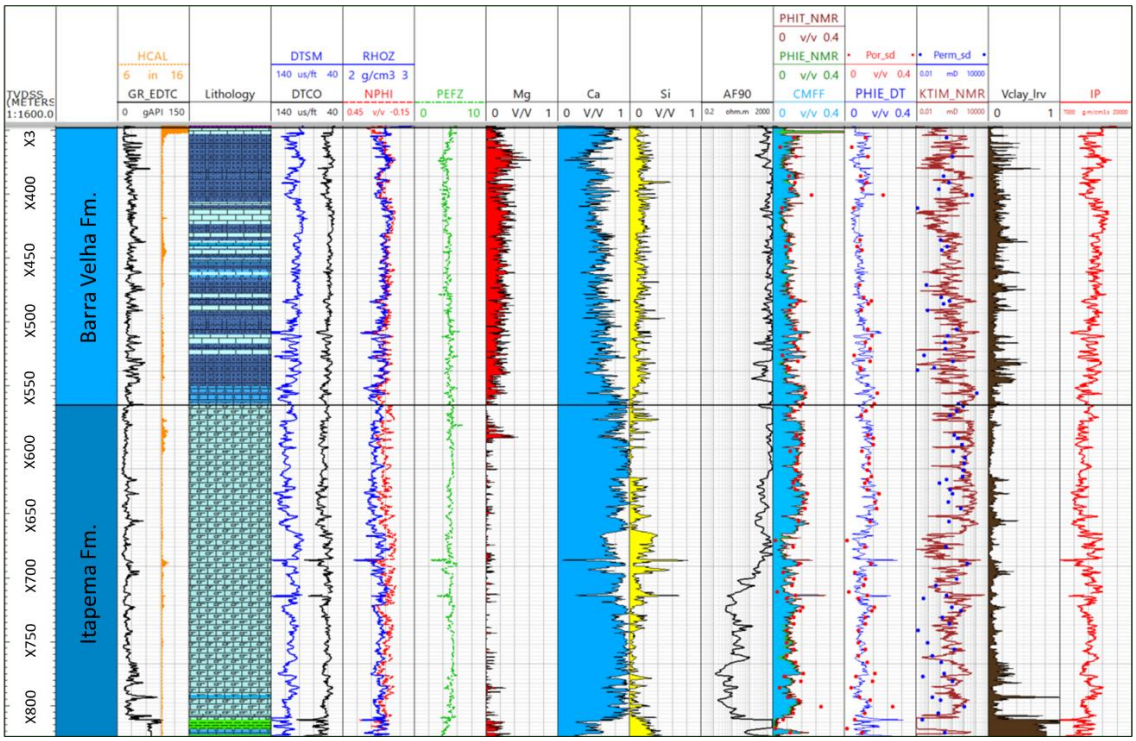

Figure 46: Layout with conventional, NMR, and estimated well logs and porosity and permeability side core samples (red and blue dots, respectively). Tracks: 1) depth by TVDSS; 2) formations; 3) Gamma rays (GR_EDTC) and caliper (HCAL); 4) Lithology by composite log; 5) Sonic transit time (DTCO and DTSM); 6) Density and neutron (RHOZ and NPHI); 7) Deep resistivity (AT90); 8) Photoelectric (PEFZ); 9) Mg ECS log; 10) Si ECS log; 11) Ca ECS log; 12) Total porosity (PHIT_NMR), effective porosity (PHIE_NMR) and Free Fluid (CMFF) by NMR; 13) Effective porosity by Sonic (PHIE_DT); 14) Micro, Meso and Macro porosity; 15) permeability by NMR (KTIM_NMR); 16) Permeability by Sonic (KTIM_DT); 17) clay volume (v/v); and 18) Acoustic Impedance (7000-20000 g.m/cm3.s).

The Itapema Fm. presents, in general, low values of the GR and Vclay logs throughout the formation. At the base, it is possible to observe higher values of GR and Vclay, as well as high silica content, and on the other hand, low permoporosity and calcium content. Furthermore, there is a tendency of the GR, Vclay, and Si values to decrease towards the top. Permeability, as well as the porosity, increases towards the top of the formation, in addition, the calcium content is high for the entire range, except for the intervals where there is a slight increase in Si, GR, and a decrease in permoporosity. It is noteworthy that in a small interval, very close to the transition of the Itapema to Barra Velha Formation, there is a subtle decrease in porosity and permeability values.

The Barra Velha Formation, on the other hand, exhibits GR and Vclay values a little higher than those seen in Itapema Fm. Furthermore, in the Barra Velha Formation it is observed that the values of the ECS logs of silica and magnesium are considerably higher than in the Itapema Formation and, conversely, the calcium content appears to be lower. Likewise, it is possible to observe, overall, a trend of decreasing permoporosity from the base to the top. Near the top of the formation, it is easy to identify a pulsed behavior of the GR log, also known as Lula Mark, which may be responsible for this decrease in permoporosity, possibly associated with the presence of clay.

Figure 47 shows that in the Itapema Formation most of the worst flow facies (FF1 and FF2) are located at the base and in the middle of the formation and these facies are mainly associated with high values of Si and/or GR and Vclay. At the base of this formation (X826 to X805.9m), there is a predominance of FF1, associated with low permoporosity, low calcium content, and high values of GR, Vclay, and silica. In this interval samples of shales, rudstones with the presence of calcite cement, and mudstones were collected.

In addition to the basal part, another interval that draws attention to the Itapema Fm. is between depths X710 and X665m. In this interval, it is possible to observe a greater presence of FF2 interspersed with FF3 and FF4, which seem to be linked to the fact that the silica content significantly increases while the calcium content and permoporosity decrease. As much as the silica content does not present such high values throughout the entire formation, it is remarkable that in this specific interval, this curve influences the permoporosity and, consequently, the flow facies. The samples collected in this interval point to a predominance of rudstones and floatstones with an abundance of calcite and quartz cementation followed by little presence of dolomitic cement.

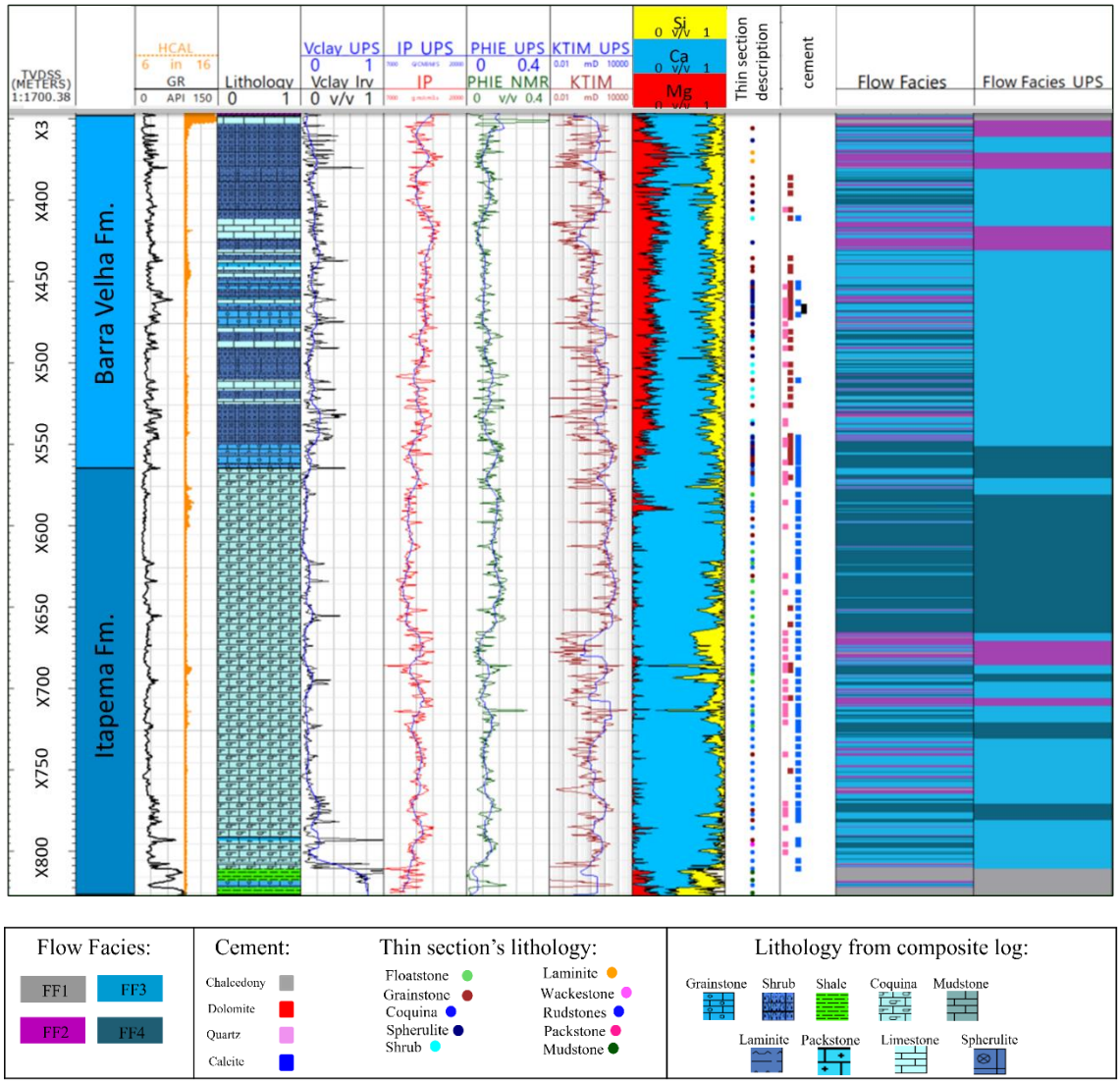

Figure 47: Layout with the main curves used to estimate the flow facies in Well C and their respective upscaled curves (blue). Tracks: 1) depth by TVDSS; 2) formations; 3) GR and HCAL; 4) Lithology; 5) Vclay (v/v); 6) PI (7000-20000 g.m/cm3.s); 7) Porosity NMR (PHIE_NMR); 8) Permeability NMR (KTIM); 9) ECS logs (Si, Ca and Mg); 10) Types of cement according to the petrographic report;11) Lithology according to the thin section description; 12) Flow facies in well-domain; 13) Upscaled flow facies.

Towards the top of this formation (X665 to X565m), as observed in wells A and B, there is an improvement in permoporous properties, lower and more stable GR and Vclay values, in addition to an increase in calcium content and a decrease in Si. This interval has a predominance of FF4, with blocks that reach more than 20m of thickness, interspersed with thin layers of FF3 and only a few layers of FF2. Sidewall sample descriptions point to a greater presence of rudstones, grainstones, and floatstones, in addition to a predominance of calcite cement.

The Barra Velha Formation has, in general, a more heterogeneous behavior of the well logs when compared to the Itapema Fm. It is possible to observe that the gamma-ray curves have spikes practically throughout the entire formation, being reflected in the Vclay log as well. Furthermore, are intercalations between FF2, FF3, and FF4 in practically the entire length of this formation. These intercalations between the flow facies also reflect a more heterogeneous character of the porosity and permeability logs. Permoporosity presents a decrease in two intervals near the top, where an increase in silica and magnesium content and a decrease in calcium content can be observed, as well as an increase in GR and PI values. Also, silica and magnesium logs have higher values than those found in the Itapema Formation.

Despite this intense intercalation between the flow facies, it is noted that the base of the formation, between the depths of X564.76 and X480.96m, there is a predominance of FF4 and FF3 with little presence of thin layers of FF2. In this range, calcium content is high, and silica and magnesium content are lower. In addition, the predominant lithologies are reworked from shrubs and spherulites, being essentially classified as grainstones, floatstones, and packstones, in addition to spherulites, shrubs, and laminites in small quantities. The predominant cement in this region is dolomitic, followed by calcite and quartz cement.

Soon after this interval, no very significant changes in the behavior of the curves and flow facies are identified, except at the depths of X430.83 and X403.85m where a drop in porosity and permeability values and calcium content is noticed, as well as an increase in the values of the magnesium and silica. As a result, there is a predominance of FF2 interspersed with FF3 and some layers of FF1. The predominant lithology is composed of reworked (grainstones), shrubs, and spherulites and the predominant cement is dolomite, in addition to containing quartz and calcite cement.

Between X403.85 and X380.96m, the behavior of the well logs are opposite to that found in the previous depths. There is an increase in permoporosity, a slight increase in calcium content, and a slight decrease in magnesium and silica contents. Furthermore, in this range, the GR and Vclay values appear to be smaller than in the previous range. Therefore, there is the presence of FF4 and FF3 interspersed with few FF2 layers. The predominant lithology is reworked from shrubs, being classified as grainstones and few samples of spherulite. The predominant cement is dolomite.

Finally, near the top of the Barra Velha Formation, in the interval between X380.96 m to the top of the Formation, it is possible to observe a significant decrease in permoporosity, as well as an increase in GR and Vclay presented in the form of nine spikes (Lula Mark), a significant increase in magnesium content, increase in silica and PI logs. The FF2 has become predominant in this region and the most present lithologies are laminites, followed by grainstones. It is noteworthy that no cement samples were collected in this interval.

It is worth paying attention to the fact that the clay matrix is quite common in the Barra Velha Formation which was diagnosed by the increase in the GR and Vclay logs as well as through the thin section descriptions collected at these intervals. This increase in the GR log, in addition to the relative increase in silica and magnesium, ends up affecting the permoporosity, decreasing it. In addition, it is good to highlight that fourteen samples of spherulites with dolomite and clay were collected along the Barra Velha Fm., as well as two samples of laminite near the top of the formation, where peaks of GR and Vclay were observed.

WELL D

The Well D contains only the Barra Velha Formation, then the well log evaluation, as well as the flow facies, will be analyzed and compared with the other wells only considering this formation. Figure 48 presents the conventional, NMR and some estimated curves. It is important to highlight the presence of igneous rocks throughout the formation influencing, in a certain way, all well-log responses and, mostly in the caliper (HCAL) tool reading. As the igneous rocks are naturally fractured, the presence of breakout in caliper logs can be usual. This well shows the presence of basalt near the base and diabase found in the middle part and the top of the formation. In the intervals that showed the presence of caliper breakout along with the presence of igneous rocks was decided to do a split of the NMR and Sonic curves and after a merge of the curves in the proposed interval. Therefore, in this well, as well as in Well B, it was used the PHIE_merged and KTIM_merged to estimate the flow facies and evaluate the responses.

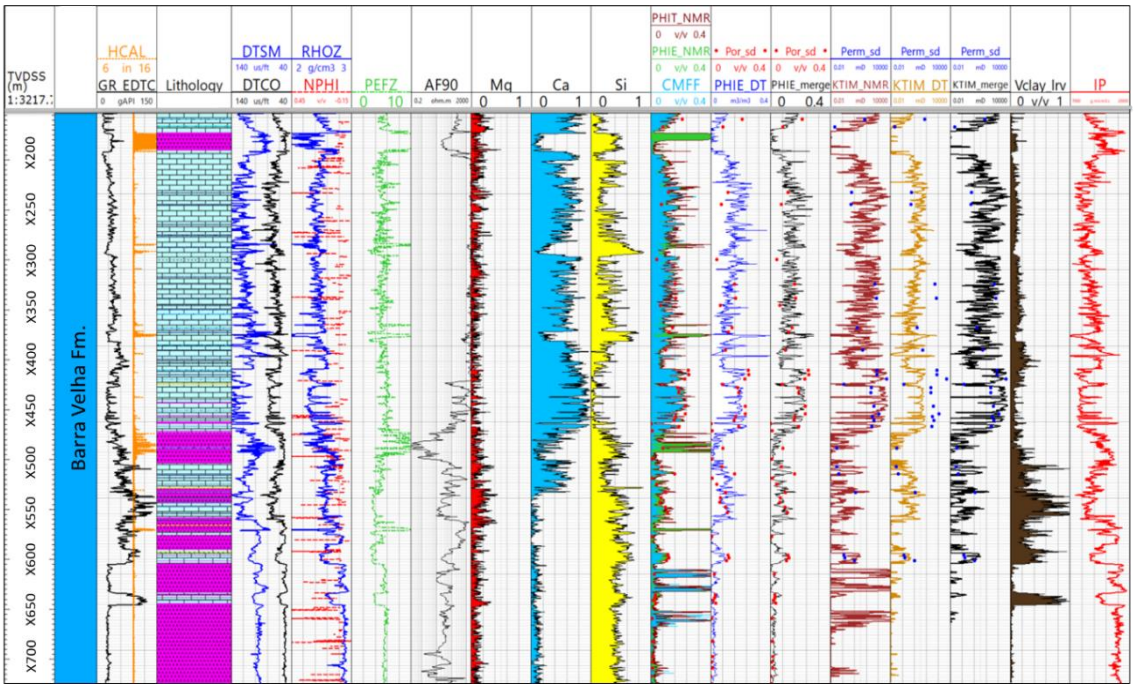

Figure 48: Layout with conventional, NMR, and estimated well-logs and porosity and permeability side core samples (red and blue dots, respectively). Tracks: 1) depth by TVDSS; 2) formations; 3) Gamma rays (GR_EDTC) and caliper (HCAL); 4) Lithology by composite log; 5) Sonic transit time (DTCO and DTSM); 6) Density and neutron (RHOZ and NPHI); 7) Deep resistivity (AT90); 8) Photoelectric (PEFZ); 9) Mg ECS log; 10) Si ECS log; 11) Ca ECS log; 12) Total porosity (PHIT_NMR), effective porosity (PHIE_NMR) and Free Fluid (CMFF) by NMR; 13) Effective porosity by Sonic (PHIE_DT); 14) merged porosity (PHIE_NMR and PHIE_DT); 15) permeability by NMR (KTIM_NMR); 16) Permeability by Sonic (KTIM_DT); 17) merged permeability (KTIM_NMR and KTIM_DT); 18) clay volume (Vclay); and 19) Acoustic Impedance (7000-20000 g.m/cm3.s).

It is noteworthy that as the intervals with the presence of igneous rocks have been showing themselves areas of low porosity and permeability and, therefore, worse flow facies (FF1 and FF2), even if the caliper has presented breakouts the flow facies estimate for these intervals were not disregarded. The presence of these rocks ends up influencing the petrophysical properties of the surrounding rocks, generally worsening the permoporosity, due to the contact metamorphism.

Figure 48 shows that, overall, the laboratory porosity and permeability measurements correlate reasonably well with the NMR porosity and permeability curves in the intervals without the presence of igneous since there are no laboratory samples in these intervals. Furthermore, it is worth noting that the GR, Vclay, and PI values tend to decrease from the bottom to the top, while the PHIE_merged, KTIM_merged, and calcium content increase. The magnesium content does not show many variations, being

higher near the base of the formation. The silica content is high at the base, decreases in the middle, and returns to increase towards the top of the Barra Velha Formation.

Figure 49 shows the estimated flow facies from the porosity and permeability log, in addition to the type of lithology and cement for the purposes of comparison and evaluation of these facies. Note that from the base to the middle of the Barra Velha Fm. (X725.85 - X470.61m) there is a predominance of FF1 with FF2 intercalations. The majority presence of FF1 may be associated with the presence of igneous rock, as well as high values of GR, Vclay, PI, and silica content and low values of porosity, permeability, and calcium. The sidewall samples collected in this interval point to the presence of diabase and basalt intercalated with laminites and mudstones and the presence of few samples of breccia, and floatstone. Quartz, calcite, and dolomite cement are the most common in this range and there is only one bitumen cement sample. Remarkably, the low permoporosities found in the areas without the presence of igneous rocks, in this interval, must be associated with contact metamorphism.

Between depths X470.61 and X409.17 m, it is possible to notice an interval where there is a significant presence of FF4 with little or no presence of FF1 and FF2. In this depth, there is a considerable decrease in the logs of GR, Vclay, PI, and Si, in addition to high values of calcium content, porosity, and permeability. Note that this interval is mainly formed by shrubs and spherulites (in situ), also containing samples of grainstones. The main type of cement found is dolomitic, also containing a few samples of calcite and quartz cement.

From X409.17 to X381.87 m it is possible to observe that there are some intervals with the presence of FF2, the permoporosity and the calcium content decrease compared to the previous interval, while the logs of GR, Vclay, Si, and PI increase. This region can be interpreted as constituted by more clayey carbonates, as they have higher GR values and lower permoporosity. The few samples collected in this interval are described as shrubs with quartz and dolomitic cement.

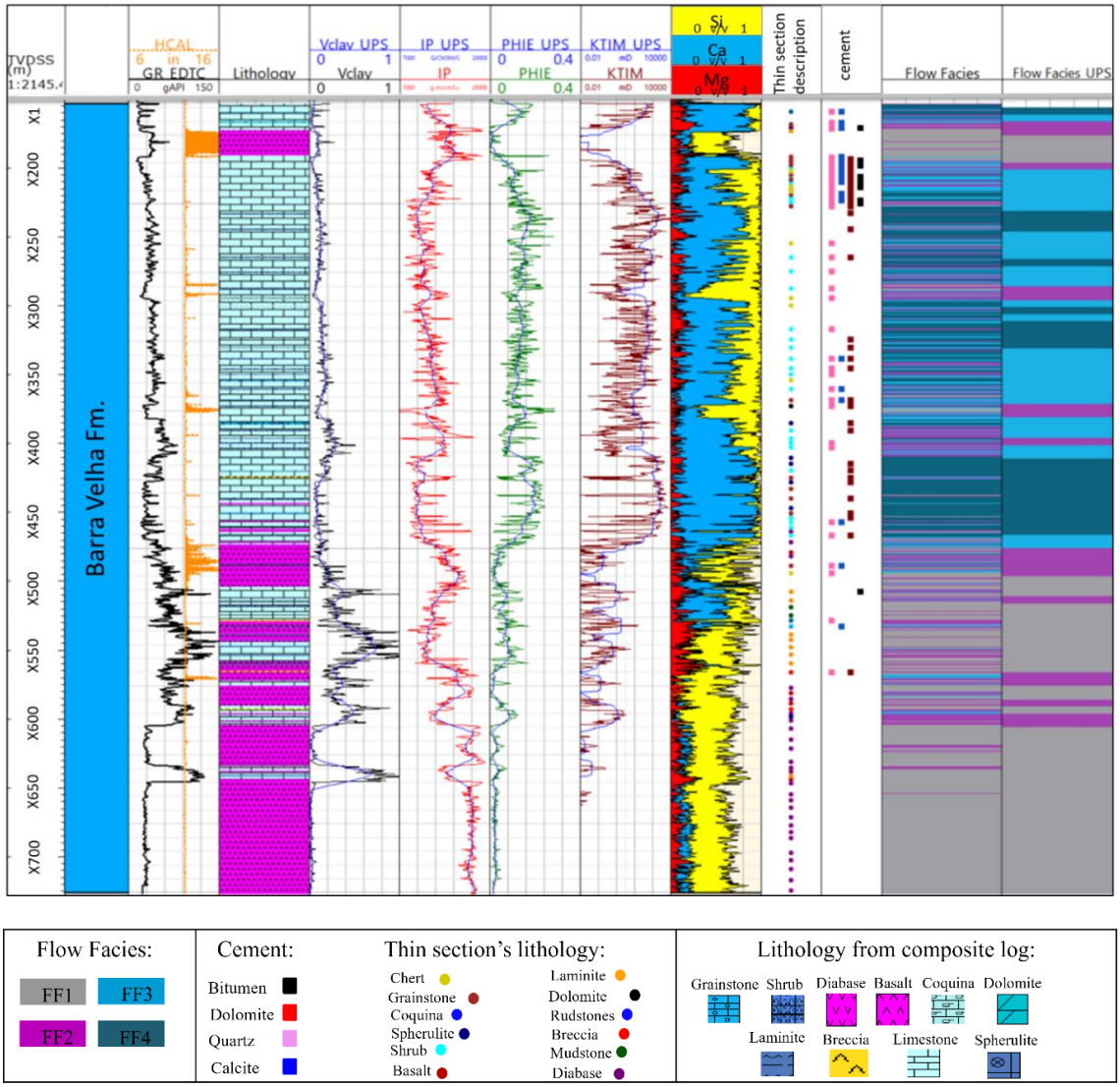

Figure 49: Layout with the main curves used to estimate the flow facies in Well D and their respective upscaled curves in blue. Tracks: 1) depth by TVDSS; 2) formations; 3) GR and HCAL; 4) Lithology; 5) clay volume (v/v); 6) PI (7000-20000 g.m/cm3.s); 7) Porosity NMR (PHIE_NMR); 8) Permeability NMR (KTIM); 9) ECS logs (Si, Ca and Mg); 10) Types of cement according to the petrographic report;11) Lithology according to the thin section description; 12) Flow facies in well-domain; 13) Upscaled flow facies.

Between X381.87 and X194.73m, a greater intercalation between the flow facies is visualized, especially FF4, FF3, and FF2. This may happen due to the large intercalation between "cleaner" carbonates with carbonates of higher silica content and/or laminated carbonates. This assumption can be supported by the sometimes high and sometimes low silica values related to permoporosity variation. Furthermore, there is a significant presence of shrubs in situ and cherts, as well as a predominance of quartz cement. The values of GR and Vclay are not high with a tendency to decrease towards the top, so the fine and/or clayey grains, in this case, are not considered a crucial factor

for the decrease in permoporosity. In addition to the above samples, the presence of grainstones (reworked facies) and dolomite were also observed.

Finally, from X194.73 m to the top of the formation, there is an igneous rock and consequently FF1. The permoporosity is close to zero both in the interval where there is igneous and in the immediately inferior and superior intervals due to the contact metamorphism that ends up tighten the pores. Silica content increases significantly and calcium content decreases.

5.3. Quantitative evaluation of flow facies

The quantitative analyzes were made for each flow facies and performed by calculating the means and medians of the main geophysical logs used to quantify and qualify them, as well as the main lithologies and types of cement found in each of these flow facies, in both Barra Velha and Itapema formations. These calculations were performed for the well logs in the well scale and with the upscale. The analyzes were done for both the four wells separately and all together. In addition to the quantitative analyses, some thin sections images from the petrography report and core plug images provided by the ANP were attached.

It should be noted that the main objective of this statistical analysis is to enable a comparison between the main properties of the Barra Velha and Itapema formations and their relationships with each estimated flow facies. In addition, it is worth noting that the arithmetic mean is sensitive to samples that have very different values, so its use is more appropriate in situations where the values do not show a large discrepancy. Therefore, even though the median also has its limitations, it was more optimistic for not considering spurious values that may occur due to breakout of the caliper and/or by the large variation of the tool, as occurs with permeability. Among all the calculated curves, permeability presented values that were farther between the mean and the median, so we will consider the median as the main measure just for this curve, and for the rest of the curves the arithmetic mean will be considered.

5.3.1. Quantitative evaluation in Well A

Figure 50 presents a pie chart with the means of each flow facies in both Barra Velha and Itapema formations. It is possible to observe that the Barra Velha Fm. has a higher percentage of FF3 and FF4 than the Itapema Formation and, therefore, a lower percentage of the worst flow facies (FF1 and FF2) when compared to the Itapema Fm.

The sum of the percentages of FF3 and FF4 is 68%, representing more than half of the formation, while the Itapema Fm. sums only 46% and is composed of more than half of FF1 and FF2.

As previously seen, the FF1 located at the base of the Itapema Formation may be associated with the presence of laminite, grainstones, and rudstones with low porosity and calcite cement (Figure 43). In the middle of this formation, there is an interval with a large presence of mudstone samples and a predominance of FF1 and FF2. The flow facies tend to improve towards the top, where the highest percentage of FF3 and FF4 is found, especially in the transition from the Itapema to Barra Velha Formation.

The Barra Velha Formation has only 4% of FF1 and 28% of FF2 which are concentrated in the middle of the formation, where there is a predominance of higher Si values, lower Ca values, and lower porosities and permeabilities (Figure 43). On the other hand, FF3 and FF4 are at intervals where there is a considerably opposite scenario to the previous one (Figure 43). FF2 represents 28% of the formation and is mostly intercalated with FF3 and may be associated with sudden increases in silica content caused by the presence of chert as well as quartz, and chalcedony cement. Both the FF3 and FF4 have a mean of 34% along the interval.

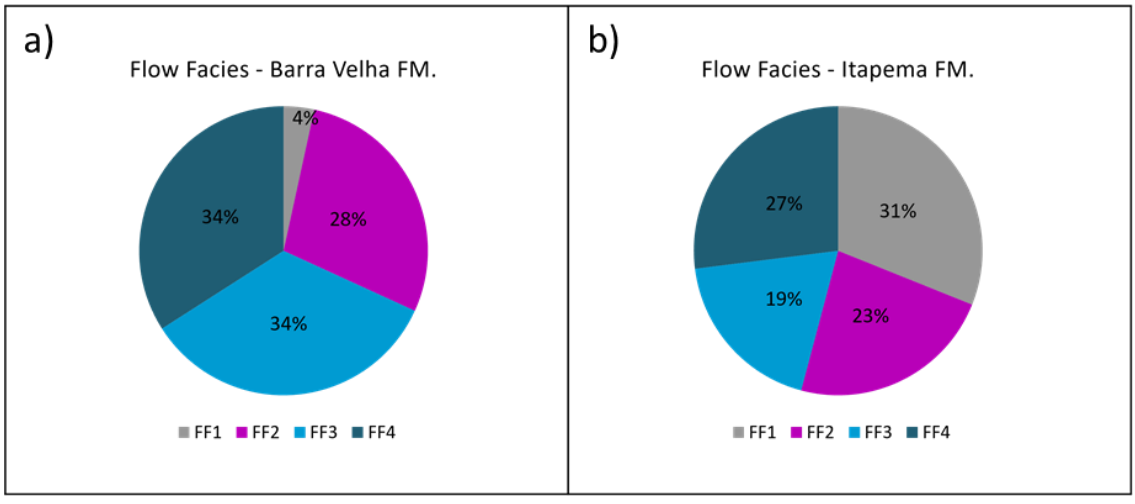

Figure 50: Pie charts with the percentage means of the flow facies for a) the Barra Velha Formation and b) for the Itapema Formation in Well A.

Table 6 shows the mean and median values for the GR, PI, KTIM, PHIE, Vclay, Ca, Mg, and Si logs of the Barra Velha and Itapema formations in Well A.

In the Itapema Formation, something that stands out is that the values of GR and Vclay are much higher than those found in the Barra Velha Formation with the highest

mean of 42,7 gAPI and 22%, respectively, for FF1 and the lowest of 31,2 gAPI and 10% for FF4, while the values of PI are lower in the Itapema Fm.

Table 6: Table with the arithmetic mean and median of the main well-logs used in this work, for each flow facies in the Barra Velha and Itapema formations in Well A.

Flow Facies	Zones	GR (gAPI)		PI(g.m/cm3.s)		KTIM (mD)		PHIE (m3/m3)		Vclay (v/v)		Ca (v/v)		Mg (v/v)		Si (v/v)	
		Mean	Median	Mean	Median	Mean	Median	Mean	Median	Mean	Median	Mean	Median	Mean	Median	Mean	Median
FF1	B. Velha	26.4	24.9	12285	12324	1.36	0.88	19%	18%	8%	7%	33%	28%	14%	14%	52%	57%
	Itapema	42.7	28.2	11706	11963	0.075	0.05	6%	6%	22%	8%	75%	88%	9%	4%	12%	4%
FF2	B. Velha	30.7	27.9	12422	12524	3.39	1.92	10%	9%	12%	9%	45%	41%	14%	13%	40%	44%
	Itapema	44.8	35.5	12509	12682	4.4	0.88	9%	8%	21%	12%	64%	64%	12%	10%	20%	19%
FF3	B. Velha	30.5	29.4	12093	11991	24.9	16.5	11%	11%	11%	10%	48%	47%	18%	18%	33%	28%
	Itapema	35.6	30.4	11686	11689	32.7	15.7	12%	11%	14%	9%	69%	70%	9%	8%	20%	19%
FF4	B. Velha	26.8	25.7	11115	11054	331	187	15%	15%	9%	8%	62%	64%	21%	21%	16%	13%
	Itapema	31.2	28.3	9838	9770	1484	524	18%	18%	10%	8%	75%	75%	11%	10%	13%	12%

The median permeability grows from FF1 (0.05 mD) to FF4 (524 mD). Porosity also increases from FF1 (6%) to FF4 (18%) and presents lower arithmetic mean and median values for FF1 and FF2 when compared to the values found in the Barra Velha formation. The calcium content is higher in all flow facies, with all measurements being greater than 64%. The magnesium content has lower values in the Itapema Fm. than in the Barra Velha Fm. and there is no growth trend from FF1 to FF4.

The silica content is significantly lower than that found in the Barra Velha Formation, having the lowest values associated with FF1 and FF4. Therefore, in the Itapema Fm., the silica content does not seem to be the main factor that exerts a strong influence on permoporosity as the clay content and the presence of calcite cement do. In addition, there is no pattern of increased calcium content and decreased permoporosity and vice versa, which may contribute to the idea that some diagenetic factors such as silicification, dolomitization, and dissolution may not have influenced this formation as much as in the Barra Velha Formation.

Two factors that possibly assume responsibility for decreasing permoporosity are the significant presence of calcite cement throughout the Itapema Formation, especially at the base of the formation (where there is greater FF1 thickness), and the presence of fine grains and/or muddy facies, found in the middle of the formation (where there is the predominance of FF1 and FF2).

In the Barra Velha Formation, the GR does not present great variations from one flow facies to another, having its maximum values with an average of around 30.7 and 30.5 gAPI (FF2 and FF3, respectively). The PI log decreases from FF1 to FF4, with lower mean and median values for FF4 (11115 and 11054 gm/cm3.s, respectively) and higher values for FF2 (average of 12422 gm/cm3.s) and FF1 (average of 12285 gm/cm3.s).

Note that FF1 and FF2 have low permeabilities, with a median of 0.88 mD and 1.92 mD, respectively, while FF3 and FF4 show a jump in permeability values, with 16.5 and 187 mD. According to North (1985 apud Ahr, 2008), the permeability for oil reservoirs can be described, in mD, as: Low (1.0 – 15.0); Moderate (15.0 - 50.0); Good (50.0 - 250.0); Very Good (250.0 - 1,000.0) and excellent (> 1,000.0). Therefore, the Barra Velha Formation in Well A points to a low permeability for FF1 and FF2, moderate for FF3, and good for FF4. The porosities, in general, present good values for all flow facies.

According to the electrofacies defined by Dias (2021) carbonates considered reservoirs have porosities above 6% and Vclay below 20%, therefore, according to these pre-established cutoffs, all flow facies of the Barra Velha Formation would be considered reservoir carbonates, however, the permeability values considered in the calculations of these facies may refute this premise. Porosity has the highest mean and median for FF1 and the lowest mean and median for FF2, while permeability has the lowest mean and median values for FF1 and FF2. These high porosity and low permeability values, especially in FF1 and FF2 may be related to the presence of diagenetic factors such as cementation and silicification that may obstruct the primary porosity, as well as dissolution and dolomitization that may generate secondary porosity, such as vug and moldic, that may have interconnectivity or not.

The means and medians of the ECS logs of Ca, Mg, and Si present very close values. Ca and Si logs show more significant opposite behaviors when compared to the magnesium. Calcium and magnesium contents follow a trend of increase from FF1 to FF4 whereas silica content decrease from FF1 to FF4. It is worth mentioning that, as seen in Figure 50, the percentage of FF1 in the Barra Velha Formation is only 4%, and therefore, not very representative. In addition to the low representativeness of this facies, it is possible to observe that the arithmetic mean of Si content (~52%) is high, and the median of permeability (~0.88) is low, even with high porosities (~19%).

Aiming to facilitate the visualization and comparison between the data, the parameters observed for each flow facies will be presented in the form of bar graphs (Figure 51), they were constructed from the arithmetic mean values of the logs of GR, PI, Vclay, PHIE, Ca, Si and Mg, and the median of KTIM which are also shown in Table 6. It is important to emphasize that in these bar graphs, each curve has its own range of values on the y axis, which, in turn, is the same for all flow facies. However, as permeability values vary greatly, generally between 0.01 and 10000 mD, it was not possible to adopt the same scale on the y-axis for this log, thus, it requires more careful analysis. This large variation in permeability curve values, and therefore different values on the y-axis, occurred in the four wells analyzed in this dissertation.

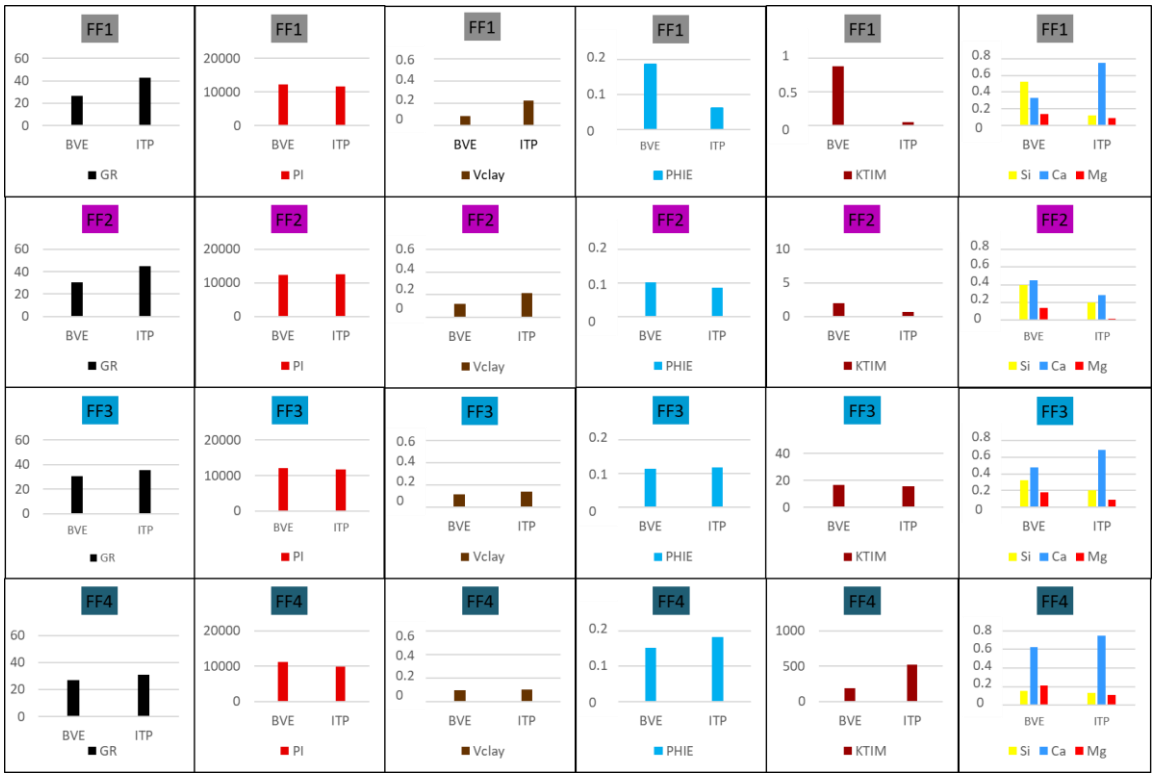

Figure 51: Bar graphs comparing different properties (GR, PI, Vclay, PHIE, KTIM, and Ca, Si, Mg, respectively) by formations (Barra Velha - BVE and Itapema – ITP, consecutively) for each flow facies in Well A. It is worth mentioning that the y-axis of the permeability values is on different scales in all the flow facies. It is worth noting that the y-axis of the permeability curve has a scale of different values for each flow facies. Therefore, it is necessary to be careful when interpreting this specific curve.

Table 7 shows the main lithologies and type of cement found in each flow facies as well as their average for the entire well, covering the two formations, Barra Velha and Itapema. Figure 52 shows some thin section images taken from the petrography report of the most present lithologies in each flow facies for each formation.

In the FF1 of the Barra Velha Formation, the predominant lithology is chert and shrubs that contain mostly quartz and chalcedony cement, whereas, in the Itapema Formation, the dominant lithologies are laminites, mudstones, and grainstones with the presence of calcite cement. In addition to chert and shrubs, FF2 has the presence of spherulite, with quartz cementation in the Barra Velha Fm., and a predominance of grainstones and laminites with calcite cementation in the Itapema Fm. FF3 has shrubs and spherulites with some samples containing quartz cement in the Barra Velha Fm. and grainstones and floatstones in the Itapema Formation. The FF4 presents a greater presence of reworked facies (grainstones), shrubs, and spherulitites in situ with dolomite cement being the predominant in the Barra Velha Fm., and in the Itapema Fm., there are facies similar to those found in FF3.

Finally, it is noted that the predominant cement throughout the Barra Velha Formation is quartz cement, whereas, in the Itapema Formation, the most common cement is calcite. Furthermore, the idea that flow facies have no direct correlation with lithology is supported, as it is possible to find the same lithologies responding to flow in different ways, and different lithologies having the same flow responses due to the diagenetic history they have gone through.

Table 7: Table with the main lithologies and types of cement present in each flow facies for both Barra Velha and Itapema formations, in addition to the percentage of each flow facies for the entire well.

	Zones	FF1	FF2	FF3	FF4
Lithology	B. Velha	chert, dolomite, shrubs	chert, shrubs, spherulitite	spherulitite, chert, shrubs	spherulitite, grainstone, shrubs
	Itapema	grainstone, laminite mudstone	grainstone, laminite	grainstone and floatstone	grainstone and floatstone
Cement	B. Velha	quartz, chalcedony	quartz, dolomite	quartz, dolomite	dolomite, quartz e calcite
	Itapema	calcite and dolomite	calcite and dolomite	calcite and quartz	calcite, dolomite and quartz
Flow Facies	Well A	16%	26%	27%	31%

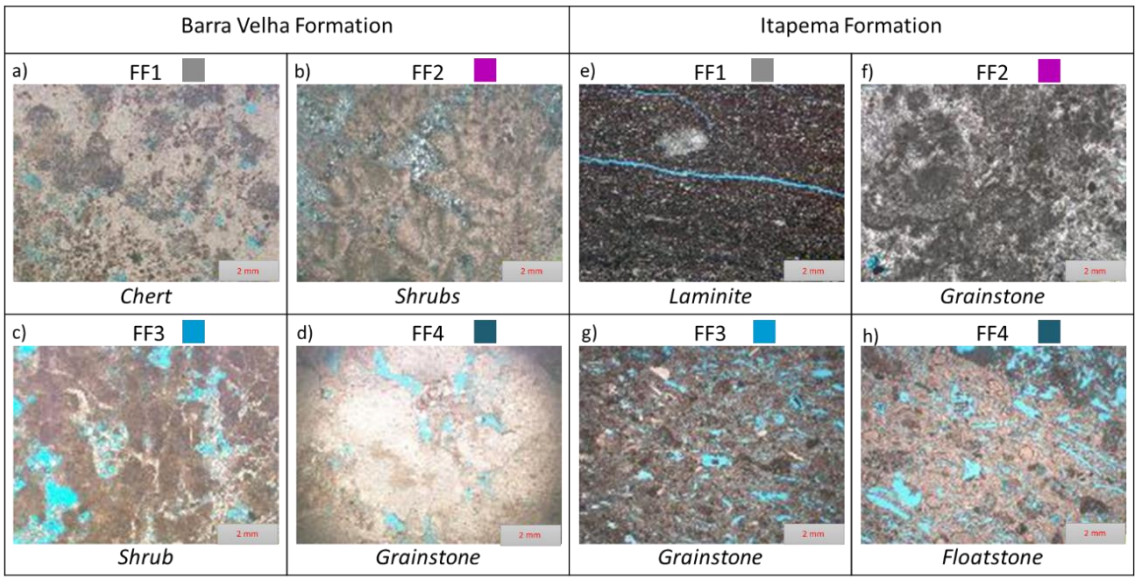

Figure 52: Images of some of the main thin section samples found in each flow facies in Well A for the Barra Velha Formation a) Chert with chalcedony as the main component, and spherulites and quartz as secondary; b) Shrubs with optical fascicular texture and mosaic, quartz and chalcedony cementation in interelement pore and quartz cementation in vugular pore; c) Shrubs with optical fascicular texture, interelement pore dolomite cementation; d) Grainstones with intraclasts and fragments of shrubs and peloids, dolomite cement and calcite in the form of sparse crystals in interparticle pore, and the Itapema e) laminite with lamination characterized by calcite, dolomite, clay, and siliciclastic grains; f) Grainstone consisting mainly of peloids, intraclasts, and bivalve mollusk bioclasts; g) Grainstone consisting mainly of bivalve mollusk bioclasts, intraclasts and with the presence of dolomitic cement; h) Floatstone with bivalve mollusc bioclasts with occurrence of calcite and quartz cement in interparticle pore.

5.3.2. Quantitative evaluation in Well B

Well B does not have a petrographic thin section analysis, nor a detailed description of the sidewall core samples. Therefore, as there is no information about the type of cement, matrix, or main constituents of the lithotypes, it is difficult to analyze and describe possible diagenetic processes. For this well, a table was created with the calculations of the mean and median of the main curves used to evaluate and estimate the flow facies. In addition to this table, two images, one containing pie charts with the mean of flow facies for each formation and the other containing some photos representing the sidewall core transversal samples collected in each flow facies, were also produced.

As previously seen in Figure 45, the Itapema Fm. has both the base and the middle dominated by FF1 with some layers of FF2. The base of this formation is mostly composed of unidentified igneous rock, and volcanic breccia, and towards the middle of the formation, there is an interval where with a significant presence of mudstones, shales,

and siltstones. Given that, Figure 53 shows that the Itapema Formation presents a higher percentage of FF1 and FF2, totaling 68% of the entire formation. On the other hand, the Barra Velha Fm. has a higher percentage of FF3 and FF4 than the Itapema Formation, totaling 81%. Besides, the Barra Velha Formation has only 7% of FF1 and 12% of FF2, and these facies are more concentrated at the top of the formation. This interval has the presence of igneous rocks, increased silica content, and reduced calcium, as well as lower porosities and permeabilities. Conversely, FF3 and FF4 are found in regions where silica content and PI are low and calcium content and permoporosity are higher.

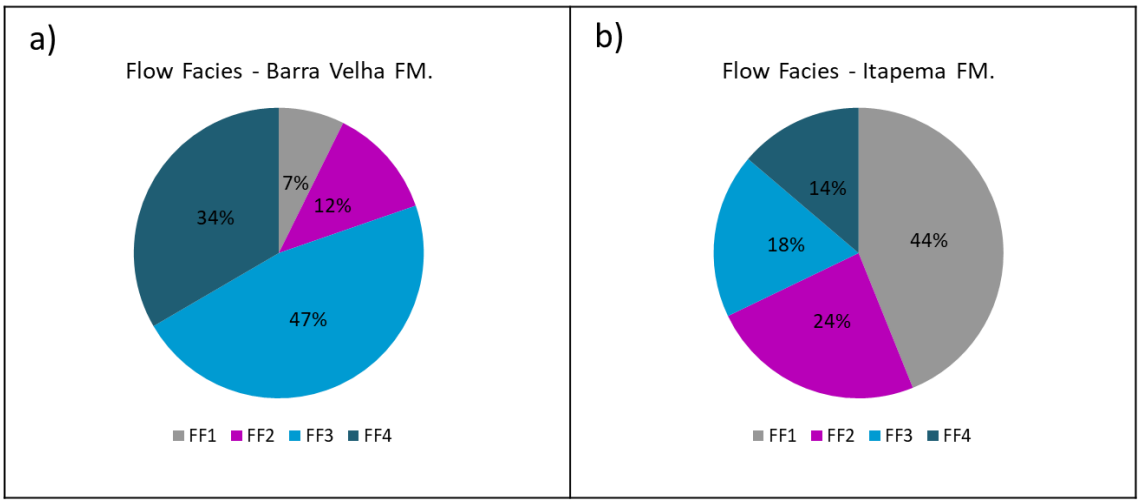

Figure 53: Pie charts with the percentage means of the flow facies for a) the Barra Velha Formation and b) for the Itapema Formation in Well B.

Table 8 shows the arithmetic mean and the median from the logs shown in Figure 45, of the Barra Velha and Itapema formations in Well B. The Itapema Formation presents GR and Vclay values for the FF1 significantly higher than those found in the Barra Velha Formation, as shown in Well A. In addition, the PI values for all the flow facies are lower when compared to the arithmetic means and medians found in the Barra Velha Formation. The means and medians for both the GR and Vclay logs and the PI log decrease from FF1 to FF4. The median of permeability has a trend of increasing from FF1 (0.009 mD, low permeability) to FF4 (83.3, mD, good permeability).

Porosity exhibits the same increasing trend. The average porosity for FF1 is 3.6%, FF2, 7%, FF3, 9.3%, and FF4, 12.8%. Furthermore, it has the arithmetic mean and median for all flow facies pretty close to those found in the Barra Velha Formation. The average of calcium content grows from FF1 (~19%) to FF4 (~92%). The magnesium content presents much lower values for all flow facies when compared to the Barra Velha Formation, having a decreasing trend from FF1 to FF4, with an average of 14% for FF1,

and only 3% for FF4. Unlike what was found in the Barra Velha Formation, the magnesium content in the Itapema Fm. seems to have a more direct relationship with permoporosity, that is, as there is an improvement in the flow facies, the Mg content decreases. Finally, the Si content has a decreasing pattern from FF1 to FF4, with the highest mean value for FF1, with 42%, and the lowest for FF4, with only 4%.

As in Well A, Well B does not present large variations in the means and medians of the GR log in the four flow facies of the Barra Velha Formation. The highest mean and median values of the GR belong to FF1 and are respectively 23.8 and 21.1 gAPI. For the rest of the flow facies, the means and medians are considerably low, being around ~20 gAPI. The same occurs for the clay volume (Vclay), having mean and median values that do not exceed 7% considering all flow facies. This behavior corroborates with the idea that the Barra Velha Formation, in this well, does not appear to have much presence of fine grains and/or muddy facies as it can be seen in Figure 45.

The mean and median of the acoustic impedance (PI) log decreases from FF1 to FF4, with an average of 16603 g.m/cm3.s in FF1 and 11689 g.m/cm3.s in FF4. Alongside Well A, Well B also presents significant variations regarding the means and medians of the permeability curves. Permeability increases from FF1 to FF4, with median close to 0 mD for FF1, 0.72 mD for FF2 (low permeability), 12.9 mD for FF3 (moderate) and 117.2 mD for FF4 (good). Porosities also follow the same pattern as the permeability, increasing from FF1 to FF4. The means and medians of porosities are not considered substantially low (except for FF1) and FF4 presents an average of 13.4%. The ECS logs have very close mean and median.

The calcium content increases from FF1 to FF4 while the magnesium and silica content behave oppositely. It is noteworthy that the magnesium log does not present significant differences in values between the flow facies, and of the three ECS logs, it is the least showing contrast from one flow facies to another. Despite this, is possible to see that the FF4 has the lowest Mg arithmetic mean, but for the other flow facies is still hard to conclude whether it is associated with worse or better flow responses.

The visualization and comparison between the data presented in the table above will be also presented in bar graphs form (Figure 54). The geophysical logs of GR, PI, PHIE, Vclay, Ca, Mg e Si are distributed according to their arithmetic means, and for KTIM the median was used.

Table 8: Table with the arithmetic mean and median of the main well-logs used in this work, for each flow facies in the Barra Velha and Itapema formations in Well B.

Flow Facies	Zones	GR (gAPI)		PI(g.m/cm3.)		KTIM (mD)		PHIE (m3/m3)		Vclay (v/v)		Ca (v/v)		Mg (v/v)		Si (v/v)	
		mean	median	mean	median	mean	median	mean	median	mean	median	mean	median	mean	median	mean	median
FF1	B. Velha	23.8	21.1	16603	17462	0.018	0.00	5.4%	3.1%	7%	5%	45%	47%	23%	23%	23%	21%
	Itapema	56.2	49.7	12880	12980	0.11	0.009	3.6%	2.3%	28%	17%	19%	14%	14%	11%	42%	44%
FF2	B. Velha	19.9	18.9	13773	13751	1.49	0.72	6.9%	6.4%	4%	3%	54%	53%	23%	23%	21%	19%
	Itapema	21.7	16.1	12655	12787	1.02	0.6	7%	6.8%	7%	3%	75%	87%	7%	1%	14%	10%
FF3	B. Velha	20.7	19.3	12782	12836	12.9	9.68	9.3%	9.2%	4%	4%	61%	60%	22%	22%	17%	15%
	Itapema	15.9	15.0	12405	12259	14.1	11.3	9.3%	9.6%	3%	3%	85%	91%	5%	0%	8%	6%
FF4	B. Velha	20.3	19.2	11689	11662	181	117.2	13.4%	13.3%	4%	4%	70%	72%	19%	19%	10%	9%
	Itapema	14.9	15.2	11395	11400	115.4	83.3	12.8%	12.6%	3%	3%	92%	94%	3%	0%	4%	4%

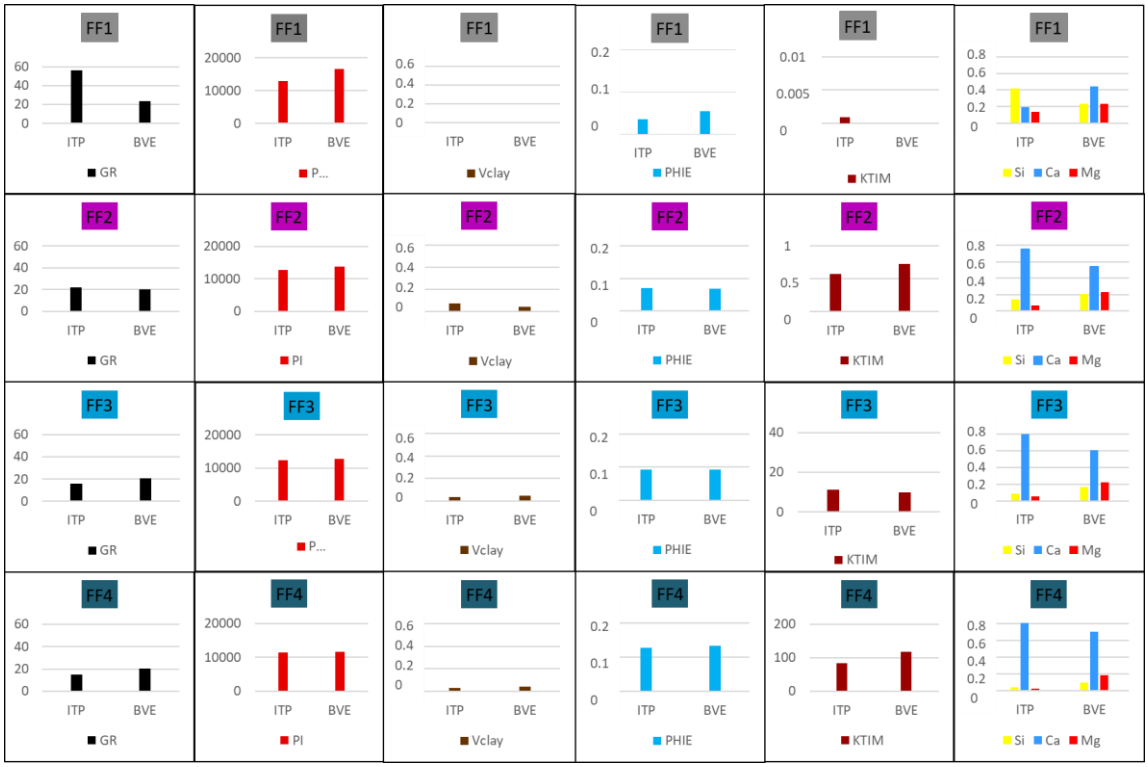

Figure 54: Bar graphs comparing different properties (GR, PI, Vclay, PHIE, KTIM, and Ca, Si, Mg, respectively) by formations (Itapema – ITP and Barra Velha – BVE, consecutively) for each flow facies in Well B. It is worth noting that the y-axis of the permeability curve has a scale of different values for each flow facies. Therefore, it is necessary to be careful when interpreting this specific curve.

Table 9 shows the main lithologies in each flow facies as well as the average of each of them for the entire well, covering the two formations, Barra Velha and Itapema.

Table 9: Table with the main lithologies present in each flow facies for both Barra Velha and Itapema formations, in addition to the percentage of each flow facies for the entire well.

	Zones	FF1	FF2	FF3	FF4
Lithology	B. Velha	Spherulite	Silicified limestone, and shrubs	Spherulite, shrubs and grainstone	Spherulite and grainstone
	Itapema	NI igneous, shale, and coquinas	Coquina and mudstone	Coquinas and grainstone	Coquinas and grainstone
Flow Facies	Well B	32%	20%	28%	20%

Figure 55 displays the transverse sidewall core sample images corresponding to the most present lithologies in each flow facies for each formation. As mentioned before, no report contains a detailed description of these photos, only a generalized description of the sidewall samples contained in the final well report provided by the ANP.

The Barra Velha Formation presents, as the predominant lithology of the FF1, spherulites with closed porosity and fissural silicification (Figure 53-a), while in the Itapema Formation the dominant lithology for this facies is shale (Figure 53-e), being possible to observe the dark color, possibly showing the presence of organic matter. A sample was collected where there is the presence of FF2 and points to silicified limestone with closed porosity in the Barra Velha Formation (Figure 53-b) while in the Itapema Formation poinst to the presence of mudstone with laminated dark gray grainstone and closed porosity (Figure 53-f). A sample corresponding to FF3, in the Barra Velha Formation, is described as limestone with spherulitic texture (Figure 53-c), and in the Itapema Formation, described as coquina with light color, good porosity (Figure 53-g). FF4 count with the presence of spherulite described as probable grainstone with good and interparticle porosity in Barra Velha Formation (Figure 53-d) and, in Itapema Formation the coquina possibly reworked with good porosity is more likely to represents this facies (Figure 53-h).

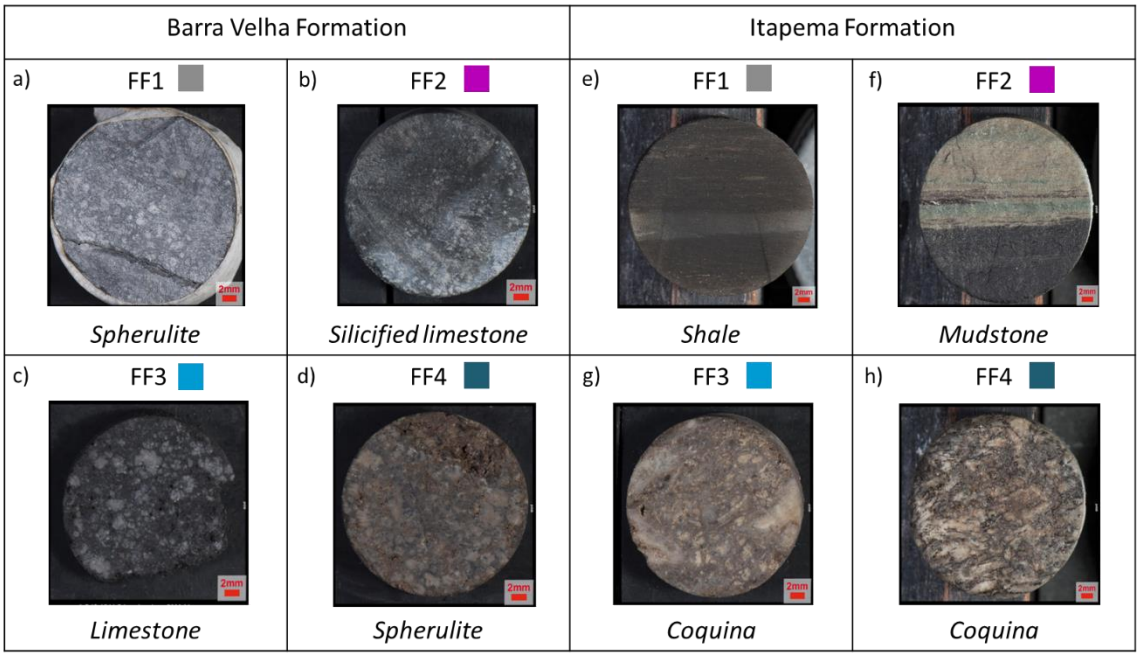

Figure 55: Images of transverse sidewall core samples for each flow facies and both Barra Velha and Itapema Formation in Well B.

5.3.3. Quantitative evaluation in Well C

This well contains information on petrographic thin sections as well as core images and sidewall core samples, so it was possible to identify the type of cement and predominant lithology in each flow facies, in addition to quantifying, through the arithmetic mean and median, patterns and behaviors of the main geophysical logs in the four estimated flow facies in both the Barra Velha and Itapema formations.

Figure 56 shows two pie charts corresponding to the two formations present in Well C. It is possible to observe that both in the Barra Velha Formation and in the Itapema Formation the percentages of FF3 and FF4 are much higher than those of FF1 and FF2 together. This behavior differs from wells A and B, which have higher averages of FF3 and FF4 only in the Barra Velha Formation. The sum of the percentages of FF3 and FF4 reaches 85% and this same sum in the Itapema Formation reaches 90%. From this, it is understood that Well C presents better permoporosity when compared to the other wells.

The Itapema Formation has only the base dominated by FF1, showing where the small percentage of FF1 (6%) of this formation probably came from. As seen previously, the basal part of this formation is composed of samples of shale and rudstones with the presence of calcite cement (Figure 47). The FF2 has a percentage of 14% being found scattered all around the formation, generally interspersed with FF3. The layers of FF2

may represent areas where possible decreases in permoporosity and calcium content, as well as an increase in silica content and GR logs have occurred. These decreases in permoporous properties and consequent worsening in flow facies may occur due to the presence of fine and/or clayey grains, that increase the values of the GR log, as well as the presence of diagenetic processes such as silicification or cementation.

The Barra Velha Formation has only 1% of FF1 and 24% of FF2. The FF2 layers are present throughout the entire range but are more concentrated from the middle to the top of the formation (Figure 47). It was also noted that where there were local increases in the Mg and Si contents and the consequent decrease in Ca, the highest concentrations of the worst flow facies were found. As observed in wells A and B, in Well C the FF3 and FF4 have the highest percentage averages of this formation, indicating that the Barra Velha Formation in Well C has, in general, good permoporous conditions.

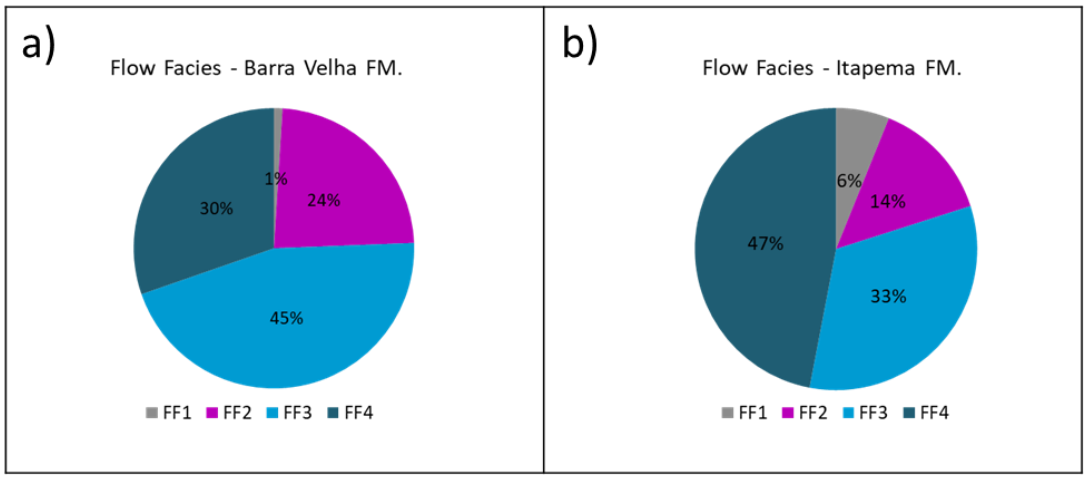

Figure 56: Pie charts with the percentage means of the flow facies for a) the Barra Velha Formation and b) for the Itapema Formation in Well C.

Through Table 10, it is possible to identify a decreasing trend in the GR, Vclay, silica, and magnesium logs from FF1 to FF4, and, in a conversely way, there is an increase in permoporosity, as well as in the calcium content from FF1 to FF4. This pattern is noted both in the Barra Velha and in Itapema formations in Well C.

The Itapema Formation has considerably higher GR and Vclay values in FF1 than the Barra Velha Formation. This same characteristic was found in Well B. The means and medians of the GR and Vclay log decrease from FF1 to FF4, having an average of 63.2 gAPI for FF1 and 23.7 gAPI for FF4. The PI values do not tend to decrease from the worst flow facies (FF1) to the best (FF4). This possibly happens because the muddy facies are not well distinguished by acoustic impedance, sometimes presenting high or low

values of PI. Permeability medians increase from FF1 (~0 mD, low permeability) to FF4 (157 mD, good permeability).

Contrary to what was found in Well B, the permeability for FF3 and FF4 is greater in the Itapema Fm. than in the Barra Velha Formation. The porosity values show the same permeability trend, increasing towards FF4, having a mean of 2% for FF1 and 14% for FF4. The arithmetic mean of the calcium content is considerably high in all flow facies all along the Barra Velha and Itapema formations. However, it is noted that the Itapema Fm. has higher values of calcium content than the Barra Velha Formation, in contrast, it has lower values of magnesium and silica. The calcium log increases from FF1 (~49%) to FF4 (~89%) and that of silica decreases from FF1 (27%) to FF4 (8%). The magnesium log does not have high values, with averages of 12.8% for FF1 and around 2% for FF2, FF3, and FF4.

As observed in Well A and Well B, Well C does not present large variations in the GR log for the four flow facies in the Barra Velha Formation. The highest mean values of the GR log belong to FF1 and FF2 with 33.31 and 32.2 gAPI, respectively, and the lowest belongs to FF4 with 24.3 gAPI. The same happens with Vclay, having an average of 26% for FF1 and 11% for FF4. Note that the GR and Vclay values are higher in Barra Velha Formation of Well C than in Well A and B, possibly due to the intervals with the presence of laminites and clay matrix diagnosed by the collected core and by the petrographic thin section samples.

The arithmetic mean and median of the PI log, in general, also show a decrease from FF1 to FF4, with an average of 14339 g.m/cm3.s in FF1 and 11775 g.m/cm3.s in FF4. As seen in the two previous wells, the means and medians of the permeability also show significant variations in Well C. The permeability medians increase from FF1 to FF4, with values of 0.02 mD (low permeability) for FF1, 0,51 mD (low) for FF2, 8.06 mD (good) for FF3 and 198.5 mD (good) for FF4. Porosity also follows the same trend, increasing from FF1 to FF4. The porosities of FF1 and FF2 are below 6% while for FF3 and FF4 are above 13%. The ECS logs have means and medians considerably close, as seen in wells A and B. The Ca content increases from FF1 to FF4 while the Mg and Si decrease.

Table 10: Table with the arithmetic mean and median of the main well-logs used in this work, for each flow facies in the Barra Velha and Itapema formations in Well C.

Flow Facies	Zones	GR (gAPI)		PI(g.m/cm3.s)		KTIM (mD)		PHIE (m3/m3)		Vclay (v/v)		Ca (v/v)		Mg (v/v)		Si (v/v)	
		mean	median	mean	median	mean	median	mean	median	mean	median	Mean	median	mean	median	mean	median
FF1	B. Velha	33.31	31.8	14339	14186	0.05	0.02	4.3%	4%	26%	25%	47%	49%	27%	25%	24%	22%
	Itapema	63.2	70.7	11180	11179	0.02	0	2%	2%	66%	81%	49%	46%	12.8%	13.3%	27%	27%
FF2	B. Velha	32.2	30.7	14084	14383	0.84	0.51	6.2%	6%	21%	19%	48%	48,7%	25%	24%	22%	21%
	Itapema	23.8	22.8	13206	13265	0.73	0.44	6%	6%	11%	6%	78%	80%	2%	0%	19%	16%
FF3	B. Velha	28.54	27.3	13278	13342	12.52	8.06	16%	14%	16%	14%	56%	58%	23%	23%	17%	16%
	Itapema	25.3	24.6	12282	12424	13.45	10.14	9%	9%	12%	9%	85%	87%%	2%	0%	12%	9%
FF4	B. Velha	24.3	23.4	11775	11871	198.5	99.51	13.5%	13%	11%	10%	59%	65%	17%	17%	11%	11%
	Itapema	23.7	22	10899	10955	266.6	157.8	14%	14%	11%	8%	89%	93%	2.4%	0%	8%	5%

Figure 57 shows the bar graphs corresponding to the arithmetic means of all logs and the median of the permeability log, for each flow facies observed in Table 10. Table 11 shows the main lithologies and cement types found in each flow facies in addition to their average for the entire well.

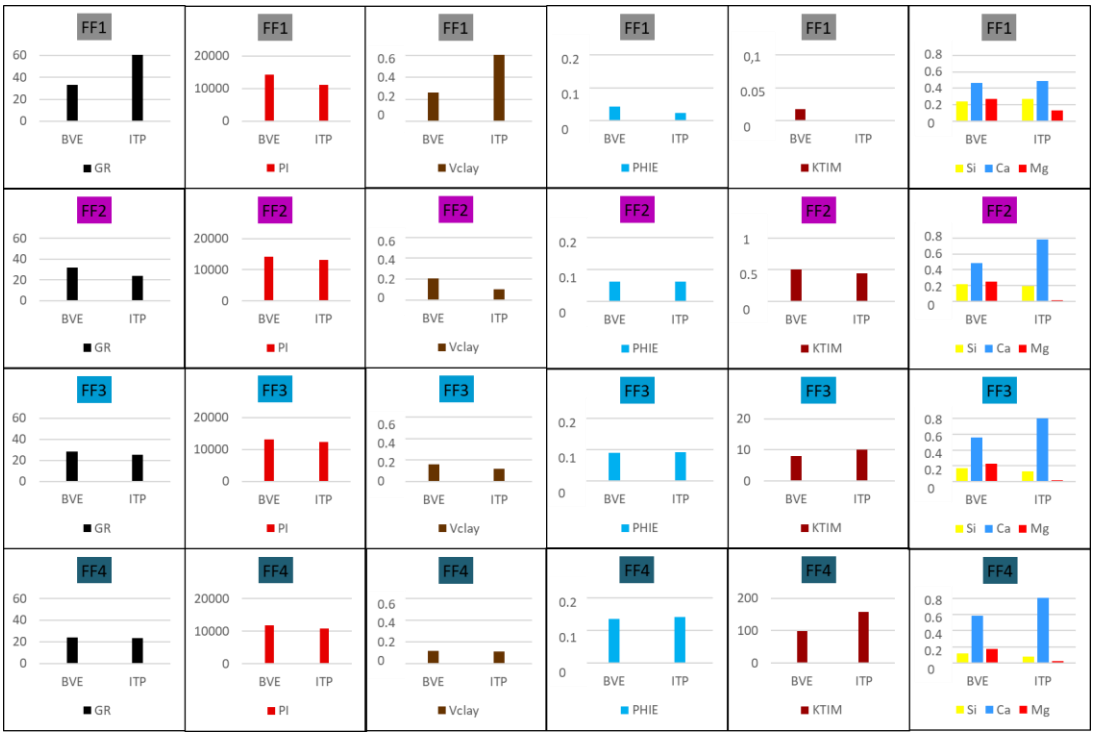

Figure 57: Bar graphs comparing different properties (GR, PI, Vclay, PHIE, KTIM, and Ca, Si, Mg, respectively) by formations (Barra Velha - BVE and Itapema – ITP, consecutively) for each flow facies in Well C. It is worth mentioning that the y-axis of the permeability values is on different scales in all the flow facies. It is worth noting that the y-axis of the permeability curve has a scale of different values for each flow facies. Therefore, it is necessary to be careful when interpreting this specific curve.

Figure 58 presents images of the petrographic thin section with examples of some of the most present lithologies in the flow facies. In the Barra Velha Formation, the FF1 contains predominantly laminites, reworked shrubs (grainstones), and shrubs in situ, with quartz and dolomite cement as the predominant ones for this facies. FF2 has a greater presence of grainstone, spherulite, some occurrences of laminite and dolomite, quartz cement, and few samples of calcite cement. FF3 and FF4 have, as predominant lithology, grainstones, shrubs, and spherulites as well as calcite, dolomite, and quartz cement. In the Itapema Formation, the dominant lithologies for the FF1 are rudstones and grainstones with calcite cement, as well as some occurrence of shales. FF2 is mostly composed of rudstones with calcite cement and some occurrences of quartz cement. Finally, FF3 and FF4 also have rudstones as dominant lithology, in addition to floatstones and calcite cement.

Table 11: Table with the main lithologies and types of cement present in each flow facies for both Barra Velha and Itapema formations, in addition to the percentage of each flow facies for the entire well.

	Zones	FF1	FF2	FF3	FF4
Lithology	B. Velha	Laminite, grainstone, shrubs	Grainstone, spherulite, laminite	Grainstone, spherulite, shrubs	Grainstone, spherulite, shrubs
	Itapema	Rudstone, grainstone	Rudstone	Rudstone, floatstone	Rudstone, floatstone
Cement	B. Velha	Quartz, dolomite	Dolomite, quartz, calcite	Calcite, quartz, dolomite	Calcite, quartz, dolomite
	Itapema	Calcite	Calcite, quartz	Calcite, quartz	Calcite, quartz
Flow Facies	Well C	4%	18%	38%	40%

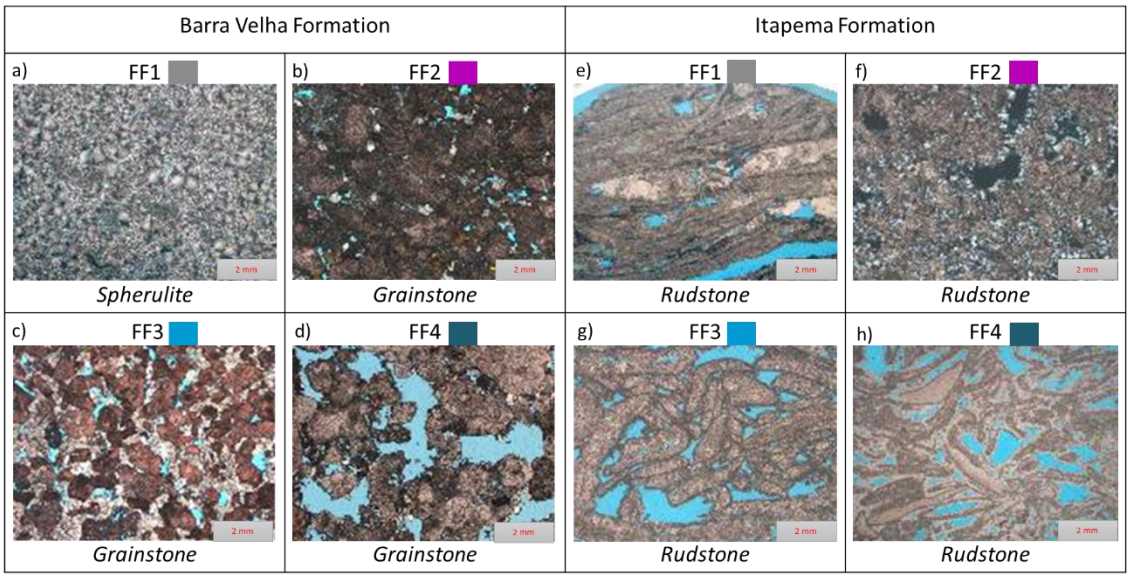

Figure 58: Images of some of the main thin section samples found in each flow facies in Well A for the Barra Velha Formation a) Spherulite with dolomite and mud with muddy matrix and quartz cementation; b) Grainstone with peloids and dolomite cementation in interparticle pores; c) Grainstone with fragments of shrub and spherulite, and dolomite cementation; d) Grainstones with fragments of shrubs and spherulites, dolomite and calcite cementation, and the Itapema e) Rudstone with micritic matrix and calcite cement; f) Rudstone consisting mainly of bioclasts, with calcite and quartz cementation; g) Rudstone consisting mainly of bivalve mollusk bioclasts, intraclasts and with the presence of dolomitic cement; h) Rudstone consisting mainly of bioclasts with the occurrence of calcite cement in an interparticle pore.

5.3.4. Quantitative evaluation in Well D

As previously seen, Well D was drilled only up to the Barra Velha Formation, therefore, for comparative purposes between the Barra Velha and Itapema formations, this well will not be considered, being used only for comparative means of the Barra Velha formations between the four wells. Well D contains a petrographic sheet report in addition to images of plugs and cores, making it possible to identify the type of lithology and cement predominant in each flow facies.

Figure 59 shows the pie chart with the average of the four flow facies of the Barra Velha Formation in Well D. It is possible to observe that the highest percentage of flow facies is concentrated in FF1 with 39% and in second place is FF4, with 25%. As seen earlier, this well is full of igneous rocks at both the base, middle, and top of the formation. The presence of igneous rocks, together with the presence of fine grains, which represents a "dirtier" interval, are mostly responsible for the greater presence of FF1 in the well. This behavior can also be observed in Well B, where there is a thick range of igneous rocks and consequently of FF1.

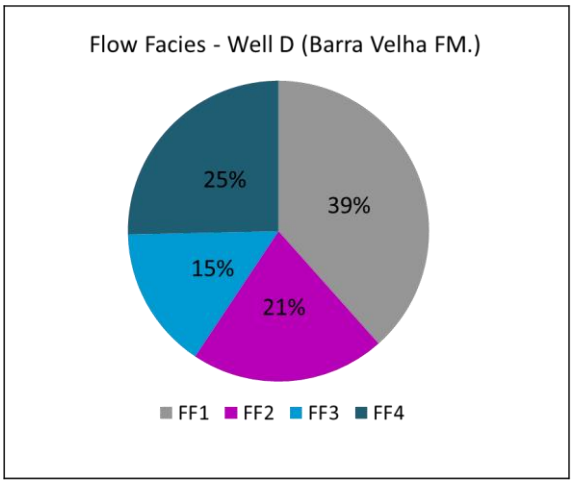

Figure 59: Pie charts with the percentage means of the flow facies for the Barra Velha Formation in Well D.

The FF2, for the most part, is related to tighten carbonates cemented with quartz and/or dolomite, as well as to rocks that have undergone diagenetic processes such as silicification (Figure 49). Furthermore, they may be related to laminated carbonates, with the presence of fine grains due to some areas with high GR and Vclay values. FF3 and FF4 are related to cleaner shrubs with the presence of cement that possibly did not fill the entire pore throat. If the thickness of the igneous rocks and FF1 related to them were not taken into account, possibly the FF4 would represent the highest average percentage of flow facies in Well D. The range that takes the middle of the formation to the base of the igneous rock present at the top, has good permoporous properties.

Table 12 shows the mean and medians of the main geophysical logs carried out in the analyzes of this work. From the outset, it is possible to observe that the GR values present higher values in the Barra Velha Formation of this well than when compared to the previously analyzed wells. The highest means of the GR log belong to FF2 with 51.32 gAPI and FF1 with 48.7 gAPI, and the lowest mean is for FF4 with 36.9 gAPI. Thus, as in the previous wells, both GR and Vclay values decrease from FF1 to FF4. FF2 has the highest mean percentage of Vclay ~22%, whereas FF4 has ~12%. The high values of the GR and Vclay logs reflect the presence of fine and/or clayey grains (e.g. laminites and mudstones).

The means and medians of the acoustic impedance log (PI) do not differ much and show the same tendency to decrease from FF1 to FF4. FF1 has a mean PI of 15293 g.m/cm3.s and FF4 of 10156 g.m/cm3.s, this difference of approximately 5000 g.m/cm3.s is due to the high acoustic impedance of some igneous rocks while cleaner and more

porous carbonates tend to have low PI values. As seen in the other wells, the merged permeability log (KTIM_merged) presents mean and median values that vary greatly from one flow facies to another. FF1, for example, has a median of 0.007 mD (low), FF2 of 0.72 mD (low), FF3 of 9.25 mD (low) and FF4 with 427.6 (very good).

The porosities show the same pattern of increasing from FF1 to FF4. The porosity means for FF1, FF2, FF3 and FF4 are, respectively, 3.4%, 8%, 9.9% and 16.5%. The Ca content has the lowest mean value for FF1 compared to wells A, B, and C, with only 16%, possibly due to the presence of igneous rocks that generally have higher silica contents. The highest mean of Ca belongs to the FF4 with 71%. The Mg content shows a slight decrease from FF1 to FF4 but nothing very significant. The Mg values are relatively low throughout the formation, with the highest percentage mean of 12% for FF1.

The silica log is interesting because, as in Well A, it presents relatively high values for all flow facies, except for FF4. This behavior can illustrate the great influence of silica and the silicification process in this well since samples of chert were collected and quartz cement is the most present throughout the entire formation. In addition, the Si content sometimes appears to significantly reduce permoporosity and sometimes not so much.

Table 12: Table with the arithmetic mean and median of the main well-logs used in this work, for each flow facies in the Barra Velha Fm. in Well D.

Flow Facies	Zone	GR (gAPI)		PI(g.m/cm3.s)		KTIM (mD)		PHIE (m3/m3)		Vclay (v/v)		Ca (v/v)		Mg (v/v)		Si (v/v)	
		mean	median	mean	median	mean	median	mean	median	mean	median	mean	median	mean	median	mean	median
FF1	B. Velha	48.7	33.82	15293	16485	0.09	0.007	3.4%	2%	19%	7%	16%	12%	12%	11%	43%	43%
FF2	B. Velha	51.32	45.58	12822	12773	2.30	0.72	8%	7%	22%	16%	38%	42%	10%	8%	40%	39%
FF3	B. Velha	40.9	38.7	12000	11938	17.17	9.25	9.9%	10%	14%	13%	52%	57%	9.1%	9%	35%	34%
FF4	B. Velha	36.9	37.4	10156	10036	869.6	427.6	16.5%	17%	12%	12%	71%	71%	10.1%	10.1%	17%	14%

Figure 60 shows a different way to visualize the arithmetic mean and median values observed in the table above for each flow facies. This well has only the Barra Velha Formation and the arithmetic means were used for all geophysical logs, except for the permeability in which the median was used.

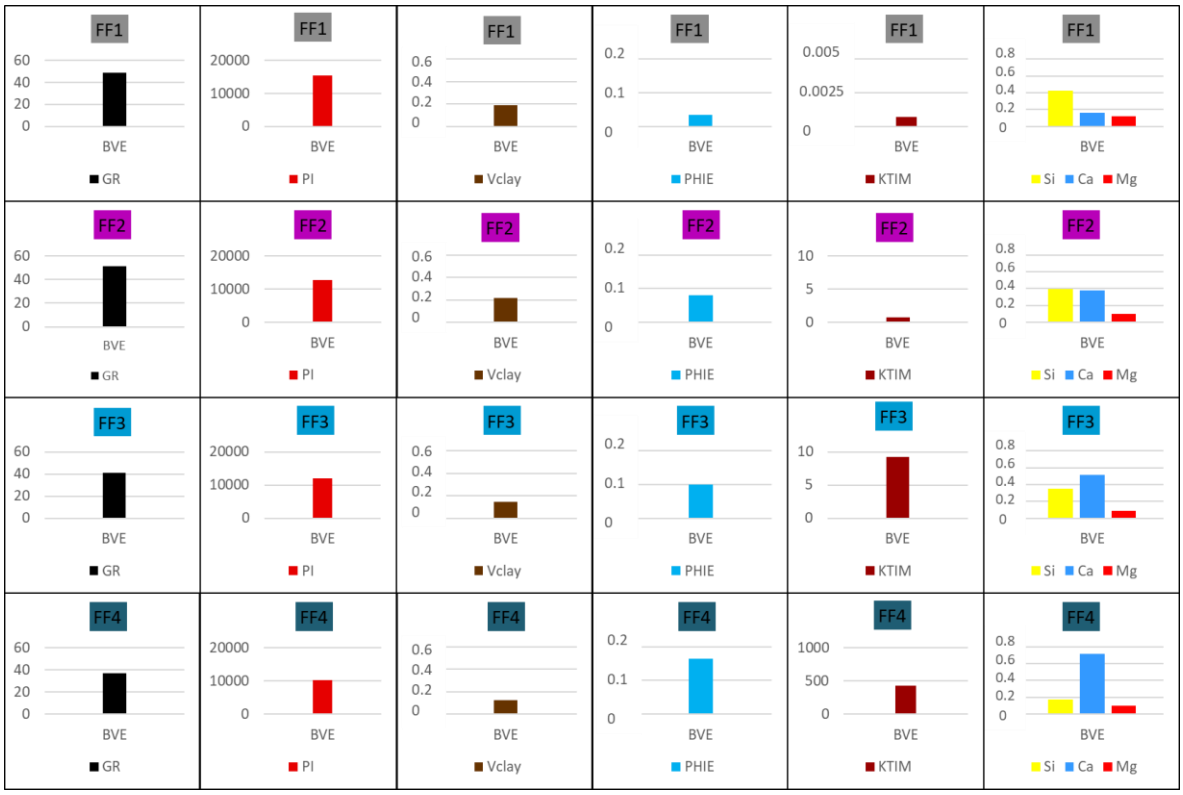

Figure 60: Bar graphs comparing different properties (GR, PI, Vclay, PHIE, KTIM, and Ca, Si, Mg, respectively) by Formation (Barra Velha – BVE) for each flow facies in Well D. It is worth noting that the y-axis of the permeability curve has a scale of different values for each flow facies. Therefore, it is necessary to be careful when interpreting this specific curve.

Table 13 shows the main lithologies and types of cement for each flow facies in the Barra Velha Formation. Figure 61 displays the images of the petrographic thin section as well as sidewall core and plug samples. The dominant lithologies of the FF1 are laminites (Figure 61-a), basalt, and diabase, as well as quartz, dolomite, and bitumen cement.

In FF2 there is a predominance of in situ shrubs with quartz cement, dolomite, as well as a few samples of breccia with quartz, dolomite, and bitumen cementation. Furthermore, FF2 is very characteristic due to the presence of chert, with intense quartz cementation and some presence of chalcedony cement. In Figure 61-b it is possible to observe the chert sample with intense quartz cementation.

The FF3 and FF4 are essentially composed of shrubs and spherulites in situ and reworked of shrubs and spherulites (grainstones) and the predominant cement is dolomite and quartz. Figure 61-c shows a very porous shrub with dolomitic cement. Figure 61-d shows the thin section and plug photos of a very porous spherulite with dolomite and dolomitic cement.

Table 13: Table with the main lithologies and types of cement present in each flow facies for Barra Velha Fm., in addition to the percentage of each flow facies for the entire well.

	Zones	FF1	FF2	FF3	FF4
Lithology	B. Velha	Laminite, diabase and basalt	Shrubs, chert and breccia	Shrubs, grainstone and spherulite	Shrubs, spherulite and grainstone
Cement	B. Velha	quartz, dolomite, bitumen	quartz, dolomite, bitumen	dolomite, quartz	dolomite, quartz
Flow Facies	Well D	39%	21%	15%	25%

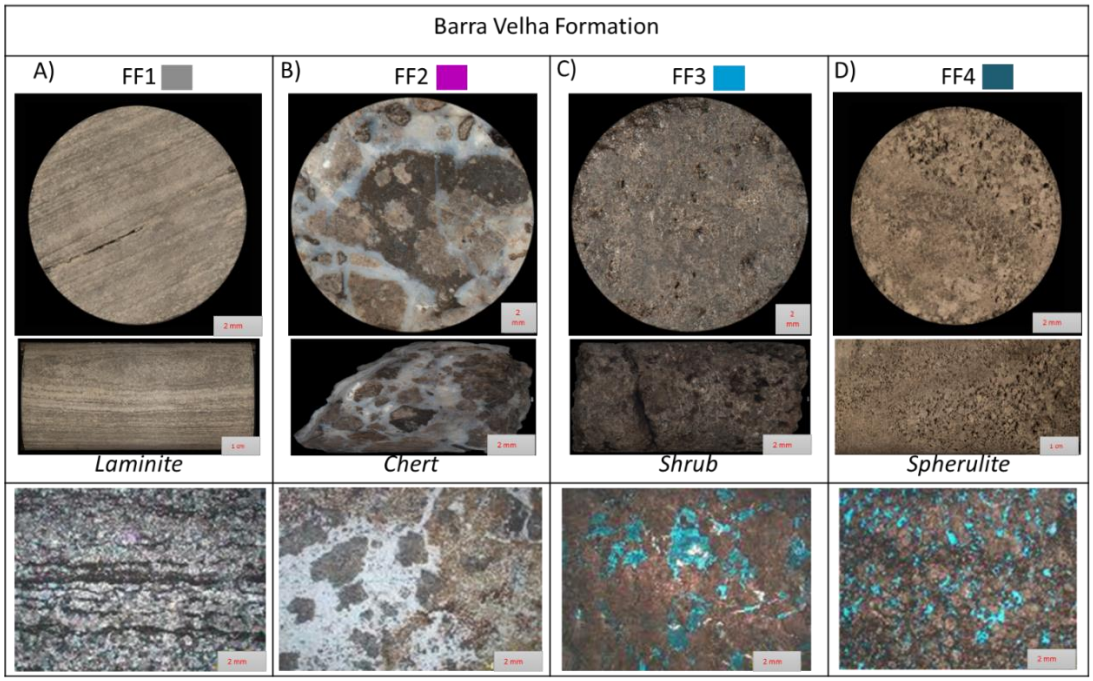

Figure 61: Images of some of the main thin section samples found in each flow facies in Well A for the Barra Velha Formation: a) Laminite characterized by calcite and organic matter, muddy and organic matrix; b) Chert consisting mainly of quartz and chalcedony in addition to shrub fragments, 15% quartz cementation; c)Shrub with dolomite and quartz cementation; d) Spherulite with dolomite and dolomitic cementate.

5.3.5. Quantitative analysis in all wells

In addition to the quantitative analysis carried out in each well separately, the arithmetic means and median of the main curves used in this work were calculated for all wells together. Thus, analyzes were carried out for each formation, both the Barra Velha

and Itapema, considering all wells. It is noteworthy that the main objective of this statistical analysis is to enable a comparison between the estimated flow facies and the behavior of the main curves in each of these facies in the Barra Velha and Itapema formations. Therefore, for comparative purposes, four wells will be considered in the Barra Velha Fm. and only three in the Itapema Fm. since Well D has only the Barra Velha Formation.

As mentioned above, the arithmetic mean is more suitable for situations where the values do not show a large discrepancy. In turn, the median can also have limitations that, by discarding the values more to the right and the left, can end up resulting in values that are lower or higher than expected. In the case of the analyzed wells, the means and medians of the curves, except for the permeability curve, presented similar values, so the arithmetic mean was considered. On the other hand, the values of the permeability logs presented very different mean and median values precisely because they present great variation and plenty of intervals with spurious points. Therefore, for the analysis of the permeability by the NMR and with the applied merge, the medians were considered.

Besides the calculations performed on the well domain, quantitative analyzes were performed for the seismic domain. These calculations were executed in order to compare the results obtained at both the well and seismic scales. In addition, the last section of this chapter will address, in more detail, the behavior of flow facies in the seismic volume as well as the prediction of the probability of occurrence of each flow facies.

Table 14 considers the Itapema and Barra Velha formations and it contains the data for the four wells. It is noted that, in general, for the four wells, both the Barra Velha and the Itapema show a tendency to decrease the GR, Vclay, PI, and Si logs from FF1 to FF4 while the porosity, permeability, and calcium content exhibit opposite behavior. The Mg content does not show any pattern of increase or decrease in the direction of FF1 to FF4 or vice versa, on the contrary, both in Barra Velha Formation and in Itapema, it appears sometimes decreasing towards FF4, sometimes increasing. However, if a more general behavior is considered, the magnesium content tends to decrease from FF1 to FF4. Furthermore, it was observed that the calcium content is higher in the Itapema Formation in all wells than in the Barra Velha Formation, on the other hand, the high silica content is, in general, more common in the Barra Velha Fm. than in Itapema.

Table 14: Table with arithmetic means of well logs by flow facies for wells A, B, C and D, and the median of permeability.

Wells	Flow Facies	Zones	GR (gAPI)	PI(g.m/cm3.s)	KTIM (mD)		PHIE (m3/m3)	Vclay (v/v)	Ca (v/v)	Mg (v/v)	Si (v/v)
			mean	mean	mean	median	mean	mean	mean	mean	mean
Well A	FF1	B. Velha	26.44	12285	1.36	0.88	19%	8%	33%	14%	52%
		Itapema	42.7	11706	0.075	0.05	6%	22%	75%	9%	12%
	FF2	B. Velha	30.7	12422	3.39	1.92	10%	12%	45%	14%	40%
		Itapema	44.8	12509	4.4	0.88	9%	21%	64%	12%	20%
	FF3	B. Velha	30.5	12093	24.9	16.5	11%	11%	48%	18%	33%
		Itapema	35.67	11686	32.7	15.7	12%	14%	69%	9%	20%
	FF4	B. Velha	26.8	11115	331.2	187.7	15%	9%	62%	21%	16%
		Itapema	31.2	9838	1484	524.8	18%	10%	75%	11%	13%
Well B	FF1	B. Velha	23.8	16603	0.018	0.00	5.4%	7%	45%	23%	23%
		Itapema	56.2	12880	0.11	0.009	3.6%	28%	19%	14%	42%
	FF2	B. Velha	19.96	13773	1.49	0.72	6.9%	4%	54%	23%	21%
		Itapema	21.7	12655	1.02	0.6	7%	7%	75%	7%	14%
	FF3	B. Velha	20.75	12782	12.9	9.68	9.3%	4%	61%	22%	17%
		Itapema	15.9	12405	14.1	11.3	9.3%	3%	85%	5%	8%
	FF4	B. Velha	20.3	11689	181	117.2	13.4%	4%	70%	19%	10%
		Itapema	14.9	11395	115.4	83.3	12.8%	3%	92%	3%	4%
Well C	FF1	B. Velha	33.31	14339	0.05	0.02	4.3%	26%	47%	27%	24%
		Itapema	63.2	11180	0.02	0	2%	66%	49%	12,8%	27%
	FF2	B. Velha	32.2	14084	0.84	0.51	6.2%	21%	48%	25%	22%
		Itapema	23.8	13206	0.73	0.44	6%	11%	78%	2%	19%
	FF3	B. Velha	28.54	13278	12.52	8.06	16%	16%	56%	23%	17%
		Itapema	25.3	12282	13.45	10.14	9%	12%	85%	2%	12%
	FF4	B. Velha	24.3	11775	198.5	99.51	13.5%	11%	59%	17%	11%
		Itapema	23.7	10899	266.6	157.8	14%	11%	89%	2,4%	8%
Well D	FF1	B. Velha	48.7	15293	0.09	0.007	3.4%	19%	16%	12%	43%
	FF2	B. Velha	51.32	12822	2.30	0.72	8%	22%	38%	10%	40%
	FF3	B. Velha	40.9	12000	17.17	9.25	9.9%	14%	52%	9.1%	35%
	FF4	B. Velha	36.9	10156	869.6	427.6	16.5%	12%	71%	10.1%	17%

Wells C and D have a dirtier Barra Velha Formation, with the highest percentage averages of the GR log for the four flow facies. In the Itapema Formation, the four wells

have the highest averages of GR belonging to FF1 with values above 42 gAPI, this is due to the presence of intervals with fine grains in the four wells (ex: mudstones, and laminites). Well A presents a very peculiar behavior when compared to other wells, mainly in the Barra Velha Formation. It has the highest means of Si content that, given the porosity values, appear sometimes affecting significantly, filling the pores, and sometimes not changing much. An example of this is the fact that FF1 has an average percentage of porosity (19%) higher than FF3 and FF4. However, permeability is a determining factor to analyze the permoporous characteristics, that is, even though FF1 has good porosity, permeability has a median of 0.88 mD, whereas FF4 has a median of 187.7 mD. Therefore, there may have occurred some diagenetic processes generating secondary porosities without great interconnectivity between them.

After estimating the arithmetic means and median in each well separately, the same statistical measurements were performed for all wells together. In Table 15 is possible to notice that the Itapema Formation has the same characteristics concerning the trends of the curves as the Barra Velha Formation, that is, at this point, it is already possible to see that the GR, Vclay, and Si curves behave in an opposite way to the porosity and permeability curves, as well as calcium content. Therefore, it is noted that the factors responsible for the decrease in permoporosity are, in general, the silica content, and the presence of fines and/or clay in both formations.

In the Itapema Formation, the Mg content appears to be more distinguishable, and its increase is also associated with lower permoporosity. Also, it is important to highlight that the averages of the GR and Vclay for FF1 are highest in Itapema Fm., with 54.03 gAPI and 39%, respectively. In contrast, the average of the PI for FF1 is lower than for FF2 and FF3, result that is different than expected. In general, as the porosity increases, the PI decreases, therefore, the FF1 should present the highest values of PI among all the flow facies because they represent the worst permoporosity. This distinct behavior can be explained by the GR and Vclay because their high values indicate the presence of clay, and the elastic parameters do not show good responses with regard to distinguishing muddy carbonates from porous carbonates, since they both have low impedances. This behavior will be noted in more detail in the next section.

In the Barra Velha Fm., the GR, Vclay, and PI logs decrease from FF1 to FF4, reaching averages of 33.06 gAPI, 15%, and 14630 g.m/cm3.s, respectively, for FF1 and 27.07 gAPI, 9%, and 11184 gm /cm3.s for FF4 The mean porosities found for FF1 and

FF2 are equal, 8%, but the median shows a difference of 3%. The porosity means and medians for FF3 and FF4 are very close, 12% and 15%, respectively. It is interesting to note that the average clay content is no more than 15% and the average porosity is greater than 8% in all flow facies. These values are considered reasonable and may even be classified as facies reservoir carbonate I (Dias, 2021). However, what will determine its permoporous quality are the permeability values.

The medians of the permeability for FF1 and FF2 are considered low according to North (1985) apud Ahr (2008), with medians of 0.01 and 0.72 mD, respectively. FF3 has a permeability considered moderate (median of 9.5 mD) and FF4 has a good permeability (median of 152.45 mD). The ECS log of calcium shows an increase pattern from FF1 to FF4 with an overall mean of 35% and 66%, respectively. Roughly speaking it can be said that the magnesium content has a slight tendency of decreasing from FF1 to FF4. Finally, the silica content, as previously observed, presents a decrease pattern from FF1 to FF4.

Table 15: Arithmetic means and medians of the geophysical logs in each flow facies for the four wells together in both Barra Velha and Itapema formations.

Flow Facies **(Four Wells)c**	Zones	GR (gAPI)		PI(g.m/cm3.s)		KTIM (mD)		PHIE (m3/m3)		Vclay (v/v)		Ca (v/v)		Mg (v/v)		Si (v/v)	
		mean	median	mean	median	mean	median	mean	median	mean	median	mean	median	mean	median	mean	median
FF1	B. Velha	33.06	28.4	14630	15336	0.37	0.01	8%	4%	15%	7%	35%	38%	19%	19%	36%	33%
	Itapema	54.03	49.7	11922	11963	0.068	0.0009	4%	2%	39%	17%	48%	46%	12%	11%	27%	27%
FF2	B. Velha	33.54	29.3	13275	13263	2	0.72	8%	7%	15%	13%	46%	45%	18%	18%	31%	30%
	Itapema	30.1	22.8	12790	12787	2.05	0.6	7%	7%	13%	6%	72%	80%	7%	1%	18%	16%
FF3	B. Velha	30.17	28.37	12539	12414	16.87	9.5	12%	11%	11%	12%	54%	58%	18%	20%	26%	22%
	Itapema	25.62	24.6	12124	12259	20.1	11.3	10%	10%	10%	9%	80%	81%	5%	0%	13%	9%
FF4	B. Velha	27.075	24.55	11184	11358	395.1	152.45	15%	14%	9%	9%	66%	68%	17%	18%	14%	12%
	Itapema	23.26	22	10710	10955	622	157.8	15%	14%	8%	8%	85%	93%	5%	0%	8%	5%

Figure 62 shows the bar graphs for the four wells together. As observed in each separate well, it is possible to notice some trends in the analyzed curves. In general, the GR and the Vclay are higher in the Barra Velha Fm. for all flow facies, except for the FF1, and in both formations there is a tendency for values to decrease from FF1 to FF4. The same behavior observed in the GR and Vclay curves can be seen in the PI values, in addition, the Barra Velha Formation presents higher values of PI for all flow facies, when compared to Itapema Formation. The values of Si and Mg also show the same behavior, decreasing from FF1 to FF4, being higher in the Barra Velha Formation. Unlike the curves mentioned above, PHIE, KTIM and Ca increase from FF1 to FF4, and the calcium

content in the Barra Velha Formation is lower than that found in the Itapema Formation, for all flow facies.

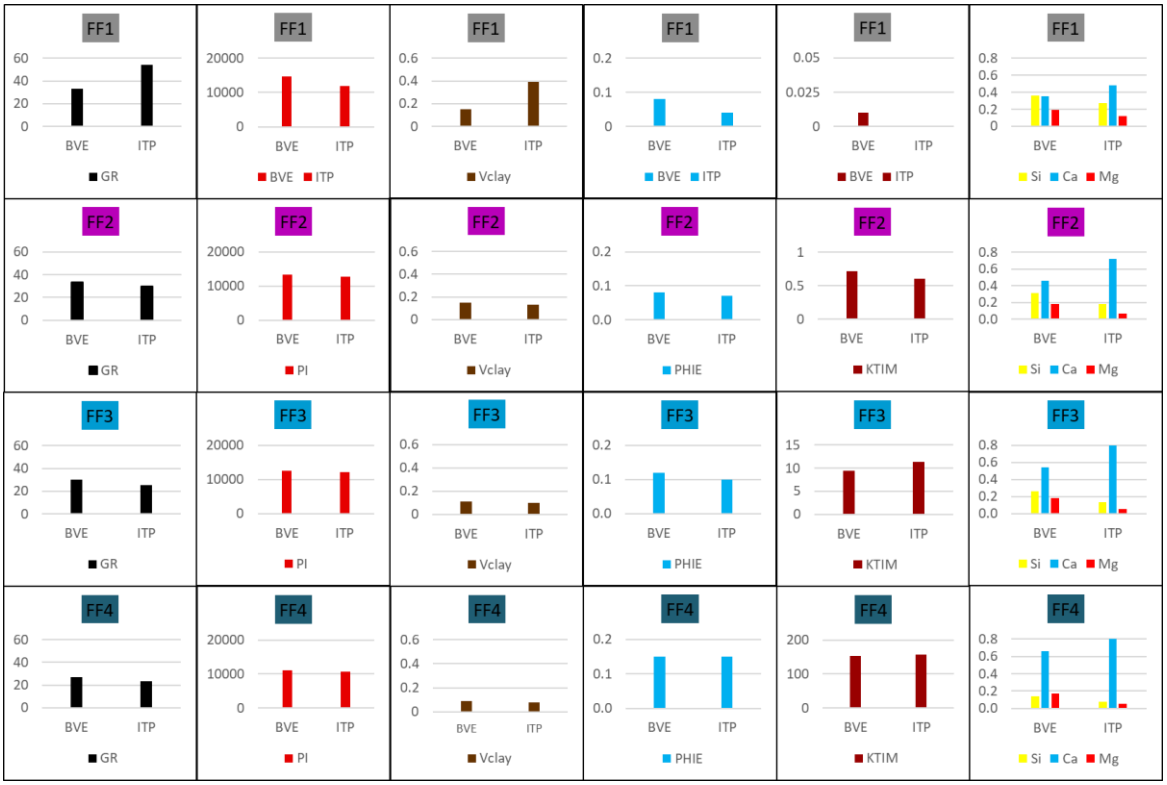

Figure 62: Bar graphs comparing different properties (GR, PI, Vclay, PHIE, KTIM, and Ca, Si, Mg, respectively) by formations (Itapema – ITP and Barra Velha – BVE, consecutively) for each flow facies in the four wells together. It is worth noting that the y-axis of the permeability curve has a scale of different values for each flow facies. Therefore, it is necessary to be careful when interpreting this specific curve.

Table 16 shows the percentage averages of each flow facies in each well for both Barra Velha and Itapema formations. In the last column of this table are the means for all wells together, at the well scale. In general, the percentage of FF1 in the Itapema Fm. is higher (25%) than in the Barra Velha Formation (13%) for all wells together. In wells A, B, and C, separated, this pattern is also observed. In wells A, B, the sum of percentages of FF1 and FF2 are higher in the Itapema Fm. than in the Barra Velha. It is worth remembering that in the Itapema Fm. of Well A there is a significant interval with the presence of fine grains and/or clay with organic matter. Moreover, Well B also has a considerable interval with the presence of muddy facies, as well as igneous rocks.

On the other hand, Well C has a higher percentage of the sum of FF3 and FF4 in the Itapema Formation and this is probably related to the presence of higher values of the GR and Vclay logs in the Barra Velha Fm., in addition to the significant presence of laminites throughout its entire formation. Also, in Well C, the silica and magnesium

content is also higher than in the Itapema Formation. In this well, FF3 and FF4 have the highest percentages of flow facies in both formations when compared to the other wells. Well D has only the Barra Velha Formation and behaves differently from the other wells. The FF1 and FF2 summed to represent the highest percentages of flow facies for this well. This is due to the fact that the well is covered with igneous rocks that, in this work, are acting as permeability barriers, in addition to the strong presence of intervals with mudstones, shales, and laminites along this formation. Furthermore, the silica and magnesium content are higher than those found in the Barra Velha Fm. of wells B and C. Finally, the average of the flow facies of all the wells together points to a higher percentage of FF3 and FF4 in the Barra Velha Formation and of FF1 and FF4 in the Itapema Formation, but when adding the best flow facies (FF3 and FF4) and the worse (FF1 and FF2) it is noted that the sum of FF3 and FF4 are greater than that of FF1 and FF2 in both formations.

Table 16: Pie charts with the percentages of each flow facies at the well scale, by Formation and by well with the corresponding thicknesses for each Formation.

Zones	WELL A	WELL B	WELL C	WELL D	ALL WELLS
Barra Velha	~273m 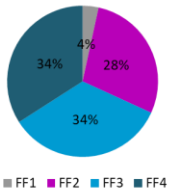	~132m 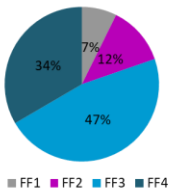	~218m 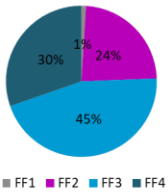	~573m 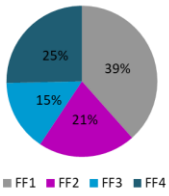	Flow Facies 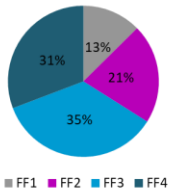
Itapema	~242m 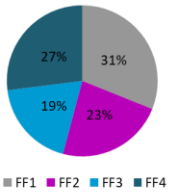	~243m 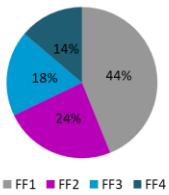	~262m 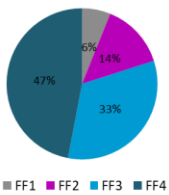		Flow Facies 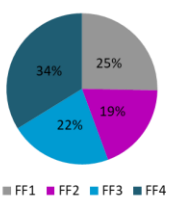

Erro! Autoreferência de indicador não válida. presents the same results as the previous one, but with the flow facies at the seismic scale, that is, after the curves have been upscaled. It is possible to observe that in the Itapema Formation the FF3 increased in all wells, FF1 practically remained the same, FF2 did not show very significant changes, and the FF4 decreases for wells A, B, and C. In the Barra Velha Formation of all wells, it can be noticed the same behavior, there was a significant increase in the percentage averages of FF3 with the upscale. Along with this, FF4 decreased, FF1 either showed a decrease or remained practically the same and FF2 increased only in Well A.

Finally, with the sum and averages of all wells, in both the Itapema and Barra Velha formations, the highest percentage averages belong to FF3. FF4 decreases significantly and FF1 and FF2 do not show major changes when compared to the well scale. It is noteworthy that both at the seismic and well scale, the sum of the percentages of FF3 and FF4 are greater for the two formations.

Table 17: Pie charts with the percentages of each flow facies with the upscale, by Formation and by well with the thicknesses corresponding to each Formation.

Zones	WELL A_UPS	WELL B_UPS	WELL C_UPS	WELL D_UPS	ALL WELLS_UPS
Barra Velha	~273m 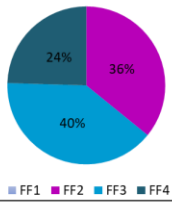	~132m 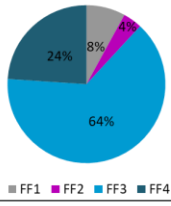	~218m 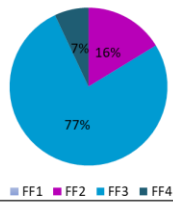	~573m 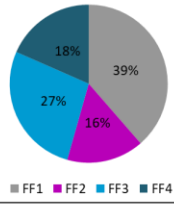	Flow Facies_UPS 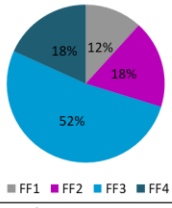
Itapema	~242m 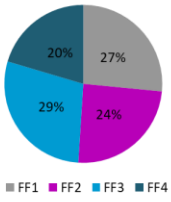	~243m 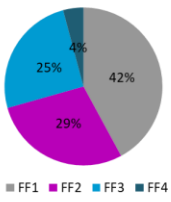	~262m 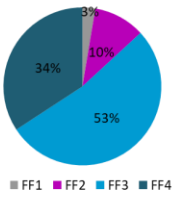		Flow Facies_UPS 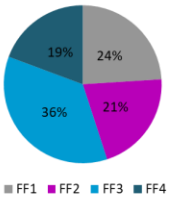

5.4. Rock physics crossplot

The crossplots that will be shown in this section were built by using acoustic and petrophysics parameters calculated from the geophysical well logs. The PI versus Ln(FZI) and PI versus PHIE crossplots were made in the four wells presented in the previous sections. The construction and analysis of crossplots aim to help understand how the flow facies distribution will be, and whether there is a visible separation of these facies when using acoustic and petrophysical parameters. The information obtained from these crossplots can serve as a basis for building a distribution model of flow facies in the seismic volume for both Barra Velha and Itapema formations.

Crossplots data were carried out for the Barra Velha and Itapema formations together, in each well, and for the four wells together. The Ln(FZI) was obtained from the NMR effective porosity and permeability curves, and in the wells with the presence of igneous, the porosity and permeability logs were used with the merge of the NMR and DT curves.

PI x Ln(FZI) crossplots

Figure 63 shows the PI versus Ln(FZI) crossplots performed in wells A, B, C, and D. As expected, the flow facies have a good correlation and, in general, it is possible to observe the behavior of each of these facies in relation to the acoustic impedance and Ln(FZI) logs. It is noteworthy that higher values of Ln(FZI) represent higher permoporosity and lower values of Ln(FZI) otherwise. The acoustic impedance values are generally influenced by the porosity of the rock, that is, more porous rocks tend to have a lower PI value and less porous and/or tighten rocks, as well as some igneous rocks, tend to have higher PI values. In other words, porosity generally has an inverse relationship with acoustic impedance. However, it is possible to see in some wells that FF1, which represents the smallest porosity or zero porosity, sometimes has high and sometimes low PI values.

This happens because in some wells the presence of fine grains and/or muddy facies, that belong to FF1, end up hinders the good relationship that exists between acoustic impedance and some petrophysical parameters such as porosity. Thus, when there is the presence of muddy facies or fine grains, FF1 can be confused with the behavior of the FF3 and FF4 which, in turn, would represent the reservoir rocks, making it a great challenge to use porosity modeling and facies classification techniques based only on the acoustic volume of PI. This superposition of PI values in pre-salt carbonates between the reservoir and non-reservoir rocks was also reported in the works by Teixeira et al. (2017), Castro and Lupinacci (2019), Mello (2020), and Penna and Lupinacci (2021).

In Well A (Figure 63-A), there is a trend of decreasing PI values and increasing Ln(FZI) values. It is possible to observe that FF2, FF3, and FF4 respect this trend, however, FF1 presents a different behavior. FF1 is between the 10,000 and 13,500 g.m/cm3.s, having PI values equal to or even lower than those found for FF3. On the other hand, FF3 is among high values of Ln(FZI) while FF1 is among lower values. It should be remembered that Well A has an interval, in the Itapema Formation, with the presence of muddy facies, such as shales and mudstones, which, according to some works such as Dias (2021), the muddy facies may have low impedance and low porosities.

The behavior observed in Well B (Figure 63-B) is similar to that found in Well A, however, it is noted that, in general, all the flow facies present PI values higher than those

in Well A. It is noteworthy that at the base of the Itapema Formation in Well B, there is an unidentified igneous rock in addition to an interval with the presence of shales and siltstones. The presence of these muddy facies may have been responsible for the low PI values as well as the presence of the igneous ones, which, depending on their characteristics, can either generate very high PI values or low values. In general, intrusive igneous ones such as diabase will present high values of PI, and extrusive igneous ones, such as basalt, low values. As we do not have information about the type of igneous rock in this well, it is difficult to conclude anything.

Well C (Figure 63-C) presents the most representative behavior of the relationship between acoustic impedance and petrophysical parameters. It is possible to observe that the few FF1 samples have higher impedance values than those observed in wells A and B, with PI values between 16,000 and 13,000 g.m/cm3.s. In addition, it is noted that the PI for FF4 is between 13,000 and 9,000 gm/cm3.s, therefore, it is possible to say that due to the small presence of muddy facies in the Itapema Formation and the presence of muddy carbonates in the Barra Velha Formation, Well C shows a better correlation between the parameters so far. It is worth mentioning that according to the PI vs. PHIE crossplots carried out by Dias (2021), sometimes, the muddy carbonates of the Barra Velha Formation present higher PI values than the muddy facies found in the Itapema Fm. which are generally associated with shales and mudstones.

Finally, Well D (Figure 63-D) is more similar to Well B due to the fact that it has igneous rocks throughout the formation and muddy carbonates such as laminites and mudstones. In this well, both intrusive (diabase) and extrusive (basalt) rocks are present. Intrusive rocks usually have high PI values, which may explain, the FF1 “cloud” between the values of 18,000 and 16,000 g.m/cm3.s. On the other hand, extrusive rocks usually have lower PI values that may justify, along with the muddy carbonates, the FF1 also scattered around lower PI values. Also, this well does not show good correlations that make distinctions and trends of the FF2 and FF3 very clear.

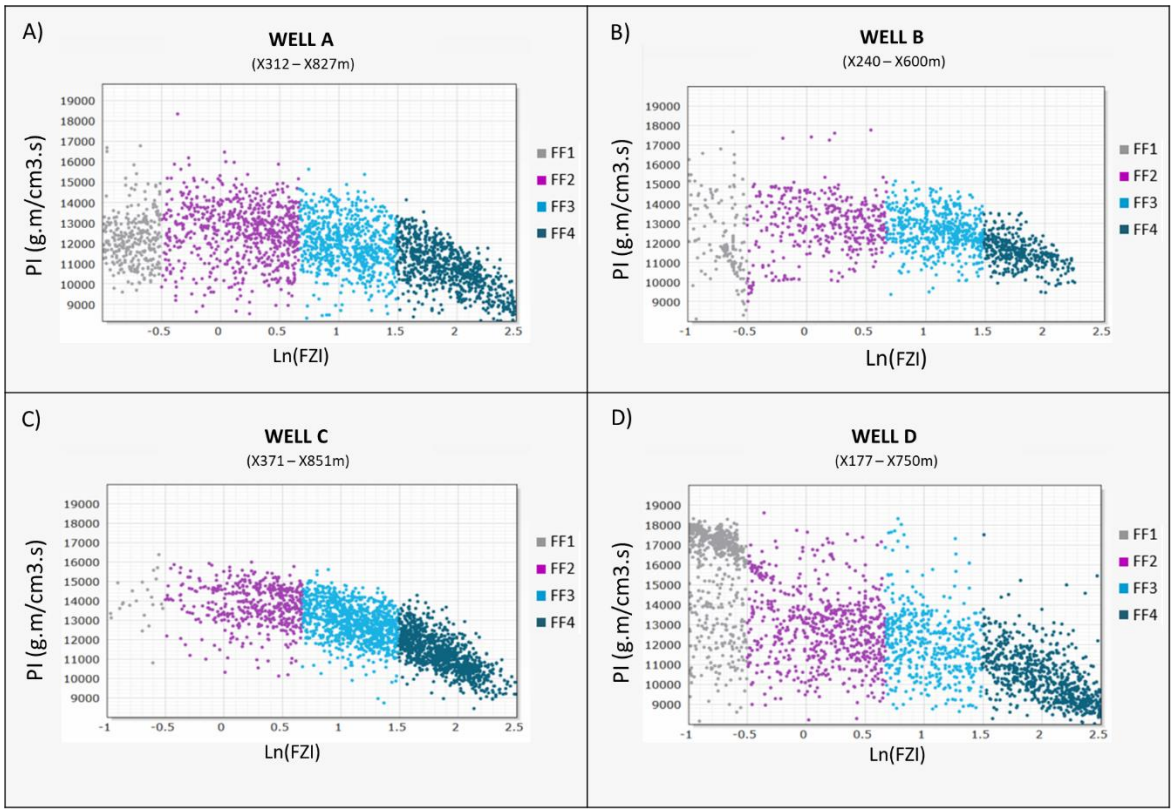

Figure 63: Crossplots of PI versus Ln(FZI) by flow facies for both Barra Velha and Itapema formations. A) Well A; B) Well B; C) Well C; D) Well D.

Figure 64 shows the PI versus Ln(FZI) crossplot for the four wells together. It is possible to observe that, as seen in each well separately, FF4 has higher values of Ln(FZI), that is, better permoporosity, and lower values of PI, being the flow facies with the most distinguishable behavior in relation to the others. It is noted that FF3 presents lower PI values, but also shows PI values pretty close to FF2. FF1 and FF2, which should be distributed between higher values of PI, have a significant portion of facies with impedance values belonging to the same range of values as FF3, and this happens due to the expressive presence of muddy facies in FF1, as well as in FF2. In contrast, there is a "cloud" of points belonging to FF1 that falls in the range of higher acoustic impedance values. As already observed in wells B and D, the presence of intrusive igneous rocks, defined as FF1, may have been responsible for these high PI values. Therefore, analyzing all wells together, FF1 has PI values between 18,000 and 10,000 gm/cm3.s, FF2 between 16,000 and 10,000 gm/cm3.s, FF3 between 15,000 and 9,500 gm/cm3.s and FF4 between 13,000 and 8,000 gm/cm3.s.

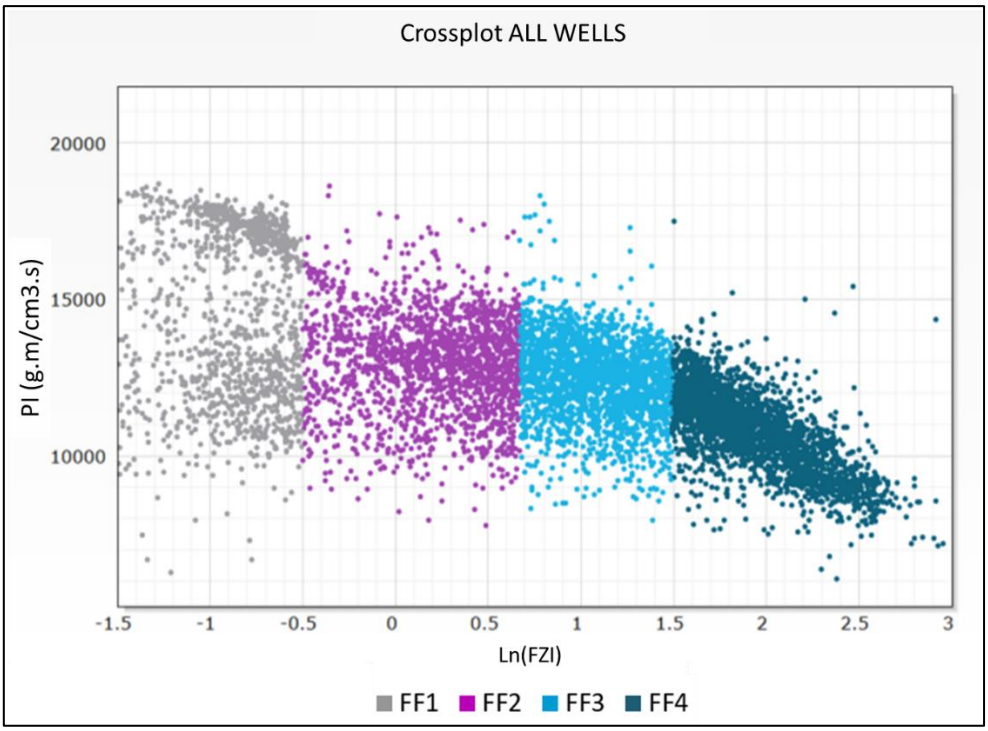

Figure 64: Crossplots of PI versus Ln(FZI) by flow facies for both Barra Velha and Itapema formations in the four wells together.

PI x PHIE crossplots

The crossplots of PI versus PHIE by flow facies were performed for the two formations Itapema and Barra Velha in each well (A, B, C, and D) and the four wells together. Based on some characteristics observed in the geophysical logs and the crossplots of PI vs. Ln(FZI), it is believed that Well B would present a similar behavior to Well D, due to the presence of igneous and muddy facies in both wells.

Figure 65 shows the PI versus PHIE crossplots for wells A, B, C, and D (Figure 65-A, Figure 65-B, Figure 65-C, and Figure 65-D, respectively). Again, it is noted that the lowest values of acoustic impedance are associated with FF3 and, mainly, with FF4. Moreover, it can be seen that the wells where a greater presence of muddy facies, igneous rocks, and/or a greater diagenetic action (e.g., silicification and/or cementation) were observed, presented a greater dispersion of data. This means that FF1 and FF2 may present, in addition to high PI values which would be expected for these lithologies, low PI values. The muddy facies represented, for the most part, by FF1 presented low PI values between 12,000 and 8,000 g.m/cm3.s, whereas the intrusive igneous rocks, also represented by FF1, have high values of PI (Dias, 2021).

Well A (Figure 65-A), as seen above, has a relatively good distribution for FF2, FF3, and FF4, where it is possible to observe that FF2 is distributed between the highest PI values (~15,000 and 12,000 g.m/cm3.s) and consequently lower porosity, while FF3 and FF4 show a trend of decreasing PI values and increasing porosity. FF1, on the other hand, presents low PI values and lower porosity values, not presenting a good distribution, being mixed with FF2. The thin section description from Well A points to a significant presence of muddy facies in the Itapema Formation, in addition to the occurrence of some diagenetic processes such as silicification and dolomitization due to the presence of chert and dolomite samples in the Barra Velha Formation. The presence of muddy facies as well as these diagenetic processes may have caused this behavior in FF1 and FF2.

Well B (Figure 65-B) is marked by the presence of an unidentified igneous rock as well as muddy facies described as siltstones, mudstones, and shales. It is possible to notice the presence of few FF1 scattered in intervals with high porosities that may be related to an intense washover zone, in addition to the presence of the igneous rocks, which may not have been able to be calibrated by the merge of the curves, and the porosity and permeability values may have been overestimated. Furthermore, there is a greater spread of FF1 between high PI values as well as low PI values. Possibly, the high PI values are related to the presence of igneous rock at the base of the Itapema Formation, and the low PI values to the presence of the muddy facies. Apart from the atypical behavior found for FF1, the FF2, FF3, and FF4 seem to have good distributions. FF2 has PI values between ~15,000 and 12,000 g.m/cm3.s, and FF4 between ~12,000 and 10,000 g.m/cm3.s. Furthermore, it is possible to notice that compared to Well A, the PI values for all flow facies present, in general, higher values in Well B (Table 14).

Well C (Figure 65-C) is the well that has the best flow facies distributions through the PI versus PHIE crossplot. The flow facies are well delimited and easy to distinguish in their corresponding intervals. The PI values for FF2 are between 15,000 and 13,000 g.m/cm3.s, for FF3 between ~14,000 and 12,000 g.m/cm3.s and for FF4 between ~12,000 and 9,000 g.m/cm3.s. The PI values along all the flow facies are also higher than those found in Well A, but there is a trend towards a decrease in PI and an increase in PHIE that is better defined between the flow facies. Furthermore, unlike Well B, Well C has no igneous rocks in the Itapema Fm. and has a narrow range of muddy facies that can correspond to this range of FF1 with low acoustic impedance values (between ~12,000 and 8000 gm/cm3.s). In addition, the Barra Velha Formation has the presence of

laminated carbonates (e.g., laminite) evidenced by GR peaks, which may explain the lower porosity values for FF2 when compared to the same flow facies in the other wells (Table 14).

Finally, Well D, has both intrusive and extrusive igneous rocks throughout the Barra Velha Formation, so it has some characteristics similar to Well B. In addition to the presence of igneous rocks, this well has a significant interval of muddy carbonates with samples described as laminites and mudstones. The high PI values associated with FF1 are possibly linked to these intrusive igneous rocks (e.g., diabase) while the low PI may be associated with the muddy and extrusive igneous facies. FF2, in general, presents higher values of PI and may be associated with tight carbonates, with low permoporosity. FF3 and FF4 represent the carbonates reservoir, with good permoporosity and low PI values. FF1 has a range of PI values between ~19,000 and 10,000 g.m/cm3.s; FF2 between ~16,000 and 12,000 g.m/cm3.s; FF3 between ~13,000 and 10,000 g.m/cm3.s; and, finally, the FF4 between 12,000 and 8000 g.m/cm3.s.

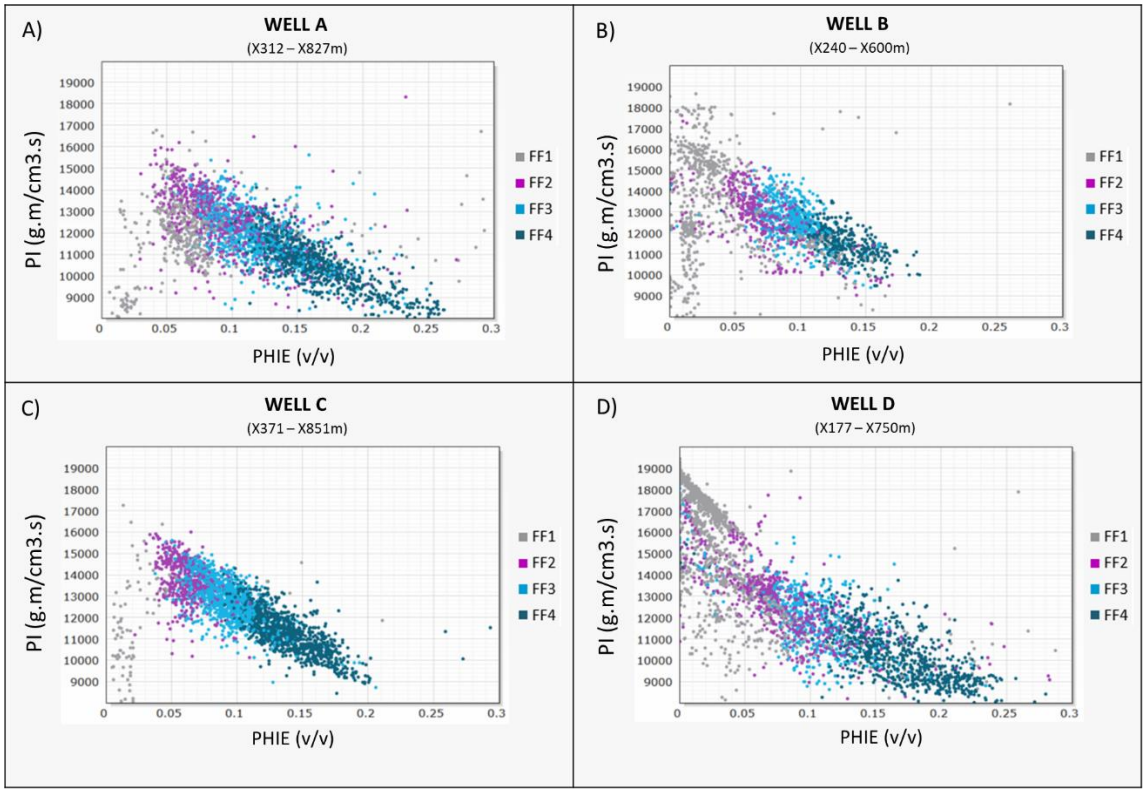

Figure 65: Crossplots of PI versus PHIE by flow facies for both Barra Velha and Itapema formations. A) Well A; B) Well B; C) Well C; D) Well D.

Finally, Figure 66 shows the PI versus PHIE crossplot for all wells together. Note that there is a good distribution between FF2, FF3, and FF4, which follow the trend of

relating the improvement in the flow facies with the decrease in the acoustic impedance values. FF1, as observed in Well A, and especially in Wells B and D, presents scattered values and a more chaotic distribution, sometimes having high PI values, sometimes low. It is noteworthy that the objective of crossplots is to evaluate and visualize how the distribution of flow facies in the seismic volume could be. In this work, this distribution will be performed using the Bayesian classification. The crossplots have already shown that there is a difficulty in separating FF1 and FF2 with low PI values which may end up being confused with FF3 or FF4 in seismic modeling when based only on the acoustic impedance volume.

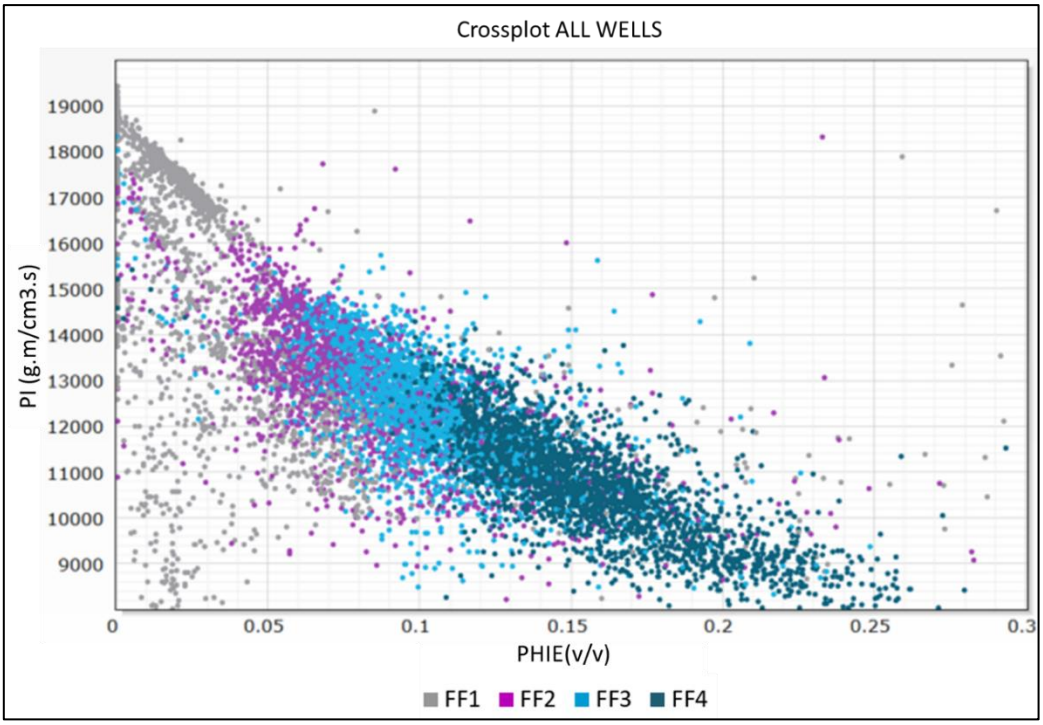

Figure 66: Crossplots of PI versus PHIE by flow facies for both Barra Velha and Itapema formations in the four wells together.

5.5. Evaluation of the model with the probability of occurrence of flow facies in the seismic volume

In section 4, it was seen that the integration of rock-log-seismic data is decisive for a proper characterization of reservoirs. In carbonate reservoirs, as they present great lateral and vertical variation, this procedure is essential for a more robust representation of their properties. Seismic data have great spatial continuity and lateral resolution, allowing the identification of structural aspects, deposit geometry, and their lateral variations. This section will show the results of the well-seismic correlation, aiming to

identify some features that can be correlated with the spatial distribution of the wells in the seismic section and their respective characteristics. Besides, aims to identify whether the wells are located near faults, in structural highs, debris zones, among others. This correlation also helps to understand the heterogeneities and distribution of the flow facies observed in the wells, bringing now to the seismic scale. Furthermore, it is necessary to emphasize that in this section, in addition to evaluating the results, brief discussions and references of authors who have developed works related to this theme will be presented with the aim of giving greater support to the results obtained.

Figure 67 presents an arbitrary section through the four wells, uninterpreted (Figure 67-A) and interpreted (Figure 67-B). In order to aid in the discussions of this arbitrary section, the upscaled flow facies track was added, representing the correct depths of each formation and unconformities. It is worth remembering that the upscale was performed using the Backus average, considering a cutoff frequency equal to 100Hz and a sampling rate of 5 meters.

The arbitrary section is practically South-North oriented and cuts the carbonate platform where wells A, B, C, and D are located. This carbonate platform is in the main structural high of the study area. Well A is located in the southernmost and in a lower portion of the carbonate platform concerning the wells B and D. Moreover, it has a thinner Itapema Formation when compared to the other wells, presenting at its base a greater presence of FF1 associated with the base of the coquinas which, as seen above, are possibly cemented. In addition, the presence of fines and/or clay towards the middle of the formation, which may suggest a deeper lake deposition environment.

Near the Pre-Alagoas unconformity, it is possible to identify an improvement in the flow facies, with a predominance of FF3 and FF4, possibly related to the area close to coquina banks, deposited in high energy shallower environments, where the action of waves could favor the reworking of these coquinas, increasing porosity and/or displacing finer sediments (Chinelatto et al., 2020), and therefore representing zones of greater permoporosity. The collected samples are mostly described as grainstones and rudstones.

The Pre-Alagoas unconformity that marks the base of the Barra Velha Fm. is characterized by intercalations between FF3 and FF4. Towards the top of this formation, there is a tendency to worsen these facies associated with intense diagenetic processes such as silicification and mainly quartz cementation. This behavior can infer bottom-to-

top shallowing and drowning cycles (Wright & Barnett, 2017; Neves et al., 2019; and Wright, 2020).

Well B was drilled under a higher location in the carbonate platform when compared to Well A. This well is located between two normal faults and the base of the Itapema Formation is extremely close to one of the faults. The base of this formation is precisely marked by the presence of igneous rock that is translated into FF1, just above this igneous rock there is a thick block of FF1 interspersed with thin layers of FF2, possibly associated with the presence of tight carbonates because of the contact metamorphism, in addition, the collected sidewall samples are described as shales, mudstones and siltstones.

The deposition of these facies may be linked to restricted lake environments and/or deposition in deeper lakes, accumulating a greater presence of fines and peloids (Chinelatto et al., 2020). Near the top of this formation, it is possible to suggest the presence of the coquinas banks structure dominated by FF3, representing better permoporosity, with possible wave action, greater reworking, and a deposition in a shallower lake configuration (Oliveira et al., 2019; Barnett et al., 2020).

The Barra Velha Formation has the smallest extension when compared to the other wells, with a predominance of FF3 with FF4 intercalations. The sidewall samples collected point to the presence of shrubs and spherulites in situ, as well as reworked facies such as grainstones, which may suggest deposition in a shallower environment (Wright and Barnett, 2015; Wright and Rodriguez, 2018). Furthermore, there is a worsening in the flow facies towards the top of this formation but mainly associated with the presence of igneous rock.

Well C is in a region of seismic debris facies that occurs close to border faults (Neves et al., 2019, Ferreira et al., 2021), with FF3 and FF4 as the major flow facies along the entire well. The Itapema Formation has low permoporosity at its base, being reflected in FF1. In this interval, laminites samples were collected. Near the top of this formation, there is an improvement in the flow facies with FF4 predominating. The Itapema Formation may be located at a region where intense reworking of coquinas may have occurred and is characterized by good permoporosity. The Barra Velha Formation presents excellent flow facies (FF3 and FF4) close to the Pre-Alagoas unconformity, towards the base of salt there is a worsening of these flow facies which can be translated

in the presence of FF2 intercalated with FF3 and FF4. These intercalations may be associated with variations at the base level of the lake (Wright and Barnett, 2015; Wright and Rodriguez, 2018).

In the region of Well D, the Barra Velha Fm. has the greatest thickness among all the wells analyzed in this work. It is located under an isolated horst conditioned by two normal faults. This well also has the presence of igneous rocks throughout the formation, mainly in the most basal part. This interval presents a predominance of FF1, and thin sections samples described as diabase and laminite.

Well D is characterized by a mound-like structure but does not have all the characteristics of a carbonate mound. This mound has igneous rocks which makes it an exception. Due to the presence of these igneous rocks and the contact metamorphism associated with them, it turns out that this seismic structure does not have such good flow facies in the places where these lithologies are found. Despite the influence of the igneous rocks, there is an improvement of the flow facies in the middle of the formation, as it is possible to notice through the greater presence of FF3 and FF4. This behavior may be associated with high fracturing in carbonate mounds in the Santos Basin observed in the works of Buckley et al. (2015), Jesus et. al (2019) and Ferreira et al. (2021) who presented the carbonate mounds as being important reservoirs, with good permoporous conditions in the pre-salt area.

For discrete well logs, like the flow facies, the upscaled facies was considered as the one that occurs with the greatest frequency given a running analysis window. Figure 64 shows how each flow facies separates in the well domain, considering the P-impedance values. As seen also in well logs in Figure 43, Figure 45, Figure 47 and Figure 49, FF1 tends to present higher values of impedances, while FF4 corresponds to lower values. This is expected, considering that FF1 and FF2 are mostly comprised of low porosity and silica cemented carbonates and igneous rocks, while FF3 and FF4 correspond to higher porosity and clean, calcium-pure carbonates. Due to the ambiguity that the presence of muddy facies as well as igneous facies with high and sometimes low PI values (Penna et al., 2019), superimposed zones between each of the four FF in the elastic domain, will possibly occur. This mean that a single P-impedance value can relate different flow facies, resulting in some level of classification errors when predicting petrophysical parameters within FF. This same analysis from the elastic characteristics was made for the lithological facies from Mero reservoir and can be seen in Penna et al. (2019).

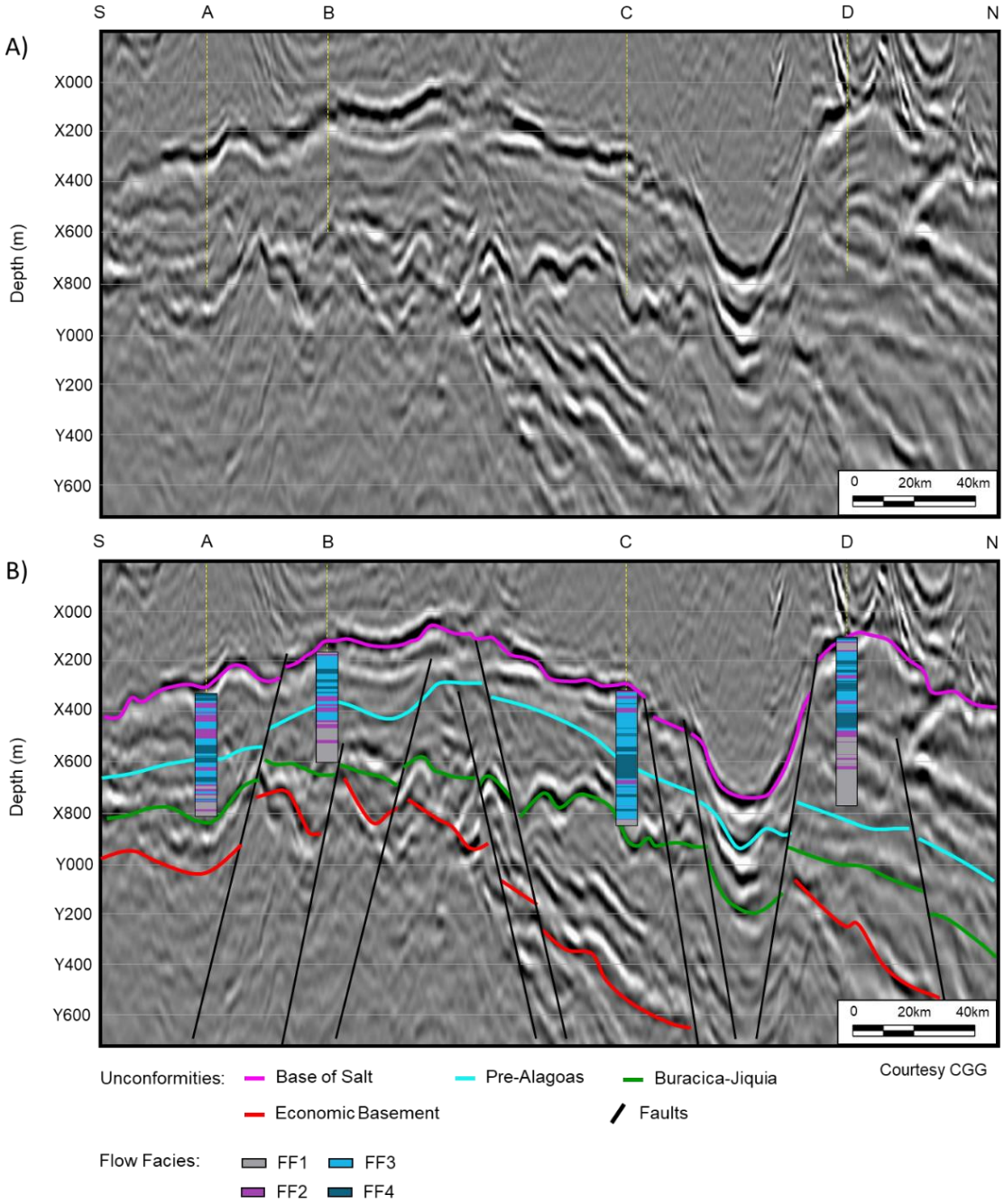

Figure 67: Arbitrary section, passing through wells A, B, C and D. (a) Uninterpreted data; (b) Seismic data with the interpretation of the main unconformities and faults, as well as a track with the upscaled flow facies, in each well.

A Bayesian classification was performed to provide a quantitative analysis of the probability occurrence from each flow facies, given the upscaled version of the well logs as inputs. As seen in section 4.1.9, Bayesian's theorem describes the posterior probability P(m|z) of the parameters model m given the observed data z. Given the discretization of

FF using seismic derived elastic property volume, it is possible to rewrite the equation as follows:

$$\mathrm{P}\left(\mathrm{FF}_i|\mathrm{PI}\right) = \frac{\mathrm{P}(\mathrm{FF}_i)\times\mathrm{P}(\mathrm{PI}|\mathrm{FF}_i)}{\mathrm{P}(\mathrm{PI})}, \quad (26)$$

where P $(\mathrm{FF}_i|\mathrm{PI})$ is the posterior probability of FF_i given PI, $\mathrm{P}(\mathrm{FF}_i)$ is a priori probability for i flow facies, the term $\mathrm{P}(\mathrm{PI}|\mathrm{FF}_i)$ corresponds to the likelihood probability density function (PDFs) adjusted for FF_i to P-impedance (PI) values, and P(PI) is the occurrence probability of PI, a normalization factor.

First, the likelihood probability density functions (PDFs) of each flow facies were calculated using the term $\mathrm{P}(\mathrm{PI}|\mathrm{FF}_i)$. The distinct PDFs were calculated from ten wells, the four wells presented in this work and six more, for both the Barra Velha and Itapema formations, and they are shown in Figure 68. The PDFs allow assessing to what extent it is possible to separate the different flow facies based, for example, on the Bayesian classification from the acoustic impedance.

The overlapping of PDFs, mainly of FF1, FF2 and FF3, due to the presence of intrusive igneous rocks as well as muddy facies, is a challenge for the flow facies modeling in the pre-salt interval using the acoustic impedance volume. When the overlap is too large, it becomes very difficult to define which PI values correspond to which facies. As an alternative, it is possible to condition a facies modeling with more than one elastic parameter a priori, using, for example, besides PI, the SI (shear impedance), or a geological model as a priori information.

In the Barra Velha Fm. (Figure 68-A), there is a better separation of the FF1, FF2 and FF3, possibly due to the lower presence of muddy intervals (e.g., mudstones, laminites) when compared to the Itapema Formation. Furthermore, the igneous rocks in the Barra Velha Formation were classified mainly as diabase (igneous intrusions) with high PI values, being easier to be distinguished. However, even with the lower presence of fines, the separation between the flow facies associated with these lithologies (FF1 and FF2) and the flow facies associated with good permoporosity (FF3), is still a challenge.

The Itapema Formation, on the other hand, (Figure 68-B) shows a greater conflict between the FF1, FF2 and FF3 PDFs, as there are significant intervals with the presence of shales, mudstones, and siltstones, which have low PI, being easily overlapped with FF3 that has also low PI values. As seen before, the PI for the Itapema Formation are lower

than those of the Barra Velha Formation and belong to a range of 9000 to 14000 g.m/cm3.s. Furthermore, the Itapema Fm. has a greater overlap of FF1 and FF3, possibly associated with the bimodal behavior of tight carbonates. This bimodal behavior is also observed in Barra Velha Fm. and is associated with the great heterogeneity of pre-salt carbonates due to silicification, dolomitization and/or cementation processes. Mello (2020) showed how the mineralogical composition of carbonates from Barra Velha Fm. impact the elastic parameters of these rocks, where it is found that rocks with greater presence of dolomite have higher values of elastic parameters than rocks with the presence of quartz.

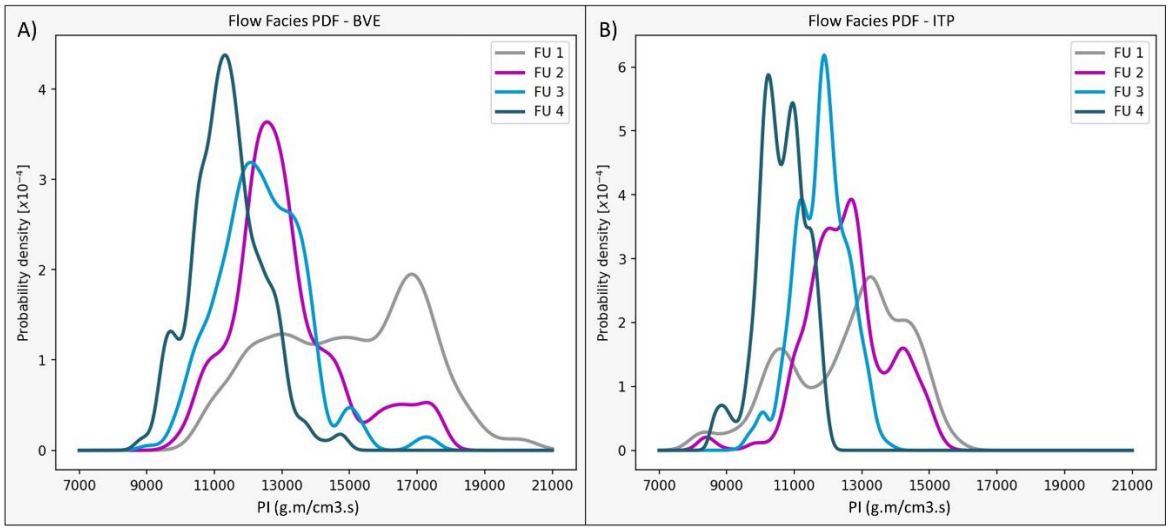

Figure 68: Prior probability density functions using data from ten wells. (A) Barra Velha Fm. (B) Itapema Fm.

Then, after having calculated the likelihood (PDFs), a priori probability of 25% was established for each flow facies, represented by $P(FF_i)$. This choice was made to reproduce a more exploratory scenario since, generally, wells are drilled in the best areas, in structural highs. Then, if the statistic is based on the ten wells in which the flow facies estimates were considered, the results would probably be biased and underestimated. Also, if the a priori probability of the ten wells together were chosen, possibly the flow facies that encompass greater heterogeneity could be extinct or represent very small percentages.

Figure 69 shows the posteriori probability density functions (PDFs), calculated through Eq. (26. With the results provided by this equation, it is possible to classify the flow facies from an acoustic impedance volume. This means that for each known PI value, there is a probability of each flow facies occurring from that given PI value, in a certain

depth. For example, in Figure 69-A, for a PI value of 18000 gm/cm3.s, the probability of being FF1 is around 0.8, FF3 is less than 0.1, FF2 is nearly 0.2, and of being FF4 is zero. The sum of these probability densities for these flow facies must always be one, and when evaluating the facies that have the highest probability density, FF1 is the highest, therefore, considering that given value of PI, for a certain depth, you are more likely to have FF1.

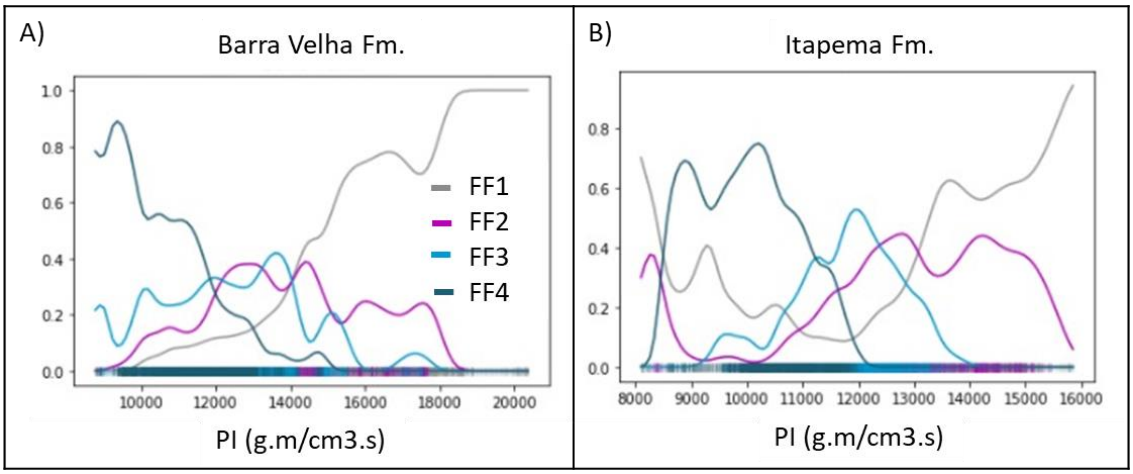

Figure 69: Posterior probability density functions using ten wells. (A) Barra Velha Fm. (B) Itapema Fm.

From these calculated PDFs, it is possible to estimate a matrix that provides information on the probability of errors and successes for each flow facies, by comparing the observed and estimated flow facies. Figure 70 shows the confusion matrix considering the well-log inputs. The main diagonal will tell you the success rate of each flow facies. The y-axis represents the observed flow facies, and the x-axis the classified flow facies through the posterioi PDFs.

In short, a confusion matrix is a table with two rows and two columns that reports the number of false positives, false negatives, true positives, and true negatives. This allows for more detailed analysis than a mere proportion of correct classifications (accuracy). The main diagonal informs the hit percentage for each flow facies. Thus, it is possible to see that in the upper part of Figure 70-A, when analyzing the first line, which compares the observed FF1 with all classified flow facies, it is observed that the hit rate for FF1 was 63.7%. It had an error of 13.1% when classifying samples as FF2, 14.6% was classified as FF3, and 8.6% as FF4. When analyzing the last line, that of FF4, it can be seen that there was a 1.4% error classifying where it was FF4 as FF1, 18.3% as FF2, 9.5% as FF3, and 70.8% classifying FF4 as FF4.

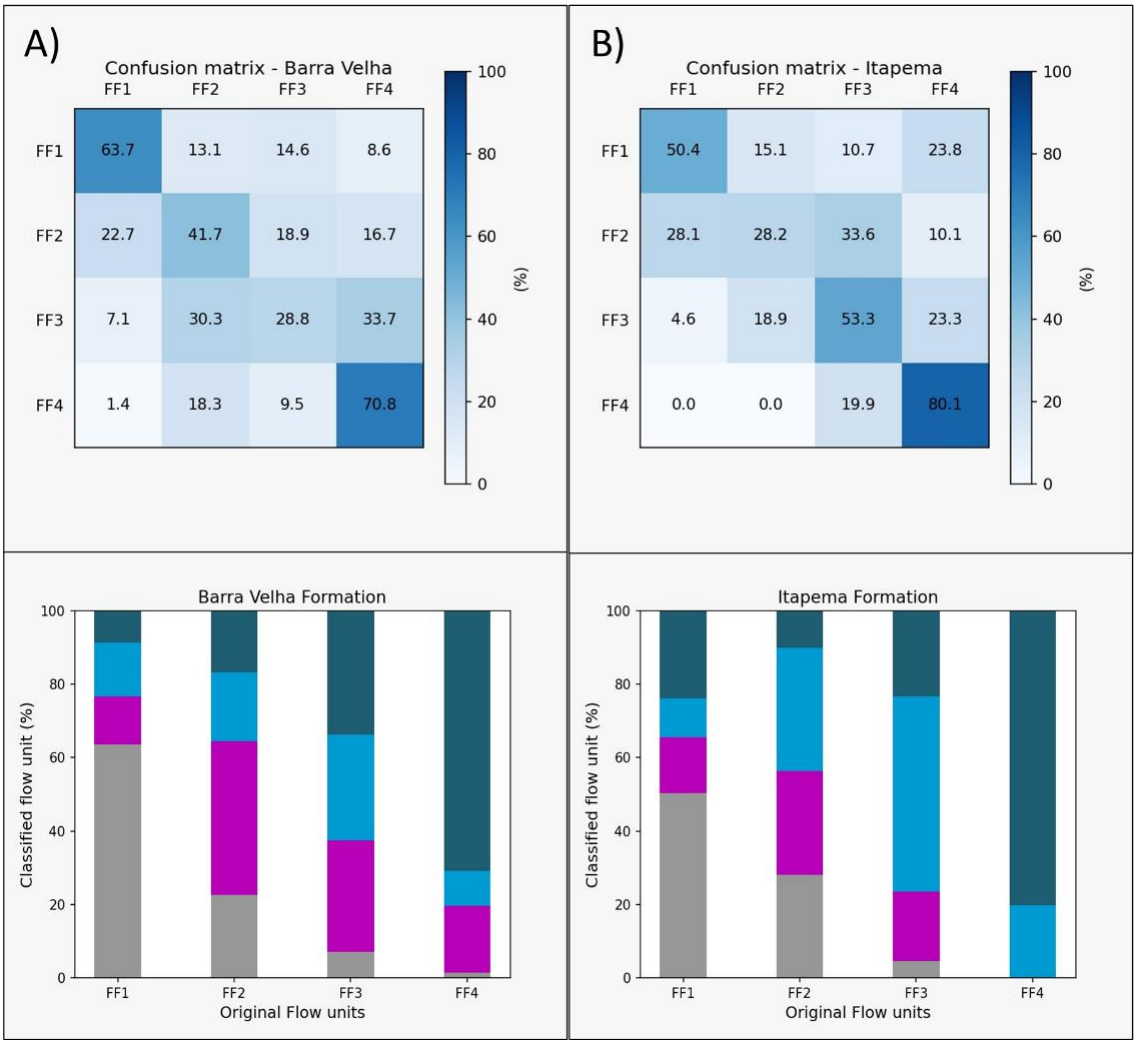

Figure 70: Confusion matrix in the upper part, and distribution of observed flow facies classified in the form of bars; A) Barra Velha Fm. and B) Itapema Fm.

The lower part of Figure 70-A shows four bars, the x-axis represents the original flow facies and the y-axis the classified ones. Note that in the first column, in FF1, more than 60% of the samples were classified as FF1, a result that could be observed in the confusion matrix. Thus, it is noted that, in the Barra Velha Formation, there is greater difficulty in classifying the FF2 and FF3, while the FF1 and FF4 are more likely to be correct. In the Itapema Formation (Figure 70-B), the FF3 has a probability of success greater than 50%. In both formations, the FF4 appears with good percentages of success, above 70%. Both the confusion matrix and the bar graphs were made for ten wells in a field in the Santos Basin.

Figure 71 shows the upscaled PI log, coming from the well-logs, the original flow facies estimated from the well data with the upscale, the probability of occurrence of each flow facies, the classified flow facies and finally, the accuracy rate in the Well C, in which

the red bars indicate where there was a misclassification. This figure shows a different way to visualize the results obtained from the posterior probability density. It is possible to observe that the base of the Itapema Formation, which presents intercalations between FF1, FF2 and FF3, showed a lot of error, classifying what was FF1 as FF4 and what was FF3 as FF2. In addition, there is a difficulty in classifying correctly FF3, which often appear to be classified as FF2.

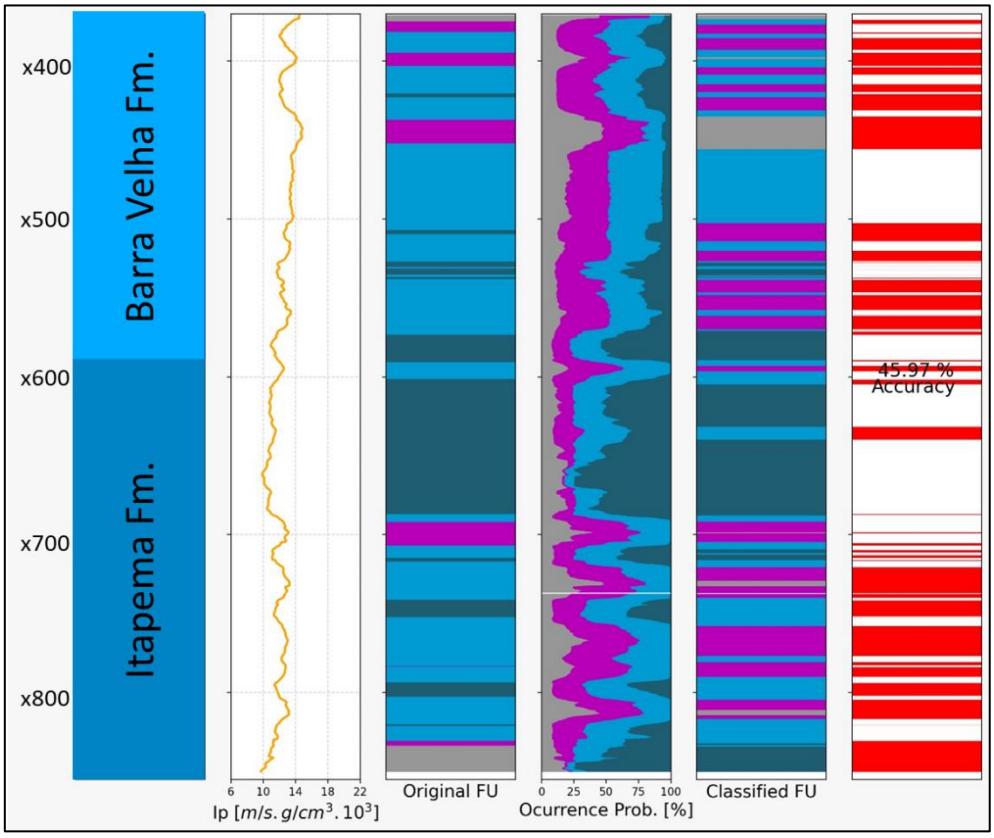

Figure 71: Layout with the PI curve and the original flow facies used to calculate the PDFs. Track 1: TVDSS (m); Track 2: PI log with upscale; Track 3: Original upscaled FF; Track 4: Occurrence probability of each flow facies; Track 5: Classified FU and Track 6: Accuracy, the red squares indicate the errors.

In the Barra Velha Formation, it is observed a greater error, towards the top of this formation, and as in the Itapema Formation, many FF3 intervals end up being classified as FF2. In this well, the GR and Vclay logs tend to increase towards the top in the Barra Velha Fm. and at the base of the Itapema Fm. Besides that, the description of some thin section samples presents some evidence of laminites. As seen earlier, the presence of fine grains and/or clay is a problem for modeling, especially using PI. This may explain a larger error at the top of the Barra Velha Formation. Finally, the entire well presented an accuracy of 45.97%.

Thus, in short, the output of the Bayesian inference was one volume that held the most probable FF volume among the four flow facies. The most probable FF volume consists of the corresponding discrete data that present a higher occurrence probability for a given sample. Each occurrence probability volume varies from zero to one, and the sum of all the probabilities for a given sample is always one.

Figure 72-A exemplifies one S-N section resulting from acoustic inversion in Wells A, B, C and D. In general, the results show a good correlation between the upscaled flow facies and the inversion impedance values, which confirm the robustness of the seismic inversion results. Most of the P-impedance errors are concentrated in the high values of the intrusive rocks or the presence of muddy facies. This happens because the intrusive rocks use to be found near the base of salt, where occurs a lot of tuning effects and high impedance contrasts between the salt and carbonate layers. In the same way, the muddy facies represents a challenge to reservoir modeling when it is done only using the acoustic impedance volume. Even though the vertical resolution is increasing with the seismic inversion, it is hard to correctly reproduce the real thickness and impedance values in these conditions.

In the Itapema Formation of Well A, predominantly low PI values are observed at the base and near the top, with some intercalations of higher values in the middle of the formation. This result is interesting since the predominant flow facies from the base to the middle of the formation is the FF1 which is characterized by the presence of fine grains and/or clayey sediments. In the Barra Velha Fm., around Well A, it is possible to notice that the base has lower PI values (orange color) and that there is an increase in PI values towards the top. This increase in PI has a good correlation with FF2, found in the middle of this formation. The top of the Barra Velha Fm. has very high PI values, possibly related to its proximity to the base of the salt.

Heading north towards Well B, it is possible to notice that Itapema Fm. has also low PI values, with some layers of higher PI values close to the basal part, possibly related to the presence of igneous rock. As in Well A, Well B also has intervals with the presence of muddy facies (e.g., laminites, mudstones and shale) with FF1, associated with lower PI values. Near the top of this formation, it is possible to notice a decrease in PI values, as well as an improvement in the flow facies (FF3). The Barra Velha Formation has medium to high PI values throughout almost the entire formation that end up showing an

interesting behavior since there is a predominance of FF3 and FF4. The basal part has lower PI values that tend to increase towards the top.

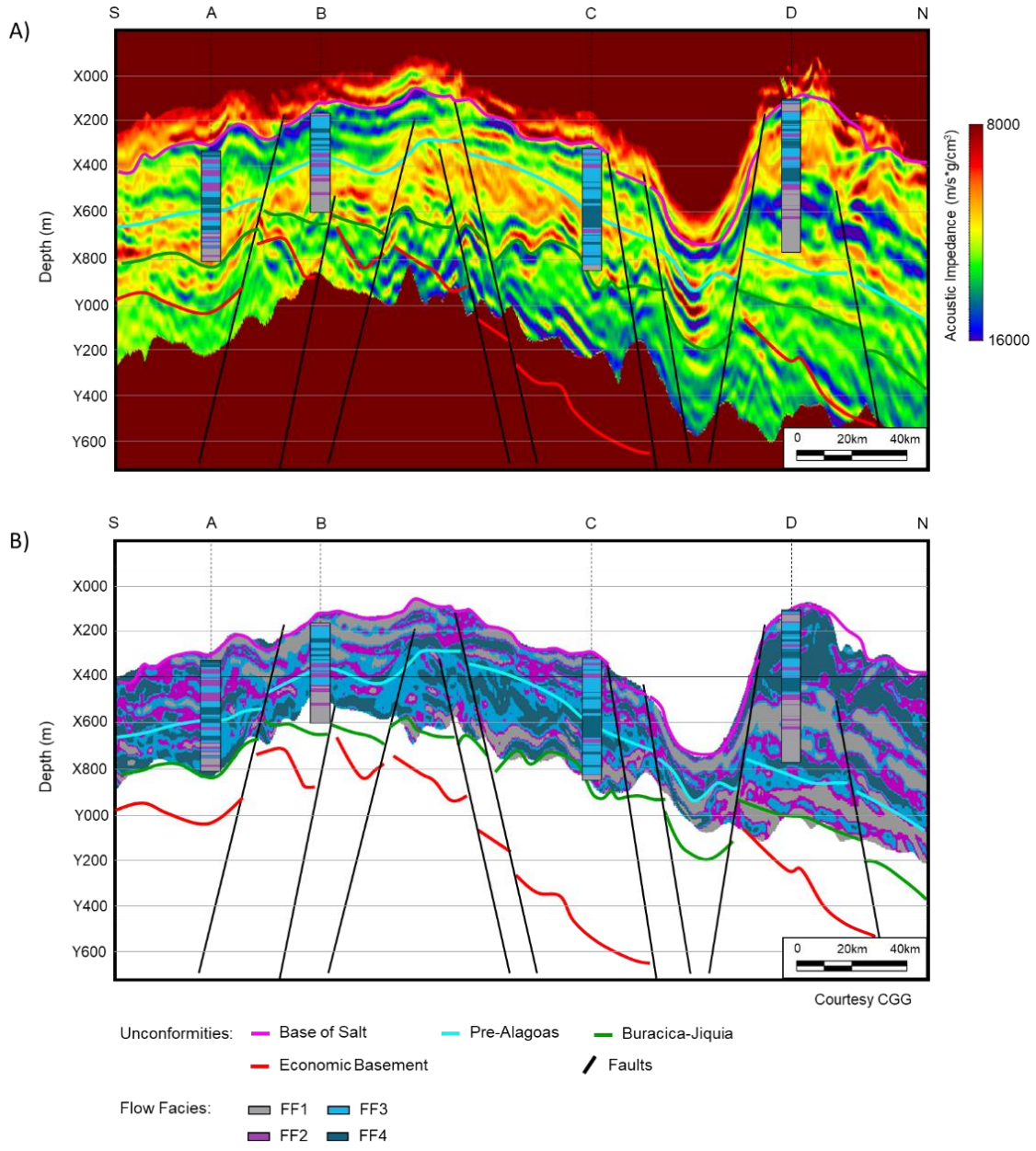

Figure 72: Interpreted arbitrary section, passing through Wells A, B, C and D. (a) P-impedance section resulting from the acoustic inversion; (b) Section S-N showing the Bayesian classification of flows facies.

Well C has higher PI values close to the base of the Itapema Formation, and a tendency to decrease towards the top with FF4 being predominant at the top of this formation. The Barra Velha Fm. has low PI values at the base, which tends to increase towards the top.

Well D has two contrasting behaviors concerning PI. In the lower part, the PI values are high (dark blue color) which corresponds to intrusive igneous intercalations,

and in the upper part, due to the mound-type structure characteristics, has low values (red color) of PI, correlated with the high permoporosity, evidenced by the greater presence of FF3 and FF4.

Figure 72-B exemplifies an S-N section with the Bayesian classification from the inversion of the acoustic impedance volume mentioned in the paragraph above. By analyzing the classifications of the flow facies in the Itapema formation, close to Well A, it is possible to see that from the base to the middle, FF1 was classified as FF3 and FF4. This discrepancy between the Bayesian classification of flow facies and the flow facies estimated in the well may have occurred due to the strong presence of muddy facies (e.g. mudstones, shale and laminites) in these intervals, which end up hindering the results as they have low PI values. At the top of this formation, the FF3 and FF4 estimated in the well were generally classified as FF2 and FF3, with some layers where both classifications match each other. The Barra Velha formation showed good classifications and a good match of the flow facies estimated from the Bayesian classification with those estimated in the well. The interleavings between FF2 and FF3 in the upper-middle part seemed to be well classified.

In the Itapema Formation of Well B, it is noted that from the base to the middle, the interval with the presence of igneous rock as well as siltite and mudstone was not modeled. From the middle to the top of the formation, it is possible to see that the FF2 and FF3 layers estimated in the well correspond very well to those estimated by the Bayesian classification. Next to the Pre-Alagoas disagreement, where it can be considered a coquina bank structure, the FF3 and FF2 were very well classified. The base of the Barra Velha Formation was also very well classified, however, towards the top of the formation the same does not happen. In the well, the predominant flow facies in this well is FF3 with few layers of FF4. However, it is observed that the flow facies estimated by the Bayesian classification resulted in a majority of FF1 and FF2, in a few areas where it was classified as FF3. This behavior may have been a result of the presence of high PI igneous at the top, as well as very close acoustic impedance values in the carbonates along and around this formation.

At the base of the Itapema Formation of Well C, the flow facies results through the Bayesian classification do not seem to match very much with those found in the well. In the middle, the results obtained through the Bayesian classification seem to match more. At the top of this formation, the same behavior can be observed, the FF4 were very

well classified around the well, which may reflect a zone where an intense rework may have occurred, thus improving the permoporosity of the region. Furthermore, the entire extent of the Pre-Alagoas unconformity that passes through this well appears to represent a configuration of an extensive reworking zone similar to that found under storm conditions in the article by Chinelatto et al. (2020). In the Barra Velha Formation, the base is also very well classified, containing only small layers where FF3 was classified around as FF2. Towards the top of this formation, the Bayesian classification does not match the results obtained in the well, this may be due to the proximity to the base of the salt, as well as the presence of laminated carbonates that can generate lower IP values.

In general, Well D showed good flow facies responses from the Bayesian classification compared to the FF found in the well. It is possible to see that at the base, where there is large intercalation of igneous rocks and the PI has considerably high values, the classifications were very good. The upper part of this formation was more classified as FF4, possibly due to the presence of the mound-type structure under which this well and its surroundings lie. Mound structures are characterized by excellent permoporous quality (Ferreira et al. 2019 and Jesus et al. 2019). In addition, some FF2 ranges in the well were also well ranked.

The predominance of FF1 is notable, in the northern part, close to the Pre-Alagoas and the Jiquia- Buracia unconformities. Besides, in the southern part, the FF1 and FF2 seem to be more close to the base of Salt. The best flow facies (FF3 and FF4) are usually found near the top of the Itapema Formation and the base of the Barra Velha Formation, except for the surroundings of Well D.

By comparing the flow facies obtained in the seismic section through the Bayesian classification (Figure 72-B) with the results obtained in Table 17, where the percentages of the flow facies with the upscale are presented, it is possible to observe that the Barra Velha Fm. in the wells A, B and C have small or no percentage of FF1, whereas when evaluating the flow facies through the Bayesian classification, in the seismic section, (Figure 72-B) there is the presence of FF1 around these wells. Therefore, it is noted that when analyzing well by well, the flow facies may not be as representative on some occasions, but when analyzing the flow facies in a seismic volume, these FF become much more representative.

6. Discussions

This chapter seeks, in addition to interpreting, analyzing, and discussing the results shown in chapter 5 to bring further discussions about the main diagenetic effects of dissolution, cementation, and silicification in the estimated flow facies. Moreover, an attempt was made to contextualize the flow facies estimated in this work with the depositional environments of the Barra Velha and Itapema formations.

First, the diagenetic effects that silica and dolomite can exert on the flow facies in the Barra Velha and Itapema formations were addressed. Then, the correlation between the wells and the identification of possible flow facies cyclicities were presented and analyzed. Finally, some ideas were shown regarding the characteristics of depositional environments, in both Barra Velha and Itapema formations.

6.1. The diagenetic effects of silica and dolomite in the flow facies

The main diagenetic effects acting in the Barra Velha Formation in Wells A, C, and D are cementation mainly of dolomite, quartz and calcite, as well as silicification which is observed in all wells, but with more prominence, in Wells A and D. It is worth mentioning that there are several records of the occurrence of diagenetic processes that act influencing the distribution of porosity and permeability in the pre-salt lacustrine carbonate reservoirs over the years (Lima and De Ros, 2019). In addition, the environments in which these carbonates were formed have extremely complex configurations that are still the subject of study and discussion to this present day. Therefore, aiming to understand all this complexity, a deeper study based on studies of petrographic thin section as well as a complete analysis of core and plugs would be necessary. Thus, the entire discussion that will be presented in this work is based on the diagenetic processes that can be observed in the rock data, and especially in the well logs.

The Itapema Formation does not show a significant presence of dolomite cement in Well C and the Mg content is extremely low. On the other hand, Well A has a greater presence of dolomitic cement in Itapema Fm. when compared to the Barra Velha Fm. However, even with the presence of dolomite cement, there are only two samples of dolomite. Therefore, dolomite does not seem to have much influence on the permoporosity and flow facies distribution in the Itapema Formation for both wells A and C. The silica content occasionally increases and generally causes a reduction in permoporosity resulting in worse flow facies in all the four wells. This increase in silica,

in the Itapema Formation, can be mainly associated with the presence of igneous rocks, as can be seen in the basal part of this formation in Well B. The presence of Mg-clays is not common in the Itapema Formation, then, the main source of silica and magnesium may be related to hydrothermal fluids from igneous intrusions.

In addition, Herlinger et al. (2017) and Lima and De Ros (2019) state that the bioclasts of the Itapema Formation were either dissolved or neomorphosed (calcitized), commonly showing a heterogeneous range of total dissolution, with variable intensity of calcite cementation of the intraparticle porosity, well connected, and moldic, poor connected, to total neomorphism. In Wells A and C in the Itapema Formation, it noticed a more cemented base, with very low porosity and permeability, with a predominance of FF1 and calcite cement. Furthermore, calcite cement is predominant in these wells in the Itapema Formation (Figure 43 andFigure 47).

The effects of the presence of silica in carbonates are even more evident with the estimation of the flow facies. In most cases, the increase in silica content leads to a reduction in permoporosity and therefore worse flow facies (FF1 and FF2). There are few exceptions, in the Barra Velha Formation, where the increase in silica does not generate significant changes in porosity yet exert a certain influence on permeability. Characteristics like these have already been reported by Herlinger et al. (2017) where they stated that the porosity in some samples of shrubs, which was dominantly developed by the dissolution of stevensite, had an average above 6% and the permeabilities were considered low, with an average of 0.8 mD. Another factor that may be associated with increased silica and little influence on permoporosity is the presence of fractures in the interval where there is a significant silica content (Fatah, 2020). Moreover, a question that can be raised is whether the fractures were already there or were generated due to the presence of silica. Lima and De Ros (2019) enunciate that in the samples analyzed by them, silicification was responsible for the extensive, yet heterogeneous formation of fractures and vugular porosity. One way to confirm the significant action of silicification, especially in the Barra Velha Formation, is the presence of quartz cement in practically all wells, but with greater expression in Wells A and D.

In Well A, ten samples of chert (totally silicified rocks) were collected and in Well D nine samples of chert were collected in addition to twelve samples described as silicified. In Well C, only three samples are described as silicified, and the presence of chert is not very common. Well B has a smaller but significant presence of silica content

mainly related to the igneous rock, however, there is no detailed information of the type of cement, in addition to not presenting a description of the petrographic thin sections.

The presence of dolomite did not show a direct relationship with the reduction or increase in porosity and consequent worsening or an improvement of the flow facies. In the Barra Velha Fm., dolomitic cement is common in wells A, C, and D, but dolomitization is recurrent only in well A and is confirmed by the presence of a large number of collected samples described as spherulite with dolomite. Well C has just one sample described as dolomitized and few samples of spherulite with dolomite. Well D has only two samples described as dolomitized.

In the upper part of the Barra Velha Formation, in Wells A and D, high silica values are observed associated with FF3, that is, with good permoporous characteristics. This peculiar characteristic may suggest some type of discontinuity in this portion possibly associated with faults and/or fractures. On the other hand, as seen in Table 14, the magnesium content, which is related to dolomite, is higher in the Barra Velha Formation in Well C than in Wells A and D. Therefore, although the Mg content is low compared to Si and Ca contents in the four wells, the greater presence of Mg in the Barra Velha Formation in Well C may be associated with the greater presence of dolomitic cement as well as the greater presence of FF2 towards the top of the Formation while the Mg content seems to increase upwards.

The ECS log of Mg is higher in wells B and C than in wells A and D but is hard to find a clear relationship between this log and the worsening or improvement of the flow facies. In Well B, the higher values of Mg content could be explained by the greater dissolution of carbonates in the Barra Velha Formation through hydrothermal fluids arising from magmatic activities, since this well has igneous rock. This dissolution has significant relevance to permoporosity, generating channels, intracrystalline aggregates, moldic porosities, and vugs, as reported by some authors (Wright and Barnett, 2015; Herlinger et al. 2017, Lima and De Ros, 2019; Wright and Barnett, 2020).

According to Herlinger et al. (2017, 2020), magnesian clays (Mg-clays) are abundantly present throughout the lacustrine deposits of the South American pre-salt and they precipitate under an extremely alkaline environment conditions. However, since they are composed of minerals that are extremely unstable and sensitive to changes in the pH, climate, and geochemistry of water, they end up being dissolved and/or replaced by other

minerals. Herlinger et al. (2017; 2020) and Lima and De Ros (2019) also claimed that Mg-clays are strongly affected by diagenesis and are often replaced by calcite, dolomite, and silica. Furthermore, as they are found in silica- and magnesium-rich settings (Herlinger et al., 2020), their dissolution may have served as a source of silica and magnesium that together with the hydrothermal fluids, helped in the formation of dolomitic and quartz cement, as well as contributed to the silicification and dolomitization.

Thus, what could be seen is, in all wells, the magnesium and silica content is generally lower and the calcium content is higher in the Itapema Formation when compared to the Barra Velha Formation. Also, in both Barra Velha and Itapema formations, the increase of silica is generally associated with a decrease in permoporosity and, consequently, the presence of FF1 and FF2. On the other hand, when the values of calcium content increase the best flow facies (FF3 and FF4) are more easily to be found.

In order to better understand the relationship between elemental capture spectroscopy logs (ECS) and flow facies distributions, as well as evaluate the impact of the mineralogical composition on these facies taking into account the most abundant minerals in carbonate rocks of the Brazilian pre-salt (calcium, magnesium, and silica), ternary plots were made for the Barra Velha and Itapema formations as well as for the entire well. In Figure 73-A it can be seen that in the Barra Velha Formation of Well A, the FF3 and FF4 are related to cleaner carbonates, with a greater abundance of clean calcite, with a lower percentage of silica and magnesium, on the other hand, there is a predominance of FF1 and mainly FF2 spread in larger percentages of silica. In the Itapema Formation (Figure 73-B) there is a greater mixture in the behavior of FF1, which is sometimes related to higher percentages of calcium and sometimes of silica. This must occur because the base of this formation is possibly cemented when presenting extremely high calcium content values and very low permoporosity. FF4 and FF3 are concentrated in higher percentages of Ca, and lower percentages of silica and magnesium, and FF1 and FF2 are concentrated in opposite configurations.

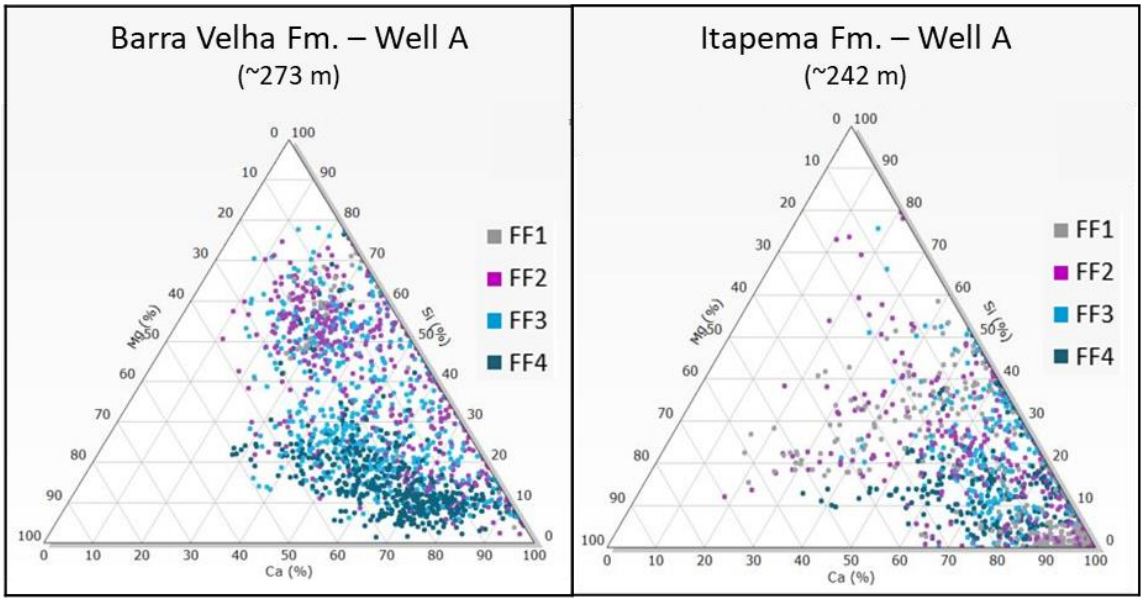

Figure 73: Ternary diagram of calcium (Ca), magnesium (Mg) and silica (Si) by the four FF in Well A. In the decametric scale (A) showing some degrees of pore obliteration due to dolomitization and silicification (Si and Mg substituting Ca) are mixed., respectively) in A) Barra Velha Fm. and B) Itapema Fm.

Well B (Figure 74-A) has its Barra Velha Formation with the same configuration as Well A, the best flow facies (FF3 and FF4) are spread over high percentages of calcium and low percentages of silica and reasonable percentages of magnesium, while FF1 and FF2, despite being few, are more close to the highest contents of silica and magnesium. In the Itapema Formation (Figure 74-B) there is a peculiar behavior due to the presence of igneous rock at the base of this formation. Unlike Well A, Well B has FF1 spread around higher values of silica and magnesium, while FF2, FF3, and FF4 are found in low percentages of magnesium and silica and high percentages of calcium.

In the Barra Velha Formation of the Well C (Figure 75-A), it is possible to see a clear separation between each flow facies point clouds. The points referring to FF4 are located where there are higher percentages of calcium and lower percentages of silica and magnesium. The FF3 is located a little above FF4 still maintaining the same pattern. The FF2 represents an increase in the percentages of silica and magnesium but with lower values when compared to wells A and B. In the Itapema Formation (Figure 75-B) the FF3 and FF4 are mostly spread around 90% calcium, 0 to 10% silica, and very low percentages of Mg. FF1, which is at the base of this formation, in turn, is distributed between higher percentages of magnesium and silica and lower values of calcium.

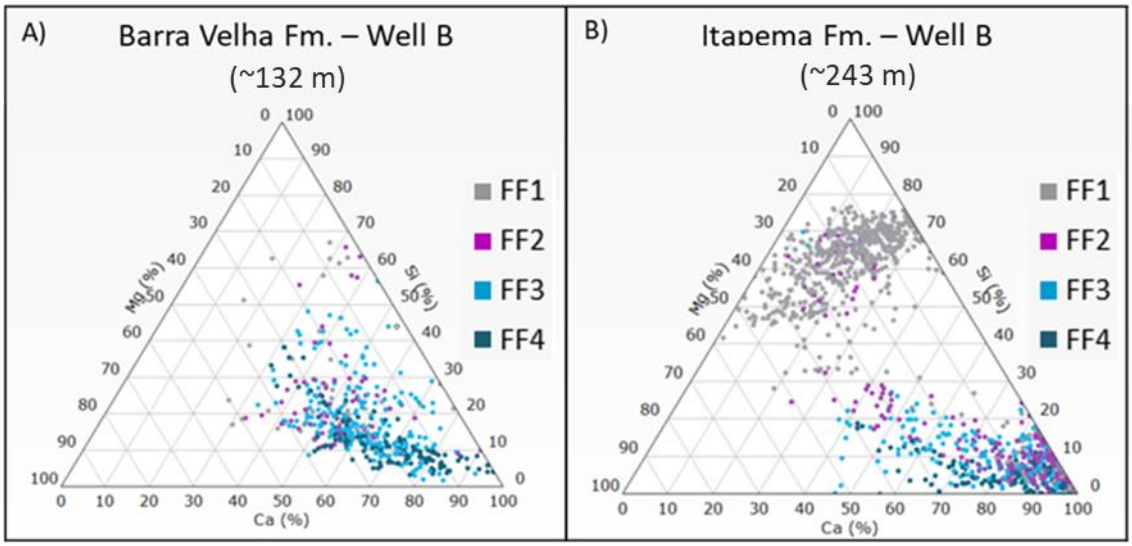

Figure 74: Ternary diagram of calcium (Ca), magnesium (Mg) and silica (Si) by the four FF in Well B, showing some degrees of pore obliteration due to dolomitization and silicification (Si and Mg substituting Ca, respectively) in A) Barra Velha Fm. and B) Itapema Fm.

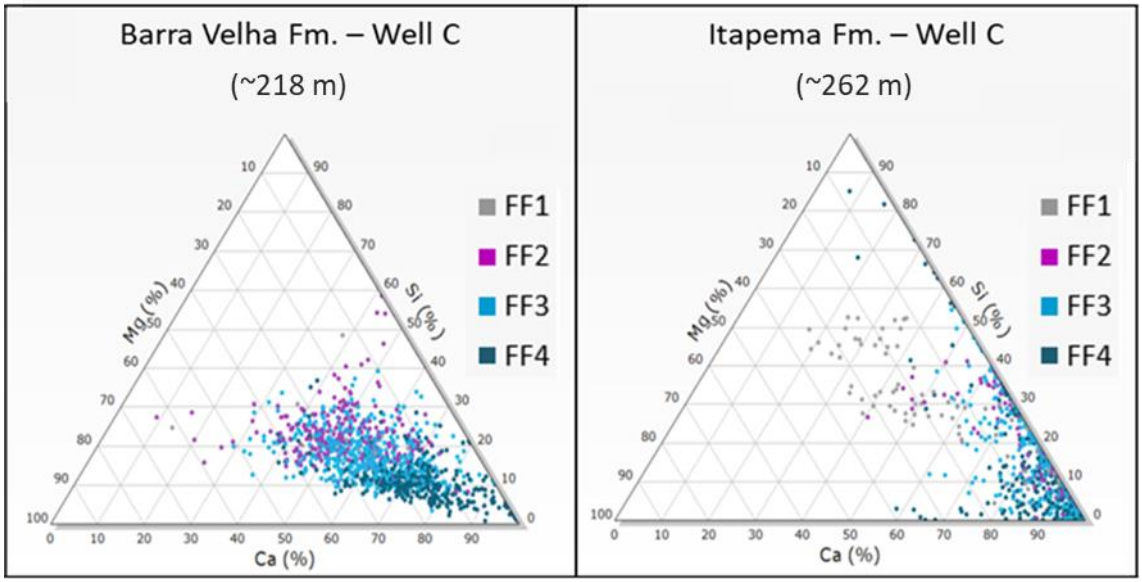

Figure 75: Ternary diagram of calcium (Ca), magnesium (Mg) and silica (Si) by the four FF in Well C, showing some degrees of pore obliteration due to dolomitization and silicification (Si and Mg substituting Ca, respectively) in A) Barra Velha Fm. and B) Itapema Fm.

In Well D, Figure 76 shows that FF1 and FF2 are scatter around higher values of silica and magnesium, as found in the other wells. It is more evident that the FF1 is found around high percentages of Mg and Si and low percentages of Ca, while the FF3 and FF4 are mostly found close to high values of calcium and low values of silica and magnesium.

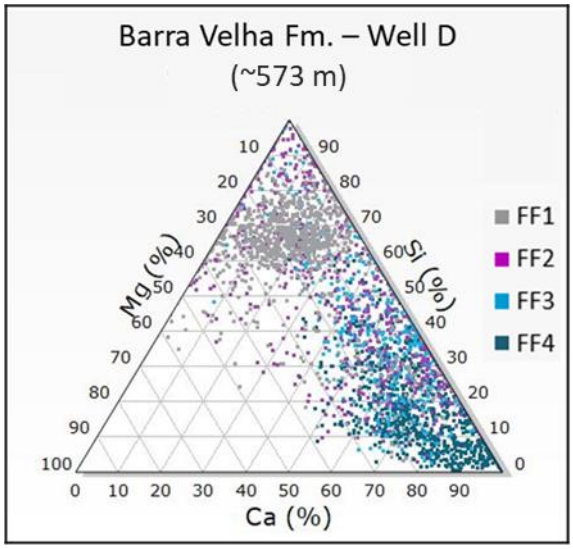

Figure 76: Ternary diagram of calcium (Ca), magnesium (Mg) and silica (Si) by the four FF in Well D, showing some degrees of pore obliteration due to dolomitization and silicification (Si and Mg substituting Ca, respectively) in A) Barra Velha Fm. and B) Itapema Fm.

Therefore, through these ternary diagrams presented above, it is possible to observe that the FF1 and FF2, with worse permoporous conditions, are related to intrusive igneous rocks as well as both silicification and dolomitization processes (silica and dolomite replacing calcite), represented as higher concentrations of magnesium, and silica, while FF3 and FF4 present dominance of clean calcite carbonates, with little diagenetic effects. These results are the same as those found by Vasquez et al. (2019) in their petroacoustic studies in Brazilian pre-salt carbonates and Penna and Lupinacci (2020) in 17 wells from pre-salt interval, Santos Basin.

6.2. Correlation of wells and cyclicity of flow facies

To identify patterns and trends and compare the results obtained in the wells analyzed in this work, this section aims to discuss whether there is any correlation between the flow facies found in all wells for both the Barra Velha and Itapema formations. By relating the main trends with the behavior of the GR and the elemental capture spectroscopy logs (ECS) of calcium, magnesium, and silica, since the union of these curves has a strong influence on permoporosity, it is possible to understand the types of flow facies encountered along formations. Finally, it is noteworthy that the correlation of these flow facies with the aforementioned logs will be made taking into account the flow facies after the upscale has been done, thus, the last track of the layouts is the one to be analyzed.

Flow facies estimation makes it possible to understand the dynamics of oil reservoirs by predicting how fluids may percolate through the subsurface during the reservoir's life cycle (Penna and Lupinacci, 2020). By considering the pore throat radius in their calculations, the flow facies estimates become an effective method to predict the permoporous qualities of a given oil-producing field. In addition, indirectly, these facies considers the diagenetic changes that the rocks may face, such as silicification, dissolution, dolomitization, cementation, among others.

Figure 77 shows the four wells, arranged according to their geographic distances with a scale of 1:300000 cm and according to their spatial locations. As already seen in section 5.5, each well has its characteristics according to its spatial positions. The dark blue lines connect the base of the Itapema Formation in the wells A, B and C, and the light blue lines link the base of the Barra Velha Formation in wells A, B, C, and D. It is noted that, in general, the base of the Itapema Formation for wells A, B, and C have FF1 as the predominant facies.

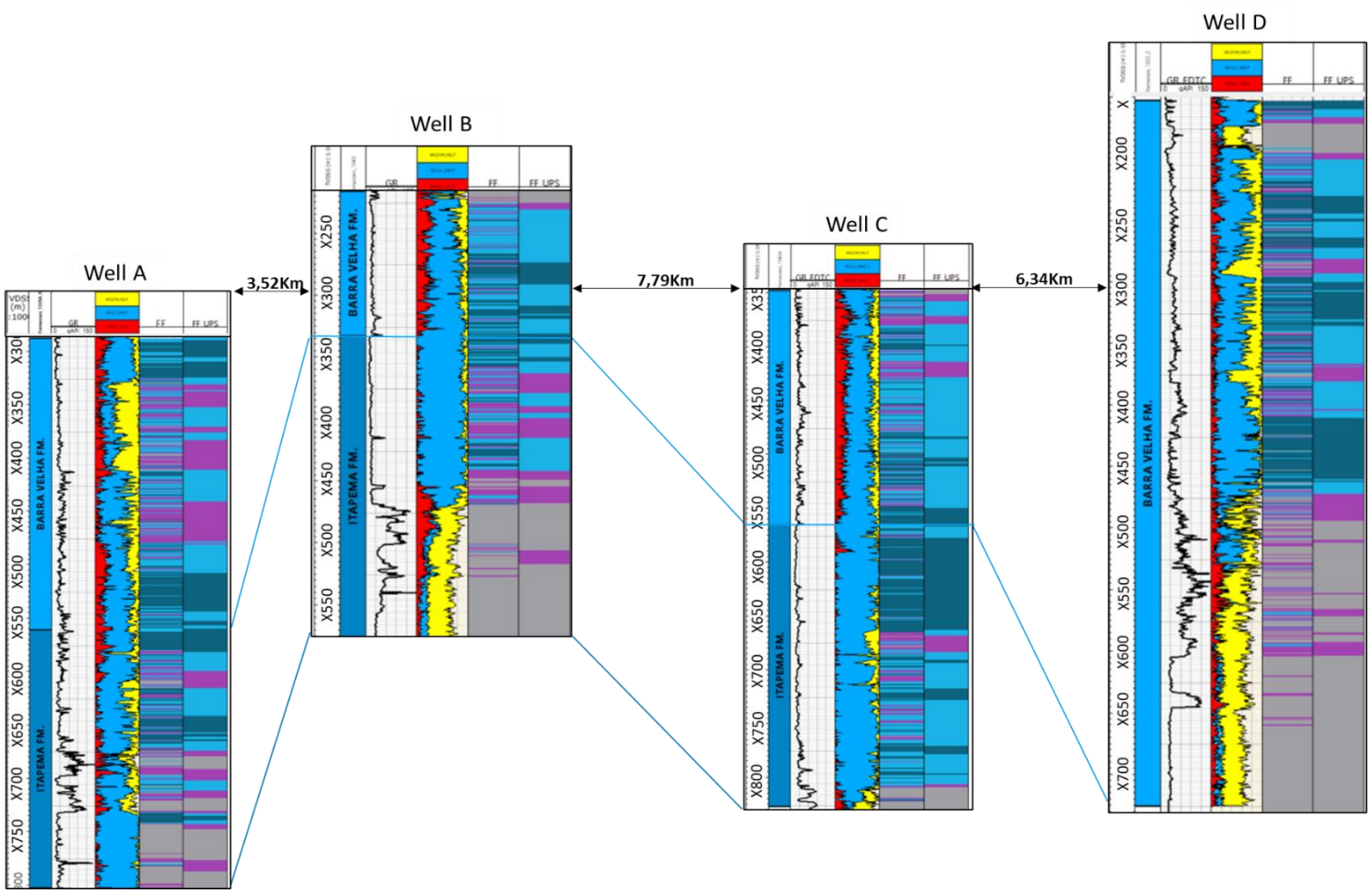

Figure 77: Correlation between the wells, respecting the geographic location in the S-N direction, as well as the spatial position of each well. The tracks are the same for all layouts: Track 1: Depth in TVDSS in meters; Track 2: Barra Velha and Itapema formations; Track 3: Gamma-ray log (GR); Track 4: ECS logs of Silica (yellow), Calcium (blue) and Magnesium (red); Track 5: well-scale flow facies; Track 6: flow facies with upscale.

Well A has at the base of the Itapema Fm. high values of calcium content and low values of Mg, Si, and GR, in contrast, Well C has high values of GR, Si, and Mg, and low values of Ca. It is inferred that these two wells may be related to a base of more closed coquinas either by calcium cementation or by the presence of fines. Castro (2019) identified closed coquinas at the base of the Itapema Formation in some wells in the Búzios Field, Santos Basin, evidenced not only in the well logs but also through the seismic reflectors. Other authors such as Chinelatto et al. (2020) and Barnett et al. (2020) also found evidence of more cemented coquinas and/or the presence of peloids in the most basal parts of the Itapema Formation.

In Well B there is the presence of igneous at the base of the formation, being responsible, together with the high values of GR, for FF1 and FF2. Furthermore, it is noted that in the middle of the Itapema Fm., in Wells A, B, and C, there is a greater presence of FF2 in addition to layers of FF3, and sometimes FF4. It is also noticed that where the silica content and GR log present greater variations, there is also a greater variation of the flow facies presenting FF1, FF2, FF3, and FF4. Because Well B has its base taken by igneous rocks, which greatly affects both the base and the middle of the formation due to the contact metamorphism, intervals of FF1 and FF2 end up being dominant.

Well C, on the other hand, has lower or little variable silica values in the middle of the formation, in addition to low GR values, thus, it has higher intercalations between FF3 and FF4, with only one FF2 range related to a sudden increase in silica content. In the three wells, it is possible to notice a trend of better flow facies towards the top of the formation, defined by the greater presence of FF3 and FF4, accompanied by a decrease in GR values, silica and magnesium content, and an increase in calcium content.

Thus, it is possible to infer that the lithologic facies found near the top of the Itapema Formation in wells A, B and C may be related to cleaner and/or reworked facies located above the Fair-Weather Wave Base (FWWB) (Chinelatto et al., 2020). These facies may have been deposited in areas close to the coquina banks or in the coquinas banks where the wave action may have had a strong influence on the good permoporosity of this interval. In these wells, the coquinas are represented by rudstones, floastones, and grainstones with good permoporosity. The coquinas banks are one of the best reservoirs of the field in terms of permoporosity, and a detailed study about the textural and taphonomic characteristics of this type of reservoir is found in Chinelatto et al. (2020).

Therefore, it is inferred that there is a cyclicity in the distribution of the flow facies in the Itapema Formation of wells A, B and C. From the base to the middle of the formation the worst flow facies (FF1 and FF2) are located, in the middle, it can be seen greater intercalation between the flow facies, especially FF2 and FF3. Towards the top of the formation, there is an improvement in permoporosity and, consequently, a greater presence of FF3 and FF4.

Barnett et. al (2020), when carrying out a study on the origin of clinoforms in lacustrine depositional environments of the Itapema Formation in three wells of the Mero Field, in the Santos Basin, found results similar to those found in this work. According to them, the base of the Itapema Formation has worse porosities associated with higher values of acoustic impedance, generally related to carbonates matrix- rich or cemented, the middle of the formation has a slight improvement in porosity and a slight decrease in PI, but still with low porosity values, and towards the top, a significant improvement in porosity and decrease in PI were found.

The estimated flow facies for the Barra Velha Formation in wells A, B, and C show similar behavior with generally a base with good permoporosity, low Si and Mg content and higher Ca. For the three wells, the base of the Barra Velha Fm. presents intercalation between FF3 and FF4. Well D, in turn, does not share the same characteristics as it has a base extremely influenced by the presence of igneous rocks, in addition to laminites and mudstones, as well as high silica and magnesium content when compared to the rest of the interval. Contact metamorphism, due to the expressive presence of igneous rocks in this well, especially at the base, can end up closing the pores and reducing permoporosity in the surrounding areas, so there is a predominance of FF1 and FF2 at the base of Well D, different from what was found in the other wells.

The middle of the Barra Velha Formation in all wells shows a predominance of FF3 with some intercalations of FF4 and FF2 associated with a decrease and increase in silica content, respectively. Note that when there is a greater variation in the silica content, it is more likely that there will be more intercalations between the FF2, FF3, and FF4 as can be seen, more clearly, in wells A and D. It is possible to note that in wells A, B, C and D, there is a general predominance of FF3 and a slight worsening of the flow facies towards the top. Well C, for example, has some FF2 layers that are possibly associated with an increase in Mg, towards the top, and variations in the GR log related to the Lula Mark. Well A presents strong intercalations between FF3 and FF2 from the middle to the

top of the formation, with thick layers of FF2 associated with an increase in silica values and a decrease in calcium content.

It is noteworthy that there is a certain pattern of behavior of the flow facies concerning the order in which they are presented. That is, the base of the Itapema Formation in wells A, B, C and the base of the Barra Velha Formation in Well D begins with FF1, after the FF1, FF2, then the FF3, and from FF3 the FF4, that is, the flow facies never jump from the FF1 to the FF3, or from the FF2 to FF4 and vice versa. They always respect a hierarchical order based on the values whether they are increasing or decreasing. This pattern of behavior of the flow facies associated with the GR and ECS logs may be related to the cyclothems based on collected core successions, proposed for the Barra Velha Fm., which are controlled by tectonics, lake water level, erosional and geochemical processes (Wright, 2012; Wright and Barnett, 2015; Wright and Tosca, 2016).

These successions consist of an evaporitic/shallowing upwards sequence with basal facies of predominantly detrital laminated carbonate muds with the occasional presence of spherulites and shrub fragments. These laminated carbonate grade into shallow water spherulitic carbonates as well as stevensite rich lithologies and finally shrub-like carbonate facies (Wright, 2012; Wright and Barnett, 2015; Wright and Tosca, 2016). It is noteworthy that these cyclothems are 0.75 to 5m thick and can be found throughout all formation. That said, it is possible to understand that the facies described by Wright and Barnett (2015) as laminated carbonates with the presence of clay (e.g., laminites and/or mudstones) are possibly associated with FF1 and FF2 as already seen in chapter 5, and the facies described as spherulites and shrubs, as well as the reworked ones (e.g., grainstones and rudstones), would represent an improvement in the permoporosity and may be related to FF3 and FF4. Therefore, as well as the cyclothems identified by the aforementioned authors, the flow facies also present a certain cyclicity and an alternation pattern.

6.3. Brief considerations on the depositional environments of the Barra Velha and Itapema formations and their relationships with the flow facies

The Itapema Fm., which occurs in wells A, B and C, has the presence of the four flow facies, having, in general, a predominance of FF1 and FF2 at its base, and FF3 and FF4 at the top of its interval. As seen before, what differentiates one flow facies from another is its permoporosity. The permeability can be a crucial factor for this distinction, for as it was observed in chapter 5, some intervals have porosities from reasonable to good, but low permeability. The average porosity for FF2 in the Itapema Formation, considering all wells, for example, is around 7% and the permeability is 2.05 mD as observed in Table 14. Some factors such as a higher amount of cement, lower degree of dissolution of the shells, and/or lower primary porosity of FF1 and FF2 may be responsible for the lower permoporosity, when compared to FF3 and FF4. In the Itapema Fm., what differs in the quality of the flow facies is the presence of fines (muddy carbonates or shales), calcitic cement, as well as the silica content, that were very present throughout this formation and that result in lower permoporosity, reflected in FF1 and FF2, mostly.

It is noteworthy that the lithological facies associated with the four flow facies for the Itapema Formation usually comprise the coquinas, most of the time, in the form of rudstones, floatstones, and grainstones, as well as mudstones, shales and laminites. Then, making a direct association of the depositional environment to the flow facies is not possible due to the strong diagenetic influence that these lithologies may have suffered. Therefore, it was decided to make a comparison between the characteristics of the geophysical logs related to each flow facies with the results of some articles that correlate the coquina facies and the type of environment to which they are linked, both in the Campos and Santos basins, approached in works such as Fick et al. (2018) and Chinelatto et. al (2020). From the depositional models developed by these authors, it is possible to expand and relate them to the flow facies found in wells A, B, and C. This correlation is made generically and is not related to degrees of selection or orientation of the shells, being just an attempt to link the flow facies with the depositional model of the coquina facies studied by the aforementioned authors.

Fick et al. (2018) investigate the role of the energy wave transformation regarding the weather conditions (e.g., fair weather and storm wave conditions) processed in shallow waters in shell concentrations. They built physical modeling of the coastal environment performed in a laboratory. The experimental setup consisted of a 2D flume, a wave generator, and a sedimentary bottom composed of quartz sand and shells (bivalves, gastropods, and fragments). They conclude that waves, storm-induced currents, the breaker, and the shoaling zone control the distribution of shell concentration.

Moreover, Chinelatto et al. (2020) enriched these experiments by conducting a study of the Itapema Formation, in the Santos Basin, in which they relate shells with preferential orientation to fair-weather conditions and, without preferential orientation and with a more chaotic distribution, to storm conditions (Figure 11). Furthermore, the authors observed from fair-weather to storm wave conditions, two main shell concentration dynamics: reworking and winnowing. The reworking dynamics (erosive) always occurred in the most proximal (and shallow) zones. These processes produce more energetic interactions with the bottom and generate intense sediment motion in the water column and on the bed of the upper and lower shoreface and foreshore. The winnowing dynamics are usually restricted to the offshore transition in fair-weather wave conditions, and offshore in storm wave conditions, occurring at an intermediate condition of energy. Well-sorted facies are generally interpreted as belonging to rework or wave breaking zones, while poorly selected facies can be correlated to an environment below the rework zone, in an offshore zone, or to restricted deposits, in a zone of lagoon and washover, especially in storm conditions (Figure 11).

In addition to the works mentioned above, others developed in the pre-salt coquinas of the Santos and Campos basins are also noteworthy, such as the one developed by Muniz (2013) and Barnett et al. (2020). After reviewing these works, it is inferred that terrigenous or muddy facies, rich in organic matter or fine grains, are found in low-energy environments, below the wave-base, where there may have been possible drowning and/or in restricted environments protected by the coast. These facies can be related to the base of the Itapema Formation and generally present worse permoporous conditions and, therefore, FF1 and FF2. Besides the facies associated with the presence of fines and/or organic matter, Barnett et al. (2020) identified, in the Itapema Formation, facies of packstones, wackestones, and bioclastic floatstones rich in matrix or cemented, also associated with low energy environments, below the wave-base or in a protected coastal

environment. Since at the top of the Itapema Formation more FF3 and FF4 were found, it can be inferred that there is an improvement in the permoporosity of the lithologic facies associated with these flow facies. Then, in a depositional model, the grainstones, rudstones and floatstones associated with FF3 and FF4, and observed in the wells analyzed in this work, would possibly be in zones under the action of waves and storms, therefore, in a high energy zone such as coquina banks or erosive surfaces.

Therefore, using the depositional model of taphofacies interpretation developed by Chinelatto et. al (2020) based on the model by Fick et al. (2018), an adaptation of this model was made with the aim of suggesting a correlation between the flow facies estimated in this dissertation and the deposits analyzed by these authors in each zone for both fair-weather and storm conditions (Figure 78-A and -B, respectively). It is noteworthy that in this interpretation, only the depositional aspects were taken into account. That is, considering the primary porosity this model works well, however, when considering a diagenetic or hybrid control - when more than one mechanism affects the formation of a pore system at different times during diagenetic history - the action of diagenesis may favor or not the relationship between porosity and permeability. Therefore, Figure 78 shows only a correlation of the flow facies with the model under depositional control, that is, with the formation of pores in carbonate rocks being controlled only by deposition processes (Ahr, 2008; Herlinger et al., 2017; Chinelatto et al., 2020).

During fair-weather conditions (Figure 78-A) FF3 and FF4 would be probably located at the shoreface and foreshore due to the reworking zone providing the best permoporous conditions, while FF2 would occur in the offshore transition, below the FWWB, where the winnowing zone is not predominant and the peloids could settle, worsening the permoporosity. At the same time, in restricted areas, peloids, setevensitic ooids, and shells with stevensite coatings are formed, inferring a greater accumulation of fine grains and, thus, low porosity and permeability. Therefore, FF2 would probably be found at the lagoon and washover, where the reworking zone is not present anymore. On the other hand, close to the transitions of the reworking to the winnowing zone, it would be possible to find FF3, due to the presence of some reworked facies as well as the action of the winnowing, generating a good permoporosity. FF1 can be found at the lake margin where mudstones may occur, as well as in the deepest parts of the lake, where the energy is low, and the currents were not strong enough to remove or displace the fine grains.

During storm surges (Figure 78-B), the zone of reworking is wider and storm waves and currents are capable of eroding previously deposited facies (red lines). Foreshore and shoreface coquinas may be eroded, transported, and deposited as washover deposits, thus it can be suggested that FF3 would be found close to the reworking zone and the FF2 near the lake margin where can be found some clay and/or fine grains, transported by waves, mixed with old and fresh shells. At the lake margin, the waves are capable of removing and transporting clay and some other terrigenous facies to this area, therefore, FF1 could be found there. In the deepest areas of the lake, where the energy is low as well as the wave and currents actions, mudstones may have been deposited and so it is more likely to have FF1. FF2 can also be found below the SWB, and close to the deepest area of the lake, where the winnowing is not predominant. The best flow facies, FF3 and FF4 can be found in the coquinas interval between the foreshore and shoreface to offshore transition, mainly as bioclastic bars or sheets and washover fans, where there are high-energy, shallow water, waves actions, and more reworking.

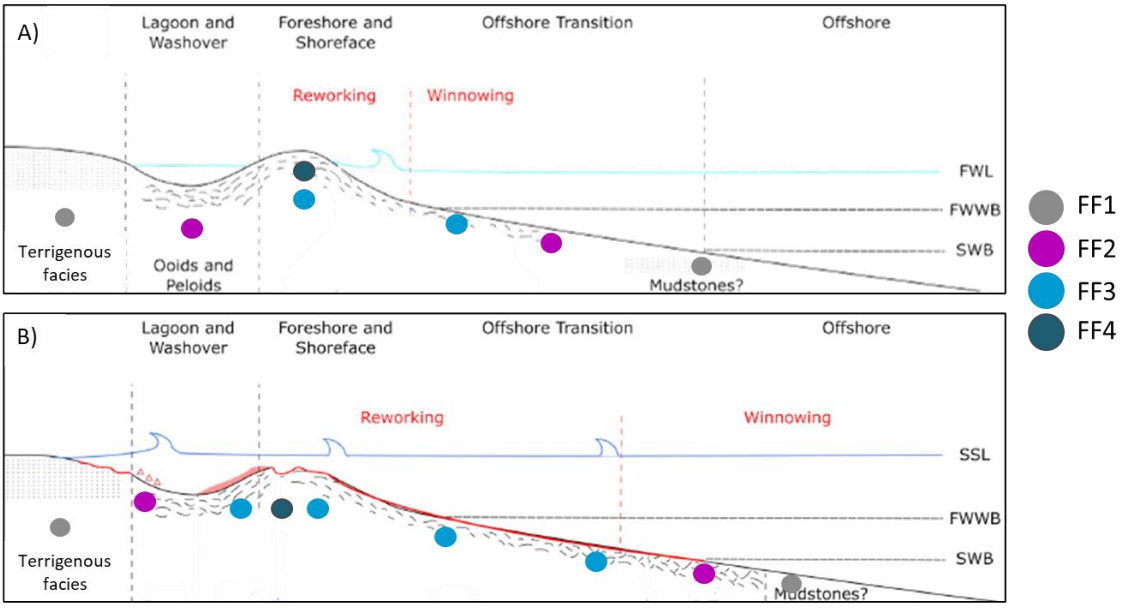

Figure 78: Correlation between the main zones of the depositional model of interpretation developed by Chinelatto et al., (2020) based on Fick et al., (2018) and the flow facies estimated in this dissertation. A) Fair-weather conditions and B) Storm conditions.

As mentioned before, Figure 78 is an attempt to correlate the flow facies with the zones interpreted in models controlled by depositional processes. However, as pre-salt carbonate reservoirs are known to be complex environments, with significant diagenesis action, it is difficult to create a model that can faithfully reproduce the relationship of diagenesis with depositional environments. Some authors such as Herlinger et al. (2017)

and Chinelatto et al. (2020) brought discussions about the diagenetic influence on the coquinas of the Coqueiros and Itapema formations, respectively. Herlinger et al. (2017) developed a table with the interpreted diagenetic sequences for the rock types studied by them (Figure 79). The authors were able to identify the main diagenetic processes observed in the bioclastic grainstones and rudstones, associating them to the time when diagenesis occurred, that is, whether it occurred right after the deposition, or in association with this process (eodiagenesis), or after deposition (mesodiagenesis).

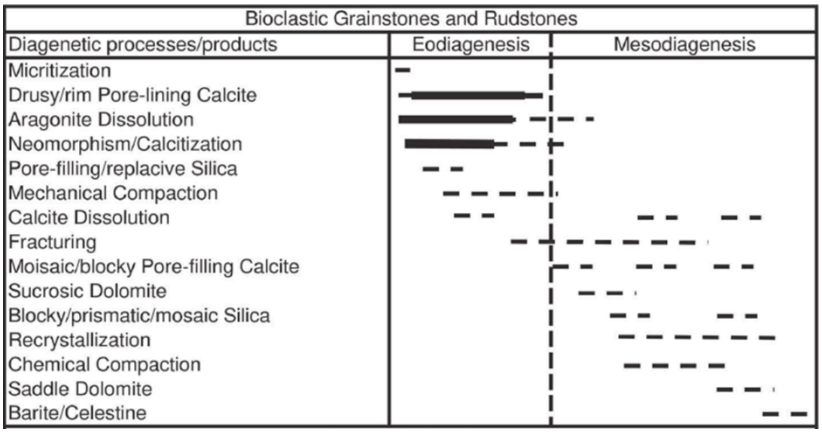

Figure 79: Diagenetic sequences interpreted for the studied rock types. Thicker lines correspond to more significant processes and products, whilst dashed lines correspond to less intense processes and products. Source: Modified from Herlinger et al. (2017).

Chinelatto et al. (2020) show the influence of calcite cementation and dissolution between the depositional and the diagenetic control of porosity, and the main pore type found in each group (Figure 12). In depositional control, the presence of fine grains, which reduces the interparticle porosity, will determine the values of porosity and permeability. In hybrid control the cementation and dissolution will control the enhancement or reduction of porosity. In diagenetic control, the high cementation obstructs the primary pores, and only secondary porosity is observed. The diagenesis reduces the primary pore, however, the dissolution of shells and matrix may promote the moldic pores and vugs. According to them, the best permoporosities were found in samples in which a great dissolution was observed.

It is noteworthy that in this dissertation, it was not possible to carry out detailed petrographic analyzes of all samples since there was not enough information to infer the possible porosity controls and diagenetic processes involved. Therefore, it becomes difficult to find a direct correlation of the flow facies with each of these processes. However, what could be observed is that calcite cementation and the silica and calcium

contents have influenced the permoporosity of the Itapema formation in the analyzed wells. Calcite cement is predominant throughout the formation and sometimes appears to be responsible for the reduction of permoporosity.

Besides the Itapema Fm., in this section, some of the main depositional models found in the literature for the Barra Velha Fm. are discussed. Also, an attempt is made to associate these environments with the flow facies. It is noteworthy that pre-salt carbonates of the Barra Velha formation are deposited in extremely complex environments, so this association of facies is merely an approximation to better understand the very multiform characteristics of this formation (Do Carmo, 2021). For this, authors such as Wright and Barnett (2015), Muniz and Bosence (2015), Wright (2020), Gomes et al. (2020), and Ferreira et al., (2021) were used as a basis for understanding the models in order to correlate them with the flow facies.

As seen in section 2.1, Wright and Barnett (2015) noted a statistically tested pattern of repetition of three main lithologies in metre-scale units: ostracod-bearing laminites, overlain by in situ spherulites, overlain by in situ shrubs (facies 3, 2, and 1, respectively; see Figure 13, section 2.1). They proposed that the cyclothems likely represented flooding and evaporation cycles. Wright (2020) adds that in some cyclothems, the shrub units are overlain, by centimeter-thick, well-sorted grainstones composed of shrub and spherulite debris, then sharply overlain by laminites.

Wright (2020) developed a model for the cyclothems in the Barra Velha Fm. shown in Figure 25, section 2.1. Stage 1 illustrates the filling of the lake with waters of low alkalinity-salinity, introducing favorable conditions for ostracods and fish. The reduced alkalinity triggered precipitation of interstitial silica gels favoring the formation of silica nodules. The lighter oxygen isotope values in this unit suggest precipitation of some calcite from these less evaporated waters. The accumulation of fine-grained carbonates implies deposition in a lower energy setting, probably below the wave-base. Earlier deposits were reworked in shallower areas along wave-dominated shorelines.

Stage 2 represents the point when evaporation triggered the formation and deposition of Mg-silicate gels, which are assumed to have been deposited below the wave-base. During the contraction of the lake, it is assumed that the wave-base may also have been shallower as fetch decreased. In stage 3 calcite was precipitated as spherulites within the gels below wave-base, and locally up-dip as shrubs where gels were not

accumulating or had been removed by falling wave-base. This is based on the observations that shrub facies are better developed, with commonly larger shrubs, in up-dip areas near minor paleo-topographic highs. Finally, in stage 4, gel deposition may have ceased and spherulite growth reached the sediment-water interface allowing shrubs to grow; further shrub growth took place in shallower settings. Later local progradation of shoreline grainstones covered the shrubs capping the cyclothems.

Gomes et al. (2020) developed an alternative conceptual model incorporating the distribution of detrital grains in order to explain the temporal variation of detrital material within the Barra Velha Formation. These alternative models were made based on modifications in the models proposed by Wright and Barnett (2015; 2017) and Farias et al. (2019) (Figure 24, section 2.1). They divided the models into three different scenarios related to climate change. The first one is the humid to arid climate with a fluctuating lake-level. During a humid climate, assuming precipitation is higher than evaporation (P > E), it would be expected an increase in fluvial detrital input associated with rising lake level, resulting in lake water dilution and a fall in pH, leading to mud deposition.

During an arid climate, assuming P < E, there would be a decrease in fluvial detrital input, associated with falling lake level, resulting in evaporative concentration and a rise in pH, leading to precipitation of Mg-clay with spherulites and then shrubs. The second is the semi-arid to arid climate, shallow-lake model. Under a semi-arid climate, assuming P≈E, there would be a decrease of aeolian detrital input (dust) and precipitation of calci/dolo/siliceous mud. During an arid climate (P < E), there is an increase in aeolian detrital input that raises the pH to high levels, being the precipitation of shrubs, spherulites, and Mg-clay with spherulites growing therein expected.

The last one is a constant lake level controlled by spill points. In this case, climate-induced changes in aeolian/fluvial detrital input, pH, and lake stratification, divorced from changes in lake level, would lead to sediment accumulation as in the first two models. Thus, Gomes et al. (2020) suggest that there were special phases of lake sedimentation during which the shrubs were formed and other phases when spherulites and Mg-clays were precipitated. The variation in thickness and facies within each basic cycle can be related to changes in accommodation and/or water chemistry.

Ferreira et al. (2021) proposed a schematic sediment succession moving from shallower to deeper lake waters, Mg-rich clays (stevensite), shrubs, spherulites, and fine-

grained carbonate muds, consecutively. The first three sediments occur in a range from 7 up to 20 m in deep water whilst in the deeper/distal portions of the lake only fine-grained carbonate mud sedimentation would take place.

In short, it can be said that Wright and Barnett (2015), Muniz and Bosence (2015), Wright (2020), Gomes et al. (2020) and Ferreira et. al (2021) attributed the formation of laminated carbonates to moments when the lake would be relatively deeper, due to a phase of humid climate, where there was a precipitation rate greater than the evaporation rate. Therefore, during this period, there was a drop in pH, greater water dilution, and greater arrival of fluvial detrital sediments with greater continental input. The worst flow facies (FF1), characterized mainly by very low permoporosity, higher values of GR, silica, and magnesium content, is linked to the presence of laminites and mudstones and may be associated with this moment.

Also, according to the aforementioned authors, the cleanest shrub and spherulite facies are formed at times when there is a shallowing at the lake level and an arid climate where the rate of evaporation is greater than that of precipitation and, therefore, a consequent increase in the concentration of salts in the water, in addition to an increase in pH and less input of fluvial detrital sediments. FF3 and FF4 have the highest porosities and permeabilities and may be associated with this period. In addition, the lithological facies that are most linked to these flow facies are grainstones, shrubs, and spherulites with lower values of GR and silica content as well as higher calcium content.

In addition to the lithological facies described in the paragraph above as shrubs and spherulites associated with the best flow facies, it is possible to find samples described as shrubs, spherulites, and grainstones related to FF2. These facies may be associated with the presence of clay laminations that impair permoporosity, high GR values, in addition to high silica content. Therefore, FF2 may be associated with a moment of drowning, where the precipitation rate is again greater than that of evaporation, thus causing a lower concentration of salts in the water, reducing alkalinity (reduction in pH). Furthermore, in this configuration, there may be an increase in the arrival of fluvial detrital sediments (Wright and Barnett, 2015; Muniz and Bosence, 2015; Gomes et al., 2020; Wright, 2020). At this moment, the lake level is deeper than at the moment mentioned in the paragraph above, however, it can be said that it is still shallower and with a higher pH and concentration of salts than the laminites deposition interval, where it is most likely to find FF1. It is possible to make this inference due to the fact that shrubs

and spherulites are not generally formed in deeper environments and/or with a low concentration of salts and low pH.

Another important aspect to be mentioned is the diagenetic action on the lithologic facies that end up influencing the estimated flow facies. Diagenetic effects such as silicification and/or cementation are post-depositional processes (Herlinger et al. 2017; Lima and De Ros, 2019), therefore, the depositional environment of these lithological facies, as well as the flow facies, may be associated with the same environments. As an example, facies described as in situ shrubs and spherulites, generally, have better permoporosity than shrubs and spherulites under the effect of silicification (ex: cherts), or with the presence of silica or dolomite cement. Therefore, even though they may belong to the same depositional environment, these facies may be associated with good and worst flow facies.

Taking into account the work developed by the authors mentioned above, Figure 80 shows an attempt to correlate one of the conceptual models proposed by Gomes et a. (2020), in the Barra Velha Formation, with the simplified schematic sediment succession developed by Ferreira et al. (2021) by positioning the flow facies according to their behavior when the lake level rises or falls.

In the humid climate is assumed that the lake level is rise and there is a drop in the pH that would lead to the mud deposition (Figure 80-A). In the Figure 80-C, this climate would be associated with the deepest parts of the lake where the energy is low and the FF1 most likely to be found. The FF2 was positioned slightly above the deepest area that indicates low energy, and where the spherulites start to appear. The reason this flow facies was positioned at these two locations is that in wells A, B and C, FF2 appear almost always interspersed with FF3, so they may be also found in the transition from humid climate to arid climate, also being considered as part of a low to moderate energy environment.

During an arid climate, the lake level is low, evaporation is higher than precipitation and the rise in pH would be favorable to the Mg-clay precipitation with spherulites and then shrubs (Figure 80-B).This climate is more likely to be related to the shallowing higher-energy trend of the lake (Figure 80-C), where the FF3 and FF4 may be encountered. As no evidence of Mg-clays were found in the samples collected in the wells

used in this work, no flow facies were positioned near the lake base level, where in Figure 80-C indicates the presence of shrubs intercalated with Mg-Clays.

Other important facies present in the Barra Velha Formation are the reworked shrubs and spherulites, mostly classified by grainstones. This generally have good permoporous characteristics, medium to low silica and magnesium contents, as well as high values of calcium content and, therefore, a predominance of FF3 and FF4. The reason of these reworking facies has different porosity and permeability values may be associated with more intense diagenetic actions, which can obstruct the primary porosities, generating secondary porosities with low interconnectivity, as well as the presence of cement and/or dissolution that can end up releasing silica or magnesium.

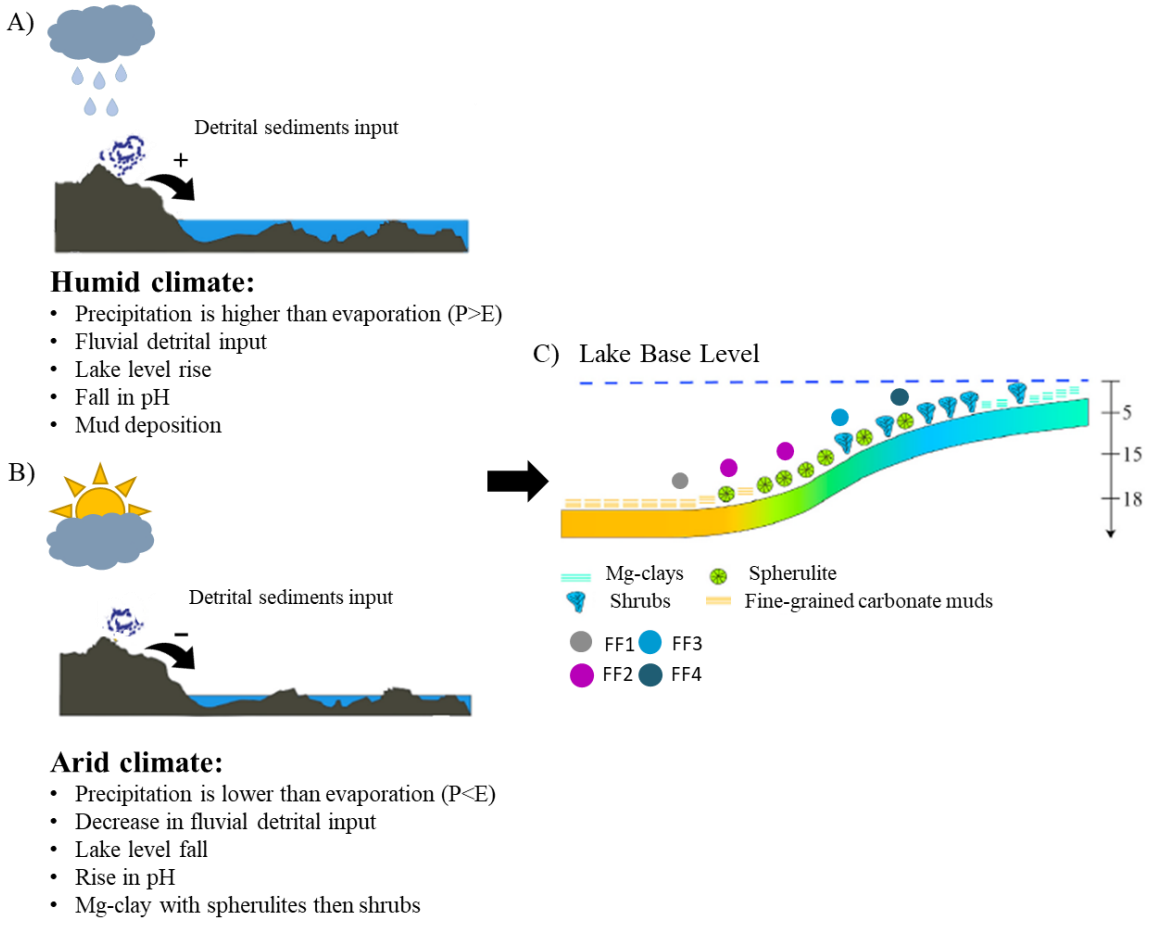

Figure 80: Modification of the humid (A) to arid climate (B) in the fluctuating lake-level model proposed by Gomes et al. (2020). Also, an attempt to relate this conceptual model with the schematic sediment succession proposed by Ferreira et al. (2021), positioning the flow facies (C) taking into account their behavior when the lake level rises or falls.

7. Conclusions

- This dissertation highlights the importance of integrating rock, well and seismic data for a better understanding of the characteristics of the carbonate reservoirs in the Itapema and Barra Velha formations in terms of acoustic impedance and, mainly, flow facies. The analyzes were performed at an intermediate scale of the seismic data and the well logs.
- The porosity and permeability logs were correlated with the ECS logs (Si, Ca and Mg). In general, with an increase in silica, magnesium and Vclay, porosity and permeability tend to decrease, and then, the worst flow facies are predominant (FF1 and FF2). However, this reduction in permoporosity is relative and, even with high silica contents, there are intervals with good flow facies (FF3).
- The presence of dolomite did not show a direct relationship with the reduction of permoporosity, as did silica, but, in general, dolomite cement, which is quite common in the Barra Velha Fm., in wells C and D, is a slight porosity reducer, depending on its quantity. This type of cement seems to occur in greater quantities in Barra Velha Fm. than in the Itapema Fm., possibly due to higher Mg content in the Barra Velha Formation.
- In the Itapema Fm., the presence of calcite cement is common and seems to reduce permoporosity especially at the base of the formation.
- In the Barra Velha formation, in all wells, the FF1 and FF2 associated with muddier facies (e.g. laminites, mudstones) with higher clay content were inferred as coming from a relatively deep environment, humid climate, P > E, lower concentration of salts in lake waters, decrease in pH, and greater input from continental sediments. On the other hand, the FF3 and FF4, with little or no clay content, characterized essentially by shrubs, spherulites and their reworking, were inferred as coming from an intermediate to shallow environment, an arid climate where E > P, the concentration of salts and pH are high and the terrigenous sediment input are very low.
- In the Itapema Formation, FF3 and FF4 were related to the depositional environment belonging to the foreshore and shoreface regions where there is constant wave action, in addition to being inserted in the reworking and

winnowing zones, in fair-weather conditions. In storm conditions, these flow facies still belong to the same regions but are more concentrated in the reworking zone, where the action of waves and currents are constant. FF1 and FF2 can be found in the offshore transition, below the winnowing zone, in restricted areas, or at the lake margin, in fair-weather conditions. In storm conditions, the worst flow facies can be found in the deepest parts of the lake, in the winnowing zone, as well as close to the washover limit to the lake margin, being transported by intense wave action.

- Most carbonates with recrystallized silica and tight carbonates were classified, in general, as FF2 with low porosity-permeability values. Low-energy carbonates with fine sediments, mudstones, and igneous were mostly classified FF1. Carbonates with better permoporous conditions were classified as FF3 or FF4, depending on the silica content and porosity/permeability values.
- Both Barra Velha and Itapema formations have good flow facies, with a predominance of FF3, in most wells, except for wells with the presence of large intervals of igneous rocks and/or intense silicification. Barra Velha Formation, in general, has higher percentages of FF3 and FF4 in all wells, apart from Well D. The Itapema Formation, in turn, has lower percentages of silica content, lower acoustic impedance and higher calcium content.
- From the seismic interpretation and the acoustic inversion, it was possible to better understand the variation in thickness of the Itapema and Barra Velha formations. For the most part, Itapema Formation presents low values of PI, mainly near its top, where the best flow facies were found (FF3 and FF4). The layers with the highest acoustic impedance values at the base of this formation are related to more cemented coquinas, and igneous rocks, reflected in more FF1 and FF2.
- The Barra Velha Formation is thicker in the Wells A, and D, and presents a very heterogeneous behavior in relation to the PI, presenting higher values than those of the Itapema Formation for all wells. In general, the base of the Barra Velha Formation, except for Well D, has low PI, as well as FF3 and FF4 predominance. From the middle to the top of this formation, there is a more heterogeneous behavior, assuming higher values, especially near the base of

the salt. As a result, there is a greater presence of FF2 and FF1 around the wells.

- The acoustic impedance probability density functions (PDFs) of the flow facies, together with the crossplots, helped in a better understanding of the distribution of the facies in the studied interval. When considering the Itapema and Barra Velha formations, the PDFs showed overlapping of the flow facies, especially the FF1, FF2 and FF3 due to the presence of muddy facies in both formations that ends up making the Bayesian classification and the separation of the PDFs hard. This overlap is a challenge for reservoir facies modeling, as it becomes difficult to define which PI values correspond to each facies.

Some suggestions for future work:

- ✓ Since many environmental models only consider depositional aspects, propose a paleoenvironmental model taking into account diagenetic effects, since flow units reflect these effects.
- ✓ Use the results of a stochastic inversion to obtain different flow facies scenarios.
- ✓ Use more than one elastic parameter for the Bayesian classification of flow facies.
- ✓ Compare the 3D modeling of reservoir properties, such as flow facies, using Bayesian classification and neural networks.
- ✓ Use a geological model or structural attribute as a priori information rather than using an equal probability for all flow facies when doing a Bayesian classification.

8. References

Adams, E.W., Grelaud, C., Pal, M., Csoma, A. E., Al Ja'aidi, O. S., and Hinai, R. A., 2011. Improving Reservoir Models of Cretaceous Carbonates with Digital Outcrop Modelling (Jabal Madmar, Oman): Static Modelling and Simulating Clinoforms, Petroleum Geoscience, 17, 309-332.

Aggoun, R. C., Tiab, D. and Owayed, J. F., 2006. Characterization of Flow Units in Shaly Sand Reservoirs – Hassi R'mel Oil Rim, Algeria. Journal of Petroleum Science and Engineering, 50: 211-226. https://doi.org/10.1016/j.petrol.2005.10.006.

Ahr, W. M., 2008. Geology of Carbonate Reservoirs: The Identification, Description, and Characterization of Hydrocarbon Reservoirs in Carbonate Rocks. John Wiley & Sons, Hoboken, pp. 296.

Aki, K., and Richards, P., 1980. Quantitative Seismology: Theory and Methods. San Francisco. W. H. Freeman, 1, 557p.

Altunbay, M., Barr, D. C., Kennaird, A. F., and Manning, D. K., 1994. Numerical Geology: Predicting Depositional and Diagenetic Facies from Wireline Logs Using Core Data. Paper presented at the SPE Asia Pacific Oil and Gas Conference, Melbourne, Australia, 7–10 November. SPE-28794-MS. https://doi.org/ 10.2118/28794-MS.

Amaefule, J., Altunbay, M., Kersey, D. G., and Keelan, D. K., 1993. Enhanced Reservoir Description: Using Core and Log Data to Identify Hydraulic (Flow) Units and Predict Permeability in Uncored Intervals/wells, Paper SPE-26436, presented at the SPE Annual Technical Conference and Exhibition, Houston, Texas, USA, 3-6 OctoberUse the "Insert Citation" button to add citations to this document.

Arienti, L. M., Souza, R. S., Viana, S., Cuglieri, M. A., Silva, R. P., Tonietto, S. N., Paula, L., and Gil, J. A., 2018. Facies Association, Depositional Systems, and Paleophysiografic Models of the Barra Velha Formation, Pre-salt Sequence – Santos Basin, Brazil. AAPG Annual Convention and Exhibition, Salt Lake City, Utah May 20–23.

Artagão, V. M., 2018. Análise estratigráfica de alta resolução aplicada aos depósitos da Formação Barra Velha, Bacia de Santos: identificação, correlação e mecanismos de controle de ciclos sedimentares. Master thesis. UERJ, Brasil (in Portuguese).

Avseth, P., Mukerji, T., and Mavko, G., 2005. Quantitative Seismic Interpretation: Applying Rock Physics Tools to Reduce Interpretation Risk, first ed. Cambridge Press, Cambridge.

Backus, G., 1962. Long-wave elastic anisotropy reduced by horizontal layering: Journal of Geophysical Research, 67, 4427–4440.

Barnett, A. J., Fu, L., Rapasi, T., Scotellaro, C., Guha, J., Cabolova, A., and Domingues, A. L., 2021. Seismic characterization and origin of clinoforms in lacustrine depositional environments: a case study from the Cretaceous of the South Atlantic. Geological Society, London, Special Publications, 509(1), 127–145. https://doi.org/10.1144/sp509-2019-148.

Basbug, Z., and Karpyn, Z., 2007. Estimation of Permeability from Porosity, Specific Surface Area, and Irreducible Water Saturation using an Artificial Neural Network. Presented in the Latin American and Caribbean Petroleum Engineering Conference, 15-18 April, Buenos Aires, Argentina. SPE-107909-MS. https://doi.org/10.2118/107909-MS.

Basso, M., Belila, A. M. P., Chinelatto, G. F., Souza, J. P. da P., and Vidal, A. C., 2020. Sedimentology and petrophysical analysis of pre-salt lacustrine carbonate reservoir from the Santos Basin, southeast Brazil. International Journal of Earth Sciences. https://doi.org/10.1007/s00531-020-01932-7

Beasley, C. J., Fiduk, J. C., Bize, E., Boyd, A., Frydman, M., Zerilli, A., Dribus, J. R., Moreira, J. L. P., and Capeleiro Pinto, A. C., 2010. Brazil's pre-salt play. Oilfield Rev 22(3):28–37.

Belila, A. M. P., Kuroda, M. C., Souza, J. P. P., Vidal, A. C., and Trevisan, O. V., 2018. Petrophysical characterization of coquinas from morro do chaves Formation (Sergipe- Alagoas basin) by X-ray computed tomography. 18. Revista do Instituto de Geociências – USP, pp. 3–13 3.

Bird, R. B., Steware, W. E., and Lightfoot, E. N., 1960. Transport Phenomena, New York, Wiley.

Boyd, A., Souza, A., Carneiro, G., Machado, V., Trevizan, W., Santos, B., Netoo, P., Bagueira, R., Polinsko, R., and Bertolini A., 2015. Pre-salt Carbonate Evaluation for Santos Basin, Offshore Brazil. Petrophysics, 56 (6), p 577–591.

Buckley, J. D., Bosence, D. W., and Elders, C. F., 2015. Tectonic setting and stratigraphic architecture of an Early Cretaceous lacustrine carbonate platform, Sugar Loaf High, Santos Basin, Brazil. Geological Society, London, Special Publications, 418, p 1–17.

Buchheim, H. P., and S. M. Awramik., 2013. Stevensite, oolite, and microbialites in the Eocene Green River Formation, Sanpete Valley, Uinta Basin, Utah, in Proceedings of the AAPG Annual Convention and Exhibition.

Bruhn, C. H. L., Gomes, J. A. T., Lucchese JR., C. D., and Johann, P. R. S., 2003. Campos Basin: reservoir characterization and management — historical overview and future challenges. Offshore Technology Conference, 5–8 Maio, Houston, Texas, USA, p 1–14.

Cainelli, C., and Mohriak, W.U., 1999. Some remarks on the evolution of sedimentary basins along the Eastern Brazilian continental mar- gin. Episodes 22(3):206–216.

Calvo, J. P., Blanc-Valleron, M. M., Rodríguez-Aranda, J. P., Rouchy, J. M., and Sanz, M. E., 1995. Authigenic clay minerals in continental evaporitic environments. In Palaeoweathering, Palaeosurfaces and Related Continental Deposits.

Carlotto, M.A., Silva, R.C.B., Yamato, A., Trindade, W., Moreira, J., and Fernandes, R., Ribeiro, O., 2017. Libra: a newborn giant in the Brazilian pre-salt province. In: Merrill, R.K., Sternbach, E. (Eds.), Giant Fields of the Decade 2000–2010, vol. 113.

Carman, P., 1937. Fluid flow through granular beds. Transactions-Institution of Chemical Engineeres, 15, 150–166.

Carminatti, M., Wolff, B., and Gamboa, L. A. P., 2008. New exploratory frontiers in Brazil. In: 19th World Petroleum Congress, Madrid, 2008.

Carminatti, M., Dias, J. L., and Wolf, B., 2009. From turbidites to carbonates: breaking paradigms in deep waters. In: Offshore Technology Conference, Houston, TX, OTC 20124, 2009.

Carvalho, M. D., Praça, U. M., Silva-Telles JR., A. C., Jahnert, R. J., and Dias, J. L., 2000. Bioclastic carbonate lacustrine facies models in the Campos Basin (Lower Cretaceous), Brazil. Tulsa, AAPG, (Studies in Geology 46), p 245–256.

Castro, T. M., 2019. Avaliação dos reservatórios carbonáticos do Pré-sal no Campo de Búzios, bacia de Santos. Dissertação (Mestrado em Dinâmica dos Oceanos e Terra) - Universidade Federal Fluminense. Advisor: Wagner Moreira Lupinacci (in portuguese).

Catuneanu, O., 2019. Scale in sequence stratigraphy. Marine and Petroleum Geology, 106(April), 128–159. https://doi.org/10.1016/j.marpetgeo.2019.04.026..

Chang, H. K., Kowsmann, R. O., Figueiredo, A. M. F., and Bender, A. A., 1992. Tectonics and stratigraphy of the East Brazil Rift system: an overview. Tectonophysics 213:97–138.

Chekani, M., and Kharrat, R., 2009. Reservoir Rock Typing in a Carbonate Reservoir-Cooperation of Core and Log Data: Case Study. Presented in the SPE/EAGE Reservoir Characterization and Simulation Conference, 19-21 October, Abu Dhabi, UAE. SPE-123703-MS. https://doi.org/10.2118/123703-MS.

Chinelatto, G. F., Vidal, A. C., Kuroda, M. C., and Basilici, G., 2018a. A taphofacies model for coquina sedimentation in lakes, (Lower Cretaceous, Morro do Chaves Formation, NE Brazil). Cretaceous. Res. 85, 1–19.

Chinelatto, G.F., Kuroda, M.C., and Vidal, A.C., 2018b. Relação entre biofábrica e porosidade, coquinas da Formação Morro do Chaves (Barremiano/Aptiano), Bacia de Sergipe- Alagoas, NE-Brasil. Geologia USP. Série científica 18, 57–72.

Chinelatto, G., Belila, A., Basso, M., Souza, J.P., and Vidal, A., 2020. A Taphofacies Interpretation of Shell Concentrations and Their Relationship with Petrophysics: A Case Study of Barremian-Aptian Coquinas in the Itapema Formation, Santos Basin- Brazil. Mar. Petrol. Geol. 116 https://doi.org/10.1016/j.marpetgeo.2020.104317,104317.

Chopra, A. K., Stein, M. H. and Ader, J. E., 1987. Development of Reservoir Description to Aid in Design of EOR Project, SPE 16370, presented at the SPE California Regional meeting, Ventura, California.

Choquette, P.W., and Pray, L., 1970. Geologic nomenclature and classification of porosity in sedimentary carbonates. AAPG (Am. Assoc. Pet. Geol.) Bull. 54, 207–250.

Craig, F. F., 1972. The Reservoir Engineering Aspects of Waterflooding: SPE Monograph Volume 3, P. 63-66.

Coates, G. R., Xiao, L., and Prammer, M. G., 1999. NMR Logging Principles, and Applications. Halliburton Energy Services Publication.

Corbett, P. W. M., Estrella, R., Rodriguez, A. M., Shoeir, A., Borghi, L., and Tavares, A. C., 2016. Integration of cretaceous Morro do Chaves rock properties (NE Brazil) with the Holocene Hamelin coquina architecture (Shark Bay, western Australia) to model effective permeability. Petrol. Geosci. 22 (2), 105–122.

De Oliveira, F. V. C. S., Gomes, R. T. M., and Silva, K. M. S. P. S., 2019. Log Features for the Characterization of Igneous Rocks in the Pre-Salt Area of Santos Basin, SE Brazil.

De Paula Faria, D. L., Dos Reis, A. T., and De Souza Jr, O. G., 2017. Three-dimensional stratigraphic-sedimentological forward modeling of an Aptian carbonate reservoir deposited during the sag stage in the Santos basin, Brazil. Marine and Petroleum Geology, 88, 676-695.

Dezfoolian, M. A., and Sanaee, R., 2012. A Comparison of Reservoir Mineralogy Prediction Utilizing Logging Data and Elastic Wave Ve- locities by Virtue of an Artificial Neural Network in South Pars Field. Petroleum Science and Technology. 30: 817–829.

Dezfoolian, M. A., 2013. Flow zone indicator estimation based on petrophysical studies using an artificial neural network in a southern iran reservoir. Petroleum Science and Technology, 31(12), 1294–1305. https://doi.org/10.1080/10916466.2010.54242. .

Dias, J. L., 2005. Tectônica, estratigrafia e sedimentação no Andar Aptiano da margem leste brasileira. Boletim de Geociências da Petrobrás, 13: p 7–25.

Dias, R. M., 2020. Interpretação sísmica quantitativa aplicada a reservatórios carbonáticos de um campo do pré-sal da bacia de santos. Dissertação (Mestrado em Dinâmica dos Oceanos e Terra) - Universidade Federal Fluminense, Equinor Brasil. Advisor: Wagner Moreira Lupinacci (in portuguese).

Dorfman, M. H., Newey, J., and Coates, G. R., 1990. New Techniques in Lithofacies Determination and Permeability Prediction in Carbonates using well Logs (1990)

113-120, in Geological Applications of Wireline Logs, A Hurst, M.A Lovell and Ae. Morton, Eds., Geological Society Special Publication No. 48.

Do Carmo, M. C., 2021. Reconhecimento de eletrofacies carbonáticas e interpretação deposicional e diagenética, com base em dois poços do pré-sal da Bacia de Santos. Dissertação (Mestrado em Dinâmica dos Oceanos e Terra) - Universidade Federal Fluminense, Equinor Brasil. Advisor: Fernando Freire (in portuguese).

Dubrule, O., and Haldorsen, R. H., 1986. Geostatistics for Permeability Estimation," Reservoir Characterization, L.W. Lake and H.B. Carroll, Jr. (eds.), Academic Press (1986) 223-247.

Dunham, R. J., 1962. Classification of carbonate rocks according to depositional texture. In: Ham, W.E. (Ed.). Classification of carbonate rocks. Tulsa. American Association of Petroleum Geologists, Memoir 1, p 108–122.

Dunn, K. -J., Bergman, D. J., and Latorraca, G. A., 2002. Nuclear Magnetic Resonance: Petrophysical and Logging Applications. Handbook of Geophysical Exploration, Pergamon, New York, 2, 176p.

Dutilleul, P., 1993. Spatial Heterogeneity and the Design of Ecological Field Experiments, Ecology, 74, 1646-1658.

D'Windt, A., Quint, E., Al-Saleh, A. and Dashti, Q., 2018. Bayesian Based Approach for Hydraulic Flow Unit Identification and Permeability Prediction: A Field Case Application in a Tight Carbonate Reservoir. Presented in the SPE International Heavy Oil Conference and Exhibition, 10-12 December, Kuwait City, Kuwait. SPE-193752-MS. https://doi.org/10.2118/193752-MS.

Ebanks, W. J., 1987. Geology in enhanced oil recovery: Reservoir Sedimentology. SEPM Special Publication: 40, 1-14.

Emani-Niri, M. and Lumley, D. E., 2016. Probabilistic Reservoir Property Modelling Jointly Constrained by 3D Seismic Data and Hydraulic Unit Analysis. SPE Reservoir Evaluation and Engineering 19 (2): 253 - 264 SPE-171444-PA. https://doi.org/10.2118/171444-PA.

Embry, A.F., and Klovan, J.E., 1971. A late devonian reef tract on northeastern banks Island, NWT. Can. Petrol. Geol. Bull. 19, 730–781.

Farias, F., Szatmari, P., Bahniuk, A., and Franca, A. B., 2019. Evaporitic carbonates in the pre-salt of Santos Basin–Genesis and tectonic implications. Marine and Petroleum Geology, 105, 251-272.

Fatah, T. Y. A., 2020. Análise de zonas de fraturas através de Perfis de Imagem em poços do pré-sal da Bacia de Santos. Dissertação (Mestrado em Dinâmica dos Oceanos e Terra) - Universidade Federal Fluminense, Equinor Brasil. Advisor: Wagner Moreira Lupinacci (in portuguese).

Ferreira, D. J. A., Lupinacci, W. M., Neves, I. A., Zambrini, J. P. R., Ferrari, L., Gamboa, L. G. P., and Olho Azul, M., 2019. Unsupervised seismic facies classification applied to a pre-salt carbonate reservoir, Santos Basin, offshore Brazil: AAPG Bulletin, 2,1–16, https://doi.org/10.1306/10261818055.

Ferreira, D. J. A., Dutra, H. P. L., de Castro, T. M., and Lupinacci, W. M., 2021. Geological process modeling and geostatistics for facies reconstruction of pre-salt carbonates. Marine and Petroleum Geology, 124(May 2020), 104828. https://doi.org/10.1016/j.marpetgeo.2020.104828.

Fick, C., Toldo JR., E. E., and Puhl, E., 2018. Shell concentration dynamics driven by wave motion in flume experiments: insights for coquina facies from lake-margin settings. Sediment. Geol. 374, 98–114.

Fitch, P., Davies, S., Lovell, M., and Pritchard, T., 2013. Reservoir Quality and Reservoir Heterogeneity: Petrophysical Application of the Lorenz Coefficient. Petrophysics, 54 (5): 465-474.

Formigli, J. M., Pinto, A. C. C., and Almeida, A. S., 2009. Santos Basin's Pre-Salt Reservoirs Development – The Way Ahead. Offshore Technology Conference, 4–7 May Houston, Texas.

Furquim, S. A. C., Graham, R. C., Barbiero, L., De Queiroz Neto, J. P., and Valles, V., 2008. Mineralogy and genesis of smectites in an alkaline–saline environment of Pantanal wetland, Brazil: Clays and Clay Minerals, v. 56, p. 579–595.

Ghanbarian, B., Lake, L., and Sahimi, M., 2019. Insights Into Rock Typing: A Critical Study. SPE Journal, 24(1), 230-242. SPE-191366-PA. https://doi.org/10.2118/191366-PA.

Girão, G., 2004. Perfilagem Geofísica de Poço. Apostilas 7: Sônico e Apostila 8: Densidade. Hydrolog Serviços de Perfilagem Ltda (in portuguese).

Goldberg, K., Kuchle, J., Scherer, C., Alvarenga, R., Ene, P. L., Armelenti, G., and De Ros, L. F., 2017. Re-sedimented deposits in the rift section of the Campos Basin: Marine and Petroleum Geology, 80, p 412–431.

Gomes, P. O., Kilsdonk, B., Minken, J., Grow, T., and Baragan, R., 2008. The outer high of the Santos Basin, southern São Paulo Plateau, Brazil: Pre-salt exploration outbreak, paleogeographic setting, and evolution of the syn-rift structures: AAPG International Conference and Exhibition, 26-29.

Gomes, P. O., Parry J., and Martins W., 2002. The outer high of the Santos Basin, Southern São Paulo plateau, Brazil: Tectonic setting relation to volcanic events and some comments on hydrocarbon potential: AAPG Hedberg Research Conference, 8-11.

Gomes, J. P., Bunevich, R. B., Tedeschi, L. R., Tucker, M. E., and Whitaker, F. F., 2020. Facies classification and patterns of lacustrine carbonate deposition of the Barra Velha Formation, Santos Basin, Brazilian Pre-salt. Marine and Petroleum Geology, v. 113, p. 104176.

Guardado, L. R., Gamboa, L. A. P., and Lucchesi, C. F., 1989. Petroleum geology of the Campos Basin, Brazil, a model for a producing Atlantic-type basin. In: Edwards, J. D. & Santogrossi, P. A. (ed.) Divergent / Passive Margin Basins. Tulsa, AAPG, (Memoir 48), p 3–7.

Gunter, G., Finneran, J., and Miller, J., 1997. Early Determination of Reservoir Flow Units Using an Integrated Petrophysical Method. Presented in the SPE Annual Technical Conference and Exhibition, 5-8 October, San Antonio, Texas. SPE-38679-MS. https://doi.org/10.2118/38679-MS.

Hearn, C., Ebanks W. J., Tye, R., and Ranganathan, V., 1984. Geological factors influencing reservoir performance of the Hartzog Draw field, Wyoming. Journal of Petroleum Technology, 36(8), 1335–1344.

Herlinger, R., Zambonato, E. E., and De Ros, L. F., 2017. Influence of diagenesis on the quality of lower cretaceous pre-salt lacustrine carbonate reservoirs from northern

Campos Basin, offshore Brazil. J. Sediment. Res. 87, 1285–1313. https://doi.org/10.2110/jsr.2017.70.

Herlinger, R., Freitas, G. D. N., Dos Anjos, C. D. W., and De Ros, L. F., 2020. Petrological and petrophysical implications of magnesian clays in brazilian pre-salt deposits. SPWLA 61st Annual Logging Symposium. https://doi.org/10.30632/SPWLA-5004.

Herz, N., 1977. Timing of spreading in the South Atlantic: information from Brazilian alkalic rocks. Geol Soc Am Bull 88:101–112.

Holford, S. P., Schofield N., Jackson C. A. -L., Magee C., Green P. F., and Duddy I. R., 2013. Impacts of igneous intrusions on source and reservoir potential in prospective sedimentary basins along the western Australian continental margin: Presented at West Australian Basins Symposium.

Horschutz, P., and Scuta, M. D. S., 1992. Fácies-perfis e mapeamento de qualidade do reservatório de coquinas da Formação Lagoa Feia do Campo de Pampo. Boletim de Geociências da Petrobrás 6 (1/2), p 45–58 (in portuguese).

Iravani, M., Rastegarnia, M., Javani, D., Sanati, A., and Hajiabadi, S. H., 2018. Application of Seismic Attribute Technique to Estimate the 3D Model of Hydraulic Flow Units: A Case Study of a Gas Field in Iran. Egyptian Journal of Petroleum 27 (2): 145-157. https://doi.org/10.1016/j.ejpe.2017.02.003.

Jennings Jr., J. W., Ruppel, S. C., and Ward, W. B., 2000. Geostatistical Analysis of Permeability Data and Modeling of Fluid-Flow Effects in Carbonate Outcrops: SPE Reservoir Evaluation and Engineering, 3, 292-303.

Jones, B., and Renaut, R. W., 1994. Crystal fabrics and microbiota in large pisoliths from Laguna Pastos Grandes, Bolivia: Sedimentology, v. 41, p. 1171–1202.

Kadkhodaie, A., and Kadkhodaie, R., 2018. A Review of Reservoir Rock Typing Methods in Carbonate Reservoir: Relation Between Geological, Seismic and Reservoir Rock Types. Iranian Journal of Oil and Gas Science and Technology 7 (4): 13-35. https://doi.org/10.22050/IJOGST.2019.136243.1461.

Kadkhodaie-Ilkhchi, A., and Amini, A., 2009. A fuzzy logic approach to estimating hydraulic flow units from well log data: A case study from the Ahwaz oilfield, South Iran. J. Pet. Geol. 32:67–78.

Kattah, S., 2015. Pre-Salt Limestone Plays in Campos and Santos Basins, Brazil: Additional Potential Identified. Offshore Technology Conference.

Kearey, P., Brooks M., and Hill, I., 2009. Geofísica de Exploração. São Paulo, Oficina de textos (in portuguese).

Kenyon, W. E., 1997. Petrophysical principles of applications of NMR logging. The Log Analyst 38, vol. 2, p 21–43.

Kenyon, W. E., Day, P. I., Straley, C., and Willemsen, J. F., 1988. A three-part study of NMR longitudinal relaxation properties of water-saturated sandstones. SPE Formation Eval. 3, vol. 3, p 622–636. https://doi.org/10.2118/15643-PA.

Kozeny, J., 1927. Uber Kapillare Leitung Des Wassers Imboden, Stiuzurgsberichte, Royal Academy of Science, Vienna, Proc. Class 1, Vol. 136, p. 271-306.

Lake, L., and Jensen, J., 1991. A Review of Heterogeneity Measures Used in Reservoir Characterization, In Situ, 15, 409-439.

Lalanne, B., and Massonnat, G., 2004. Impacts of Petrophysical Cut-Offs in Reservoir Models. Presented in the SPE Annual Technical Conference and Exhibition, 26-29 September, Houston, Texas. SPE-91040-MS. https://doi.org/10.2118/91040-MS.

Larionov, W. W., 1969. Radiometry of boreholes, NEDRA, Moscou.

Lawrence, J. J., Maer, N. K., Corwin, L. W., and Idol, W. K., 2002. Jay Nitrogen Tertiary Recovery Study: Managing a Mature Field, Paper SPE-78527, presented at the 10th Abu Dhabi International Petroleum Exhibition and Conference, Abu Dhabi, UAE, 13-16 October.

Lebre, M. B. S., Comparação de metodologias para estimativa de propriedades de reservatório aplicadas nos carbonatos do pré-sal do Campo de Búzios, Bacia de Santos. Trabalho de Conclusão de Curso em Geofísica - Universidade Federal Fluminense. Advisor: Wagner Moreira Lupinacci (in portuguese).

Li, P., Zheng, M., Bi, H., Wu, S. and Wang, X., 2017. Pore Throat Structure and Fractal Characteristics of Tight Oil Sandstones: A Case Study in the Ordos Basin, China. Journal of Petroleum Science and Engineering. 149. 665-674. 2017.

Lima, B., and De Ros, L. F., 2019. Deposition, diagenetic and hydrothermal processes in the Aptian Pre-Salt lacustrine carbonate reservoirs of the northern Campos Basin, offshore Brazil. Sedimentary Geology 383: 55-81. https://doi.org/10.1016/j.sedgeo.2019.01.006.

Lorenz, M. O., 1905. Methods of Measuring Concentration of Wealth, Journal of the American Statistical Association, 9(70), 209-219.

Mahjour, S. K., Correia, M. G., dos Santos, A. A., and Schiozer, D., 2017. Flow Units Characterization Methods in a Synthetic Carbonate Reservoir Model. Presented at the 9th Brazilian Oil and Gas Research and Development Congress. Maceio, Brazil. 09-11 September, 2017.

Mello, V. L., 2020. Classificação de Rochas Carbonáticas do Pré-Sal com relação à composição mineralógica a partir de parâmetros elásticos. (Mestrado em Dinâmica dos Oceanos e Terra) - Universidade Federal Fluminense. Advisor: Wagner Moreira Lupinacci (in portuguese).

Mizuno, T. A., Mizusaki, A. M. P., Lykawka, R., 2018. Facies and paleoenvironments of the Coqueiros Formation (Lower Cretaceous, Campos Basin): a high frequency stratigraphic model to support pre-salt “coquinas” reservoir development in the Brazilian continental margin. J. S. Am. Earth Sci. 88, 107–117.

Moreira, J. L. P., Madeira, C. V., GIL, J. A., and Machado, M. A. P., 2007. Bacia de Santos. Boletim de Geociências da Petrobras 15, p 531–549 (in portuguese).

Mohriak W., Nemčok M., and Enciso G., 2008. South Atlantic divergent margin evolution: rift-border uplift and salt tectonics in the basins of SE, Brazil, vol 294. Geological Society, London, pp 365–398.

Mohriak, W. U., Perdomo, L. V., Plucenio, D. M., and Saad, J. L., 2015. Challenges for petrophysical characterization of pre-salt carbonate reservoirs. 14th International Congress of the Brazilian Geophysical Society and EXPOGEF, Rio de Janeiro, Brazil, pag. 623-627.

Moore, C. H., 2001. Carbonate Reservoirs: Porosity Evolution and Diagenesis in a Sequence Stratigraphic Framework: Amsterdam, Elsevier, Developments in Sedimentology 67, 444p.

Mu L., Huang S., and Jia A., 1996. New technology of reservoir description Proceedings of Oil and Gas Field Development of China National Petroleum Corporation Beijng Petroleum Industry Press 1-10.

Muniz, M. C., 2013. Tectono-Stratigraphic evolution of the Barremian-Aptian Continental Rift Carbonates in Southern Campos Basin, Brazil. PhD thesis presented to Royal Holloway, University of London. The Grants Register 2021, 726–728. https://doi.org/10.1057/978-1-349-95988-4_768.

Muniz, M. C. and Bosence, D. W. J., 2015. Pre-salt microbialites from the Campos Basin (Offshore Brazil): image log facies, facies model, and cyclicity in lacustrine carbonates. Geological Society, London, Special Publications, 418, p 221– 242.

Nascimento, A. C. F., 2015. Métodos para identificação de unidades de fluxo e cálculo de permeabilidade no pré-sal da bacia de santos. nota técnica e&p-exp/afoe/afp (in portuguese).

Neves, I. D. A., Lupinacci, W. M., Ferreira, D. J. A., Zambrini, J. P. R., Oliveira, L. O. A., Olho Azul, M., Ferrari, A. L., & Gamboa, L. A. P., 2019. Pre-salt reservoirs of the Santos Basin: Cyclicity, electrofacies, and tectonic-sedimentary evolution. Interpretation, 7(4), SH33–SH43. https://doi.org/10.1190/INT-2018-0237.1.

Ohen, H. and Ajufo, A., 1995. A Hydraulic (Flow) Unit Based Model for the Determination of Petrophysical Properties from NMR Relaxation Measurements. Presented in the SPE Annual Technical Conference and Exhibition, 22-25 October, Dallas, Texas. SPE-30626-MS. https://doi.org/10.2118/30626-MS.

Oliveira M. L. L., 2019. Reconhecimento de eletrofácies em reservatórios turbidíticos da formação Carapebus no Parque das Baleias, Bacia de Campos. Dissertação (Mestrado em Geofísica Aplicada) - Universidade Federal Fluminense, Niterói, RJ (in portuguese).

Penna, R., Araujo, S., Geisslinger, A., Sansonowski, R., Oliveira, L., Rosseto, J. and Matos, M., 2019. Carbonate and Igneous Rock Characterization Through Reprocessing, FWI Imaging and Elastic Inversion of a Legacy Seismic Data Set in Brazilian Pre-salt Province. The Leading Edge 38 (1) 11-19. https://doi.org/10.1190/tle38010011.1.

Penna, R., Lupinacci, W. M., 2020. Decameter-Scale Flow-Unit Classification in Brazilian Pre-salt Carbonates. SPE Res Eval & Eng 23 (04): 1420–1439. https://doi.org/10.2118/201235-PA.

Penna, R., Lupinacci, W. M., 2021. 3D modelling of flow units and petrophysical properties in Brazilian pre-salt carbonate. Marine and Petroleum Geology 124: 104829. https://doi.org/10.1016/j.marpetgeo.2020.104829.

Pereira, M. J. & Feijó, F. J., 1994. Bacia de Santos. Estratigrafia das Bacias Sedimentares do Brasil (in portuguese).

Petersohn, E., 2013. Bacia de Santos: Sumário Geológico e área em oferta. ANP – Agência Nacional de Petróleo, Gás Natural e Biocombustíveis – Seminário Técnico, 34p (in portuguese).

Pietzsch, R., Oliveira, D. M., Tedeschi, L. R., Neto, J. V. Q., and Figueiredo, M. F., 2018. Palaeohydrology of the Lower Cretaceous pre-salt lacustrine system, from rift to post-rift phase, Santos Basin, Brazil. Palaeogeography, Palaeoclimatology, Palaeoecology 507, p 60−80.

Planke, S., Rasmussen T., Rey S. S., and Myklebust R., 2005. Seismic characteristics and distribution of volcanic intrusions and hydro- thermal vent complexes in the Vøring and Møre basins: Geological Society of London, Petroleum Geology Conference Series, 6, no. 1, 833–844, https://doi.org/10.1144/0060833.

Pozo, M., and Casas, J., 1999. Origin of kerolite and associated Mg clays in palustrine-lacustrine environments. The Esquivias deposit (Neogene Madrid Basin, Spain). Clay Miner. 34, p 395–395.

Pranter, M. J., Reza, Z. A., and Budd, D. A., 2006. Reservoir-Scale Characterization and Multiphase Fluid-Flow Modelling of Lateral Petrophysical Heterogeneity Within Dolomite Facies of the Madison Formation, Sheep Canyon and Lysite Mountain, Wyoming, USA, Petroleum Geoscience, 12, 29-40.

Prasad, M., 2003. Velocity-permeability relations within hydraulic units. Geophysics 68 (1), 108–117. https://doi.org/10.1190/1.1543198.

Pritchard, T., Scotellaro, C., and Webber, R., 2010. Carbonate Facies and Permeability Estimation using Rock Physics and Flow-Zone Facies. Presented at the SEG 2010

Annual Meeting, Denver. USA. Technical Program Expanded Abstracts: 2654-2658. https://doi.org/10.1190/1.3513392.

Qiu Y., and Wang Z., 1996. New technology of reservoir description Proceedings of Oil and Gas Field Development of China National Petroleum Corporation Petroleum Industry Press 62-72.

Quirk D. G., Hertle M., Jeppesen J. W., Raven M., Mohriak W. U., Kann D., Norgaard M., Howe M. J., Hsu D., Coffey B., Mendes M. P., 2013. Rifting, subsidence and continental break-up above a mantle plume in the central South Atlantic, vol 369. Geological Society, London.

Riding, R., 2008. Abiogenic, microbial and hybrid authigenic carbonate crusts: components of Precambrian stromatolites: Croatian Geology, v. 61, p. 73–103.

Rodrigues, R., 1995. A geoquimica orgânica na Bacia do Parnaíba. Tese de Doutorado – Universidade Federal do Rio Grande do Sul, RS (in portuguese).

Sartorato, A. C. L., 2018. Caracterização faciológica, estratigráfica e diagenética dos reservatórios carbonáticos da Formação Barra Velha, Bacia de Santos. Dissertação de Mestrado – Universidade Estadual do Rio de Janeiro, RJ (in portuguese).

Sartorato, A. C. L., Tonietto, S. N., and Pereira, E., 2020. Silicification and dissolution features in the brazilian Pre-salt Barra Velha Formation: impacts in the reservoir quality and insights for 3D geological modeling. Rio Oil and Gas Expo and Conference, 20(2020), 68–69. https://doi.org/10.48072/2525-7579.rog.2020.068.

Schmalz, J. P., and Rahme, H. D., 1950. The Variation of Waterflood Performance with Variation in Permeability Profile, Production Monthly, 15(9), 9-12.

Schön, J., 2015. Propriedades físicas das rochas aplicadas à engenharia: Fundamentos teóricos e práticos. 1 ed. Rio de Janeiro, Elsevier (in Portuguese).

Sibley, M. J., Bent, J. V., and Davis, D. W., 1997. Reservoir Modeling and Simulation of a Middle Eastern Carbonate Reservoir, Paper SPE-36540, SPE Reservoir Engineering, 12(2), 75-81.

Silva, A. P. P., 2018. Estudo de reservatórios carbonatados em dois poços do pré-sal da Bacia de Santos: caracterização faciológica e diagenética, síntese comparativa

integrada. Dissertação (Mestrado em Dinâmica dos Oceanos e Terra) - Universidade Federal Fluminense (in portuguese).

Silva, R. C., 2021. Construção de um modelo tectono-estratigráfico com foco no reservatório carbonático do pré-sal do prospecto de Gato do Mato, Bacia de Santos. (Mestrado em Dinâmica dos Oceanos e Terra) - Universidade Federal Fluminense. Advisor: Wagner Moreira Lupinacci (in portuguese).

Shenawi, S., Al-Mohammadi, H., and Faqehy, M., 2009. Development of generalized porosity- permeability transforms by hydraulic units for carbonate oil reservoirs in Saudi Arabia. SPE/EAGE Reservoir Characterization and Simulation Conference.

Shirer, J. A., Langston, E. P., and Strong, R. B., 1988. Application of Field-Wide Conventional Coring in the Jay-Little Escambia Creek Unit," lPT (December 1978) 1774-1780.

Stiles, J. H., Jr. and Hutfilz, J. M., 1988. The use of Routine and Special Core Analysis in Characterizing Brent Group Reservoirs, U.K. North Sea, SPE 18388.

Strasser, A., Hilgen, F. J., Heckel, P. H., 2006. Cyclostratigraphy e concepts, definitions, and applications. Newsl. Stratigr. 42, 75e114.SZATMARI, P. & E. J. MILANI. Tectonic control of the oil-rich large igneous-carbonate-salt province of the South Atlantic rift. Marine and Petroleum Geology, vol. 77, p 567–596, 2016.

Tanaka, A. P., Faria, D. L. P., Gomes, J. P. B., Souza Jr., O.G., 2018. Geological characterization and modeling of an Aptian carbonate reservoir in the Santos basin, Brazil. In: AAPG 2018 AAPG Annual Convention and Exhibition, Salt Lake City, Utah, May 20–23.

Tavares, A. C., Borghi, L., Corbett, P., Nobre-Lopes, J., Câmara, R., 2015. Facies and depositional environments for the coquinas of the Morro do Chaves Formation, Sergipe- Alagoas Basin, defined by taphonomic and compositional criteria. Braz. J. Geol. 45 (3), 415–429.

Terra, G. J. S., Spadini, A. R., França, A. B., Sombra, C. L.; Zambonato, E. E., Juschaks, L. D. S., and Winter, W. R., 2010. Classificação de rochas carbonáticas aplicável às bacias sedimentares brasileiras. Boletim de Geociências Petrobrás, 18, 9-29.

Tiab, D., and Donaldson, E. C., 2000. Petrophysics – Theory and Practice of Measuring Reservoir Rock and Fluid Transport Properties. Second edition, Elsevier, 2000, 889 p.

Tiab, D., and Donaldson, E., 2004. Petrophysics (2nd ed.). Gulf Publishing. Watson, A., Gatens, J., & Lane, H. (1988, March). Model Selection for well Test and Production Data Analysis. SPE Formation Evaluation, 3(1), 215–221. doi: https://doi.org/10.2118/15926-PA.

Timur, A., 1968. An Investigation of Permeability, Porosity and Residual Water Saturation Relationships. Trans. SPWLA Ninth Annual Logging Symposium (1968) Paper K.

Tiwary D. K., Bayuk I. O., Vikhorev A. A., and Chesnokov E. M., 2011. Comparison of seismic upscaling methods: From sonic to seismic. Geophysics 74(2): https://doi.org/10.1190/1.3054144.

Thomaz Filho, A., Mizusaki, A. M. P., and Antonioli, L., 2008. Magmatismo nas bacias sedimentares Brasileiras e sua influência na geologia do petróleo: Revista Brasileira de Geociências, 38, no. 2, 128–137.

Thompson, D. L., Stilwell, J. D., Hall M., 2015. Lacustrine carbonate reservoirs from Early Cretaceous rift lakes of Western Gondwana: pre-salt coquinas of Brazil and West Africa. Gondwana Res. 28: 26–51.

Tosca, N. J., and Wright, V. P., 2014. The Formation and diagenesis of Mg-clay minerals in lacustrine carbonate reservoirs. In Adapted from oral presentation given at 2014 AAPG Annual Convention and Exhibition, Houston, Texas.

Vasquez, G. F., Morschbacher, M. J., Dos Anjos, C. W. Di., Silva, Y. M. P., Madrucci, V., and Justen, J. C. R., 2019. Petroacoustics and composition of presalt rocks from Santos Basin. Leading Edge, 38(5), 342–348. https://doi.org/10.1190/tle38050342.1.

Wendt, W. A., Sakurai, S., and Nelson, P. H., 1986. Permeability Prediction from well Logs Using Multiple Regression: Reservoir Characterization, L.W. Lake and RB. Carroll, Jr. (eds.), Academic Press (1986): 181-221.

Williams, H. D., Wright, V. P., Della Porta, G., Granjeon, D., 2011. Investigating carbonate platform types: Multiple controls and a continuum of geometries. In: Journal of Sedimentary Research, vol. 81, no. 1, p 18–37.

Winter, W. R., Jahnert, R. J., Franca, A. B., 2007. Bacia de Campos. Boletim de Geociências da Petrobrás 15 (2), p 511–529 (in portuguese).

Wright, V. P., and Rodriguez K., 2018. Reinterpreting the South Atlantic pre-salt 'microbialite' reservoirs: Petrographic, isotopic and seismic evidence for a shallow evaporitic lake depositional model: First Break, 36, p 71–77.

Wright, P., and Tosca, N., 2016. A geochemical model for the Formation of the pre-salt reservoirs, Santos Basin, Brazil: Implications for understanding reservoir distribution. AAPG Search and Discovery, article, 51304.

Wright, V. P. & Barnett, A. J., 2017. Critically Evaluating the Current Depositional Models for the Pre-Salt Barra Velha Formation, Offshore Brazil. AAPG Search and Discovery, Article #51439.

Wright, V. P., 2020. The mantle, CO2 and the giant Aptian chemogenic lacustrine carbonate factory of the South Atlantic: Some carbonates are made, not born. Sedimentology.

Wright, V. P.; and Barnett, A. J., 2015. An abiotic model for the development of textures in some South Atlantic early Cretaceous lacustrine carbonates. Geological Society, London, Special Publications, 418(1), 209-219.

Wright, V. P.; and Barnett, A. J., 2020. The textural evolution and ghost matrices of the Cretaceous Barra Velha Formation carbonates from the Santos Basin, offshore Brazil. Facies, 66(1), 1-18. https://doi.org/10.1007/s10347-019-0591-2.

Wyllie, M. R. J.; Gregory, A. R.; Gardner, L. W., 1956. Elastic wave velocities in heterogeneous and porous media. Geophysics, Society of Exploration Geophysicists, 41-70.

Zahaf, K., and Tiab, D., 2002, Vertical Permeability from In Situ Horizontal Measurements in Shaly-Sand Reservoirs, Paper PS-02-08-01, Journal of Canadian Petroleum Technology, 41(8), 1-8.

Zhao, J.; Oliveira, M. J. R.; Zhao, J.; Ren, K.; Oliveira, L. C.; Carmo, I. O.; Rancan, C. C.; and Deng, Q., 2019. Fault Activity and its Influences on Distribution of

Igneous Rocks in Libra Block, Santos Basin: Semi-Quantitative to Quantitative Assessment of Fault Activity Based on High-Resolution 3D Seismic Data. Offshore Technology Conference, Brasil. OTC-29691-MS.

Zielinski, J.P.T., Vidal, A.C., Chinelatto, G.F., Coser, L., Fernandes, C.P., 2018. Evaluation of pore system properties of coquinas from Morro do Chaves Formation by means of x-ray microtomography. Braz. J. Geophysics. 36 (4).